UNIVERSIDADE FEDERAL DE PERNAMBUCO

LABORATORIO DE IMUNOPATOLOGIA KEIZO ASAMI

PROGRAMA DE PÓS GRADUAÇÃO EM BIOLOGIA APLICADA A SAÚDE

MARIA AMÉLIA CARLOS SOUTO MAIOR BORBA

MEDICINA DE PRECISÃO EM ONCOLOGIA: ANÁLISE DE POTENCIAIS MARCADORES MOLECULARES PARA O CARNCINOMA HEPATOCELULAR E O CÂNCER DE MAMA

Recife

2019

MARIA AMÉLIA CARLOS SOUTO MAIOR BORBA

MEDICINA DE PRECISÃO EM ONCOLOGIA: ANÁLISE DE POTENCIAIS MARCADORES MOLECULARES PARA O CARNCINOMA HEPATOCELULAR E O CÂNCER DE MAMA

Tese de Doutorado apresentada ao Programa de Pós-graduação em Biologia Aplicada à Saúde do Laboratório de Imunopatologia Keizo Asami – LIKA/UFPE, como requisito para a obtenção do título de doutora.

Área de Concentração: Biologia Aplicada à Saúde

Orientador: Profª. Drª. Danyelly Bruneska Gondim Martins

Recife

2019

Catalogação na fonte:
Bibliotecária Claudina Queiroz, CRB4/1752

Borba, Maria Amélia Carlos Souto Maior
Medicina de precisão em oncologia: análise de potenciais marcadores moleculares para o carcinoma hepatocelular e o câncer de mama / Maria Amélia Carlos Souto Maior Borba - 2019.
179 folhas: il., fig., tab.

Orientadora: Danyelly Bruneska Gondim Martins
Tese (doutorado) – Universidade Federal de Pernambuco. Centro de Biociências. Programa de Pós-Graduação em Biologia Aplicada à Saúde. Recife, 2019.

Inclui referências e apêndices.

1. Medicina de precisão 2. Câncer 3. Biologia molecular
I. Martins, Danyelly Bruneska Gondim (Orientadora) II. Título

616.994 CDD (22.ed.) UFPE/CB-2020-092

MARIA AMÉLIA CARLOS SOUTO MAIOR BORBA

MEDICINA DE PRECISÃO EM ONCOLOGIA: ANÁLISE DE POTENCIAIS MARCADORES MOLECULARES PARA O CARNCINOMA HEPATOCELULAR E O CÂNCER DE MAMA

Tese do Doutorado apresentada ao Programa de Pós-graduação em Biologia Aplicada à Saúde do Laboratório de Imunopatologia Keizo Asami – LIKA/UFPE, como requisito para a obtenção do título de doutora.

Aprovada em 28 de novembro de 2019

COMISSÃO EXAMINADORA

_____

Profª Drª Danyelly Bruneska Gondim Martins/UFPE

_____

Prof. Drº Jones Oliveira de Albuquerque/UFRPE

_____

Prof. Drº José Luiz de Lima Filho/UFPE

_____

Prof. Drº Luiz Carlos Alves/UFPE

_____

Profª Drª Maria de Mascena Diniz Maia/UFRPE

Dedico este trabalho aos colegas cientistas: que a ciência e a curiosidade sejam sempre frutos de inspiração, mesmo nos tempos mais difíceis.

AGRADECIMENTOS

À Deus pelo dom da vida e por todas as graças alcançadas.
Aos meus pais por tudo que me ensinaram e pelo caráter que construíram em mim
Aos meus avós por todo apoio, torcida e acolhimento.
A Renato pelo companheirismo e inspiração.
Aos meus orientadores, Danyelly Bruneska e José Luiz, pelas oportunidades, pela amizade e por terem aberto para mim as portas do mundo.
Ao LIKA, e todos que o fazem, por ser casa e família.
Aos amigos e familiares por compreenderem as ausências e celebrarem as vitórias comigo.
A equipe de mastologia do Hospital Barão de Lucena pela parceria.
Aos pacientes e familiares por terem aceito participar dos estudos que fizeram esta tese possível.

“Nature often gives us hints to her profoundest secrets”

(COLEY, 1891)

RESUMO

A medicina passa neste momento por uma transformação onde as análises moleculares têm sido associadas com desfechos clínicos e contribuído para as decisões terapêuticas; dando origem a medicina de precisão. Esta se fundamenta no princípio de que cada indivíduo é único em sua identidade genética, metabólica e ambiental. O avanço das tecnologias em saúde tem impulsionado a pesquisa e validação de novos biomarcadores, e a oncologia é uma das áreas terapêuticas que tem maior evolução. O objetivo foi avaliar potencias marcadores moleculares do câncer de mama e hepatocelular. Um artigo Editorial comenta o papel dos dispositivos *point-of-care* na aplicação da medicina de precisão e discute a importância de estudos clínicos randomizados prospectivos e retrospectivos baseados na individualidade dos pacientes. Três diferentes abordagens moleculares foram utilizadas para aplicar estes conceitos no estudo da oncologia. A primeira trata de um caso clínico de carcinoma hepatocelular no qual o perfil genômico de mutações nos genes BRAF, CTNNB1, ERBB2, FBXW7, HF1A, KRAS, NRAS, PIK3CA, TP53permitiu associar as alterações nas vias metabólicas com o desenvolvimento clínico do paciente, que não seguiu o prognóstico esperado. A segunda abordagem foi baseada na análise *in silico* de mutações em alelos pobre metabolizadores do gene CYP2D6 (CYP2D6*7 e CYP2D6*14A), e permitiu avaliação impacto estrutural e funcional na enzima, demonstrando como estas alterações podem prejudicar o metabolismo do tamoxifeno, o pilar do tratamento endócrino do câncer de mama. A terceira abordagem molecular foi focada no estresse oxidativo e seu papel na saúde e na doença, que foi revisado no capítulo de livro e deu origem a uma hipótese de via molecular testada no câncer de mama. Desta forma, foi avaliada a expressão gênica dos genes PPARG, SIRT1, NFE2L2, UCP2 e RAC1 em amostras teciduais de câncer de mama. Os resultados demonstram correlação significativa entre os genes PPAGR e SIRT1 (p=0,0156), PPARG e NFE2L2 (p=0,0182); e NFE2L2 e RAC1 (p=0,0043), demonstrando o que pode haver um eixo de regulação metabólica e anti-oxidante no câncer de mama entre esses genes. Além disso, a expressão de PPARG foi associada ao estadiamento (p=0,00335 I vs III), a de RAC1 ao estadiamento [I *vs* II (p=0,0165) e I *vs* III (p= 0,0161)], tamanho do tumor (T1 *vs* T3, p=0,0347) e subtipos [HER2 *vs* Luminal (p=0,0036) e HER2 *vs* Triplo Negativo (p=0,0152). Em conclusão, o presente trabalho demonstrou, corroborando com outros estudos, que as ferramentas moleculares

constituem o caminho para a oncologia de precisão, levando ao desenvolvimento tecnológico, à otimização dos custos e a eficiência para o tratamento do câncer.

Palavras-chave: Medicina de Precisão. Câncer. Biologia Molecular. Oncologia.

ABSTRACT

Medicine is currently undergoing a transformation where molecular analysis has been associated with clinical outcomes and contributed to therapeutic decisions; giving rise to precision medicine. Precision medicine is based on the principle that individuals are unique in their genetic, metabolic and environmental identity. Advances in health technologies have driven research and validation of new biomarkers, and oncology is one of the most evolving therapeutic areas. The objective was to evaluate potential molecular markers of breast and hepatocellular cancer. The Editorial article comments on the role of point-of-care devices in the application of precision medicine and discusses the importance of prospective and retrospective randomized clinical trials based on patient individuality. Three different molecular approaches were used to apply these concepts in the study of oncology. The first is a clinical case of hepatocellular carcinoma in which the genomic profile of mutations in the genes BRAF, CTNNB1, ERBB2, FBXW7, HF1A, KRAS, NRAS, PIK3CA, TP53 allowed the association of metabolic pathway alterations with the patient's clinical development, which did not follow the expected prognosis. The second approach was based on in silico analysis of mutations in poor metabolizing alleles of the CYP2D6 gene (CYP2D6*7 and CYP2D6*14A), and allowed for structural and functional impact assessment on the enzyme, demonstrating how these changes may impair tamoxifen metabolism, the backbone of breast cancer endocrine therapy. The third molecular approach focused on oxidative stress and its role in health and disease, which was reviewed in the book chapter and gave rise to a molecular pathway hypothesis tested in breast cancer. At this point, the gene expression of NRF2, SIRT1, PPARG, UCP2 and RAC1 genes in breast cancer tissue samples was evaluated, and the results correlated to clinical parameters such as molecular subtypes, staging and tumor grade. Significant correlation between PPAGR and SIRT1 (p=0.0156), PPARG and NFE2L2 (p=0.0182) and NFE2L2 and RAC1 (p=0.0043) genes was demonstrated; indicating what may be an axis of metabolic and antioxidant regulation in breast cancer between these genes. In addition, PPARG expression was associated with tumor stage (p = 0.00335 I vs III), and RAC1 expression was associated with tumor stage (p = 0.0165 I vs II and p = 0.0161 I vs III), tumor size (p = 0.0347 T1 vs T3) and subtype (p = 0.0036 HER2 vs Luminal and p = 0.0152 HER2 vs Triple Negative). In conclusion, the present study demonstrated, corroborating with other studies, that molecular tools constitute

the path to precision oncology, leading to technological development, cost optimization and efficiency for cancer treatment.

Key words: Precision medicine. Cancer. Molecular Biology. Oncology.

LISTA DE FIGURAS

LISTA DE TABELAS

SUMÁRIO

1 INTRODUÇÃO

A história da medicina é marcada por revoluções que acompanham o desenvolvimento de novas tecnologias, como a microscopia e a robótica. Nas últimas décadas, após o projeto genoma humano entre 1990 e 2003, a medicina tem passado por mais uma transformação. O desenvolvimento de tecnologias em saúde gera novos dados em velocidade recorde e dentre estes, os dados de análise genômica. Com todos estes novos dados, e com tecnologias computacionais que permitem a análise em larga escala, é possível traçar o perfil genético e molecular de cada paciente, viabilizando não só o aconselhamento genético, mas também um planejamento terapêutico que é dosado para cada paciente. Estas ações são parte desta nova era na medicina, a era da precisão.

A medicina de precisão, ou personalizada, aplica na clínica médica os princípios farmacogenômicos para que o tratamento certo seja feito no momento certo para o paciente certo. No entanto, para a implementação destes princípios em toda a medicina, existem alguns desafios importantes: um dos principais é de como transferir todo o volume de informações médicas provenientes das mais diversas plataformas e bancos de dados, da pesquisa molecular, até à pesquisa clínica e, por fim, à prática clínica. Uma das áreas terapêuticas que vive intensamente esta transformação é a oncologia; onde o conhecimento e aplicação de informações genéticas mudou a história de vários tumores, a exemplo o câncer de pulmão e de ovário.

É nesta fronteira de desafio que se situa a hipótese desta tese que através de prospecção molecular translacional utilizou três diferentes abordagens para estudar potenciais marcadores moleculares no carcinoma hepatocelular e da mama. As seguintes abordagens foram utilizadas: análises *in silico* para predição de impacto funcional e estrutural de mutações não-sinônimas no gene da CYP2D6; análise de perfil de mutações e identificação de alterações a nível de vias metabólicas em paciente com carcinoma hepatocelular que teve desfecho diferente do prognóstico previsto; análise de expressão gênica em amostras de câncer de mama para avaliar a associação de vias do estresse oxidativo com parâmetros e desenvolvimento clínico. Os resultados apresentados nesta tese demonstram que através da utilização destas ferramentas de prospecção molecular é possível contribuir para que a medicina de precisão seja uma realidade na oncologia clínica.

1.1 OBJETIVOS

1.1.1 Objetivo Geral

- Avaliar potenciais marcadores moleculares no câncer de mama e no carcinoma hepatocelular

1.1.2 Ojetivos Específicos

- Avaliar o potencial dos marcadores moleculares na medicina personalizada aplicada ao câncer de mama
- Avaliar o papel de mutações associadas com o carcinoma hepatocelular no desfecho clínico do paciente;
- Avaliar os níveis de expressão dos genes envolvidos na regulação celular e no estresse oxidativo: de NFE2L2, SIRT1, UCP2, PPARG e RAC1 em amostras de pacientes com câncer de mama.

2 REVISÃO BIBLIOGRÁFICA

2.1 MEDICINA DE PRECISÃO

O Projeto Genoma Humano (OLSON, 1993) foi um grande marco na história da medicina, uma vez que revolucionou o modo como as patologias são estudadas (FRANCKE, 2013; HAMAZAKI et al., 2017) e abordadas na prática clínica (**Figura 1)**. Essa quebra de paradigma levou a percepção de que cada indivíduo possui um *background* genético único que influencia a susceptibilidade ou a proteção a doenças (HAMAZAKI et al., 2017).

Figura 1. O impacto do Projeto Genoma Humano na Medicina: como os dados moleculares se aplicam na clínica médica.

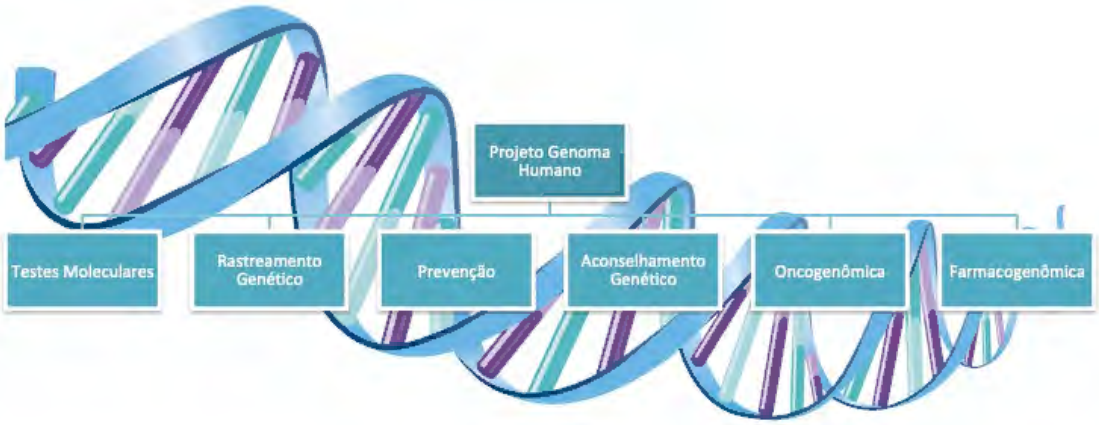

Fonte: Adaptado de Francke et al, 2013.

O princípio fundamental sob o qual se baseia a medicina de precisão é unir parâmetros clínicos e patológicos bem estabelecidos com os avanços da biologia molecular que permite traçar perfis genéticos. Deste modo, espera-se criar estratégias de diagnóstico, prognóstico e tratamento que são baseadas e balanceadas para as necessidades de cada paciente (MIRNEZAMI; NICHOLSON; DARZI, 2012). Existem, contudo, grandes desafios para implementação da medicina personalizada, incluindo o manejo de dados multi-paramétricos e proficiência em interpretação de informações “ômicas”. Estes desafios são globais e envolvem profissionais de saúde, cientistas e autoridades públicas, embora a realidade não seja tão linear, existem alguns papeis delimitados que norteiam essa ação (**Tabela 1)**.

Tabela 1. O papel dos envolvidos em implementar a medicina de precisão.

Instituições/Grupos	Papéis
Governo	- Desenvolver leis transparentes de privacidade; - Identificar áreas socioeconômicas prioritárias a se beneficiar com estratégias de medicina de precisão; - Realizar consultas públicas sobre opção de adesão à estratégias de pesquisa.
Pesquisadores	- Desenvolver ferramentas eficientes para suportar a decisão clínica e integração com registros de saúde eletrônicos; - Desenhar e conduzir estudos pilotos adequados para obtenção de dados em áreas alvo da medicina de precisão - Desenvolver tecnologias sustentáveis
Comunidade biomédica	- Mudar o treinamento da graduação para compreender melhor os mecanismos moleculares das doenças; - Desenvolver e contribuir com um novo sistema de classificação de doenças que incorpora informações moleculares; - Introduzir um papel mais transparente e participativo para os pacientes elegíveis para recrutamento nos testes clínicos.
Indústria farmacêutica	- Desenvolver testes diagnósticos eficientes, com ou sem um agente terapêutico associado, para gerir as condições identificadas como de maior peso socioeconômico.
Pacientes	- Participar cada vez mais de iniciativas de saúde e bem-estar - Utilizar novos meios de fornecer informações para pesquisas, tais como redes sociais e aplicativos para telefones.
Agências Regulatórias	- Assegurar que as medidas regulatórias garantam a segurança dos pacientes, mas que não impeçam o progresso científico.

Fonte: Adaptado de Reza Mirnezami, Jeremy Nicholson e Ara Darzi (2012).

É neste cenário de transformação que a medicina se direciona para o preconizado por Leroy Hood, que propôs o conceito de medicina 4P: preditiva, preventiva, personalizada e participativa (HOOD et al., 2004; HOOD; BALLING; AUFFRAY, 2012). Este conceito 4P faz parte do que se entende por medicina sistêmica, que aplica biologia sistêmica para o desafio das doenças humanas, utilizando ferramentas tecnológicas e computacionais inclusive a participação e feedback dos pacientes (FLORES et al., 2013) (**figura 2**). A perspectiva é que esta

abordagem sistêmica viabilizará a transição da prática tradicional medicina de forma reativa para uma medicina 4P proativa que é focada no bem-estar. Adicionalmente, acredita-se que neste novo modelo ocorrerá uma reversão dos custos para desenvolvimento de drogas, o que terá grande impacto social e econômico (HOOD; BALLING; AUFFRAY, 2012).

Figura 2. Diagrama ilustrativo dos quatro pilares que constituem a medicina 4P.

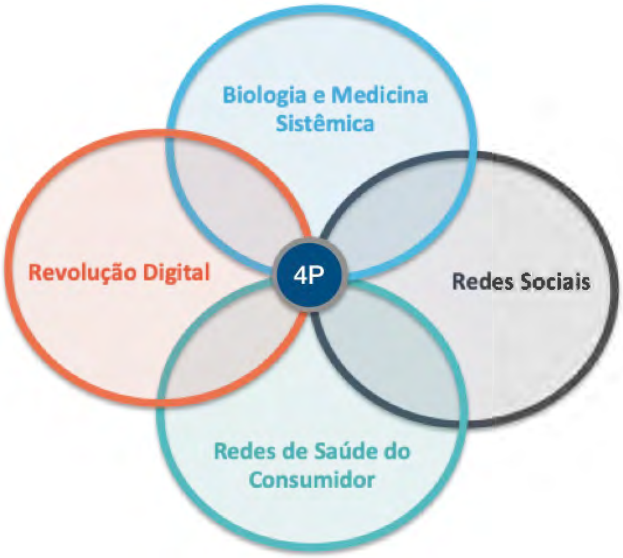

Fonte: Adaptado de Flores, 2013.

De fato, a consciência da necessidade de personalizar as abordagens terapêuticas já causa impacto quando se trata dos altos custos de medicamentos inovadores e, consequentemente, do acesso limitado a estes (GRONDE; UYL-DE GROOT; PIETERS, 2017). Um exemplo de doença que reflete essa transformação é o câncer de pulmão, onde a relevância terapêutica de realizar testes genéticos, como mostra o volume de testes representado na **figura 3**, é indiscutível e acumula cada vez mais evidências com a chegada de novas drogas alvo que trazem significativo ganho de sobrevida (VANDERLAAN et al., 2018). O grande desafio nesse contexto é que se por um lado o diagnóstico molecular do câncer de pulmão requer diversos testes, tais como mutações no gene EGFR, translocações de ALK e de ROS1, e expressão tumoral do PD-L1 (HERBST; MORGENSZTERN; BOSHOFF, 2018); por outro lado os testes em si, e as drogas que seguem a indicação elevam significativamente os custos do tratamento desses pacientes (LOUBIÈRE et al., 2018; YU et al., 2018).

.

Figura 3. O uso de biomarcadores moleculares ao longo dos anos, o exemplo do câncer de pulmão de como a descoberta de novos alvos aumentou o número de testes na clínica médica.

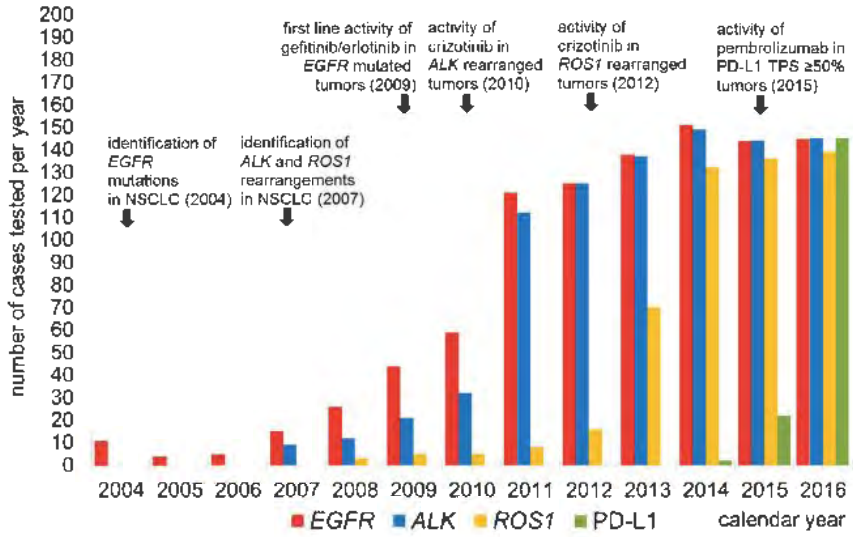

Fonte: (VANDERLAAN et al., 2018)

Essa discussão se estende até o ponto em que a dúvida é como as ferramentas moleculares, que não são baratas, irão poder auxiliar na implementação de uma medicina mais precisa. É preciso considerar, no entanto, que com a evolução das técnicas o custo da informação caiu bastante, por exemplo o sequenciamento do genoma humano. Enquanto o primeiro sequenciamento completo custou aproximadamente U$ 3bi, o mesmo serviço hoje é oferecido por menos de U$ 1000 (WETTERSTRAND, 2017). Ademais, o valor da informação genética pode ser mais significativo do que seu custo financeiro, oferecendo uma estratégia que viabiliza um tratamento mais seguro e eficaz através da prospecção de biomarcadores. Desta forma, surge o racional da busca por criar estratégias que permitam que a abordagem personalizada na oncologia, baseada em perfis moleculares individuais, seja um recurso para decisões regulatórias. Ainda que os ensaios clínicos randomizados sejam o padrão ouro para definir a eficácia de determinadas drogas, desenhar estudos que unam o perfil molecular tumoral e incorporar dados de vida real (*real world evidence – RWE*) pode ser o caminho para tornar a implementação da oncologia de precisão, mais prática (SALGADO et al., 2019).

2.1.1 Marcadores Moleculares

Para colocar em prática a medicina de precisão é essencial identificar biomarcadores, seja utilizando dados "-ômicos" puros ou associados à fatores ambientais e de hábitos de vida. A realidade é que os avanços tecnológicos impulsionam a biomedicina e consolidam o maior desafio deste cenário: transformar o imenso volume de dados em biomarcadores utilizados na prática com valor preditivo, prognóstico, diagnóstico e farmacogenômico (WANG et al., 2017a).

Na era da medicina oncológica personalizada, os diagnósticos moleculares estão na linha de frente da prescrição terapêutica. Neste sentido, a seleção de pacientes baseada no perfil molecular e *background* genético de cada um foi estabelecida com a chegada dos inibidores de quinase e as terapias alvo. Este valor é provado pela diferença significativa que aparece na taxa de resposta a estas terapias dada a presença ou ausência de biomarcadores específico (DE CASTRO et al., 2013). A Tabela 2 apresenta exemplos de biomarcadores moleculares usados na prática clínica para guiar decisões no diagnóstico e tratamento de diferentes tipos de câncer.

Tabela 2. Exemplos de usos de biomarcadores na prática clínica com valor diagnóstico, prognóstico, preditivo e de monitoramento de diversos tipos de câncer**.**

Diagnóstico		
Leucemias Agudas	PML-RARA	Classificação das Leucemias pela OMS
	BCR-ABL1	
	CBFB-MYH11	
	ETV6-RUNX1T1	
	MLL-rearranged	
	TCF3-PBX1	
	RBM15-MKL1	
MPD	JAK2	Mutações confirmam diagnóstico de MPD
Sarcomas	SS18-SSX1/SSX2	Sarcoma sinovial
	PAX3/PAX7-FOXO1A	Rabdomiosarcoma alveolar
	EWSR1-FLI1	Sarcoma de Ewing
	EWSR1-ERG	

	EWSR1-NR4A3	Condrosarcoma mixoide extra-esquelo
	TAF15-NR4A3	
	EWSR1-ATF1	Sarcoma de células claras (e histiosarcoma fibroso angiomatóide)
	EWSR1-CREB1	
	ASPSCR1-TFE3	Sarcoma alveolar de partes moles (e carcinoma de células renais)
	FUS-DDIT3	Liposarcoma mixoide
	FUS-CREB3L2	Sarcoma fibromixoide de baixo grau
	JAZF1-SUZ12	Sarcoma estromal endometrial
	ETV6-NTRK3	Fibrosarcoma congênito (e câncer de mama secretório)
Preditivos		
NSCLC	EGFR	Mutação prediz resposta a inibitor de tirosina quinase
	ALK	Rearranjo prediz resposta a inibidores de ALK
GIST	KIT and PDGFRA	Mutações predizem resposta a inibidores de c-KIT/PDGFRA
mCRC	KRAS	Mutações predizem não resposta a inibidores de EGRF
Melanoma	BRAF	Mutações predizem resposta a inibidores específicos de BRAF
Câncer de Mama	HER2	Amplificação prediz resposta a anticorpos anti-HER2
Prognóstico		
CLL	TP53	Mutações indicam prognóstico ruim
	IGHV	Ausência de mutações indica prognóstico ruim
AML	FLT3-ITD	Mutações indicam prognóstico ruim
mCRC	BRAF	Mutações indicam prognóstico ruim
Câncer de Mama	OncotypeDx	Estratificação de risco por um painel de expressão de 21 genes
	Mammaprint	Estratificação de risco por um painel de expressão de 70 genes
	IHC4	Estratificação de risco por expressão de 4 genes através de imuno-histoquímica
Monitoração da doença		
CML	BCR-ABL1	Detecção de doença mínima residual
APML	PML-RARA	Detecção de doença mínima residual
ALL	IGHT-TCR (rearranjos)	Detecção de doença mínima residual

Legendas: ALL, leucemia linfoblástica aguda; AML, leucemia mielóide aguda; APML, leucemia promielocítica agura; CLL, leucemia linfocítica crônica; CML, leucemia mielóide crônica; EGFR, receptor do fator de crescimento epidermal; GIST, tumores estromais gastro-intestinais; HER2, receptor 2 do fator de crescimento epidermal

humano; mCRC, câncer coloretal metastático; MPD, doenças mieloproliferativas; NSCLC, câncer de pulmão de células não pequenas; OMS, organização mundial da saúde. Fonte: Adaptado de (DE CASTRO et al., 2013)

A lógica da padronização na pesquisa biomédica por identificar e validar os novos biomarcadores é baseada na formação de *network* de dados, de modo que a integração de informações de múltiplas fontes, seja o alicerce da validação prática (VARGAS; HARRIS, 2016). Essa network integra os dados e fornece informações tanto para a pesquisa biomédica, quanto para a medicina clínica e para a pesquisa preventiva (**Figura 4**).

Figura 4. Esquema ilustrativo da integração de dados e formação de network para identificação e validação de biomarcadores.

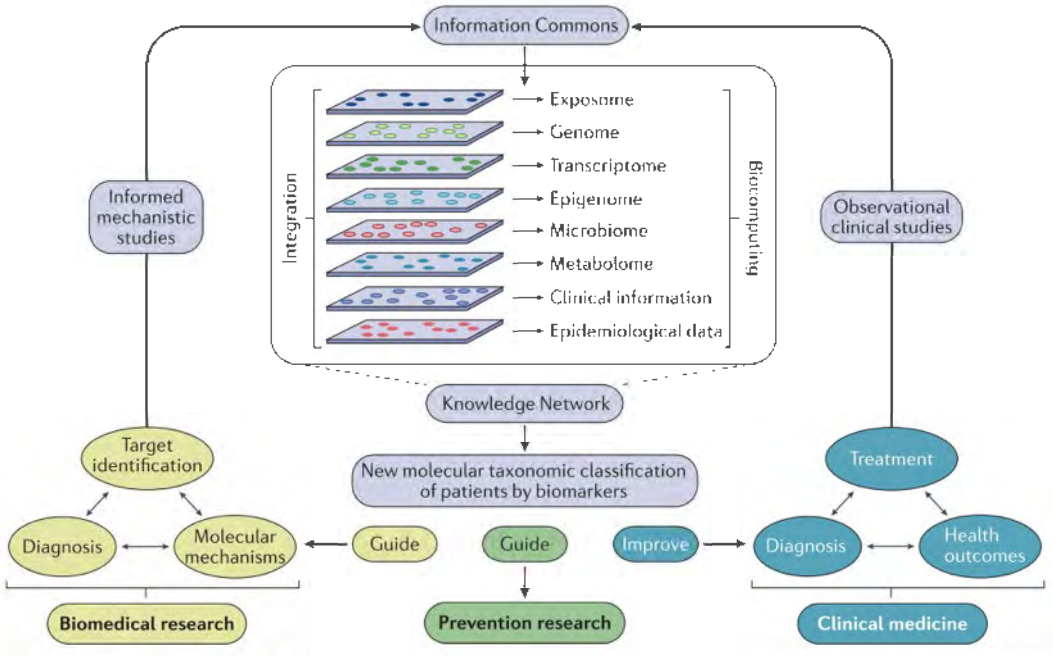

Fonte: (VARGAS; HARRIS, 2016).

Uma importante ferramenta que possibilita a integração, análise e reporte dos dados gerados pela pesquisa biomédica é a bioinformática. Esta ciência é fundamentada no princípio de que a biologia é constituída por dados. A lógica é compreender a informação genética e incorporar a técnicas e procedimentos da matemática e da computação (BARTLETT; PENDERS; LEWIS, 2017). As três principais ramificações da bioinformática são: o desenvolvimento de algoritmos e métodos estatísticos para avaliar a relação entre membros de bases de dados distintas; a análise de dados diversos, tais como sequencias de nucleotídeos ou aminoácidos e estrutura terciária das proteínas; e desenvolvimento de ferramentas

que permitem acesso e organização de vários tipos de informação, notavelmente, o *big data* (FANDO; KLAVDIEVA, 2018).

No estudo do câncer as ferramentas de bioinformática têm sido empregadas para auxiliar as análises clínicas e moleculares, sendo uma aliada para alcançar a medicina de precisão na oncologia (KATO, 2016; LU et al., 2018). São exemplos das aplicações da bioinformática no estudo do câncer: desenvolvimento de plataforma proteômica do câncer (TYANOVA; COX, 2018), análise diferencial de RNA circulante associado a resistência à radioterapia em câncer de esôfago (SU et al., 2016); identificação de genes e vias metabólicas no câncer colo retal (LIANG; LI; ZHAO, 2016) e a avaliação e caracterização de mutações genéticas (FUJIMOTO et al., 2016; MENSCHAERT; FENYÖ, 2017).

Esta funcionalidade da bioinformática de avaliar mutações genéticas é implementada através de algoritmos (VERLI, 2014) que aplicam métodos de classificação como o *Support Vector Machine* (SVM), *Neural Network* (NN) ou *Random Forest* (RF) para definir se uma mutação tem provável efeito deletério nas proteínas com impacto clínico (KANDOI; ACENCIO; LEMKE, 2015; KUMAR et al., 2014). Para realizar esta classificação, são aplicados algoritmos que utilizam diferentes técnicas, a exemplo do Mutation Assessor e o SIFT que avaliam dados de conservação obtidos através de alinhamentos de múltiplas sequências. Por outro lado outas ferramentas também associam outros fatores a esta análise, como as propriedades físico-químicas dos aminoácidos envolvidos na troca; a localização de regiões funcionais; a estrutura secundária e a topologia da proteína, a exemplo dos algoritmos PolyPhen2, SNPs&GO e MutPred, usados no âmbito da pesquisa e do diagnostico (FROUSIOS et al., 2013).

2.1.2 Metabolismo do Câncer

As células tumorais apresentam um conjunto de características comuns que as conferem diferentes capacidades para garantir o contínuo crescimento e proliferação. Este conjunto de características é conhecido como *Hallmarks* do câncer e dentre esses, a desregulação do metabolismo energético celular é importante pois garante a célula tumoral a adaptação necessária para sustentar a progressão do tumor (HANAHAN; WEINBERG, 2000, 2011).

Em condições aeróbicas, as células normais metabolizam a glicose à piruvato através da glicólise no citoplasma e então a dióxido de carbono nas mitocôndrias; em

condições anaeróbias a glicólise é favorecida e menos piruvato é enviado às mitocôndrias. Nas células tumorais, mesmo em presença de oxigênio, há desvio do metabolismo energético que fica restrito a glicólise, criando um efeito de glicólise aeróbia, também chamada de Efeito Warburg (**Figura 5**). A perda do metabolismo mitocondrial do piruvato através de fosforilação oxidativa, decorrente deste efeito, reduz a eficiência energética na célula tumoral, que compensa esta perda através do aumento de expressão de transportadores de glicose, como o GLUT-1 (HANAHAN; WEINBERG, 2011).

Figura 5. O Efeito Warburg nas células tumorais: ilustração do desvio metabólico que leva a glicólise aeróbia.

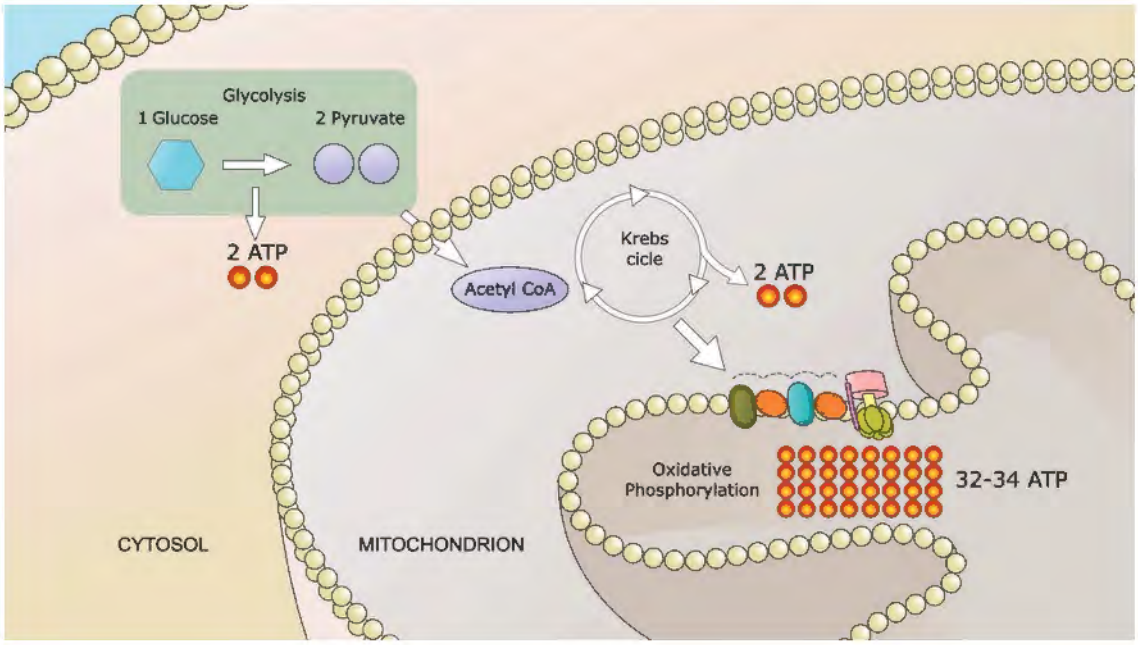

Fonte: (SCHMIDT, 2017)

O efeito Warburg é uma característica chave do metabolismo energético tumoral, no entanto, este é complexo e envolve diversas outras vias de sinalização intracelulares. Enquanto nas células normais o estímulo através de fatores de crescimento da via PI3K/AKT/mTOR promove a síntese proteica e de ácidos graxos; as células tumorais frequentemente apresentam alterações nessa via que conferem independência da sinalização pelos fatores de crescimento (**figura 6**). A ativação aberrante da molécula mTORC1 induz o crescimento anabólico tumoral, pois aumenta a síntese de nucleotídeos, proteínas e lipídeos. Por outro lado, a perda de genes supressores de tumor, como p53, ou ativação de oncogenes, como MYC, favorece a

transcrição de genes anabólicos. Este controle da expressão gênica sofre interferência ainda dos diversos mecanismos epigenéticos de acetilação, metilação e dos radicais livres de oxigênio (ROS) (DEBERARDINIS; CHANDEL, 2016; RINALDI; ROSSI; FENDT, 2018).

Figura 6. Ilustração esquemática das principais vias metabólicas que participam da regulação do metabolismo tumoral.

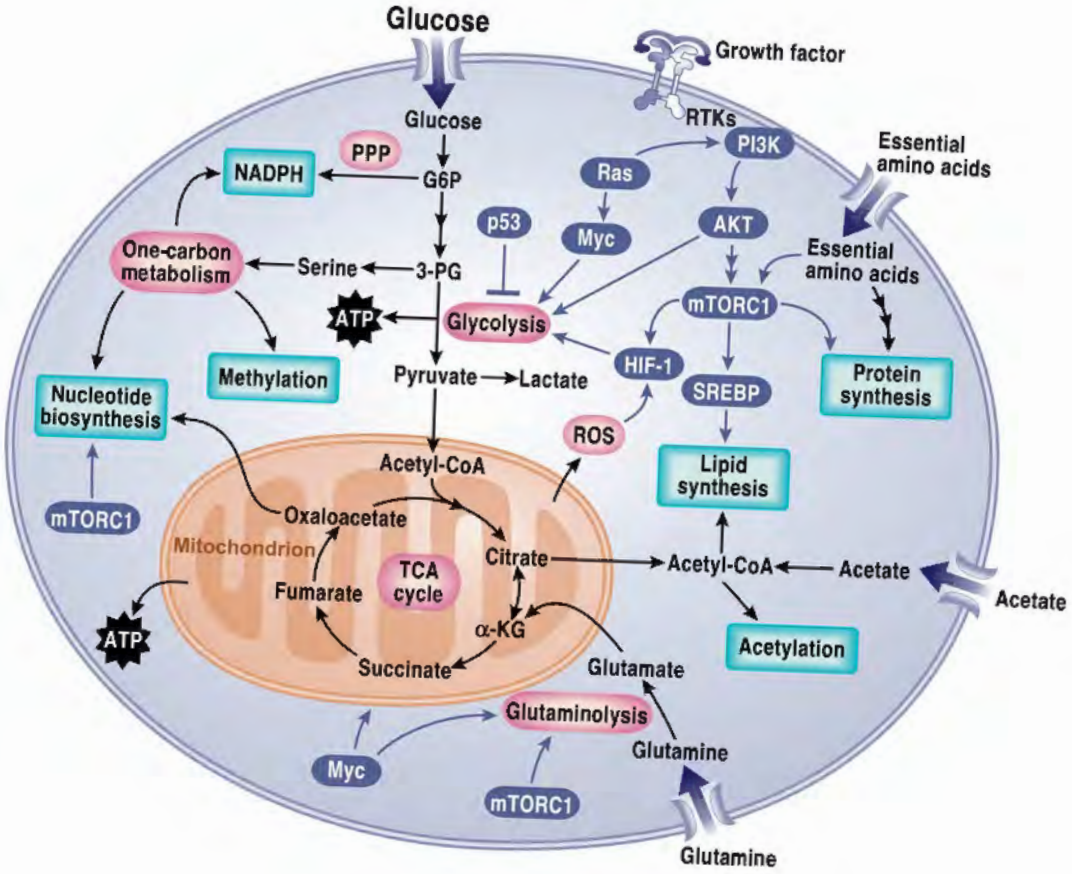

Fonte: (DEBERARDINIS; CHANDEL, 2016)

A desregulação metabólica nas células tumorais, tem sido, portanto, associada também a aberrações genômicas e isso se dá não somente pelo metabolismo da glicose, mas também pelos metabolismos do folato, do fosfato de pentose e o metabolismo mitocondrial. Esta complexa rede de alterações está associada a perda do controle do equilíbrio redox, com aumento de ROS. Neste cenário, o ganho de mutações em oncogenes como KRAS, MYC, PI3K combinado com o aumento do estresse oxidativo pode estar associado não só com a tumorigenênse, mas também com a resposta aos tratamentos. Por exemplo, o uso do quimioterápico 5-flourouracil (5-FU) é baseado em sua analogia com o dUMP, levando a inibição da síntese da

timina e tem indicação em vários tipos de câncer, incluídos os de mama e pulmão (DE SANTIS et al., 2018).

Outro exemplo de como o metabolismo do câncer pode interferir no tratamento se dá quando essas alterações moleculares podem ser detectadas clinicamente e utilizadas como alvo terapêutico e/ou como biomarcadores diagnósticos (KAUSHIK; DEBERARDINIS, 2018). É o caso da lactato desidrogenase (LDH), enzima que participa do metabolismo energético na interconversão de lactato para piruvato, alimentando o ciclo de Krebs. No melanoma os níveis de LDH séricos auxiliam na determinação do estadiamento tumoral e tem sido considerados também como potencial alvo terapêutico na combinação com drogas inibidoras de *check-point* imunológico, tais como pembrolizumabe, nivolumabe e ipilimumabe (DANESHMANDI; WEGIEL; SETH, 2019).

2.1.3 Estresse Oxidativo

O estresse oxidativo é o resultado de um desequilíbrio entre as vias oxidativas e anti-oxidantes, este processo faz parte da homeostase celular. Se por um lado, a presença de radicais livres de oxigênio (ROS) ou nitrogênio (RNS) favorece a resposta inflamatória à patógenos; por outro lado, está associada ao aumento de doenças metabólicas, autoimunes e ao desenvolvimento do câncer (ANDRISIC et al., 2018).

As células tumorais possuem um conjunto de propriedades que garantem a progressão tumoral e caracterizam os *hallmarks* do câncer, como ilustra a **figura 7** (HANAHAN; WEINBERG, 2011). Dentre estas características, a desregulação do metabolismo energético permite que a célula prolifere e sobreviva em microambientes em que a célula normal morreria. Uma das principais consequências destas alterações metabólicas é o aumento da produção ROS/RNS e a redução das vias anti-oxidantes, caracterizando o estresse oxidativo (POSTOVIT et al., 2018).

Figura 7. Os hallmarks do câncer. No esquema são demonstrados os hallmarks do câncer em sua versão mais atual, em roxo está representada a desregulação do metabolismo energético e o Efeito Warburg.

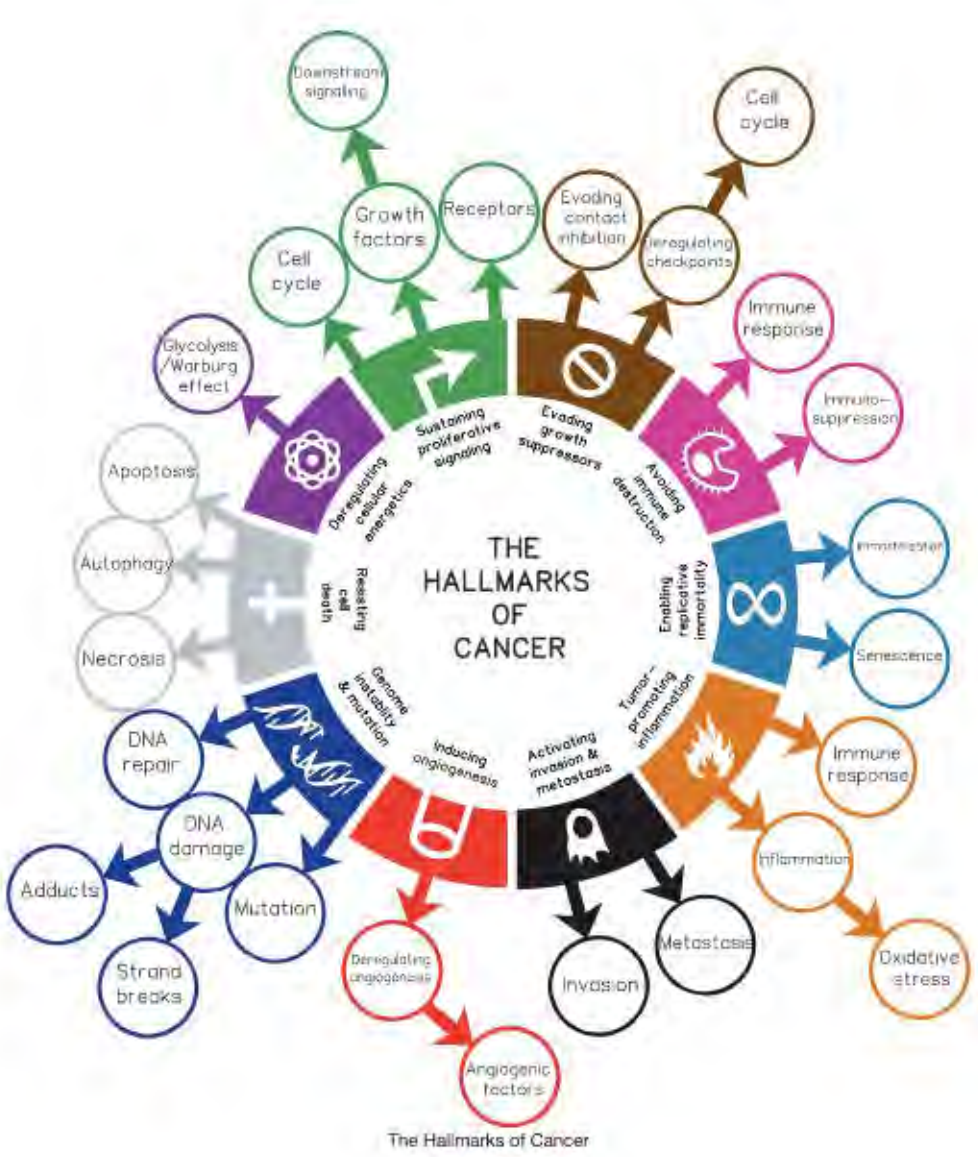

Fonte:(BAKER et al., 2017)

No entanto, a relação entre o câncer o estresse oxidativo é complexa e multifatorial, envolvendo diversas vias metabólicas, sendo a via do metabolismo da glutationa uma das principais (**Figura 8**). O estresse oxidativo tem um relacionamento dinâmico com o tumor, desempenhando um papel diferente a cada fase desde a oncogênese até a progressão do câncer.

Figura 8. Representação esquemática das vias metabólicas relacionadas ao estresse oxidativo que estão alteradas no câncer. Nesta representação gráfica o tamanho dos círculos é proporcional à importância da via e os círculos mais a direita são os representativos

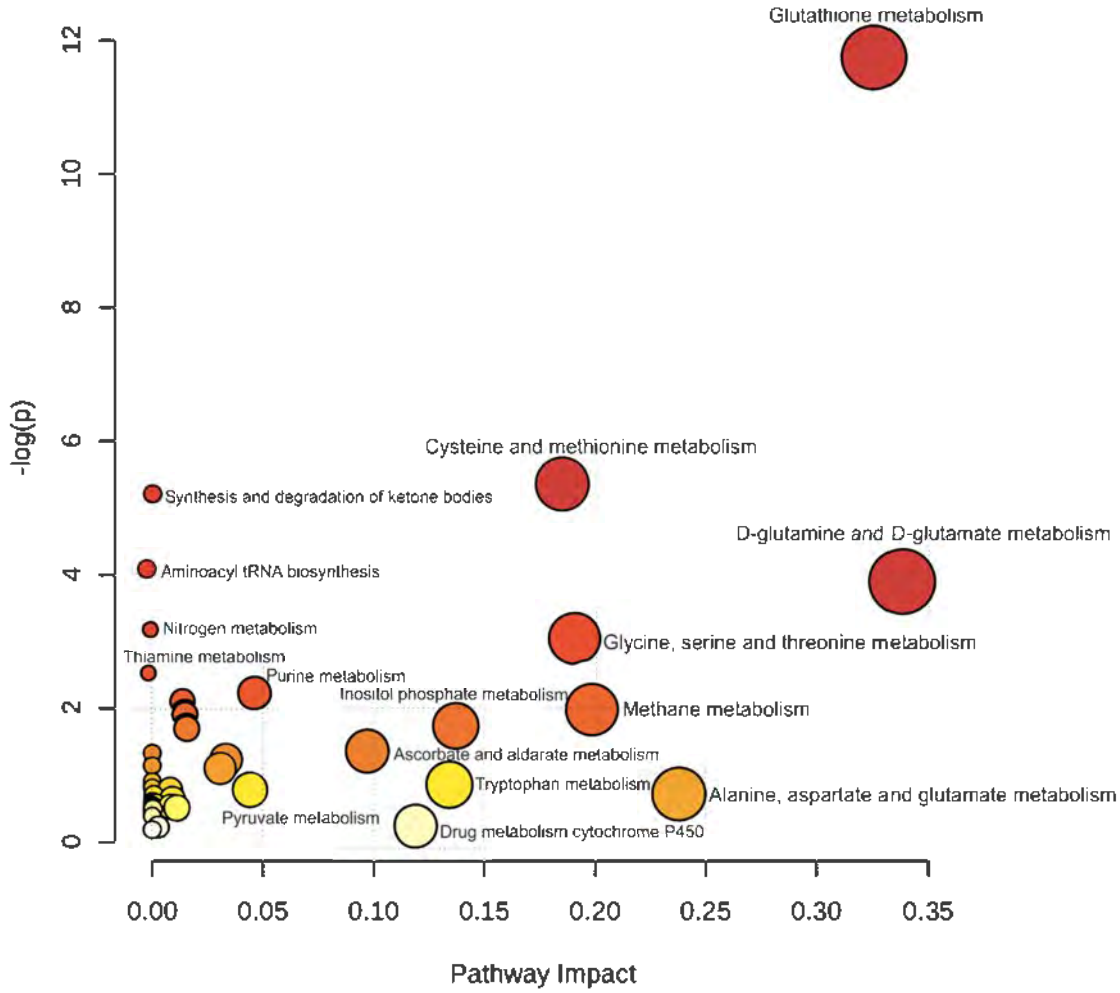

Fonte: (ANDRISIC et al., 2018).

A presença de radicais livres de oxigênio (ROS) no tumor é resultado da dinâmica metabólica tumoral, e portanto, varia em cada fase do câncer (**Figura 9**). Os danos causados pelos ROS às macromoléculas, como DNA, podem ser um fator que favorece a iniciação do câncer. Por outro lado, quando os níveis de ROS estão baixos, vias de sinalização que mediam a proliferação, sobrevivência e progressão tumoral são ativadas, podendo levar ao fenótipo metastático. Mas se na presença de alto nível de ROS, vias que mediam a morte celular são ativadas, favorecendo também a formação de células tronco, que podem induzir a recorrência local dos tumores (STORZ, 2013).

Figura 9. Gráfico ilustrativo dos níveis de radicais livres de oxigênio na célula normal e ao longo da evolução tumoral, correlacionando com as diferentes etapas metabólicas e anti-oxidantes**.**

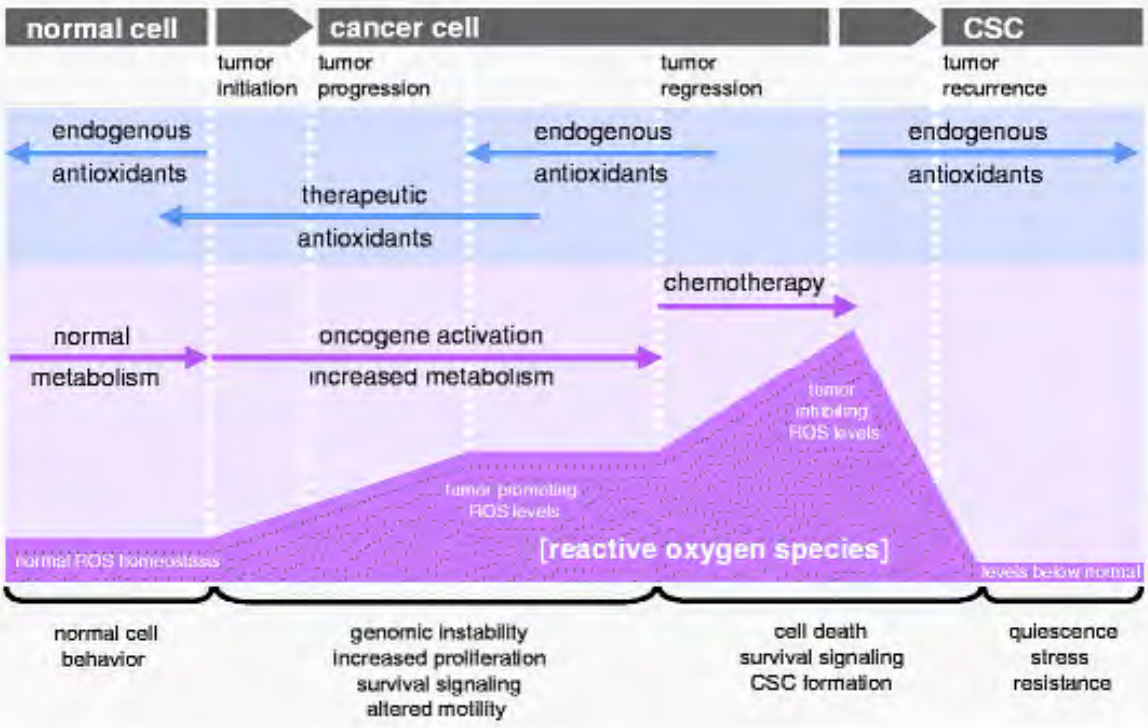

Fonte: (STORZ, 2013)

Ao longo do processo carcinogênico, o equilíbrio REDOX no microambiente tumoral sofre influência do metabolismo tumoral e das alterações moleculares na célula do câncer. Este processo é finamente regulado por moléculas chave que estão relacionadas a transcrição e expressão gênica, que modulam o fenótipo tumoral, como as sirtuínas (CARAFA; ALTUCCI; NEBBIOSO, 2019).

2.1.4 As Sirtuínas

Sirtuínas (SIRT), são uma classe de proteínas que tem atividade de desacetilase dependente da nicotinamida adenina dinucleotídeo (NAD+), sendo classificadas como desacetilases de classe III (KIDA; GOLIGORSKY, 2016). Estas moléculas desempenham papéis importantes na homeostase celular e estão envolvidas em diversos processos, tais como o metabolismo energético e a resposta ao estresse (DAI et al., 2018). Em humanos estão descritas sete isoformas, denominadas SIRT1-7, e estas têm diferentes localizações e funções, que variam de acordo com seus substratos, conforme descrito na **tabela 3.** As SIRT1, SIRT6 e SIRT7 são

prioritariamente nucleares e regulam fatores de transcrição e modificações nas histonas para coordenar a expressão gênica, direcionando o metabolismo celular. A SIRT2 é majoritariamente citoplasmática e está envolvida com a dinâmica dos microtúbulos e com a atividade de fatores de transcrição que também sejam citoplasmáticos. As sirtuínas mitocondriais; SIRT3, SIRT4 e SIRT5, por sua vez, se localizam na matriz da mitocôndria e conseguem regular a atividade metabólica de diversas enzimas (GERMAN; HAIGIS, 2015).

Tabela 3. As sirtuínas e suas diferentes funções de acordo com seus substratos

Sirtuína	Atividade	Localização	Substrato e/ou Alvo	Função
SIRT1	Desacetilase	Núcleo	H3K9, H3K56, H4K16, H1K26, SUV39H1, p300, PCAF	Regulação da cromatina e transcrição
			HDAC1, PARP1, p53, KU70, NBS1, E2F1, RB, XPA, WRN, survivin, β-catenin, MYC, NF-κB, TOPBP1	Reparo do DNA e sobrevivência celular
			PGC1α, FOXO1, FOXO3A, FOXA2, CRCT1, CRCT2, PPARα, PPARγ, LXR, FXR, RARβ, SREBP1C, SREBP2, HNF4α, HIF1α, HIF2α, CREB, NKX2-1, STAT3, TFAM, MYOD, NHLH2, UCP2, TSC2, eNOS, LKB1, SMAD7, AKT, ATG5, ATG7, ATG8, 14-3-3ζ, PGAM1, ACECS1, PTP1B, S6K1	Metabolismo
SIRT2	Desacetilase	Citoplasma	Tubulin, keratin 8, PAR3 and PRLR G6PD, LDH, PEPCK1, ACLY, MEK1, ITPK1, S6K1, PGAM	Diferenciação Metabolismo
		Núcleo	H4K16, H3K56, H3K18, CDC20, APC/C, CDK9, BUBR1	Ciclo celular
			FOXO1, FOXO3A, p300, NF-κB, HIF1α	Metabolismo
SIRT3	Desacetilase	Mitocôndria	LCAD, VLCAD, HMGCS2, NDUFA9, SKP2, SDHA, ACECS2, GDH, IDH2, MRPL10, PDP1, SOD2, OTC, CYPD, OPA1, PDH, FOXO3, GOT2	Metabolismo

SIRT4	ADP-ribosilase, Lipoamidase e desacetilase	Mitocôndria	GDH, IDE, SLC25A5, PDH, MCD	Metabolismo
SIRT5	Deacilase e Desacetilase	Mitocôndria	CPS1, HMGCS2, PDH, SDH, SOD1, GAPDH	Metabolismo
SIRT6	Deacilase, Desacetilase e ADP-ribosilase	Núcleo	H3K9, H3K56, CtIP, GCN5, SNF2H, G3BP, FOXO3, PARP1	Regulação da cromatina e Reparo do DNA
			MYC, HIF1α, NF-κB, TNF, SREBP1, SREBP2, USP10	Metabolismo
SIRT7	Desacetilase	Núcleo	MYC, H3K18, PAF53, HIF1α, HIF2α, ELK4, RNA Pol I, MYBBP1A, TFIIIC2, p53	Regulação da Transcrição
			mTOR, DCAF1, DDB1, CUL4B, GABPβ1	Metabolismo

Fonte: Adaptado de (CHALKIADAKI; GUARENTE, 2015)

No câncer as sirtuínas estão significativamente envolvidas com a regulação do metabolismo energético e seu papel varia de acordo com a fase do desenvolvimento tumoral, como ilustra o esquema na **figura 10**. Na fase inicial, de desenvolvimento do câncer uma redução na expressão das sirtuínas favorece a oncogênese, dado que a manutenção da homeostase metabólica é um fator protetor contra o câncer. Em humanos, foi observada redução da expressão de mRNA da SIRT3 em câncer de mama e de ovário e da SIRT4 em tumores de pulmão, bexiga, estômago e mama (GERMAN; HAIGIS, 2015).

Figura 10. Fluxograma do desenvolvimento tumoral e como ele se relaciona com estresse oxidativo e as sirtuínas.

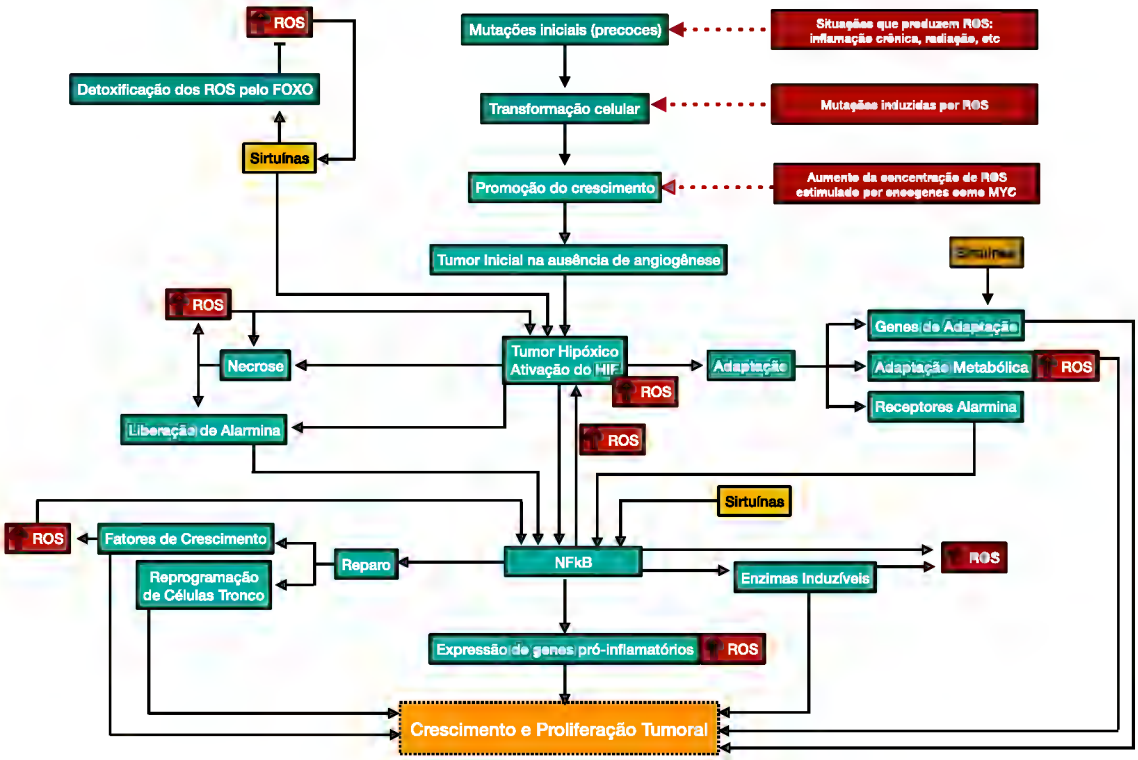

Fonte: Adaptado de (TAFANI et al., 2016)

Por outro lado, uma vez que os tumores estão em fase mais avançada e bem estabelecidos, as sirtuínas podem desempenhar um papel pró-tumoral através da manutenção da sobrevivência celular numa situação de significativo estresse metabólico. Por exemplo, a manutenção da expressão de SIRT1 parece ser essencial para a sobrevivência da célula tumoral, tendo sido associada a resistência a agentes quimioterápicos devido aumento na expressão do “Multi Drug Resistance 1” (MDR1) (GERMAN; HAIGIS, 2015). Na **figura 11** estão ilustradas as vias moleculares pelas quais as sirtuínas regulam o estresse oxidativo na célula tumoral. Como demonstrado na figura, as funções das sirtuínas nas células do câncer influenciam o balanço oxidativo com redução da concentração de ROS através de diversos mecanismos que vão desde a regulação da transcrição gênica até a ativação de moléculas como o FOXO e o PGAM.

Figura 11. Esquema das vias metabólicas onde se demonstra arelação molecular entre as sirtuínas e o estresse oxidativo.

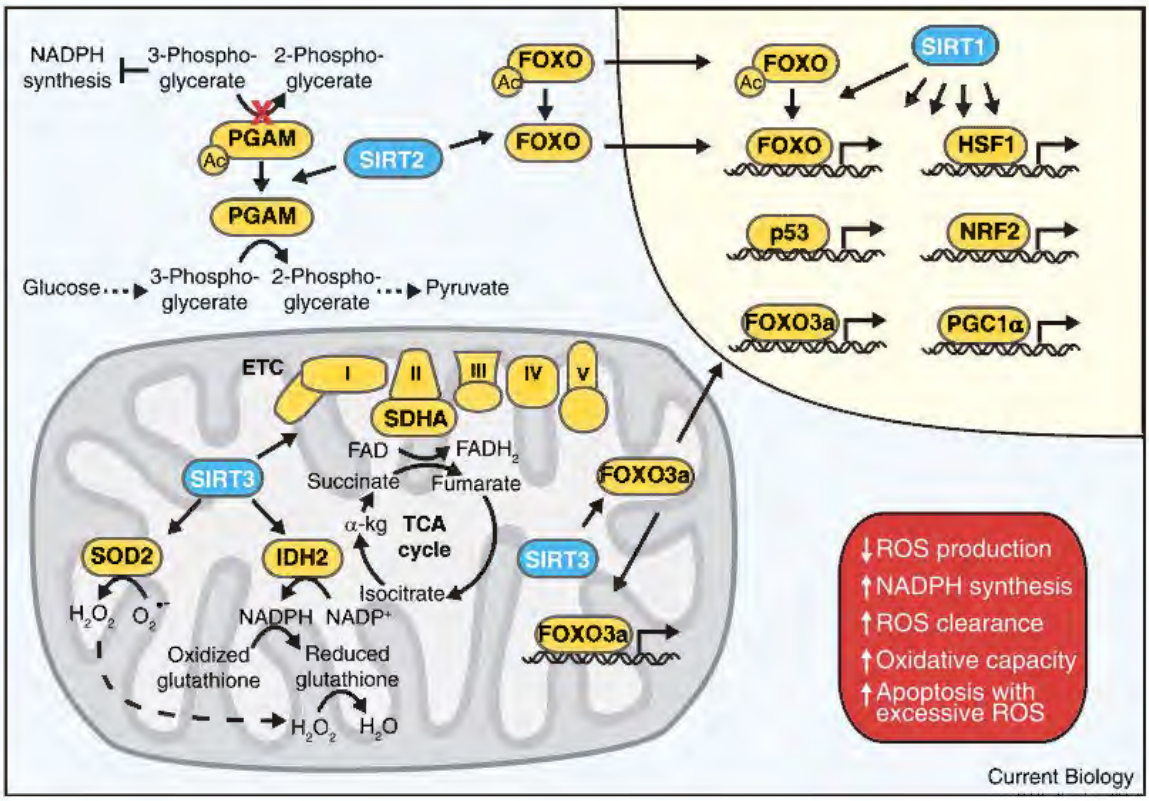

Fonte: (GERMAN; HAIGIS, 2015)

A SIRT1, no núcleo, é responsável por desacetilar fatores de transcrição regulatórios, tais como o p53 e o NRF2, que levam a transcrição de genes antioxidantes – controlando a produção de ROS ou direcionando a célula para apoptose caso a concentração destes seja muito elevada (GERMAN; HAIGIS, 2015). No citoplasma a SIRT2, que parece ter sua expressão regulada em resposta ao estado energético, atua como um sensor energético que desempenha um papel na proteção contra os ROS através da desacetilação do FOXO (que fica apto a se translocar para o núcleo) e do PGAM (que ativo promove resposta antioxidante pelo aumento da concentração de NADPH) (ELKHWANKY; HAKKOLA, 2018). A SIRT3, na matriz mitocondrial, é capaz de (i) responder à alta concentração de ROS através do FOXO3a; (ii) aumentar a produção de NADH através da desacetilação do IDH2, (iii) metabolizar o superóxido pela ativação da SOD2; e (iv) regular a produção de ROS na cadeia transportadora de elétrons através da ativação do metabolismo oxidativo pela desacetilação de diversas enzimas mitocondriais (GERMAN; HAIGIS, 2015; KWON et al., 2015). Esta função mitocondrial da SIRT3 é parcialmente mediada

pelo transportador UCP2 (do inglês, Uncoupling Protein 2), que funciona como um canal de prótons, revertendo o fluxo de H^+ e resultando na redução da produção de ATP. Aparentemente, o UCP2 regula a ação da SIRT3 através do controle da proporção de NAD^+/NADH, levando a produção do PGC1α, que por sua vez forma complexos transcricionais com NRF1, NRF2 e ERRα. (SU et al., 2017)

2.2 CÂNCER DE FÍGADO - HEPATOCELULAR CARCINOMA

2.2.1 Epidemiologia e fatores de risco

O câncer no fígado é, segundo o tipo de câncer em número de mortes, atrás apenas do câncer de pulmão (**Figura 12**). Na estimativa de 2018 da *International Agency for Research on Cancer* (IARC/World Health Organization), são esperados 841.080 novos casos e 781.631 mortes por câncer no fígado (BRAY et al., 2018)**.**

No Brasil a estimativa do INCA não incluiu o câncer no fígado, mas um levantamento no DATASUS baseado nos dados de carcinoma hepatocelular entre 2011 e 2016 mostrou 28.822 casos, sendo mais de 70% já diagnosticados em estágio avançado, sem chance de cura (RAMOS et al., 2018).

Figura 12. Número estimado de mortes por câncer no mundo em 2018, mostrando o câncer de fígado como o segundo mais letal.

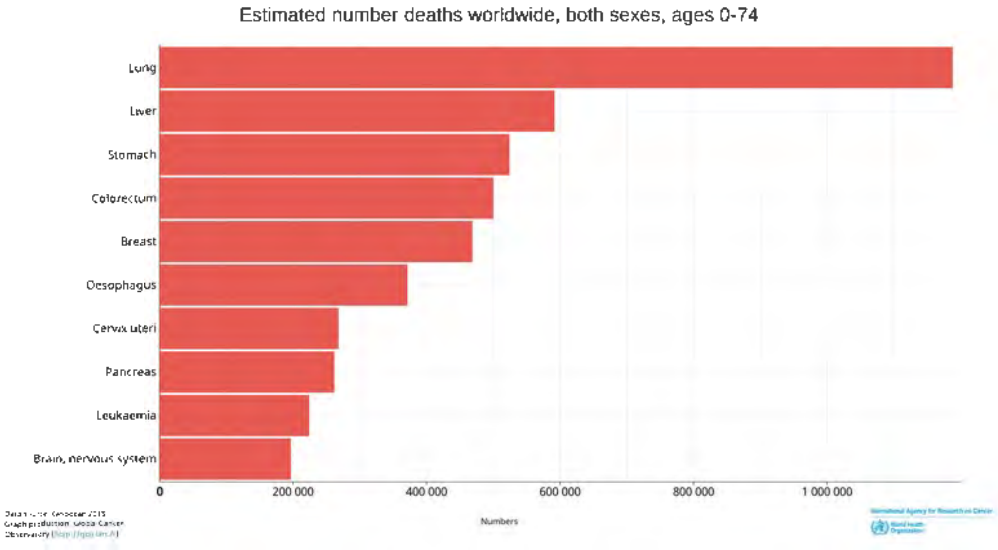

Fonte: Agência Internacional para Pesquisa de Câncer, Organização Mundial da Saúde

No HCC observa-se uma relação particular de incidência com os fatores de risco. Ao contrário do que acontece em outros canceres, para o HCC os fatores de risco estão bem estabelecidos. A incidência de câncer de fígado é maior na Ásia e na

África Sub-Saariana (**Figura 13**), onde há maior prevalência do Vírus da Hepatite B (HBV), o principal fator de risco para desenvolvimento de HCC. Além deste, também são fatores de risco infecção pelo Vírus da Hepatite C (HCV), abuso de álcool e a esteatose não-alcoólica em pacientes com síndrome metabólica e diabetes. Existem ainda os chamados c-fatores de risco, que estão associados à aumento da incidência do HCC se algum dos fatores de risco estiver presente; são eles o tabagismo e a exposição à aflatoxina B (SIA et al., 2016).

Figura 13. Distribuição da incidência do câncer de fígado no mundo em 2018.

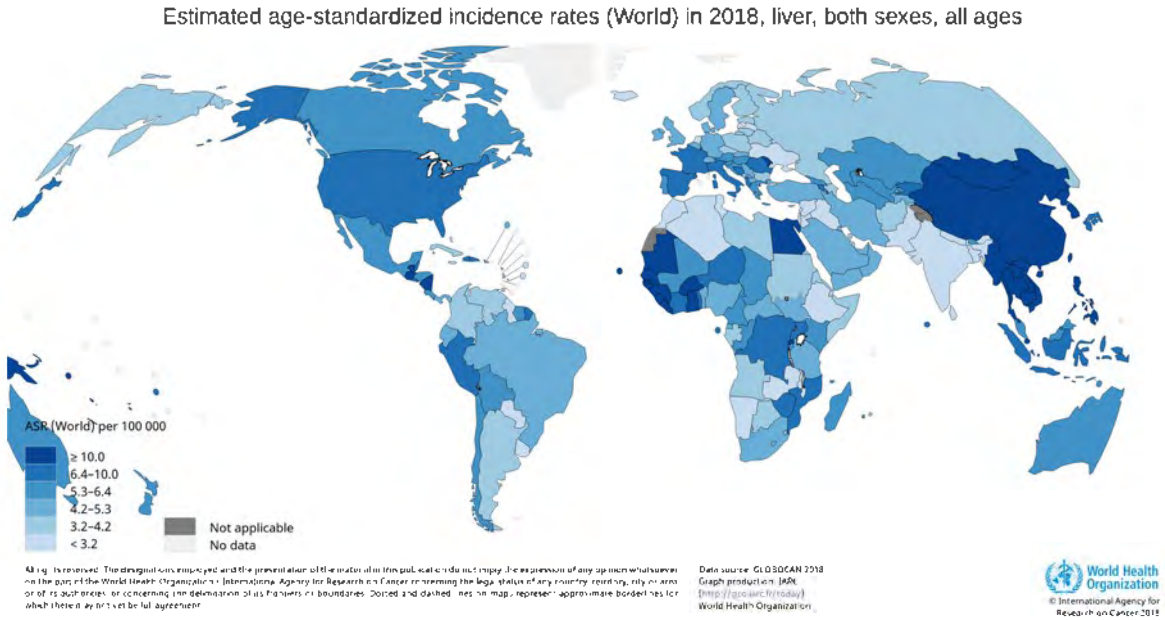

Fonte: Agência Internacional para Pesquisa de Câncer, Organização Mundial da Saúde.

2.2.2 Biologia e Classificação do Carcinoma Hepatocelular

A denominação de câncer de fígado abrange um conjunto heterogêneo de doenças malignas, com características histológicas e prognósticas distintas. Os tumores hepáticos podem ser carcinoma hepatocelular (HCC), colangiocarcinoma intrahepático (iCCA), misto carcinoma hepatocelular e colangiocarciona (HCC-CCA), HCC fibrolamelar e hepatoblastoma, uma neoplasia infantil. Dentre todos os tipos, o HCC e o iCCA são os mais comuns e correspondem a aproximadamente 99% dos casos, sendo 90% só o HCC (SIA et al., 2016).

O carcinoma hepatocelular é um tumor heterogêneo, no qual as células neoplásicas crescem em cordas de espessuras variáveis, alinhadas às células

endoteliais e mimetizando as trabéculas e sinusóides do fígado normal (CALDERARO et al., 2017).

Durante o desenvolvimento do HCC ocorre também uma evolução histológica do tumor. Nas fases iniciais pequenos nódulos podem ser detectados em testes de rastreio, são hipovasculares, possui o mesmo grau de diferenciação de uma displasia de alto grau, pode apresentar gordura, mas microinvasão vascular é rara. Neste estágio a biópsia por punção pode não detectar a malignidade, que é caracterizada pela invasão estromal. Em estágio avançado, por outro lado, o HCC raramente apresenta alguma diferenciação e pode apresentar uma cápsula bem definida e invasão microvascular. Análises de imunohistoquímica (IHC) podem auxiliar no diagnóstico de HCC, sendo analisadas a expressão da *heat shock protein*-70, glipicana-3, glutamina sintetase e clatrina cadeia pesada. No entanto, o diagnóstico radiológico é considerado padrão-ouro para o HCC, com a vantagem de ser não-invasivo (BRUIX; REIG; SHERMAN, 2016).

O estadiamento do HCC pode ser feito de diversas maneiras (LIU et al., 2016), mas o sistema de classificação *Barcelona Clinic Liver Cancer (BCLC)* associa o estadiamento com prognóstico, sendo endossado cientificamente. O sistema BCLC leva em consideração a condição clínica do paciente, a função hepática e a carga tumoral, conforme esquematizado na **Figura 14** (AYUSO et al., 2018).

Figura 14. Sistema de classificação do HCC da Barcelona Clinic Liver Cancer (BCLC) e sua correlação com o prognóstico, tratamento e expectativa de sobrevida.

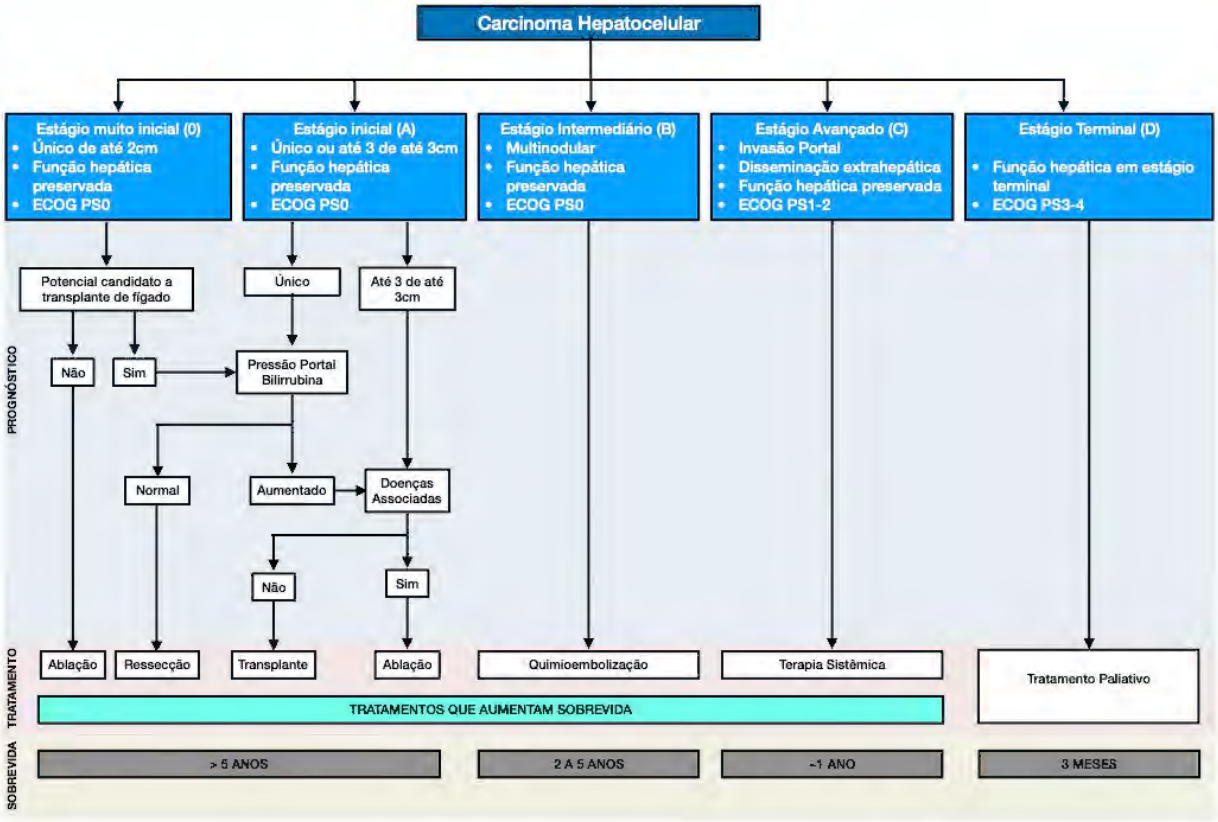

Fonte: Adaptado de (AYUSO et al., 2018)

2.2.3 Medicina de Precisão no Carcinoma Hepatocelular

A classificação molecular do HCC (**Figura 15**) foi feita ao longo do tempo através de painéis de expressão gênica e mais recentemente, dada a tecnologia de sequenciamento de nova geração, através de perfis mutacionais. Essa classificação levou a caracterização de dois subtipos distintos: um proliferativo e o outro não proliferativo. O tipo proliferativo é mais agressivo, mantém vias de proliferação super-expressas, como a do IGF1 (*insulin-like growth fator 1*), a do mTOR e a Notch. Achados epigenéticos e citogenéticos também associam o subtipo proliferativo com maiores taxas de recorrência e menor sobrevida. O subtipo não-proliferativo, por outro lado, é mais indolente e usualmente mantem características semelhantes as dos hepatócitos, alguns mantém a via Wnt canônica ativada, principalmente através de mutações no gene CTNNB1. As análises de perfil mutacional do HCC são capazes de indicar a história do tumor, pois as assinaturas genéticas têm sido associadas à exposição a álcool, cigarro, aflatoxina B1 ou ácido aristolóquico (SIA et al., 2016).

Figura 15. Esquema ilustrado da classificação molecular do HCC através de diferentes técnicas de análise, com caracterização das alterações genéticas encontradas em cada subclasse.

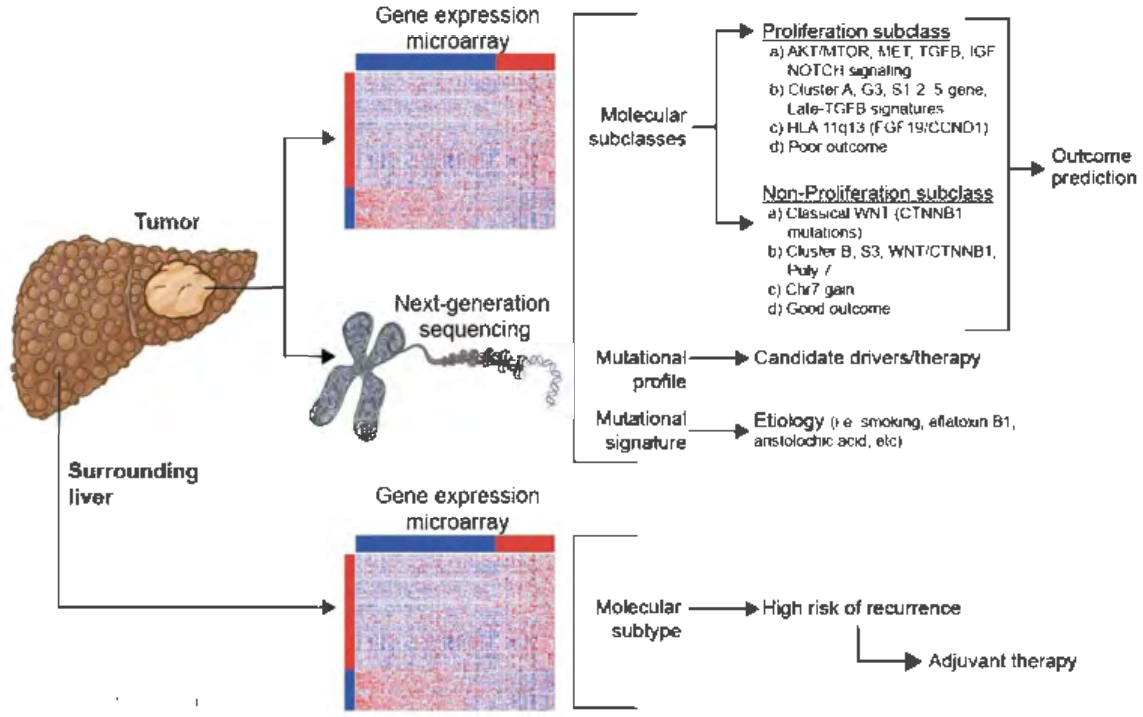

Fonte: (SIA et al., 2016).

De modo geral, apenas um terço dos pacientes de HCC é diagnosticado em estágio onde a cura é possível (DING et al., 2017). Por isso, o número de evidências apontando a eficácia de utilizar as ferramentas moleculares para aplicar a abordagem de precisão no diagnóstico e tratamento de HCC é crescente (SIA et al., 2016). É neste contexto que nas últimas décadas vários estudos clínicos foram conduzidos para identificar e validar novos potenciais alvos terapêuticos no HCC, especialmente para o tratamento dos pacientes em estágio avançado (LLOVET et al., 2018). Na **Figura 16** está representada esquematicamente uma célula de HCC e os atuais e potenciais alvos terapêuticos.

Figura 16. Esquema ilustrado das vias metabólicas no HCC e as terapias de alvo molecular para que estão disponíveis ou em desenvolvimento.

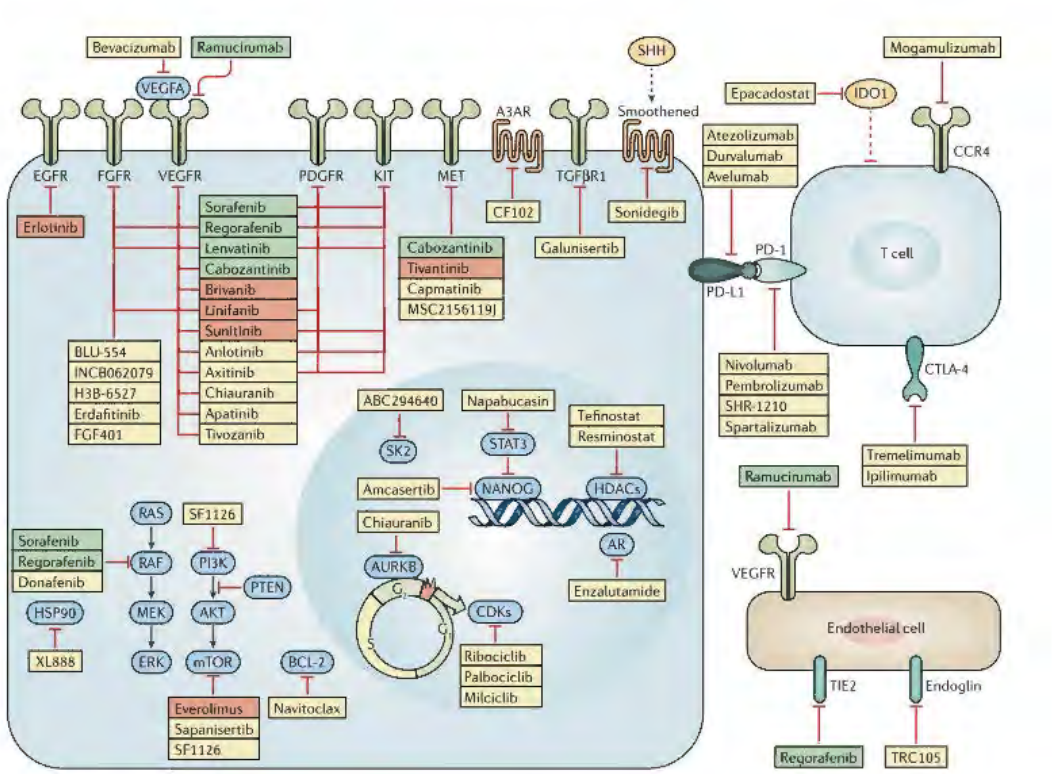

Fonte: (LLOVET et al., 2018). Nas caixas verdes estão drogas com resultado positivo em estudos de fase 3; caixas vermelhas para drogas com resultado negativo em estudo de fase 3; caixa amarela para droga em desenvolvimento (fase 1, 2 ou 3).

2.3 CÂNCER DE MAMA

2.3.1 Epidemiologia & Fatores de risco

De acordo com a última publicação da *International Agency for Research on Cancer* (IARC/World Health Organization), o câncer de mama é o mais incidente, com 1.810.231 novos casos em 2018; e o quinto em número de mortes com 468.739 registradas em 2018 (**Figura 17**) (BRAY et al., 2018)**.**

Figura 17. O câncer de mama é o mais incidente no mundo: número estimado de casos e mortes por câncer em 2018

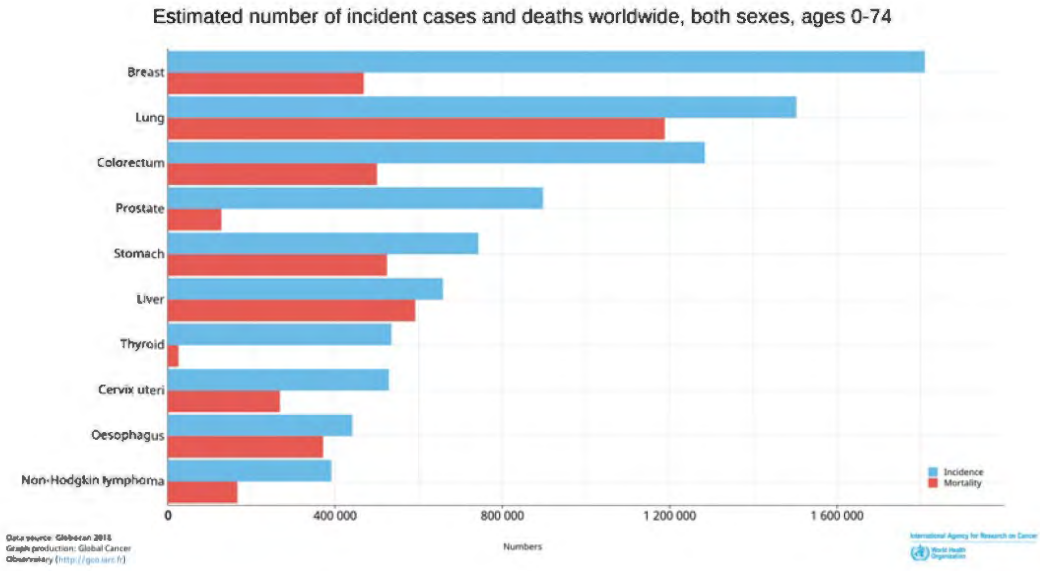

Fonte: Agência Internacional para Pesquisa de Câncer, Organização Mundial da Saúde.

No Brasil, a estimativa do Instituto Nacional do Câncer para o biênio 2018-2019 (**Figura 18**) aponta que são esperados 59.700 novos casos de câncer de mama, sendo o mais frequente (INSTITUTO NACIONAL DE CANCER JOSÉ ALENCAR GOMES DA SILVA, 2018). Deste modo, no Brasil, assim como no mundo, o câncer de mama é o mais frequente na população de mulheres.

Figura 18. Incidência do câncer no Brasil estimada para o biênio 2018-2019

Distribuição proporcional dos dez tipos de câncer mais incidentes estimados para 2018 por sexo, exceto pele não melanoma*

Localização Primária	Casos	%			Localização Primária	Casos	%
Próstata	68.220	31,7%	Homens	Mulheres	Mama Feminina	59.700	29,5%
Traqueia, Brônquio e Pulmão	18.740	8,7%			Cólon e Reto	18.980	9,4%
Cólon e Reto	17.380	8,1%			Colo do Útero	16.370	8,1%
Estômago	13.540	6,3%			Traqueia, Brônquio e Pulmão	12.530	6,2%
Cavidade Oral	11.200	5,2%			Glândula Tireoide	8.040	4,0%
Esôfago	8.240	3,8%			Estômago	7.750	3,8%
Bexiga	6.690	3,1%			Corpo do Útero	6.600	3,3%
Laringe	6.390	3,0%			Ovário	6.150	3,0%
Leucemias	5.940	2,8%			Sistema Nervoso Central	5.510	2,7%
Sistema Nervoso Central	5.810	2,7%			Leucemias	4.860	2,4%

*Números arredondados para múltiplos de 10.

Fonte: Instituto Nacional do Câncer

O risco de desenvolver câncer de mama aumenta com a idade (DESANTIS et al., 2017), mas também há grande participação de fatores genéticos, hormonais e ambientais (HOLM et al., 2017). Existe uma subclassificação dos fatores de risco entre aqueles que podem ser evitados, como o alcoolismo, tabagismo e uso de anticoncepcionais hormonais. Já os fatores de risco que não podem ser evitados incluem fatores genéticos (até 10% dos casos de câncer de mama são hereditários), menarca precoce e menopausa tardia (**Figura 19**).

Figura 19. Fatores de risco e prevenção para o câncer de mama.

Fonte: A autora.

2.3.2. Biologia e Classificação do câncer de Mama

A biologia do câncer de mama envolve importantes processos metabólicos e estruturas celulares (**Figura 20**). No tecido mamário normal (A1) as células epiteliais formam o ducto, estabelecem junções com as células vizinhas e com a membrana basal, constituindo uma forma de controlar a proliferação celular e garantir a manutenção da polaridade celular (A2), através de inibição por contato. Por outro lado, no tecido cancerígeno, as células ductais perdem a estrutura polarizada que é fornecida por uma matriz densa de colágeno, e desta forma, se proliferam e migram (B1). O microambiente tumoral é complexo e envolve a matriz extracelular, células cancerígenas, além de diversos outros tipos de células, inclusive fibroblastos e células do sistema imune. Esta complexidade celular é responsável por garantir

autossuficiência em fatores de crescimento, bem como manter o ambiente inflamatório e oxidante, favorecendo a angiogênese (B2) (VIDEIRA; REIS; BRITO, 2014).

Figura 20. Ilustração do tecido mamário normal e tumoral, demonstrando as alterações nos elementos biológicos.

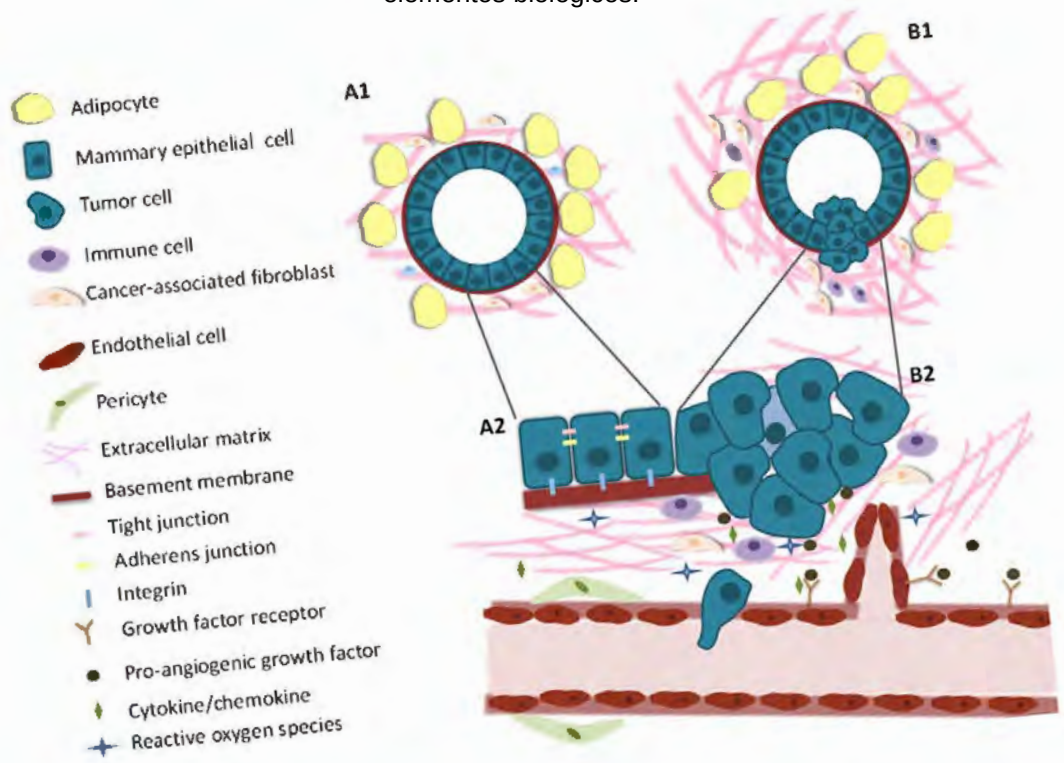

Fonte: (VIDEIRA; REIS; BRITO, 2014).

A classificação do câncer de mama segue o estadiamento TNM, de acordo com as recomendações do NCCN (National Comprehensive Cancer Network). Dentro destes critérios, os tumores da mama são avaliados com relação ao (T) tamanho; (N) número de linfonodos comprometidos, podendo ser subdivididos em (cN) se por avaliação clínica ou (pN) se por avaliação patológica; e (M) presença de metástases distantes (LURIE et al., 2018). A **Tabela 4** resume a classificação do câncer de mama por estes critérios

Tabela 4. Classificação do câncer de mama pelo critério pTNM**.**

Estágio	Tamanho do Tumor Primário	Número de Linfonodos Comprometidos	Presença de Metástases
IA	≤20mm	N0	Ausente
IB	≤20mm	Micro metástases (>0,2mm <2,0 mm)	Ausente
IIA	≤20mm >20mm ≤50mm	N1 N0	Ausente
IIB	>20mm ≤50mm >50mm	N1 N0	Ausente
IIIA	≤50mm >50mm	N2 N1 ou N2	Ausente
IIIB	Atinge parede torácica e/ou pele	N0 a N2	Ausente
IIIC	Qualquer tamanho	N3	Ausente
IV	Qualquer tamanho	N0 a N3	Detectável

Fonte: Adaptado de *American Joint Committee on Cancer* (https://cancerstaging.org)

O câncer de mama é ainda caracterizado de acordo com suas propriedades histológicas e moleculares (**Figura 21**). Pelo perfil histológico são classificados em ductais ou lobulares e ainda entre *in situ* ou invasivo (ARAÚJO et al., 2017). A classificação molecular, por sua vez se estabeleceu após o estudo do Perou que fez análise de expressão gênica por microarranjo (PEROU et al., 2000), e tem valor prognóstico e preditivo, uma vez que auxilia na decisão terapêutica. A partir das observações deste estudo, foi proposta uma sub-classificação molecular em: Luminal A e B, Basal-like, HER2 super-expresso e mama normal. O tipo basal-like é positivo para CK5/6, p-caderina, caveolinas 1 e 2, nestina, EGFR, entre outros; esse subtipo é frequentemente confundido com os tumores triplo negativos, no entanto, 30% dos tumores basais não tem o fenótipo triplo negativo (BADVE et al., 2011). O câncer de mama denominado de triplo negativo é caracterizado por não apresentar os receptores de estrógeno (RE) e/ou progesterona (RP) e HER2. Por outro lado, os cânceres de mama denominados Luminais expressam os RE e RP, mas o Luminal A não apresenta HER2 e tem baixo Ki67, um marcador de proliferação celular, em contraste ao tipo B que pode ser HER2+ e tem alto Ki67 (LEE, 2016; PEROU et al., 2000). Outro subtipo foi posteriormente descrito, o *claudin-low* se refere a tumores

que exibem propriedades de células tronco mamárias e mesenquimais, esse subtipo tem sido frequentemente associado a células resistentes à quimioterapia (O'REILLY et al., 2015).

Figura 21. Esquema da classificação histológica e molecular do câncer de mama

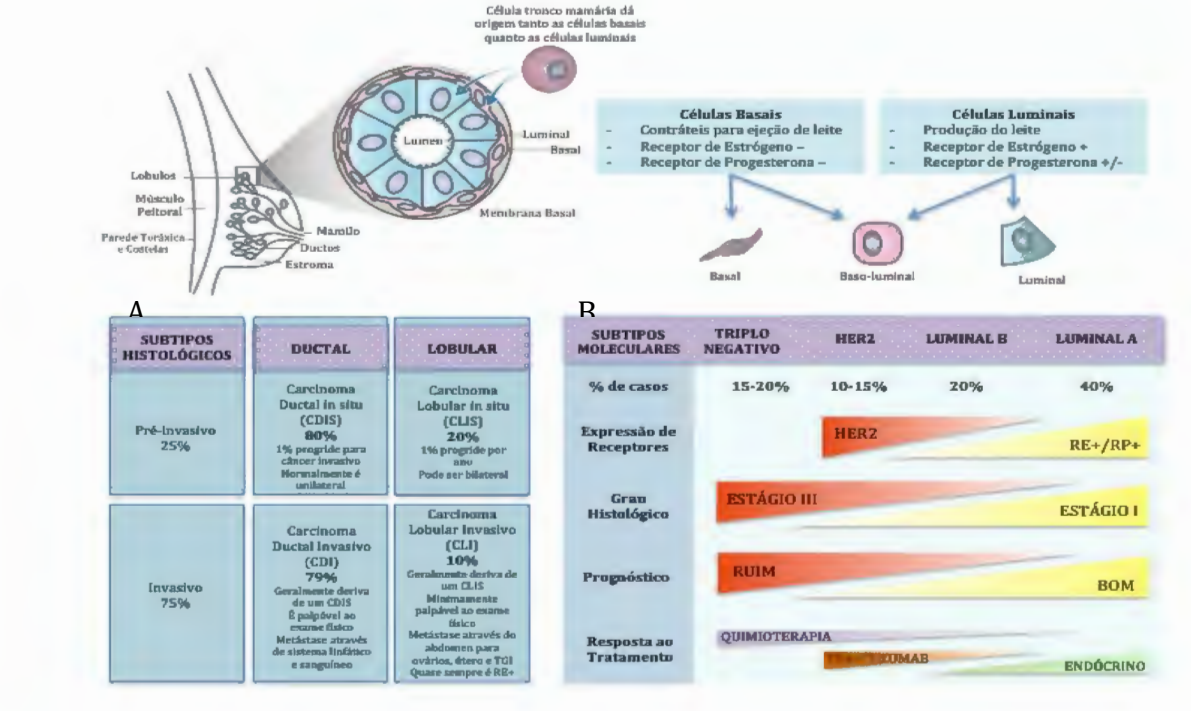

Fonte: Adaptado de http://www.pathophys.org/breast-cancer/

2.3.3 Tratamento e Medicina de Precisão no Câncer de Mama

O câncer de mama é um dos tipos de câncer onde mais está aplicado o conceito de medicina de precisão. A decisão terapêutica é primariamente baseada na classificação molecular (**Figura 22**), podendo ser resumida da seguinte forma: nos tumores que apresentam receptores hormonais (HR) é necessário utilizar a terapia endócrina (TE), que consiste em inibidores de aromatase (anastrozol, letrozol, examestano, por exemplo) e inibidores do RE (tamoxifeno, raloxifeno, fulvestranto, por exemplo); nos tumores com amplificação do HER2, esta via molecular é inibida por anticorpos monoclonais anti-HER2 (tais como trastuzumabe e pertuzumabe, entre outros); no caso dos tumores triplo negativos, a terapia é majoritariamente baseada em quimioterápicos, exceto em casos específicos onde há marcadores moleculares presentes (GODONE et al., 2018; SENKUS et al., 2015).

Figura 22. Tratamento do câncer de mama

Fonte: A autora

Nos tumores triplo negativos com presença de mutação de BRCA, foi visto que a quimioterapia baseada em carboplatina é superior a baseada em docetaxel (TUTT et al., 2018). Em paralelo, surgem novas drogas com mecanismos de ação precisamente desenvolvidos para agir nas células com mutação em BRCA (*breast cancer*). A classe de inibidores da PARP (poli-ADP Ribose polimerase) é composta por drogas como o olaparibe e o talazoparibe, que ao inibir o mecanismo de reparo de DNA por excisão de base exercido pela PARP, acarretam em letalidade sintética (**figura 23**). Essas drogas estão aprovadas pelo FDA para tratamento de tumores de mama HER2- pois demonstraram significativo aumento na sobrevida livre de progressão das pacientes (LITTON et al., 2018; ROBSON et al., 2017).

Figura 23. Inibidores da PARP e a letalidade sintética das células com mutação de BRCA, um exemplo da aplicação clínica e terapêutica de marcadores moleculares no câncer de mama.

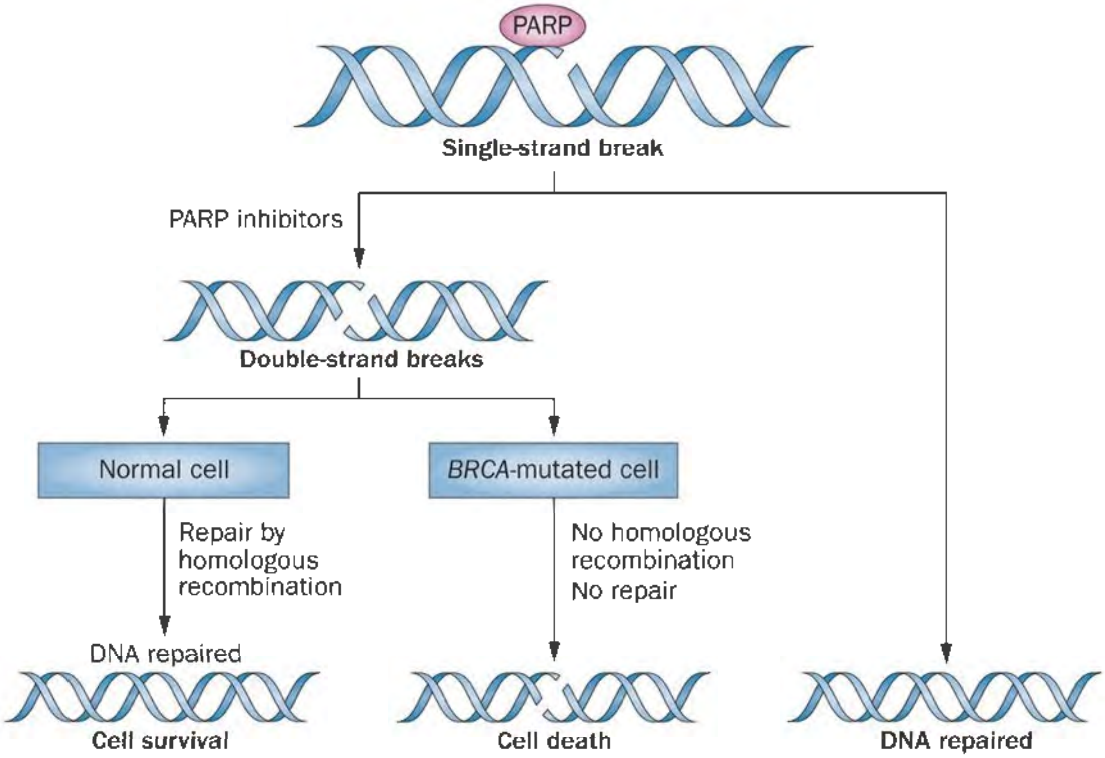

Fonte: (SONNENBLICK et al., 2015)

É com o objetivo de personalizar e tornar cada vez mais eficaz o tratamento do câncer de mama que várias iniciativas tem sido tomadas, desde abordagens no rastreamento (SHIEH et al., 2017) até o cenário metastático (ARNEDOS et al., 2015), incluindo análises de painéis genéticos que podem auxiliar na decisão de tratamento (CARDOSO et al., 2016). Isto por que, dada a alta capacidade adaptativa das células tumorais, o câncer de mama torna-se resistente as abordagens terapêuticas. Cada um dos subtipos do câncer de mama tem os seus próprios mecanismos de resistência aos tratamentos. Os tumores triplo negativos, embora quimiossensíveis, desenvolvem quimiorresistência ao longo da história da doença o que limita as opções de quimioterapia a cada nova recorrência ou progressão de doença (KIM et al., 2018; O'REILLY et al., 2015). Já os tumores HR+ são mais indolentes, mas 50% dos casos desenvolvem resistência as terapias endócrinas através da ativação de vias secundárias, principalmente a via do PI3K-AKT-mTOR (GUERRERO-ZOTANO; MAYER; ARTEAGA, 2016; GUL et al., 2018). No entanto, a resistência ao tratamento endócrino também poderá ser do tipo primária, ou seja, intrínseca, e neste caso diz respeito principalmente a deficiências no metabolismo das drogas ou mutações no

receptor do estrógeno (BRUFSKY; DICKLER, 2018; JESELSOHN et al., 2015; SZOSTAKOWSKA et al., 2019).

É através de uma resistência primária ao tamoxifeno que até 50% das pacientes com câncer de mama HR+ recorrem na doença. Neste caso em específico, são três os principais mecanismos de resistência ao tratamento com tamoxifeno: (i) alteração no RE; (ii) alterações nos segundos mensageiros da via sinalizada pelo RE e (iii) defeitos de metabolismo (GROENENDIJK; BERNARDS, 2014). O metabolismo do tamoxifeno envolve o citocromo P450 onde é realizada a conversão para os metabólitos ativos endoxifeno e 4OH-tamoxifeno (MÜRDTER et al., 2011). A **figura 24** ilustra as fases do metabolismo do tamoxifeno e seu mecanismo de ação, destacando o protagonismo da enzima CYP2D6.

Figura 24. Ilustração esquemática do metabolismo (farmacocinética) e mecanismo de ação (farmacodinâmica) do tamoxifeno, destacada em vermelho a CYP2D6.

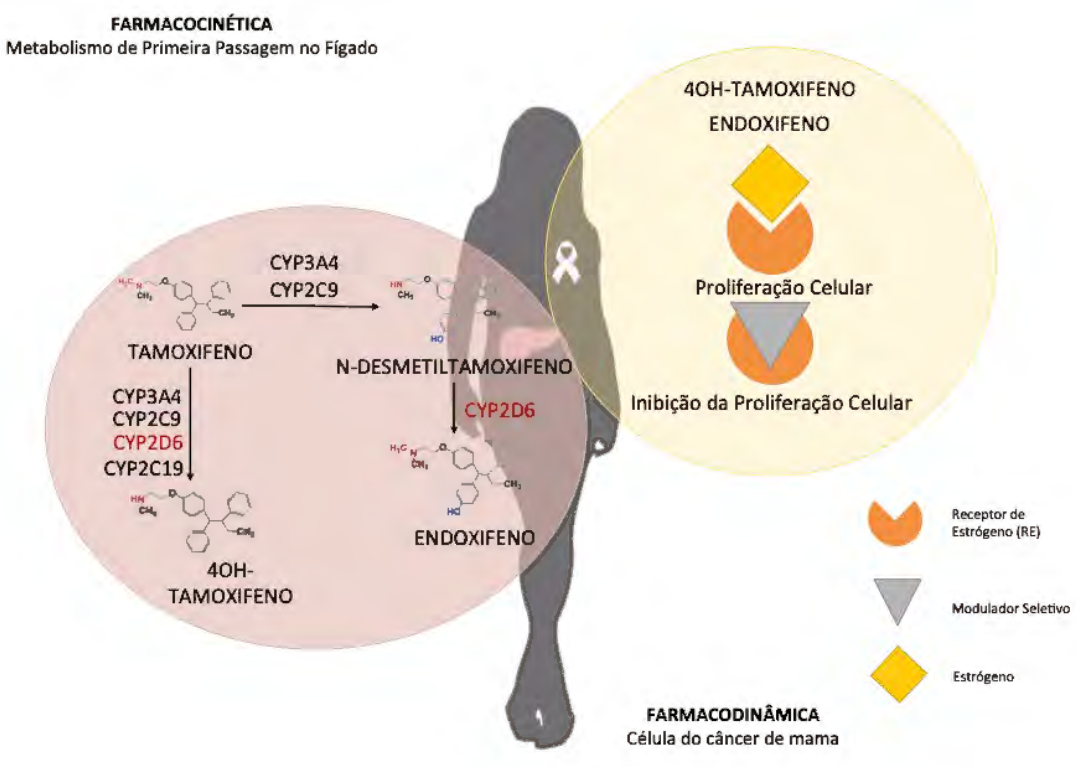

Fonte: A autora.

O gene que codifica a enzima CYP2D6 é altamente polimórfico, ou seja, apresenta diversas variações em sua sequência que acarretam em diferentes capacidades metabólicas da enzima (KIM et al., 2013). De acordo com esta

capacidade metabólica, foi desenvolvido um sistema de classificação fenotípica da CYP2D6 que leva em consideração os conjuntos de alterações genéticas nos alelos do gene. A classificação se dá da seguinte forma: (i) pobres metabolizadores – PM, que tem dois alelos não funcionais; (ii) metabolizadores intermediários – IM, um alelo funcional ou dois alelos de atividade reduzida; (iii) metabolizadores extensivos – EM, que tem dois alelos funcionais – considerados normais; e (iv) metabolizadores ultrarrápidos – UM, que tem duplicação de alelos funcionais (BAUMANN, 2015).

3 RESULTADOS

3.1 ARTIGO 1

ARTIGO EDITORIAL PUBLICADO: POINT-OF-CARE DEVICES: THE NEXT FRONTIER IN PERSONALIZED CHEMOTHERAPY

Editorial

Future Science OA

Point-of-care devices: the next frontier in personalized chemotherapy

"Combined systems of drug delivery and biosensing are breaking paradigms in the timeline from the clinical investigation of symptoms to starting the treatment."

First draft submitted: 8 May 2017; **Accepted for publication:** 10 May 2017; Published online: 14 July 2017

Keywords: cancer • chemotherapy • point-of-care devices • precision medicine

Maria Amélia Carlos Souto Maior Borba*[,1], Carlos Henrique Madeiros Castelletti[1,2], José Luiz de Lima Filho[1,3] & Danyelly Bruneska Gondim Martins[1,3]

[1]Molecular Prospection & Bioinformatics Group (ProspecMol) - Laboratory of Immunopathology Keizo Asami (LIKA), Federal University of Pernambuco (UFPE), Av. Prof. Moraes Rego 1235, 50670 -901, Cidade Universitária, Recife, PE, Brazil

[2]Agronomic Institute of Pernambuco (IPA), Av. General San Martin 1371, 50761 -000, Bongi, Recife, PE, Brazil

[3]Biochemistry Department, Federal University of Pernambuco (UFPE), Av. Prof. Moraes Rego 1235, 50670--901, Cidade Universitária, Recife, PE, Brazil

*Author for correspondence: mborba@prospecmol.org

The 'standard-of-care' is the commonest type of treatment, determined by averaging responses across large cohorts. However, every patient has their own genetic background and lifestyle, which indicates that each one should receive individualized care as based on clinical trials. The 'Precise Medicine' era has emerged to achieve successful treatment for each patient based on their personal characteristics and it is pushing forward 'point-of-care' (POC) devices [1]. The POC concept relies on portable, user-friendly and robust devices to perform sensitive and specific detection anywhere. This technology can also be linked to a cell phone coupled to a detection device [2]. One of the prime fields for application of this technology is cancer therapy, focusing on evaluating the treatment scheme for each patient.

Point-of-care devices

The global population has grown and the maximum age has been raised together with cancer incidence. The world-wide landscape of cancer treatment costs US$ 2 trillion/year [3], which impacts not only public programs but also the patient budget [4]. Besides, chemotherapy does not always achieve the expected results [5,6], so the patient relapses and the treatment costs increase. Combined systems of drug delivery and biosensing are breaking paradigms in the timeline from the clinical investigation of symptoms to starting the treatment. As an example, patch nanotechnology has shown promising results with doxorubicin delivery and also in diabetes and chronic viral infections fields [7]. Therefore, the concept of using POC devices goes beyond the clinician's office; it achieves patient empowerment.

An additional advantage in POC testing is the possibility of monitoring disease progression through specific biomarker-based dosage and monitoring treatment effectiveness, in real time, by dosing drug and metabolites ratios. Real-time patient monitoring can be integrated with wireless data collection and analysis, as observed for a POC device dedicated to acute stress that sends the vital signs to mobile applications (US FDA approved) [8]. The possibilities for similar devices in the clinical oncology routine are endless and they are also near to becoming a reality.

Computational techniques have been used for prospecting drug targets in metabolic pathways based on the humongous amount of human genome data available. New tools have emerged to reduce the computational costs, creating accessible and intuitive resources and allowing the use of systems biology insight. The computational approach is the best to perceive the individual phenotype and then develop a therapeutic approach. Other *in silico* tools evaluate how a point mutation affects the protein's

FUTURE SCIENCE part of fsg

function and its intermolecular interactions on three dimensional simulation software, which allows the understanding of protein–drug interaction, an important application in pharmaceuticals industries [9,10]. These predictive computational methodologies are a prebench step that saves time and reduces the costs of the *in vitro* tests, being crucial to cancer research due to the disease's complexity.

Chemoresistance & precision medicine

Each tumor has its own characteristics, composed of its particular and heterogeneous pool of cells. Once exposed to chemotherapy, drugs kill the sensitive cells but a small set of cells may be resistant to therapy and allows a clonal expansion that changes the tumor characteristics and determines treatment failure. On the other hand, genetic and epigenetic alterations lead to extrinsic resistance that occurs secondarily to exposure to the drug [11]. Both intrinsic and extrinsic resistance are traceable through POC devices using specific biomarkers. However, to develop precise and efficient POC devices, it is mandatory to understand how cancer cells evade therapy.

Among the mechanisms of cellular resistance to treatment, some are universal and others are disease related. A classic universal drug resistance mechanism is increased drug efflux, mediated by the overexpressed proteins of the ATP-binding cassette family, also known as multidrug resistance and P-glycoprotein [12]. An example of disease-related resistance is observed in luminal breast cancer treated with tamoxifen, a selective modulator of the estrogen receptor. The tamoxifen nonresponsive patients may have: dysfunction in tamoxifen metabolism, such as *CYP2D6* gene polymorphisms, the major metabolizing enzyme on CYP450; or polymorphisms on the estrogen receptor or its downstream effectors [13]. Another example in breast cancer was observed in a study that evaluated 14 metastatic sites of a breast cancer patient harboring *PIK3CA*-activating mutations. In those foci that presented BYL719-resistance, *PTEN* mutations were identified, evidencing a selective therapeutic pressure that conferred to the tumor temporal heterogeneity [14].

> "Going forward, in the technological era, it is not acceptable that clinicians have to test the best therapy instead of initiating the treatment under accurate molecular evaluation."

The so-called 'n of 1' approach arises to overcome these mechanisms that lead to chemotherapy failure, exploring a new interpretation of clinical trial results [15]. This comprises looking for the exceptional responders – the individuals that were different to the majority and achieve optimal responses in failed clinical trials. On the other hand, it is the nonresponders that can also contribute to revealing new possible approaches because, potentially, their genomes hold the keys to solving the therapeutic paradigm of promising *in vitro* studies that fail in clinical trials. These studies highlight the need to review the drug testing methods to create a precision-driven approach. Rather than consider the patient as a number in a thousand, it is necessary to observe and consider genetics and environmental factors [16]. Upon the application of this reasoning, the use of POC devices will allow monitoring patient response and drug metabolism efficiency, thus leading to more accurate conclusions at the trials.

Not that long ago cancer diagnosis was a death sentence. Nowadays this reality has changed, but the survival expectancy upon cancer diagnosis is still often given in months and is potentially influenced by the treatment choices. Going forward, in the technological era, it is not acceptable that clinicians have to test the best therapy instead of initiating the treatment under accurate molecular evaluation. So, what is keeping us from the next step? We need to recruit professionals, such as bioinformaticians and computer scientists, clinicians, biomedical engineers and pharmaceuticals to work in this field to empower the patient, so they will not be a simple number at statistics, but a whole and complex individual.

Acknowledgements

The authors thank Renato Pessoa e Melo Neto for his valuable contribution in English correction.

Financial & competing interests disclosure

This work was supported by Pernambuco State Science and Technology Support Foundation (FACEPE), Coordination for the Improvement of Higher Education Personnel (CAPES) and National Council for Scientific and Technological Development (CNPq). The authors have no other relevant affiliations or financial involvement with any organization or entity with a financial interest in or financial conflict with the subject matter or materials discussed in the manuscript apart from those disclosed.

No writing assistance was utilized in the production of this manuscript.

References

1 Syedmoradi L, Daneshpour M, Alvandipour M, Gomez FA, Hajghassem H, Omidfar K. Point of care testing: the impact of nanotechnology. *Biosens. Bioelectron.* 87, 373–387 (2017).

2 Calabria D, Caliceti C, Zangheri M, Mirasoli M, Simoni P, Roda A. Smartphone–based enzymatic biosensor for oral fluid L-lactate detection in one minute using confined multilayer paper reflectometry. *Biosens. Bioelectron.* 94, 124–130 (2017).

3 World Economic Forum Annual Meeting 2015 | World Economic Forum. World Econ. Forum. www.weforum.org/events

4 Markman M, Luce R. Impact of the cost of cancer treatment: an internet-based survey. *J. Oncol. Pract.* 6(2), 69–73 (2010).

5 Kartal-Yandim M, Adan-Gokbulut A, Baran Y. Molecular mechanisms of drug resistance and its reversal in cancer. *Crit. Rev. Biotechnol.* 8551, 1–11 (2015).

6 Kalia M. Biomarkers for personalized oncology: recent advances and future challenges. *Metabolism* 64(3), S16–S21 (2015).

7 Wang M, Hu L, Xu C. Recent advances in the design of polymeric microneedles for transdermal drug delivery and biosensing. *Lab Chip* 17(8), 1373–1387 (2017).

8 Chan A, Narasimhan R, Selvaraj N, Doan T. US20160338640 A1 (2016).

9 Patani H, Bunney TD, Thiyagarajan N *et al.* Landscape of activating cancer mutations in FGFR kinases and their differential responses to inhibitors in clinical use. *Oncotarget* 7(17), 1949–2553 (2016).

10 Borba MA, Melo-Neto RP, Leitão GM, Castelletti CH, Lima-Filho JL, Martins DB. Evaluating the impact of missenses mutations in CYP2D6*7 and CYP2D6*14A: does it compromise tamoxifen metabolism? *Pharmacogenomics* 17(6), 561–570 (2016).

11 Buhagiar A, Ayers D. Chemoresistance, cancer stem cells, and miRNA influences: the case for neuroblastoma. *Anal. Cell. Pathol.* 2015, 150634 (2015).

12 Housman G, Byler S, Heerboth S *et al.* Drug resistance in cancer: an overview. *Cancers (Basel)* 6(3), 1769–1792 (2014).

13 Ciccolini J, Fanciullino R, Serdjebi C. Pharmacogenetics and breast cancer management: current status and perspectives. *J. Expert Opin. Drug Metab. Toxicol.* 11(5), 719–729 (2015).

14 Pareja F, Marchiò C, Geyer FC, Weigelt B, Reis-Filho JS. Breast cancer heterogeneity: roles in tumorigenesis and therapeutic implications. *Curr. Breast Cancer Rep.* 9(1), 34–44 (2017).

15 Ledford H. Cancer researchers revisit "failed" clinical trials. *Nature* doi:10.1038/nature.2013.12835 (2013) (Epub ahead of print).

16 Schork NJ. Personalized medicine: time for one-person trials. *Nature* 520(7549), 609–611 (2015).

3.2 ARTIGO 2

MANUSCRITO: A BAD OUTCOME ON HEPATOCELLULAR CARCINOMA WITH EXTRA-HEPATIC HCV INFECTION CAUSED BY MUTATIONS IN TP53, CTNNB1 AND FBXW7 GENES

Submetido após contato com Editor para a revista:
Pharmacogenomics
ISSN (print): 1462-2416 | ISSN (online): 1744-8042
Impact Factor: 2.265 (2018)

Case report

A bad outcome on hepatocellular carcinoma with extra-hepatic HCV infection caused by mutations in TP53, CTNNB1 and FBXW7 genes

Maria A.C.S.M. Borba[1], Luiz A. Mattos[1,2,3], Julia C. Smith[1], Laís W. Silva[1], Claudio M. Lacerda[5], Norma A. Filgueira[2,5], Fábio M. Barros[6], José L. Lima-Filho[4,7], Danyelly B.G. Martins[1,4]

[1]Grupo de Prospecção Molecular e Bioinformática – Laboratório de Imunopatologia Keizo Asami – Universidade Federal de Pernambuco

[2]Hospital das Clínicas – Universidade Federal de Pernambuco

[3]Departamento de Clínica Médica – Universidade Federal de Pernambuco

[4]Departamento de Bioquímica – Universidade Federal de Pernambuco

[5]Hospital Universitário Oswaldo Cruz – Universidade de Pernambuco

[6]Real Hospital Português de Beneficência em Pernambuco

[7]Laboratório de Imunopatologia Keizo Asami – Universidade Federal de Pernambuco

Corresponding author: Danyelly Martins, M.Sc., Ph.D.

Laboratório de Imunopatologia Keizo Asami,

Av. Prof. Moraes Rego 1235, 50670-901, Cidade Universitária, Recife - PE, Brazil.

E-mail: bruneska@prospecmol.org

Tel: +55 81 21268484

ABSTRACT

Hepatocellular carcinoma (HCC) is one of the most lethal cancers. Its aetiology is related to Hepatitis Virus infections and genetic alterations, becoming difficult to treat although largely preventable. In this paper, we evaluated the mutation profile of patients with HCC and its effect for clinical parameters and outcome. A Mutation PCR Array was used to evaluate the presence of 85 mutations in liver tissue obtained from four patients diagnosed with HCC and referred to liver transplantation. Only one patient presented a mutation profile with five variants in three genes (TP53, CTNNB1, and FBXW7) associated to regulatory pathways, and never observed together in a patient. The synergic effect of the mutated genes over the metabolism could explain the extra-hepatic HCV infection and also the patient's poor outcome. These findings highlight the importance of precision medicine as molecular tool for assisting clinical decisions in HCC treatment.

KEWORDS: Hepatocellular carcinoma; p53; FBXW7; β-catenin

INTRODUCTION

Liver cancer is a challenge in public health, with 39,230 new cases estimated to 2016, combined with intrahepatic bile duct cancer [1]. Hepatic carcinogenesis starts with external liver stimuli leading to hepatocytes alterations, followed by cell death and cellular proliferation (regeneration). Chromosomal alterations, telomere shortening, mutations and deregulated gene expression were observed for TP53, CTNNB1, JAK, STAT, AXIN1, PTEN, CDKN2A and TERT genes, leading to activation of oncogenic pathways in Hepatocellular Carcinoma (HCC) [2].

The ‘Precise Medicine’ era has emerged to achieve successful treatment for each patient based on their personal characteristics, once each tumour has its own characteristics [3]. Furthermore, the improvement of current available data on both genetics and therapeutics fields is continuously required to also improve patient’s life quality. Even though a sensitive advance had been achieved in the genetic field concerning to HCC genesis and evolution, it had not been translated to clinical practice [4]. Therefore, our study evaluates the genetic profile of four HCC patients that underwent liver transplantation, highlighting the importance of genetic tests for understanding the biochemical changes that can support the clinical decisions.

METHODS

Samples

Formalin fixed paraffin embedded tissue (FFPE) was obtained from four patients referred to orthotropic liver transplantations (OLT) at Liver Institute of Pernambuco, Brazil. Patients enrolled in this study signed Informed Consent before collecting clinical sample and data.

Genotype Profile

Three slides of 10µm FFPE tissue were used for DNA purification through QIAamp DNA FFPE Tissue Kit (Qiagen, Hilden, Germany). Eluted DNA was evaluated in Nanodrop 2000 (Thermo Scientific - Waltham, Massachusetts, EUA) prior to the genotype analysis, that was performed through qBiomarker Somatic Mutation PCR Array Human Liver Cancer (SMH-034A) (Qiagen, Hilden, Germany). This assay evaluates 85 mutations in 9 genes (BRAF, CTNNB1, ERBB2, FBXW7, HF1A, KRAS, NRAS, PIK3CA, TP53).

RESULTS

Four patients referred to OLT were selected for this study, one woman and three men over 60 years old with hepatitis C and cirrhosis history **(Table 1)**. Patients #2 and #3 had good outcome and no genetic mutations were found in these patients. Patient #1 showed a synchronic gallbladder carcinoma as an incidental finding during the OLT. No mutations were found, but surgery complications triggered his death 23 days after the transplantation. By another hand, patient #4 showed increased alpha-fetoprotein (AFP) levels 3 months after OLT, with bad outcome within 18 months. He had 2 mutations in CTNNB1, 2 mutations in TP53 and 1 mutation in FBXW7 (**Table 1**). Further analysis revealed history of arterial hypertension, splenomegaly, schistosomiasis and use of illicit drugs. Histological evaluation showed fibrosis (**Figure 1A**), an extensive area of necrosis (**Figure 1B**) and inflammatory infiltrate (**Figure 1C**) in explanted liver. Alpha-fetoprotein monitoring after OLT showed abnormal profile **(Figure 1D)**, with a membranous glomerulonephritis diagnosed with nephrotic levels,

extra-hepatic focus of HCV, with complement consumption but negative cryoglobulinemia.

In CTNNB1, two mutation lead to a change in two Serines (p.Ser37Phe and p.Ser45Ala) of the β-catenin, both important for its regulation. In TP53, p.Arg342* mutation leads to the complete loss of p53 function once introduces an early stop codon, while p.Met246Val affects the site for DNA-binding and repair (**Figure 2A**). In FBXW7, p.Arg465Cys changes a strong basic residue by a neutral one, affecting the local charge in this site which increases the hydrophobic surface and reduces its ability to bind to the substrates (**Figure 2B**). The genomic background of patient #4 could have led to a biochemical impairment (**Figure 3**) that, combined with the presence of extra-hepatic HCV, contributed to the clinical deterioration.

DISCUSSION

In this analysis, we conducted a genetic evaluation in four patients diagnosed with HCC to determine the influence of mutations in the clinical parameters. Only one patient presented mutation in the PCR Array for Human Liver Cancer and, in face of patient's relapse, his genomic background seems to have contributed to a biochemical impairment and bad outcome.

HCV is known to cause chronic hepatitis in 80% of the cases and has up to 20 times more chances of causing liver cirrhosis, due to the ability of C, NS3, NS5A and NS5B viral proteins to impair DNA repair, and apoptosis mechanisms. The NS3 protein is able to directly bind and inhibit p53 and p21 proteins, contributing to HCV carcinogenesis. The viral C protein also promotes cell proliferation through the inhibition of p53 synthesis [5]. TP53 gene encodes for p53 transcription factor responsible for regulating genes with a broad range of functions, notably: DNA repair,

cell cycle arrest, apoptosis, and senescence. The p.Arg342* mutation leads to complete loss of p53, avoiding its tumor-suppressing activity. In addition, p.Met246Val mutation may also lead to a loss of function, once it change the structure of Loop-3 (residues 237 to 250) in the DNA-binding domain (DBD) core structure, affecting the DNA binding and repair [6].

The acute and chronic HCV infection was also associated to 5 to 10 times increase in mutation occurrence in TP53 and CTNNB1 genes, although mutations in these genes were assumed as mutually exclusive [7]. Regarding their aetiology, TP53 mutations are more common in HBV-related HCC while CTNNB1 mutations appears more often in alcohol-related HCC [5]. Curiously, the patient #4 presented both genes mutated and critical AFP increment (monitor response to treatment and relapse detection), an evidence already associated with more TP53 mutations, less CTNNB1 mutations, with larger tumors, vascular invasion and early recurrence [8]. Nevertheless, this patient had no history of HBV infection or abusive alcohol intake.

Mutations in CTNNB1 were reported in up to 25% of HCC patients, frequently associated with the infection by hepatitis C virus [9]. This gene codifies for β-catenin, a key molecule in Wnt pathway, involved in the transcriptional activation of genes related to cell proliferation, differentiation, angiogenesis, and cancer. This pathway remains inactivated in adult cells due the presence of Frizzled receptor antagonists or through β-catenin inhibition. It occurs in the Wnt canonical pathway through phosphorylation of β-catenin residue Ser45 mediated by Casein Kinase 1 (CK1) upon Axin binding to β-catenin; followed by successive phosphorylation at residues Ser33, Ser37 and Ser41, mediated by glycogen synthase kinase 3β (GSK3β). These events allow β-catenin to be transferred from Axin to adenomatous polyposis coli (APC) molecule, signaling to proteasome degradation [10]. The two mutations found on

patient #4 result in loss of Ser45 and Ser37 residues in β-catenin, avoiding the phosphorylation cascade and increasing β-catenin nuclear translocation and gene transcription. In patient #4, the HCV infection could also contribute for activating Wnt pathway through NS5A protein, which binds and stabilizes β-catenin [5].

FBXW7, the third gene mutated on patient #4, has an important role in avoiding HCV genome replication, once it is involved in the ubiquitization of NS5B, targeting it to proteasome degradation [11]. In non-cancer cells FBXW7 is involved in many cellular and physiological functions, mostly related to cell cycle regulation [12], and its downregulation leads to accumulation of Myc, Notch and Cyclin E, and tumorigenesis promotion [13]. Mutations in FBXW7 are already hotspots for cancer, which p.Arg465Cys is reported at 29% frequency in HCC patients [14], the same found on patient #4. It is located at the β-propeller surface, a symmetrical fold composed of WD40 domains repeated in four-stranded antiparallel β-sheet and involved in protein-protein interactions [12]. The Arginine residues positively charged are responsible for interacting with the phosphorylated substrates, and mutation in Arg465 and Arg479 residues avoids the proper bind to Cyclin E and leads to substrate accumulation [14,15]. Thus, it could have contributed to the cell cycle deregulation and also prevented the NS5B proteassomal degradation, allowing its accumulation in cell and inducting genome replication.

An integrative overview shows that in normal cells p53 induces FBXW7 expression [16], while β-catenin inhibits it [17] and FBXW7 protein degrades β-catenin through ubiquitization, inhibiting Wnt pathways [18]. The cumulative effect of the mutations on patient #4 results in poor or inefficient function of p53, reducing the expression of FBXW7 that will show a reduced ability to bind to oncoproteins and β-catenin. This event avoids the oncoproteins degradation in proteasome and, together with the lack

of β-catenin phosphorylation and inhibition, also induces the β-catenin translocation to the nucleus to induce genes related to cell proliferation and differentiation, and angiogenesis. Therefore, the effect of the mutations in TP53, CTNNB1 and FBXW7 genes, combined with the presence of extra-hepatic HCV, contributed to the hepatocellular carcinoma development and the fast clinical deterioration of this patient.

This molecular scenario could be a key for understanding the patient's bad outcome, even after liver transplantation. Nevertheless, this knowledge could have been used to revert β-catenin activity by non-steroidal anti-inflammatory drugs (NSAIDs) administration, based on a crosstalk with Wnt pathway through prostaglandin E2 (PGE2) inhibition [19]. It is also important to know that patient #4 would benefit from 5-flourouracil or cisplatin oncotherapy, but not Doxorubicin due to the lack of efficiency already reported for patients with p53 mutation in L3 [20]. Our study demonstrates the importance of implementing molecular genetic panels in HCC treatment for increasing the patient's life quality through a supportive precise medicine.

LIST OF ABBREVIATIONS

HCC - Hepatocellular Carcinoma

FFPE - Formalin Fixed Paraffin Embedded Tissue

OLT - Orthotropic Liver Transplantations

DNA - deoxyribonucleic acid

PCR - Polymerase Chain Reaction

AFP - Alpha-Fetoprotein

HCV - Hepatitis C Virus

NS3 - Non-Structural 3

NS5A - Non-Structural 5A

NS5B - Non-Structural 5B

DBD - DNA Binding Domain

HBV – Hepatitis B Virus

CK1 - Casein Kinase 1

GSK3β - Glycogen Synthase Kinase 3β

APC - Adenomatous Polyposis Coli

NSAIDs - Non-Steroidal Anti-Inflammatory Drugs

PGE2 - Prostaglandin E2

L3 - Loop3

DECLARATIONS

Ethics Approval and Consent to Participate

All procedures performed in studies involving human participants were in accordance with the ethical standards of the institutional research committee and 1964 Helsinki declaration. The study was performed following the protocol approved by Research Ethics Committee at Human Health Centre of the Federal University of Pernambuco, Brazil.

Consent for publication

Not applicable.

Availability of data and supporting materials section

Data sharing not applicable to this article as no datasets were generated or analysed during the current study.

Competing Interests

The authors declare no competing interests

Funding

This work was supported by scholarship from Pernambuco State Science and Technology Support Foundation (FACEPE).

Authors' Contributions

LAM, CML, NAF, FMB analysed and interpreted the clinical patient data. MACSMB and LWS performed the molecular experiments. LAM, MACSMB, DBGM and JLLF were responsible for experimental design, data analysis and manuscript writing. All authors revised and approved the final manuscript.

Acknowledgements

Qiagen (Hilden, Germany) donated the kits for genotyping analysis. The authors thank Vinícus Tigre for pathways figures design.

REFERENCES

1. Siegel RL, Miller KD, Jemal A. Cancer statistics. CA Cancer J Clin. 2016;66:7–30.

2. Kan Z, Zheng H, Liu X, Li S, Barber TD, Gong Z, et al. Whole-genome sequencing identifies recurrent mutations in hepatocellular carcinoma. Genome Res. Cold Spring Harbor Laboratory Press; 2013;23:1422–33.

3. Borba MACSM, Castelletti CHM, Filho JL de L, Martins DBG. Point-of-care devices: the next frontier in personalized chemotherapy. Futur. Sci. OA. Future

Science Ltd London, UK ; 2017;3:FSO219.

4. Zucman-Rossi J, Villanueva A, Nault JC, Llovet JM. Genetic Landscape and Biomarkers of Hepatocellular Carcinoma. Gastroenterology. Elsevier Ltd; 2015;149:1226–39.

5. Tornesello ML, Buonaguro L, Izzo F, Buonaguro FM. Molecular alterations in hepatocellular carcinoma associated with hepatitis B and hepatitis C infections. Oncotarget. 2016;7:25087–102.

6. Bullock AN, Henckel J, Fersht AR. Quantitative analysis of residual folding and DNA binding in mutant p53 core domain: definition of mutant states for rescue in cancer therapy. Oncogene. 2000;19:1245–56.

7. Guichard C, Amaddeo G, Imbeaud S, Ladeiro Y, Pelletier L, Maad I Ben, et al. Integrated analysis of somatic mutations and focal copy-number changes identifies key genes and pathways in hepatocellular carcinoma. Nat. Genet. 2012;44:694–8.

8. Peng SY, Chen WJ, Lai PL, Jeng YM, Sheu JC, Hsu HC. High α-fetoprotein level correlates with high stage, early recurrence and poor prognosis of hepatocellular carcinoma: Significance of hepatitis virus infection, age, p53 and β-catenin mutations. Int. J. Cancer. 2004;112:44–50.

9. Wang W, Pan Q, Fuhler GM, Smits R, Peppelenbosch MP. Action and function of Wnt/β-catenin signaling in the progression from chronic hepatitis C to hepatocellular carcinoma. J. Gastroenterol. Springer Japan; 2016;1–13.

10. Peifer M, Polakis P. Wnt signaling in oncogenesis and embryogenesis - A look outside the nucleus. Science (80-.). 2000;287:1606–9.

11. Chen J, Wu X, Chen S, Chen S, Xiang N, Chen Y, et al. Ubiquitin ligase Fbw7 restricts the replication of hepatitis C virus by targeting NS5B for ubiquitination and degradation. Biochem. Biophys. Res. Commun. 2016;470:697–703.

12. Uddin S, Bhat AA, Krishnankutty R, Mir F, Kulinski M, Mohammad RM. Involvement of F-BOX proteins in progression and development of human malignancies. Semin. Cancer Biol. Elsevier Ltd; 2016;36:18–32.

13. Xu W, Taranets L, Popov N. Regulating Fbw7 on the road to cancer. Semin. Cancer Biol. Elsevier Ltd; 2016;36:62–70.

14. Akhoondi S, Sun D, Von Der Lehr N, Apostolidou S, Klotz K, Maljukova A, et al. FBXW7/hCDC4 is a general tumor suppressor in human cancer. Cancer Res. 2007;67:9006–12.

15. Singh T. Functionalzation of cancer-associated mutant alleles of human CDC4 (FBXW7). [Vancouver]: The University of British Columbia; 2013.

16. Kimura T, Gotoh M, Nakamura Y, Arakawa H. hCDC4b, a regulator of cyclin E, as a direct transcriptional target of p53. Cancer Sci. Blackwell Publishing Ltd; 2003;94:431–6.

17. Wu WJ, Shi J, Hu G, Yu X, Lu H, Yang ML, et al. Wnt/b-catenin signaling inhibits FBXW7 expression by upregulation of microRNA-770 in hepatocellular carcinoma. Tumor Biol. 2016;37:6045–51.

18. Jiang J, Sun C, Tian S, Yu C, Chen M, Zhang H. Tumor suppressor Fbxw7 antagonizes WNT signaling by targeting β-catenin for degradation in pancreatic cancer. Tumor Biol. Springer Netherlands; 2016;37:13893–902.

19. Ahmed K, Shaw H V., Koval A, Katanaev VL. A second WNT for old drugs: Drug repositioning against WNT-dependent cancers. Cancers (Basel). 2016;8:1–27.

20. Geisler S, Lønning PE, Aas T, Johnsen H, Fluge Ø, Haugen DF, et al. Influence of TP53 Gene Alterations and c-erbB-2 Expression on the Response to Treatment with Doxorubicin in Locally Advanced Breast Cancer. Am. Assoc. Cancer Res. 2001;61:2505–12.

FIGURES

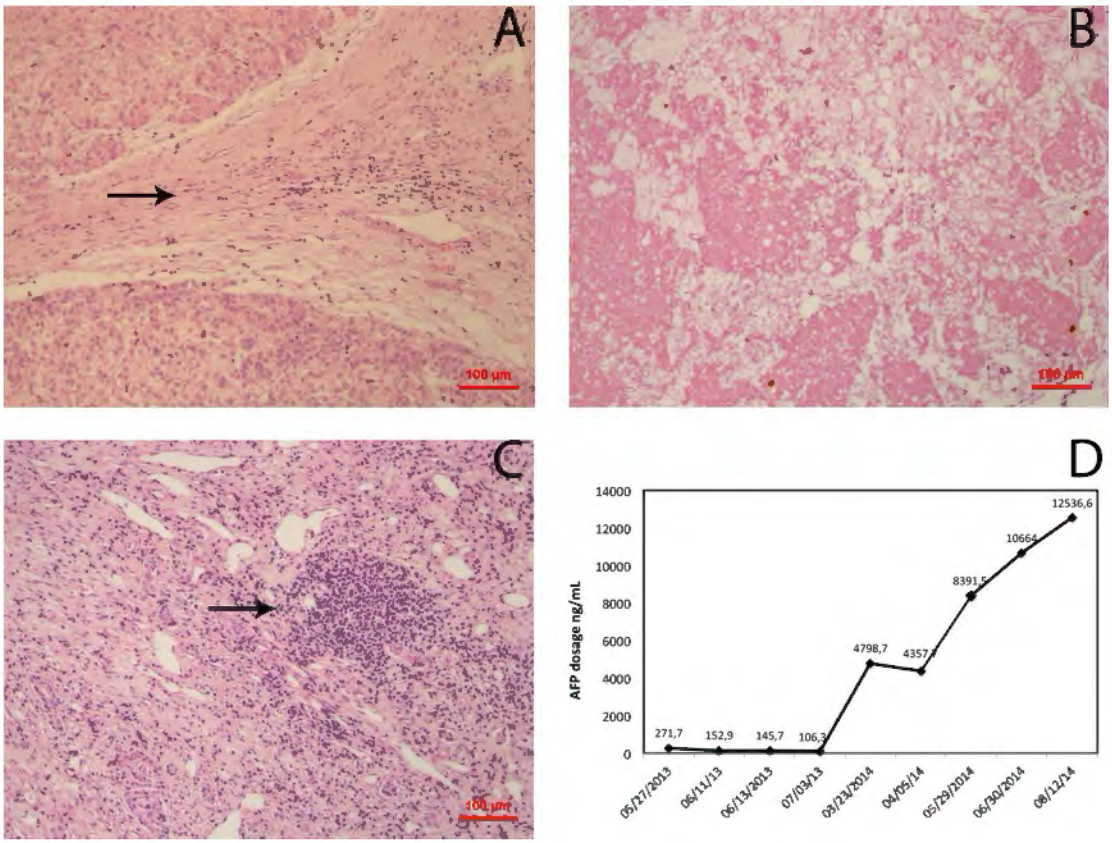

Fig.1 Histological analysis of HCC tissue, and Alpha-fetoprotein dosage evolution observed in patient #4. Panel A shows the liver tissue medium differentiation with fibrosis (black arrow); Panel B shows the extensive necrosis post-TACE; Panel C shows the presence of inflammatory infiltrate (black arrow); Panel D is the graphic representation of AFP levels during patient evolution post-TACE. Tissue images were obtained with optical microscopy ZEISS Imager.M2m (50x magnification) coupled with ZEISS AxioCam HRc.

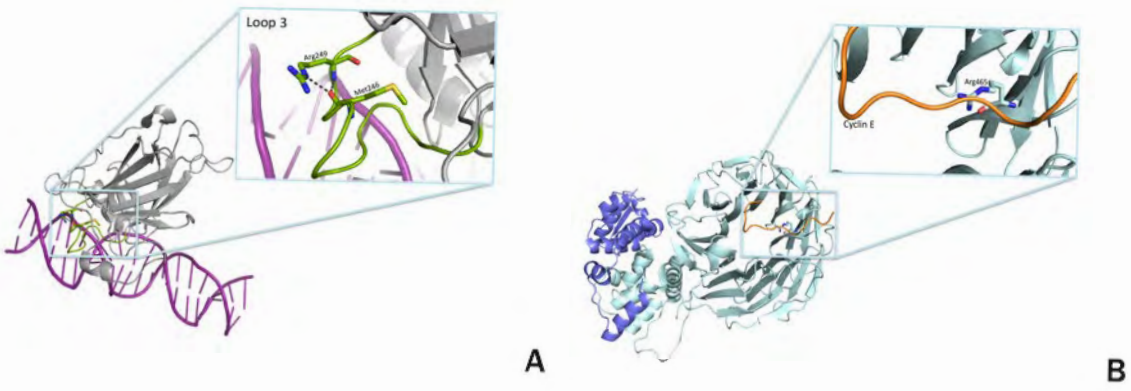

Fig.2 3D structure of p53 and FBXW7 regions related to the missense polymorphisms. Panel A shows the p53 residue Met246 establishing two hydrogen bonds (black) with Arg249 to stabilize L3 (green) in DBD of p53 molecule (gray); DNA is presented in purple. The presence of p.Met246Val mutation at p53 leads to reduced ability for DNA interacting. Panel B shows FBXW7 (light blue) binding with SCF (a complex of F-box + Skp1, Cullin 1 and Roc1/Rbx1/Hrt1) and a fragment of the substrate Cyclin E (orange). The residue Arg465 is positively charged, and interacts with phosphorylated substrates through electrostatic affinity, but p.Arg465Cys mutation prevents FBXW7 proper function. PyMol (The PyMOL Molecular Graphics System, Version 1.7.4, Schrödinger, LLC, NY, USA) was used to assess 3D conformation of the crystallographic structures of the molecules p53 (PDB: 5LGY) and FBXW7 (PDB: 2OVQ).

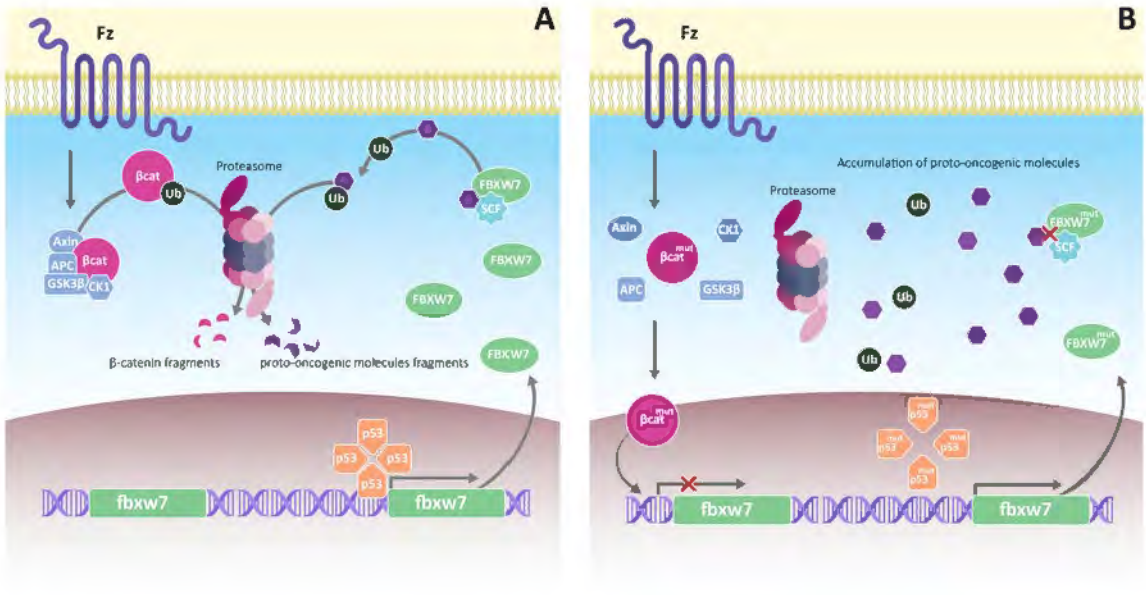

Fig.3 Pathway interaction of p53, β-catenin, and FBXW7 proteins. The Panel A shows the regular crosstalk between p53, β-catenin and FBXW7 functions. Panel B represents the scenario of the molecular pathways interaction between the three proteins mutated on patient #4, which could lead to FBXW7 downregulation and defective function with consequent oncoprotein accumulation in the cell. The pathways design was made based on literature review using the terms “Hepatocellular carcinoma”, “HCV”, “TP53”, “CTNNB1”and “FBXW7”.

3.3 ARTIGO 3

ARTIGO PUBLICADO: EVALUATING THE IMPACT OF MISSENSES MUTATIONS IN CYP2D6*7 AND CYP2D6*14^{A}: DOES IT COMPROMISE TAMOXIFEN METABOLISM?

Short Communication

For reprint orders, please contact: reprints@futuremedicine.com

Pharmacogenomics

Evaluating the impact of missenses mutations in *CYP2D6*7* and *CYP2D6*14A*: does it compromise tamoxifen metabolism?

CYP2D6 is a high polymorphic enzyme from P450, responsible for metabolizing almost 25% of drugs. The distribution of different mutations among *CYP2D6* alleles has been associated with poor, intermediate, extensive and ultra-metabolizers. **Aim:** To evaluate how missenses mutations in *CYP2D6*7* and *CYP2D6*14A* poor metabolizer alleles affect CYP2D6 stability and function. **Materials & methods:** CYPalleles database was used to collect polymorphisms data present in 105 alleles. We selected only poor metabolizers alleles that presented exclusively missenses mutations. They were analyzed through seven algorithms to predict the impact on CYP2D6 structure and function. **Results:** H324P, the unique mutation in *CYP2D6*7*, has high impact in enzyme function due to its occurrence between two alpha-helixes involved in active site dynamics. G169R, a mutation that occurs only in *CYP2D6*14A*, leads to the gain of solvent accessibility and severe protein destabilization. **Conclusion:** Our *in silico* analysis showed that missenses mutations in *CYP2D6*7* and *CYP2D6*14A* cause CYP2D6 dysfunction.

First draft submitted: 4 December 2015; Accepted for publication: 28 January 2016; Published online: 4 April 2016

Keywords: algorithms • bioinformatics • CYP2D6 • *CYP2D6*7* • *CYP2D6*14A* • poor metabolizers • tamoxifen

Maria ACSM Borba*[1], Renato P Melo-Neto[1], Glauber M Leitão[1,2], Carlos HM Castelletti[1,3], José L Lima-Filho[4,5] & Danyelly BG Martins[1,4]

[1]Molecular Prospection and Bioinformatics Group (ProspecMol) – Laboratory of Immunopathology Keizo Asami (LIKA), Federal University of Pernambuco (UFPE), Av. Prof. Moraes Rego 1235, 50670-901, Cidade Universitária, Recife, PE, Brazil
[2]Clinical Hospital – Federal University of Pernambuco (UFPE), Av. Prof. Moraes Rego 1235, 50670-901, Cidade Universitária, Recife, PE, Brazil
[3]Agronomic Institute of Pernambuco (IPA), Av. General San Martin 1371, 50761-000, Bongi, Recife, PE, Brazil
[4]Biochemistry Department, Federal University of Pernambuco (UFPE), Av. Prof. Moraes Rego 1235, 50670-901, Cidade Universitária, Recife, PE, Brazil
[5]Laboratory of Immunophatology Keizo Asami (LIKA), Federal University of Pernambuco (UFPE), Av. Prof. Moraes Rego 1235, 50670-901, Cidade Universitária, Recife, PE, Brazil
*Author for correspondence: mborba@prospecmol.org

Breast cancer is the second most common cancer in the world and, by far, the most frequent cancer among women with an estimated 1.67 million new cancer cases diagnosed in 2012 (25% of all cancers). Breast cancer ranks as the fifth cause of death from cancer overall (522,000 deaths), while it is the second most frequent cause of cancer death in women from America's region (92,058 deaths, 14.9% of total) [1].

Tamoxifen, is the standard treatment for estrogen receptor (ER)-positive breast cancer (70–80% of the cases), it is a compound known as selective ER modulator that acts as ER antagonist in breast tissue [2]. However, endocrine therapy using tamoxifen is known to fail in up to 50% of patients, due to alterations in estrogen receptor; alterations in pathways signaled by estrogen receptor; and bypass mechanisms, that includes metabolic defects, mainly by CYP2D6 dysfunction [3].

Tamoxifen has a weak affinity to the ER and is regarded as a prodrug, extensively metabolized by several members of the CYP450 family and Phase II conjugation enzymes. Multiple CYP enzymes are involved in the tamoxifen metabolism, including CYP3A4, CYP2B6, CYP2C9, CYP2C19 and CYP2D6. Endoxifen and 4-hydroxytamoxifen, which are the main metabolites, have equivalent antiestrogenic potentials and are 30–100 times more active than tamoxifen. Because of the five- to tenfold higher plasma concentrations of endoxifen compared with 4-hydroxytamoxifen, endoxifen is believed to be the principal active metabolite [4]. It is also the only metabolite that binds to ER and leads to proteasomal degradation, decreasing ER levels [5].

Future Medicine part of fsg

CYP2 family contains 16 full-length genes, spread over different chromosomes and organized in multigene clusters, which all have nine exons and eight introns. CYP genes involved in pharmacological response are highly polymorphic, notably CYP2D6 [6], a tetramer heme-containing structure that acts over substrates that have a basic nitrogen and a planar aromatic ring [7]. It plays an important role in the metabolism of almost 25% of drugs, including analgesics, antidepressants and antineoplastic [6,8]. According to CYP Allele Nomenclature Database [9], there are 105 alleles for *CYP2D6*. These alleles have been associated with four drug metabolization phenotypes: poor, intermediate, extensive and ultra-metabolizers [10]. However, this association is still unclear to be applied in the guidelines for breast cancer treatment [11]. Some multicenter studies revealed a clear association between *CYP2D6* alleles and the success of tamoxifen treatment [12,13], while many others demonstrated the failure of tamoxifen regardless of *CYP2D6* genotype [14,15].

Nowadays, there is an intuitive rationale for using pharmacogenomics to guide medical treatment. So, the understanding of *CYP2D6* alleles value in predicting the efficiency of tamoxifen through pharmacogenomics markers could improve the implementation of personalized medicine in the clinical oncology [16]. However, there is no well-established correlation between phenotypic and clinical data, despite the large volume of genomic data.

Therefore, bioinformatics approaches have been used as powerful tools to handle and understand genomic data [17,18]. Multiples algorithms were developed for predicting the structural, functional and evolutional impact of genomic mutations based on protein sequence and 3D structure data. These tools provide support for experimental validation of disease-related alleles, emphasizing changes that could affect the structure and function of the protein [19,20]. There is also a class of methods, referred as template-based modeling, which relies on detectable similarity spanning most of the modeled sequence and at least one known structure [21]. As a small change in protein sequence usually results in a change in its 3D structure, the integration of algorithms data and 3D models leads to a more reliable conclusion.

The aim of this study was to evaluate the impact of missenses mutations in *CYP2D6*7* and *CYP2D6*14A* poor metabolizer alleles, using ***in silico*** approaches for predicting the structural and functional impact on the CYP2D6 molecule.

Materials & methods

Dataset construction

CYPalleles database [9] was used to collect polymorphisms data present in 105 alleles. Only 33 alleles were associated with poor metabolizer phenotype, containing four types of mutations: insertion, deletion, duplication and base substitution. Additional screening step was performed to identify *CYP2D6* alleles that contain exclusively missenses mutations, selecting only two alleles: *CYP2D6*7* and *CYP2D6*14A*.

The mutations identified were validated through dbSNP and Ensembl databases using the follow criteria: multiple observations (cluster), validation in 1000 Genomes Project and presence of mutation frequency (MAF). Since CYPalleles and dbSNP use different assemblies (M333.88 and GRCh38, respectively), the Leiden Open Variation Database platform (LOVD database – [22]) was accessed to correlate data from both and to provide additional genomic information about polymorphisms position.

Functional & structural impact of missenses mutations

A total of seven algorithms were used to evaluate the impact of each mutation on CYP2D6 structure and function (Table 1). To determine whether a polymorphism is deleterious or not, a threshold for each algorithm was established based on the algorithm description. Thus, a classification system was adopted as follow: 1 was attributed when the prediction indicates deleterious effect; 0 was attributed when the algorithms prediction showed no effect of the mutation on enzyme structure or function.

The SNPeffect output shows the variation of Gibbs free energy after the mutation changes in the molecule, classifying it into seven classes ranging from 'no effect in stability' to 'greatly enhanced stability' [23]. MuPro is a structural algorithm based on Support Vector Machine or Neural Network, but only Support Vector Machine results were analyzed, following the author's recommendation [24]. MutPred algorithm generates two scores: a general score (g), predicting the chance for a mutation to be deleterious or disease associated; and a property score (p) with the top five properties that may be impacted by the polymorphism [25]. SNAP2 is based on SIFT [30] and Polyphen2 [31] output data, generating a score associated with the prediction of one mutation as deleterious or not for the molecule [26]. SNPs&GO is dedicated to gene ontology analysis based on PHANTER data output [32] but also shows PhD-SNP [33] prediction as the result [27]. SNPs&GO showed to be useful for removing false positive results from data output [20]. MutationTaster2 is a Bayes classifier that provides conservational scores (Philo-P and PhastCons) and provide a general score for amino acid substitution impact. Philo-P score was used as threshold once mutations in conserved residues and regions show

Table 1. Algorithms applied to *in silico* analysis.

Algorithm	Method	Analysis	Threshold	Remarks	Ref.
SNPeffect	Naive bayes	Structural	>0.5	FoldX prediction in ΔΔG	[23]
MuPro	SVM and neural network	Structural	<-0.5	SVM output is more accurate	[24]
MutPred	Random forest	Structural/ functional	g >0.75	High sensibility and specificity	[25]
SNAP2	Neural network	Functional	>50 score	Dataset construction and training included a specific data for enzymes	[26]
SNPs&GO	SVM	Functional	>0.5; RI ≥5	Utilizes gene ontology and is indicated for identifying false positives	[27]
Mutation Taster2	Bayes classifier	Functional	1	Provides conservational scores Phylo-P and PhastCons	[28]
SDM	Statistical	Structural	± 2 kcal mol^{-1}	Analysis of multiple chains mutated	[29]

Δ: Variation; RI: Reliability index; SVM: Support sector machine.

a higher probability to impact the protein structure and function [28].

The Site Direct Mutator (SDM) algorithm was used to analyze the structural impact generated by accumulative mutations in the CYP2D6 tetramer. The variants were generated by incrementing each mutation in each monomer following the chain organization. SDM uses statistical potential energy function that predicts the effect of missenses mutation in the stability of proteins, and its output includes side-chain solvent accessibility that ranges from inaccessible (<17%) and partially accessible (17–43%) to accessible (>47%). It also gives a score of pseudo ΔΔG that measures the variation of free energy between unfolded and folded protein, thus, giving a prediction of protein stability and disease association in protein variants [29]. SDM do not distinguish the impact of the chain affected according to molecule assembly, only the cumulative effect according to the number of chains mutated in the 3D model.

Tridimensional analysis

The CYP2D6 crystallographic structure was used for structural prediction. 2F9Q file (Protein Database – PDB) corresponds to CYP2D6 tetramer of four identical chains (A–D) containing 479 residues in each one, with 3.0 Å resolution. This 3D structure initiates at residue 34 and lacks the residues 42–51, but is the only one available for CYP2D6 without substrate or inhibitor. PyMOL (The PyMOL Molecular Graphics System, Version 1.7.4, Schrödinger, LLC, NY, USA) was used to observe the 3D structure of CYP2D6 and also to generate the variants models to analyze the cumulative effect of each mutation through SDM.

Results

*CYP2D6*7* poor metabolizer showed only one missense mutation, described as the cause of enzyme inactivation. The polymorphism 2935A>C, present only in this allele, occurs in exon 6 resulting in H324P mutation. *CYP2D6*14A* allele shows the same phenotype caused by four missenses mutations, each one in a different exon. R296C and S486T are well distributed in all metabolizer phenotypes; while G169R is present only in *CYP2D6*14A*. P34S mutation is present in both intermediate and poor metabolizers phenotypes.

Figure 1 represents the CYP2D6 3D structure, showing the catalytic site and the point of each mutation for *CYP2D6*7* and *CYP2D6*14A*. Table 2 shows the algorithms prediction output for the effect of each mutation in *CYP2D6*7* and *CYP2D6*14A* over protein stability and function. Table 3 shows the SDM data output related to each mutation and the cumulative effect of the mutation in more than one chain.

Allele *CYP2D6*7*

The substitution of a polar for a nonpolar amino acid leads to an extreme change in the hydrophobicity degree, ranging from 0.165 for Histidine to 0.711 for Proline. For H324P mutation, the structural algorithms SNPeffect and MuPro predict a decrease in enzyme stability. SDM predictions show a great loss in solvent accessibility when Proline is replaced by Histidine, changing from partially accessible to a

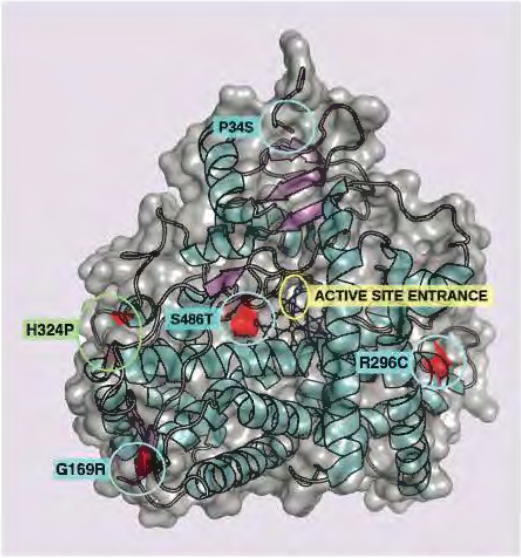

Figure 1. CYP2D6 3D structure showing the active site entrance (yellow) with the heme group; the H324P mutation carried by *CYP2D6*7* (green) and the set of mutations for the allele *CYP2D6*14A* (blue).

buried condition in the molecule, with around 22% overall reduction. The presence of H324P in only one CYP2D6 chain leads to a molecular destabilization, but its accumulation in other chains increases this impact. SDM prediction is related to the decrease of pseudo ΔΔG, leading to an increased deleterious effect that could be associated with the enzyme dysfunction.

SNPs&GO, SNAP2 and MutPred, all algorithms for functional prediction, also showed deleterious effect of H324P. MutationTaster2 analysis showed association with disease due to the functional impact; with Phylo-P conservation full score 1.00 indicating this mutation occurs in a conserved region, leading to high functional impact.

The Proline is an imino acid that imposes severe restriction on angles accessible to the pre-proline residues in the sequence. The CY2PD6 present another proline in position 325, therefore, this mutation occurs in a two residues junction region connecting J-helix and I-helix. The I-helix contains six residues (L302, A305, G306, T309, T310 and T313) composing the P450 active site pocket (Figure 2). So, this new restriction certainly reduces the states accessible to the backbone for 324-'PP'-325, consequently, restricting the relative position freedom of I-helix and J-helix.

Allele CYP2D6*14A

P34S mutation showed no effect on CYP2D6 stability according to SNPeffect while MuPro prediction showed an increase of CYP2D6 structural stability (Supplementary Table 1). SDM also predicted mutation effect, due to the increase of pseudo ΔΔG, but only when P34S occurs in two or more chains. This mutation results in additional H-bond between the Ser34 in the loop and Ser70 in a β-sheet when Proline is substituted by the Serine (Figure 3). Phylo-P conservation output showed the highest score, indicating P34S functional impact prediction.

CYP2D6*14A G169R leads to a notable reduction in hydrophobicity degree once nonpolar glycine (0.501) is substituted for a polar arginine (0.000). SNPeffect and MuPro predicted a decrease in structural stability. SDM predicted an increase in solvent accessibility in 53%, with an increase in molecule destabilizing. Disease association occurs only when G169R is present in two or more chains. All functional algorithms predict damage, with a very confident hypothesis of gain of solvent accessibility ($p = 0.0037$) according to MutPred. G169R mutation shows the great importance for CYP2D6 stability, probably due to its presence in a monomer interface region (Figure 4), which could difficult the tetramer assembly.

*CYP2D6*14A* R296C polymorphism showed no effect on molecule structure according to SNPeffect while MuPro predicted the destabilizing effect of this mutation. SDM predicts high stabilizing effect with disease association even when the mutation is present

Table 2. Algorithms predictions for missenses mutations in *CYP2D6*7* and *CYP2D6*14A* alleles.

ID	Allele	Exon	AA change	CYPalleles (M333.88)	SNPeffect	MuPro	MutPred	SNAP2	SNPs&GO	Mutation Taster2 (Phylo-P)
rs5030867	*7	6	H324P	2935A>C	1	1	1	1	1	1
rs1065852	*14A	1	P34S	100C>T	0	1	1	1	1	1
rs5030865	*14A	3	G169R	1758G>A	1	1	1	1	1	0
rs16947	*14A	6	R296C	2850C>T	0	1	0	0	0	ND
rs1135840	*14A	9	S486T	4180G>C	0	0	0	0	0	ND

Deleterious predictions are classified as 1, and null variant are classified as 0, following the established threshold.
ND: Not determined.

Table 3. SDM outputs for amino acids solvent accessibility is showed in percentage. A is for accessible; P for partially accessible and B is for buried or inaccessible. The prediction for disease association is represented as 1 for disease-associated, and 0 for non-disease associated, following the established threshold.

Missenses mutations	Number of mutated chains	Amino acid solvent accessibility	Amino acid Δ solvent accessibility (%)	Pseudo ΔΔG	Prediction	
					Stability	Disease
H324P	Wild-type	35.95% (P)				
	1	13.9% (B)	-21.9	-1.68	Destabilizing	0
	2	12.8% (B)	-23.7	-3.35	Highly destabilizing	1
	3	12.1% (B)	-24	-5.03	Highly destabilizing	1
	4	13.4% (B)	-22	-6.71	Highly destabilizing	1
P34S	Wild-type	25.17% (P)				
	1	16.6% (B)	-7.6	1.57	Stabilizing	0
	2	15.2% (B)	-6.7	2.07	Highly stabilizing	1
	3	18.1% (B)	-8.6	9.96	Highly stabilizing	1
	4	17.3% (B)	-3.4	9.78	Highly stabilizing	1
G169R	Wild-type	13.85% (B)				
	1	66.1% (A)	53	-1.82	Destabilizing	0
	2	72.5% (A)	57.7	-3.65	Highly destabilizing	1
	3	66.4% (A)	51.5	-5.47	Highly destabilizing	1
	4	71.9% (A)	59.3	-7.3	Highly destabilizing	1
R296C	Wild-type	27.55% (P)				
	1	12.1% (B)	-15.6	2.47	Highly stabilizing	1
	2	11.9% (B)	-16.8	4.93	Highly stabilizing	1
	3	11.7% (B)	-14.4	7.4	Highly stabilizing	1
	4	11.5% (B)	-16.8	9.86	Highly stabilizing	1
S486T	Wild-type	52.37% (A)				
	1	47.4% (P)	-4	0.97	Slightly stabilizing	0
	2	54.3% (P)	1	1.94	Stabilizing	0
	3	47.8% (P)	-4	2.91	Highly stabilizing	1
	4	55.7% (P)	2.7	3.88	Highly stabilizing	1

SDM outputs for amino acids solvent accessibility is showed in percentage. The prediction for disease association is represented as 1 for disease-associated, and 0 for non-disease associated, following the established threshold.
Δ: Variation; A: Accessible; B: Buried or inaccessible; P: Partially accessible.

Figure 2. Polymorphism H324P from *CYP2D6*7* found between helixes J and I. The wild residue histidine is presented in dark blue, the mutated amino acid proline appears in light blue. Heme group is represented in green near to I-helix extremity.

in only one chain. It may appear counterintuitive that increased protein stability can lead to protein malfunction. However, according to SDM authors, protein flexibility is essential for enzyme catalysis. MutPred also predicted R296C as low probability of causing loss of enzyme function but pointed an actionable hypothesis to cause loss of disorder (p = 0.0411). SNPs&GO and SNAP2 showed no effect of R296C over protein function.

*CYP2D6*14A* S486T shows no structural damage according to SNPeffect. Despite MuPro predicted the increase of structural stability; the result has low confidence score (Supplementary Table 1). SDM output shows disease association, but only if the mutation occurs in at least three chains, increasing structure stabilization due to S486T accumulation. No functional effect was found for this mutation.

Discussion

CYP2D6 is a clinically important enzyme that metabolizes numerous therapeutic drugs. The enzyme is responsible for the oxidative metabolism of up to 25% of commonly prescribed drugs such as antidepressants, antipsychotics, opioids, antiarrhythmics and tamoxifen. The ultra-rapid metabolizer phenotype is recognized as a cause of therapeutic inefficacy of antidepressant, whereas an increased risk of toxicity has been reported in poor metabolizers with several psychotropics. However, conflicting results have been reported regarding the association between *CYP2D6* genotype and tamoxifen effects. In this way, the *CYP2D6* genotyping may be useful in selecting an adjuvant hormonal therapy in postmenopausal women [34]. The present study provides *in silico* analysis regarding functional alterations of *CYP2D6*7* and *CYP2D6*14A* variant proteins. To assess the effects of *CYP2D6* variant allele's, algorithms were applied to the wild and mutant sequence/structure.

*CYP2D6*7* was first described by Evert *et al.* (1994), so-called mutation 'E.' The author suggested that H324P occurs near to the active site and also associates this mutation to a complete loss of enzyme function [35]. Later, the same author performed tests with recombinant DNA proving the null activity of H324P variant once it prevents the correct folding and the incorporation of heme group to CYP2D6 [36]. The expression of H324P mutation by recombinant baculovirus results in a protein that was practically insoluble, thus demonstrating that it also strongly influences subcellular localization of recombinant synthesized *CYP2D6*7* [36]. In our analysis, this structural/functional effect of H324P showed to be due to mutation occurrence in a high-conserved amino acid. This fact leads to the reduction of flexibility in the α-helix involved in the stabilization of heme group, extending it impact to the active site dynamics.

The effect of H324P over the molecule seems to be so relevant that it is the only mutation described for *CYP2D6*7*. By another side, *CYP2D6*7* seems to be either absent or rare allele, according to the population studied. Among 112 Hungarian individuals the frequency for *CYP2D6*7* was 0.4% [37], while among 165 Caucasian women of Geneva the frequency was

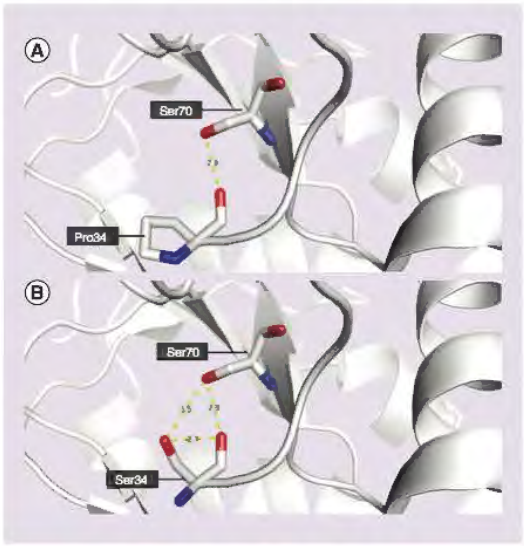

Figure 3. 3D representation of mutated CYP2D6 protein with P34S polymorphism from *CYP2D6*14A* allele. In Figure 3A is presented the wild Proline-34 residue making an H-bond (yellow) with Serine-70. Figure 3B shows the mutated residue 34 with Serine substitution and the additional H-bond added upon polymorphism. Supplementary Table 1: Algorithms original outputs without any threshold applied.

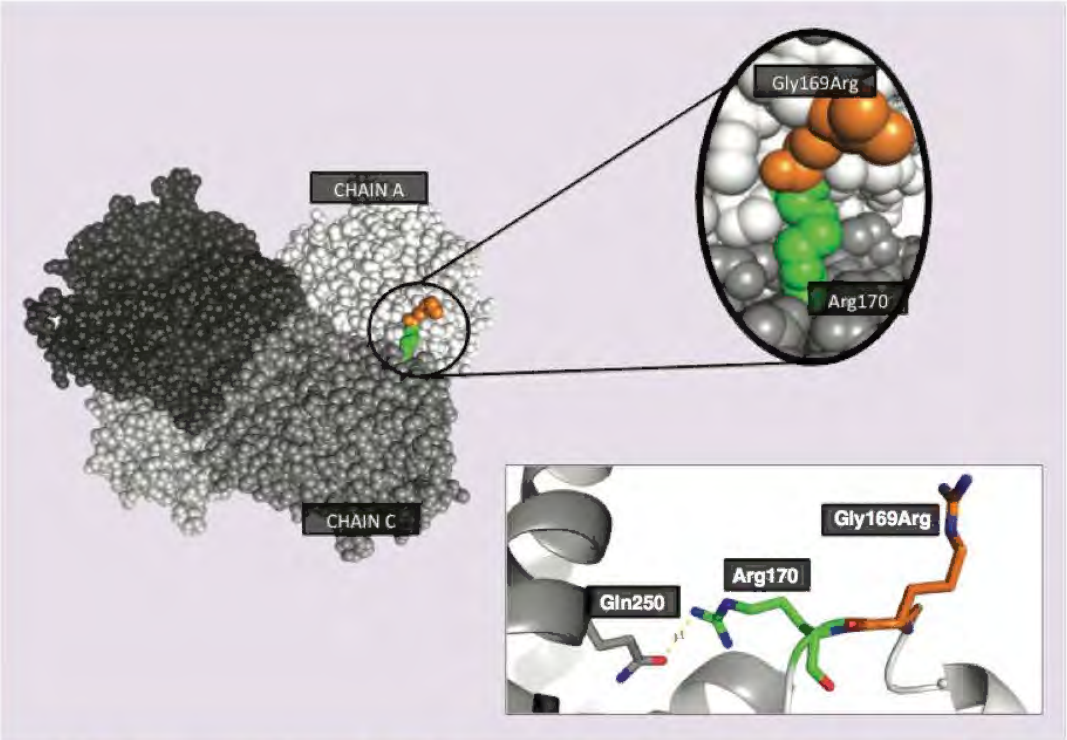

Figure 4. 3D representation of mutated CYP2D6 protein with G169R polymorphism from *CYP2D6*14A* allele. The replacement of a glycine for an arginine (orange) in position 169 occurs in the interface region between chains A and C. The Arginine-170 (green) in chain A, contributes to tetramer stabilization through an H-bond formation with Glutamine-250 from chain C.

0.3% [38]. No frequency was observed in 264 Mexican American [39], 105 Spanish [40] and 323 German Caucasian [41] individuals. Since there are few reports about *CYP2D6*7*, the frequency in the multiracial population is not well reported neither its influence in breast cancer treatment.

The *CYP2D6*14* allele has two subtypes. *CYP2D6*14A* carries the P34S, G169R, R296C and S486T substitutions and reports only detectable activity while *CYP2D6*14B* carries G169R, R296C and S486T missenses substitutions, which results in high enzyme activity. These data suggest that the relatively high activity of *CYP2D6*14B* may be attributed mainly to the absence of the P34S substitution [42]. Regarding this mutation, the presence of Serine tends to reverse the enhanced flexibility, given that it removes the typical proline restrictions on backbone angles.

According to SDM, P34S increases the stability of the enzyme in such a way that causes loss of function. Experimental analysis showed that the decrement in metabolic activity by G169R mutation is not dramatic as P34S mutation [43]. Information theory-based analysis also predicted G169R to be leaky and to be consistent with decreased (but not totally abolished) mRNA production, once its presence at the end of exon 3 reduces splice site use at least eightfold [44]. R296C mutation generates a loss disorder, despite no great deleterious effect can be observed.

This result was also observed in cloning experiments in *Escherichia coli* resulting in <10% of enzyme activity [45]. However, experimental tests with eukaryotic cells, which have a better protein folding, could be performed to understand its influence in the enzyme active site. By another side, cloning experiments for S486T in eukaryotic cells showed no consequence for CYP2D6 function [46], as we observed in our analysis.

*CYP2D6*14* allele showed to be more frequent in the Asian population, with 1.4% in 295 Chinese individuals [47] and 2.2% in 162 Japanese [48]. However, among 90 individual from Sri Lanka (Sinhalese, Tamils and Moors), no *CYP2D6*14* was found [49]. No frequency was observed in Mexican–American [39], Spanish [40] and Saudi Arabian populations [50]. The combination of G169R with P34S, R296C and S486T mutations may have further diminished the metabolic activity of CYP2D6 [43], and would be very interesting to perform *in silico* tests for the possible additive effect of these four mutation sites in the same molecule.

Conclusion

In silico analysis have shown evidence that missenses mutations in *CYP2D6*7* and *CYP2D6*14A* cause CYP2D6 dysfunction. We demonstrated that conformational 3D alterations were responsible for the CYP2D6 malfunction that leads to tamoxifen underperformance. Further analysis should be performed to all *CYP2D6* alleles associated with poor metabolizer phenotype to improve the pharmacogenomics application in breast cancer therapy.

Future perspective

CYP2D6 is an emerging biomarker that has been extensively investigated, but current guidelines do not recommend routine genetic testing of it [51]. Even so, determining whether a patient will or not benefit from tamoxifen therapy is of paramount importance in the clinical course of cancer treatment. The ROCHE AmpliChip is the closest technology available to *CYP2D6* genotyping [38], but the cost is still too high that its use is limited. To allow the development of new devices for fast, precise and low-cost detection of *CYP2D6* polymorphisms is necessary to recognize the most important ones regarding poor metabolization phenotype. Toward to the near future, *CYP2D6* genotyping will be part of breast cancer routine treatment, and then new point-of-care devices will be used in hospitals and outpatient to guide and monitor the treatment.

Supplementary data

To view the supplementary data that accompany this paper, please visit the journal website at: www.futuremedicine.com/doi/full/10.2217/psg-2015-0003

Acknowledgements

The authors thank AM da Silva Neto for the contributions in the discussion and figures design. They also thank P Radivojac and coworkers for their support and availability in elucidating MutPred results.

Financial & competing interests disclosure

This work was supported by Pernambuco State Science and Technology Support Foundation (FACEPE). The authors have no other relevant affiliations or financial involvement with any organization or entity with a financial interest in or financial conflict with the subject matter or materials discussed in the manuscript apart from those disclosed.

No writing assistance was utilized in the production of this manuscript.

Executive summary

Background

- *CYP2D6* polymorphisms may be the cause of tamoxifen failure in breast cancer treatment.
- CYP2D6 is a high polymorphic enzyme from P450 cytochrome, responsible for metabolizing almost 25% of drugs.
- Tamoxifen is an antineoplastic prodrug for estrogen receptor positive breast cancer that depends on CYP2D6 to be metabolized and generate the active metabolites.
- Almost 50% of breast cancer patients do not benefit from tamoxifen treatment.

Methods

- *In silico* analysis were performed over *CYP2D6*7* and *CYP2D6*14A* poor metabolizer alleles mutations to access the impact of missenses mutation on protein stability and function.

Results

- The allele *CYP2D6*7* have only one mutation described; H324P predictions showed high deleterious impact on CYP2D6 structure and function.
- The allele *CYP2D6*14A* has four missenses mutations, and three of them are associated with loss of enzyme stability and function.

Conclusion

- This study was the first one to predict the structural impact of the missenses mutations on CYP2D6 catalysis. This information supports the hypothesis that *CYP2D6* can be a good marker for tamoxifen pharmacogenomics.

References

1 Ferlay J, Soerjomataram I, Ervik M *et al.* Breast cancer estimated incidence, mortality and prevalence worldwide in 2012. http://globocan.iarc.fr

2 Lumachi F, Santeufemia DA, Basso SM. Current medical treatment of estrogen receptor-positive breast cancer. *World J. Biol. Chem.* 6(3), 231–239 (2015).

3 Groenendijk FH, Bernards R. Drug resistance to targeted therapies: déjà vu all over again. *Mol. Oncol.* 8(6), 1067–1083 (2014).

4 Binkhorst L, Mathijssen RHJ, Jager A, van Gelder T. Individualization of tamoxifen therapy: much more than just *CYP2D6* genotyping. *Cancer Treat. Rev.* 41(3), 289–299 (2015).

5 Klein DJ, Thorn CF, Desta Z, Flockhart DA, Altman

RB, Klein TE. PharmGKB summary: tamoxifen pathway, pharmacokinetics. *Pharmacogenet. Genomics* 23(11), 1199–1216 (2013).

6 Zanger UM, Schwab M. Cytochrome P450 enzymes in drug metabolism: regulation of gene expression, enzyme activities, and impact of genetic variation. *Pharmacol. Ther.* 138(1), 103–141 (2013).

7 Rowland P, Blaney F, Smyth M *et al.* Crystal structure of human cytochrome P450 2D6. *J. Biol. Chem.* 281(11), 7614–7622 (2006).

8 Hertz DL, Snavely AC, McLeod HL *et al. In vivo* assessment of the metabolic activity of *CYP2D6* diplotypes and alleles. *Br. J. Clin. Pharmacol.* 80(5), 1122–1130 (2015).

9 The Human Cytochrome P450 (*CYP*) Allele Nomenclatre Database. www.cypalleles.ki.se/cyp2d6.htm

10 Chin FW, Chan SC, Abdul Rahman S, Noor Akmal S, Rosli R. *CYP2D6* genetic polymorphisms and phenotypes in different ethnicities of malaysian breast cancer patients. *Breast J.* 22(1), 54–62 (2015).

11 Province M, Goetz MP, Brauch H *et al. CYP2D6* genotype and adjuvant tamoxifen: meta-analysis of heterogeneous study populations. *Clin. Pharmacol. Ther.* 95(2), 216–227 (2014).

12 Goetz MP, Suman VJ, Hoskin TL *et al.* CYP2D6 metabolism and patient outcome in the Austrian Breast and Colorectal Cancer Study Group trial (ABCSG) 8. *Clin. Cancer Res.* 19(2), 500–507 (2013).

13 Schroth W, Goetz MP, Hamann U *et al.* Association between *CYP2D6* polymorphisms and outcomes among women with early stage breast cancer treated with tamoxifen. *JAMA* 302(13), 1429–1436 (2014).

14 Regan MM, Leyland-Jones B, Bouzyk M *et al. CYP2D6* genotype and tamoxifen response in postmenopausal women with endocrine-responsive breast cancer: The Breast International Group 1–98 trial. *J. Natl Cancer Inst.* 104(6), 441–451 (2012).

15 Rae JM, Drury S, Hayes DF *et al. CYP2D6* and *UGT2B7* genotype and risk of recurrence in tamoxifen-treated breast cancer patients. *J. Natl. Cancer Inst.* 104(6), 452–60 (2012).

16 Ruddy KJ, Desantis SD, Gelman RS *et al.* Personalized medicine in breast cancer: tamoxifen, endoxifen, and *CYP2D6* in clinical practice. *Breast Cancer Res. Treat.* 141, 421–427 (2013).

17 Cannataro M, Santos RW Dos, Sundnes J. Biomedical and bioinformatics challenges to computer science: bioinformatics, modeling of biomedical systems and clinical applications. *Procedia Comput. Sci.* 4, 1058–1061 (2011).

18 Bellazzi R, Masseroli M, Murphy S, Shabo A, Romano P. Clinical bioinformatics: challenges and opportunities. *BMC Bioinformatics* 13(S14), 1471–2105 (2012).

19 Dong C, Wei P, Jian X *et al.* Comparison and integration of deleteriousness prediction methods for nonsynonymous SNVs in whole exome sequencing studies. *Hum. Mol. Genet.* 24(8), 2125–2137 (2015).

20 Frousios K, Iliopoulos CS, Schlitt T, Simpson M. Predicting the functional consequences of non-synonymous DNA sequence variants – evaluation of bioinformatics tools and development of a consensus strategy. *Genomics* 102(4), 223–228 (2013).

21 Fiser A. Template-based protein structure modeling. *Methods Mol. Biol.* 673, 73–94 (2010).

22 Leiden Open Variation Database. www.lovd.nl/3.0/home

23 De Baets G, Van Durme J, Reumers J *et al.* SNPeffect 4.0: on-line prediction of molecular and structural effects of protein-coding variants. *Nucleic Acids Res.* 40(D1), D935–D939 (2012).

24 Cheng J, Randall A, Baldi P. Prediction of protein stability changes for single-site mutations using support vector machines. *Proteins* 62(4), 1125–1132 (2006).

25 Li B, Krishnan VG, Mort ME *et al.* Automated inference of molecular mechanisms of disease from amino acid substitutions. *Bioinformatics* 25(21), 2744–2750 (2009).

26 Hecht M, Bromberg Y, Rost B. Better prediction of functional effects for sequence variants. *BMC Genomics.* 16(Suppl 8), S1 (2015).

27 Calabrese R, Capriotti E, Fariselli P, Martelli PL, Casadio R. Functional annotations improve the predictive score of human disease-related mutations in proteins. *Hum. Mutat.* 30(8), 1237–1244 (2009).

28 Schwarz JM, Cooper DN, Schuelke M, Seelow D. MutationTaster2: mutation prediction for the deep-sequencing age. *Nat Methods.* 11(4), 361–362 (2014).

29 Worth CL, Preissner R, Blundell TL. SDM – a server for predicting effects of mutations on protein stability and malfunction. *Nucleic Acids Res.* 39(Web Server issue), 215–222 (2011).

30 Ng PC, Henikoff S. Predicting deleterious amino acid substitutions. *Genome Res.* 11, 863–874 (2001).

31 Adzhubei Ia, Schmidt S, Peshkin L *et al.* A method and server for predicting damaging missense mutations. *Nat. Methods* 7(4), 248–249 (2010).

32 Thomas PD, Kejariwal A, Guo N *et al.* Applications for protein sequence-function evolution data: mRNA/protein expression analysis and coding SNP scoring tools. *Nucleic Acids Res.* 34(Web Server issue), 645–650 (2006).

33 Capriotti E, Calabrese R, Casadio R. Predicting the insurgence of human genetic diseases associated to single point protein mutations with support vector machines and evolutionary information. *Bioinformatics* 22(22), 2729–2734 (2006).

34 Samer CF, Lorenzini KI, Rollason V, Daali Y, Desmeules JA. Applications of CYP450 testing in the clinical setting. *Mol. Diagn. Ther.* 17(3), 165–184 (2013).

35 Evert B, Griese E, Eicheibaum M. A missense mutation in exon 6 of the CYP2D6 gene leading to a histidine 324 to proline exchange is associated with the poor metabolizer phenotype of sparteine. *Naunyn Schmiedebergs Arch. Pharmacol.* 350, 434–439 (1994).

36 Evert B, Eichelbaum M, Haubruck H, Zanger UM. Functional properties of CYP2D6 1 (wild-type) and CYPD26 7 (His324Pro) expressed by recombinant baculovirus in insect cells. *Naunyn Schmiedebergs Arch. Pharmacol.* 355(3), 309–318 (1997).

37 Rideg O, Háber A, Botz L *et al.* Pilot study for the characterization of pharmacogenetically relevant *CYP2D6, CYP2C19* and *ABCB1* gene polymorphisms in the Hungarian population. *Cell Biochem. Funct.* 29(7), 562–568 (2011).

38 Rebsamen MC, Desmeules J, Daali Y *et al.* The AmpliChip CYP450 test: cytochrome P450 2D6 genotype assessment and phenotype prediction. *Pharmacogenomics J.* 9(1), 34–41 (2009).

39 Luo H-R, Gaedigk A, Aloumanis V, Wan Y-JY. Identification of CYP2D6 impaired functional alleles in Mexican Americans. *Eur. J. Clin. Pharmacol.* 61(11), 797–802 (2005).

40 Menoyo A, del Rio E, Baiget M. Characterization of variant alleles of cytochrome *CYP2D6* in a Spanish population. *Cell Biochem. Funct.* 24(5), 381–385 (2006).

41 Stamer UM, Bayerer B, Wolf S, Hoeft A, Stüber F. Rapid and reliable method for cytochrome P450 2D6 genotyping. *Clin. Chem.* 48, 1412–1417 (2002).

42 Sakuyama K, Sasaki T, Ujiie S *et al.* Functional characterization of 17 *CYP2D6* allelic variants (CYP2D6.2, 10, 14A-B, 18, 27, 36, 39, 47–51, 53–55, and 57). *Pharmacology.* 36(12), 2460–2467 (2008).

43 Wang SL, Lai MD, Huang JD . G169R mutation diminishes the metabolic activity of CYP2D6 in Chinese. *Drug Metab. Dispos.* 27(3), 385–388 (1999).

44 Rogan PK, Svojanovsky S, Leeder JS. Information theory-based analysis of CYP2C19, CYP2D6 and CYP3A5 splicing mutations. *Pharmacogenetics* 13(4), 207–218 (2003).

45 Kim J, Lim Y-R, Han S *et al.* Functional influence of human *CYP2D6* allelic variations: P34S, E418K, S486T, and R296C. *Arch. Pharm. Res.* 36(12), 1500–1506 (2013).

46 Kagimoto M, Heim M, Kagimoto K, Zeugin T, Meyer U. Multiple mutations of the human cytochrome P450IID6 (CYP2D6) in poor metabolizers of debrisoquine. *J. Biol. Chem.* 265(26), 17209–17214 (1990).

47 Cai WM, Chen B, Zhang WX. Frequency of *CYP2D6*10* and *14 alleles and their influence on the metabolic activity of CYP2D6 in a healthy Chinese population. *Clin. Pharmacol. Ther.* 81(1), 95–98 (2007).

48 Nishida Y, Fukuda T, Yamamoto I, Azuma J. CYP2D6 genotypes in a Japanese population: low frequencies of *CYP2D6* gene duplication but high frequency of *CYP2D6*10. Pharmacogenetics* 10(6), 567–570 (2000).

49 Tharanga TD, Jinadasa CM, Risama MF, Galappatthy P, Jayakody RL, Dissanayake VH. Genetic variants in the cytochrome P450 2D6 gene in the Sri Lankan population. *Indian J. Hum. Genet.* 19(4), 392–396 (2013).

50 Al-Dosari MS, Al-Jenoobi FI, Alkharfy KM *et al.* High prevalence of *CYP2D6*41* (G2988A) allele in Sandi Arabians. *Environ. Toxicol. Pharmacol.* 36(3), 1063–1067 (2013).

51 Kalia M. Biomarkers for personalized oncology: recent advances and future challenges. *Metabolism* 64(3), S16–S21 (2015).

4.1 Material Suplementar

Supplementary Figure 1

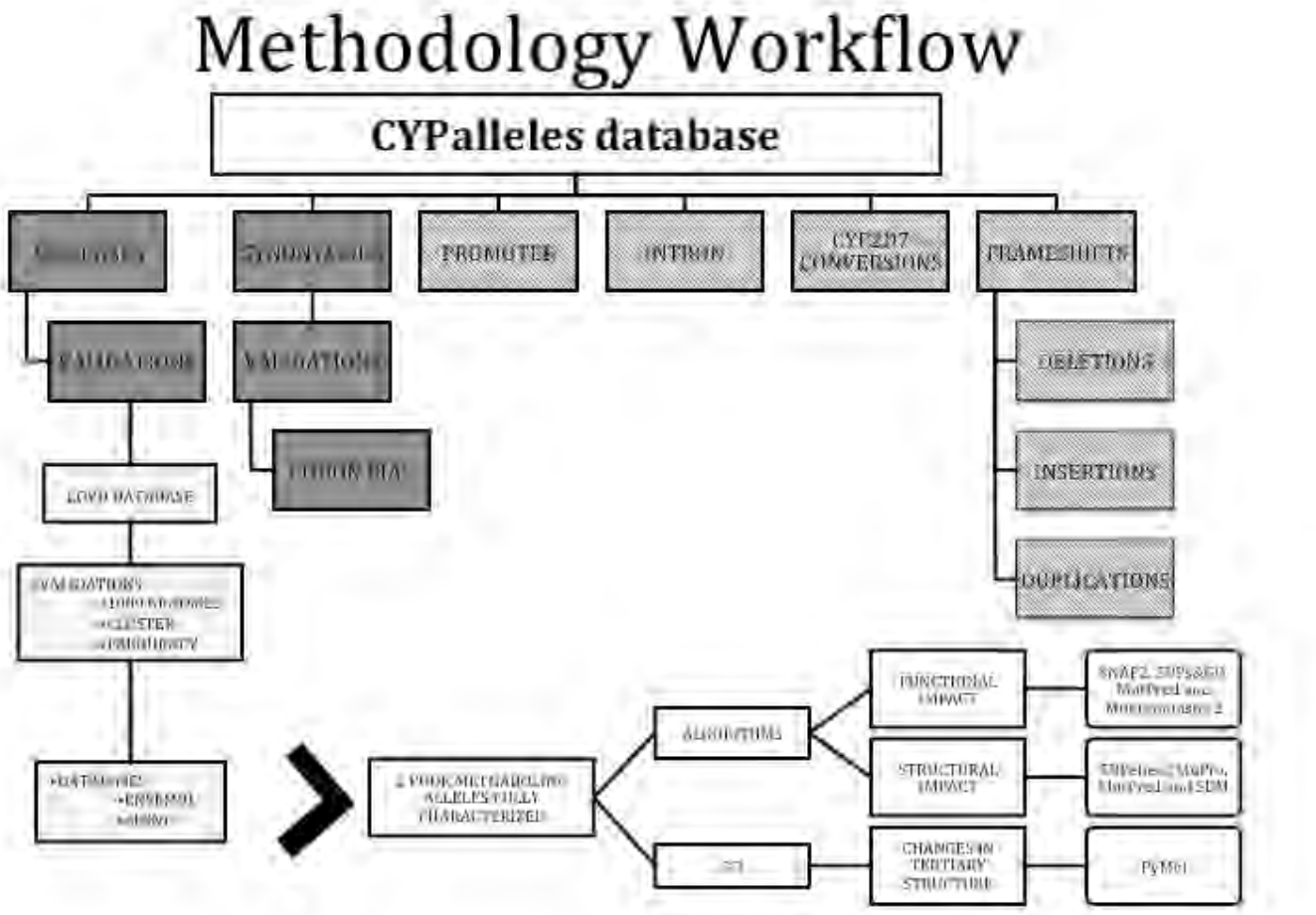

Supplementary Table 1: Algorithms original outputs without any threshold applied.

	SNPeffect		MutPred			MutPred		SNAP2		SNPs&GO output			MUTATION TASTER2		
	ΔΔG (kcal/mol)	FoldX prediction	Effect	Combined score	Score	Hypothesis	Prediction	Score	Accuracy	PREDICTION	RI	PROBABILITY	Score	PhastCons	PhyloP
H324P	5.75	Severe reduction	Decrease	-0.673 88892	0.701	Confident: Gain of catalytic residue at H324 (P = 0.0186)	Effect	79	85%	Disease	5	0.772	77	2.854	1
P34S	0.38	Null	Decrease	-0.982 78866	0.752	Actionable: Loss of catalytic residue at P34 (P=0.0091); Loss of glycosylation at P34 (P = 0.0373); Gain of loop (P = 0.0433)	Effect	66	80%	Disease	0	0.515	74	4.426	1
G169R	1.84	Reduction	Decrease	-0.11462576	0.883	Very Confident: Gain of solvent accessibility (P = 0.0037)	Effect	27	63%	Disease	5	0.766	125	0.797	0.419
R296C	-0.31	Null	Decrease	-0.936 25891	0.595	Actionable: Loss of disorder (P = 0.0411)	Neutral	-69	82%	Neutral	7	0.157	ND	ND	ND
S486T	0.42	Null	Increase	0.17381188	0.291	-	Neutral	-98	97%	Neutral	9	0.033	ND	ND	ND

CONCLUSÕES

Esta tese teve sua fundamentação na medicina de precisão e o seu objetivo principal foi demonstrar como diferentes abordagens para prospecção molecular podem ser empregadas para o estudo de potenciais marcadores moleculares na oncologia. Ao longo dos cinco capítulos que constituem o corpo deste trabalho foi demonstrada importância do desenvolvimento de novas tecnologias para viabilizar a implementação da medicina de precisão, baseada na individualidade de cada paciente. Através do relato de caso de hepatocarcinoma exemplificamos como o acesso ao perfil genômico do paciente pode impactar na tomada de decisão clínica, podendo afetar o desfecho médico, como no caso apresentado.

Outra abordagem utilizada foi o uso de ferramentas *in silico* para avaliar o impacto de mutações genéticas no metabolismo do tamoxifeno, pilar do tratamento endócrino do câncer de mama. Neste capítulo demonstramos que, através da combinação de diferentes métodos de análises computacionais, é possível determinar o impacto de mutações na prática da oncologia clínica, permitindo o desenho de medicamentos mais eficientes e o desenvolvimento de ferramentas preditivas mais eficientes.

REFERÊNCIAS

ABDULJABBAR, R. et al. Prognostic and biological significance of peroxisome proliferator-activated receptor-gamma in luminal breast cancer. **Breast Cancer Research and Treatment**, v. 150, n. 3, p. 511–522, 1 abr. 2015.

AHMAD, I. et al. Sleeping beauty screen reveals Pparg activation in metastatic prostate cancer. **Proceedings of the National Academy of Sciences of the United States of America**, v. 113, n. 29, p. 8290–8295, 19 jul. 2016.

ANDRISIC, L. et al. Short overview on metabolomics approach to study pathophysiology of oxidative stress in cancer. **Redox Biology**, v. 14, n. August 2017, p. 47–58, 2018.

ARAÚJO, T. et al. Classification of breast cancer histology images using Convolutional Neural Networks. **PLOS ONE**, v. 12, n. 6, p. e0177544, 1 jun. 2017.

ARNEDOS, M. et al. Precision medicine for metastatic breast cancer-limitations and solutions. **Nature Reviews Clinical Oncology**, v. 12, n. 12, p. 693–704, 2015.

AYUSO, C. et al. Diagnosis and staging of hepatocellular carcinoma (HCC): current guidelines. **European Journal of Radiology**, v. 101, p. 72–81, 2018.

AYYASAMY, V. et al. Cellular model of Warburg Effect identifies tumor promoting function of UCP2 in breast cancer and its suppression by genipin. **PLoS ONE**, v. 6, n. 9, p. e24792, 15 set. 2011.

BADVE, S. et al. Basal-like and triple-negative breast cancers: a critical review with an emphasis on the implications for pathologists and oncologists. **Modern Pathology**, v. 24, n. 2, p. 157–167, 2011.

BAFFY, G. Hanging in the balance: mitochondrial uncoupling protein-2 and the tumor microenvironment. **Precision Cancer Medicine**, v. 2, p. 12–12, 2019.

BAGLIA, M. L. et al. Alcohol, smoking, and risk of Her2-overexpressing and triple-negative breast cancer relative to estrogen receptor-positive breast cancer. **International Journal of Cancer**, v. 143, n. 8, p. 1849–1857, 2018.

BAKER, S. et al. Cancer Hallmarks Analytics Tool (CHAT): A text mining approach to organize and evaluate scientific literature on cancer. **Bioinformatics**, v. 33, n. 24, p. 3973–3981, 15 dez. 2017.

BARTLETT, A.; PENDERS, B.; LEWIS, J. Bioinformatics: Indispensable, yet hidden in plain sight? **BMC Bioinformatics**, v. 18, n. 1, p. 1–4, 2017.

BAUGHER, P. J. et al. Rac1 and Rac3 isoform activation is involved in the invasive

and metastatic phenotype of human breast cancer cells. **Breast cancer research : BCR**, v. 7, n. 6, p. R965-74, 30 dez. 2005.

BAUMANN, P. **CYP2D6: Genetics, Pharmacology and Clinical Relevance**. London: Future Medicine, 2015. v. 1

BORDONE, L. et al. Sirt1 Regulates Insulin Secretion by Repressing UCP2 in Pancreatic β Cells. **PLoS Biology**, v. 4, n. 2, p. e31, 27 dez. 2005.

BRAY, F. et al. Global cancer statistics 2018: GLOBOCAN estimates of incidence and mortality worldwide for 36 cancers in 185 countries. **CA: A Cancer Journal for Clinicians**, 12 set. 2018.

BRUFSKY, A. M.; DICKLER, M. N. Estrogen Receptor-Positive Breast Cancer: Exploiting Signaling Pathways Implicated in Endocrine Resistance. **The Oncologist**, v. 23, n. 5, p. 528–539, maio 2018.

BRUIX, J.; REIG, M.; SHERMAN, M. Evidence-Based Diagnosis, Staging, and Treatment of Patients with Hepatocellular Carcinoma. **Gastroenterology**, v. 150, n. 4, p. 836–853, 2016.

CALDERARO, J. et al. Histological subtypes of hepatocellular carcinoma are related to gene mutations and molecular tumour classification. **Journal of Hepatology**, v. 67, n. 4, p. 727–738, 2017.

CALEFFI, M. et al. The AMAZONA Project: Retrospective Cohort Study Describing Breast Cancer Patients' Characteristics and Survival in Brazil. **Journal of Global Oncology**, n. 4_suppl_2, p. 219s-219s, out. 2018.

CARAFA, V.; ALTUCCI, L.; NEBBIOSO, A. Dual tumor suppressor and tumor promoter action of sirtuins in determining malignant phenotype. **Frontiers in Pharmacology**, v. 9, n. JAN, 2019.

CARDOSO, F. et al. 70-Gene Signature as an Aid to Treatment Decisions in Early-Stage Breast Cancer. **New England Journal of Medicine**, v. 375, n. 8, p. 717–729, 2016.

CHALKIADAKI, A.; GUARENTE, L. The multifaceted functions of sirtuins in cancer. **Nature Reviews Cancer**, v. 15, n. 10, p. 608–624, 2015.

CHO, H. Y. et al. Nrf2-regulated PPARγ expression is critical to protection against acute lung injury in mice. **American Journal of Respiratory and Critical Care Medicine**, v. 182, n. 2, p. 170–182, 2010.

CUADRADO, A. et al. Transcription factors NRF2 and NF-κB are coordinated effectors of the rho family, GTP-binding protein RAC1 during Inflammation. **Journal of**

Biological Chemistry, v. 289, n. 22, p. 15244–15258, 30 maio 2014.

DAI, H. et al. Sirtuin activators and inhibitors: Promises, achievements, and challenges. **Pharmacology and Therapeutics**, v. 188, p. 140–154, 2018.

DANESHMANDI, S.; WEGIEL, B.; SETH, P. Blockade of Lactate Dehydrogenase-A (LDH-A) Improves Efficacy of Anti-Programmed Cell Death-1 (PD-1) Therapy in Melanoma. **Cancers**, v. 11, n. 4, p. 450, 29 mar. 2019.

DE CASTRO, D. G. et al. Personalized Cancer Medicine: Molecular Diagnostics, Predictive biomarkers, and Drug Resistance. **Clinical Pharmacology and Therapeutics**, v. 93, n. 3, p. 252–259, 2013.

DE SANTIS, M. C. et al. Signaling Pathways Regulating Redox Balance in Cancer Metabolism. **Frontiers in Oncology**, v. 8, n. April, 2018.

DEBERARDINIS, R. J.; CHANDEL, N. S. Fundamentals of cancer metabolism. **Science advances**, v. 2, n. 5, p. e1600200, 1 maio 2016.

DERDAK, Z. et al. The mitochondrial uncoupling protein-2 promotes chemoresistance in cancer cells. **Cancer Research**, v. 68, n. 8, p. 2813–2819, 15 abr. 2008.

DESANTIS, C. E. et al. Breast cancer statistics, 2017, racial disparity in mortality by state. **CA: A Cancer Journal for Clinicians**, v. 67, n. 6, p. 439–448, 1 nov. 2017.

DING, X.-X. et al. Precision medicine for hepatocellular carcinoma: driver mutations and targeted therapy. **Oncotarget**, v. 8, n. 33, p. 55715–55730, 2017.

DOKMANOVIC, M. et al. Rac1 contributes to trastuzumab resistance of breast cancer cells: Rac1 as a potential therapeutic target for the treatment of trastuzumab-resistant breast cancer. **Molecular Cancer Therapeutics**, v. 8, n. 6, p. 1557–1569, 2009.

DU, J. et al. PI3K and ERK-Induced Rac1 Activation Mediates Hypoxia-Induced HIF-1α Expression in MCF-7 Breast Cancer Cells. **PLoS ONE**, v. 6, n. 9, p. e25213, 27 set. 2011.

ELKHWANKY, M. S.; HAKKOLA, J. Extranuclear Sirtuins and Metabolic Stress. **Antioxidants and Redox Signaling**, v. 28, n. 8, p. 662–676, 2018.

FANDO, R.; KLAVDIEVA, M. Bioinformatics: Past and Present. **2018 International Conference on Engineering Technologies and Computer Science (EnT)**, p. 34–36, 2018.

FENG, Y. et al. **Breast cancer development and progression: Risk factors, cancer stem cells, signaling pathways, genomics, and molecular pathogenesisGenes and Diseases**Chongqing yi ke da xue, di 2 lin chuang xue yuan Bing du xing gan yan yan jiu suo, , 1 jun. 2018.

FLORES, M. et al. P4 medicine: how systems medicine will transform the healthcare sector and society. **Personalized Medicine**, v. 10, n. 6, p. 565–576, 2013.

FRANCKE, U. How will genomic information become integrated into the health care system? **Molecular Genetics & Genomic Medicine**, v. 1, n. 2, p. 67–70, 2013.

FROUSIOS, K. et al. Predicting the functional consequences of non-synonymous DNA sequence variants - evaluation of bioinformatics tools and development of a consensus strategy. **Genomics**, v. 102, n. 4, p. 223–228, 2013.

FUJIMOTO, A. et al. Whole-genome mutational landscape and characterization of noncoding and structural mutations in liver cancer. **Nature Genetics**, v. 48, n. 5, p. 500–509, 1 maio 2016.

GERMAN, N. J.; HAIGIS, M. C. Sirtuins and the Metabolic Hurdles in Cancer. **Current Biology**, v. 25, n. 13, p. R569–R583, 2015.

GODONE, R. L. N. et al. Clinical and molecular aspects of breast cancer: Targets and therapies. **Biomedicine and Pharmacotherapy**, v. 106, n. January, p. 14–34, 2018.

GOLDSTEIN, J. T. et al. Genomic activation of PPARG reveals a candidate therapeutic axis in bladder cancer. **Cancer Research**, v. 77, n. 24, p. 6987–6998, 2017.

GONG, M. T. et al. Comprehensive integrated analysis of gene expression datasets identifies key anti-cancer targets in different stages of breast cancer. **Experimental and Therapeutic Medicine**, v. 16, n. 2, p. 802–810, 1 ago. 2018.

GORRINI, C. et al. Estrogen controls the survival of BRCA1-deficient cells via a PI3K-NRF2-regulated pathway. **Proceedings of the National Academy of Sciences of the United States of America**, v. 111, n. 12, p. 4472–7, 25 mar. 2014.

GRADISHAR, W. J. et al. **NCCN Guidelines Version 3.2019 Breast Cancer**. [s.l: s.n.].

GROENENDIJK, F. H.; BERNARDS, R. Drug resistance to targeted therapies: déjà vu all over again. **Molecular oncology**, v. 8, n. 6, p. 1067–83, 2014.

GRONDE, T. VAN DER; UYL-DE GROOT, C. A.; PIETERS, T. **Addressing the challenge of high-priced prescription drugs in the era of precision medicine: A systematic review of drug life cycles, therapeutic drug markets and regulatory frameworks**. [s.l: s.n.]. v. 12

GUERRERO-ZOTANO, A.; MAYER, I. A.; ARTEAGA, C. L. PI3K/AKT/mTOR: role in breast cancer progression, drug resistance, and treatment. **Cancer and Metastasis Reviews**, v. 35, n. 4, p. 515–524, 1 dez. 2016.

GUL, A. et al. A combination of the PI3K pathway inhibitor plus cell cycle pathway

inhibitor to combat endocrine resistance in hormone receptor-positive breast cancer: a genomic algorithm-based treatment approach. **American journal of cancer research**, v. 8, n. 12, p. 2359–2376, 2018.

HAMAZAKI, T. et al. Concise Review: Induced Pluripotent Stem Cell Research in the Era of Precision Medicine. **STEM CELLS**, v. 35, n. 3, p. 545–550, mar. 2017.

HANAHAN, D.; WEINBERG, R. A. The hallmarks of cancer. **Cell**, v. 100, n. 1, p. 57–70, 7 jan. 2000.

HANAHAN, D.; WEINBERG, R. A. Hallmarks of cancer: the next generation. **Cell**, v. 144, n. 5, p. 646–74, 4 mar. 2011.

HAYES, J. D.; DINKOVA-KOSTOVA, A. T. The Nrf2 regulatory network provides an interface between redox and intermediary metabolism. **Trends in Biochemical Sciences**, v. 39, n. 4, p. 199–218, 2014.

HERBST, R. S.; MORGENSZTERN, D.; BOSHOFF, C. The biology and management of non-small cell lung cancer. **Nature**, v. 553, n. 7689, p. 446–454, 2018.

HOLM, J. et al. Assessment of Breast Cancer Risk Factors Reveals Subtype Heterogeneity. **Cancer Research**, v. 77, n. 13, p. 3708–3717, 1 jul. 2017.

HOOD, L. et al. Systems biology and new technologies enable predictive and preventative medicine. **Science**, v. 306, n. 5696, p. 640–643, 2004.

HOOD, L.; BALLING, R.; AUFFRAY, C. Revolutionizing medicine in the 21st century through systems approaches. **Biotechnology Journal**, v. 7, n. 8, p. 992–1001, 2012.

HORVATH, B. et al. Uncoupling protein 2 (UCP2) lowers alcohol sensitivity and pain threshold. **Biochemical Pharmacology**, v. 64, n. 3, p. 369–374, 1 ago. 2002.

IMAI, K. et al. UCP2 expression may represent a predictive marker of neoadjuvant chemotherapy effectiveness for locally advanced uterine cervical cancer. **Oncology Letters**, v. 14, n. 1, p. 951–957, 2017.

INSTITUTO NACIONAL DE CANCER JOSÉ ALENCAR GOMES DA SILVA, I. **Estima 2018: Incidência de Câncer no Brasil**. [s.l: s.n.].

ISHII, T.; WARABI, E. Mechanism of rapid nuclear factor-e2-related factor 2 (Nrf2) activation via membrane-associated estrogen receptors: Roles of NADPH oxidase 1, neutral sphingomyelinase 2 and epidermal growth factor receptor (EGFR). **Antioxidants**, v. 8, n. 3, p. 1–17, 2019.

JANANI, C.; RANJITHA KUMARI, B. D. **PPAR gamma gene - A reviewDiabetes and Metabolic Syndrome: Clinical Research and Reviews**Elsevier Ltd, , 1 jan. 2015.

JESELSOHN, R. et al. **ESR1 mutations-a mechanism for acquired endocrine**

resistance in breast cancerNature Reviews Clinical Oncology Nature Publishing Group, , 24 out. 2015.

KALLIORA, C. et al. Dual PPARα/γ activation inhibitsSIRT1-PGC1α axis and causes cardiac dysfunction. **JCI Insight**, v. 4, n. 17, 5 set. 2019.

KANDOI, G.; ACENCIO, M. L.; LEMKE, N. Prediction of Druggable Proteins Using Machine Learning and Systems Biology: A Mini-Review. **Frontiers in Physiology**, v. 6, n. December, 2015.

KATO, M. Bioinformatics in Cancer Clinical Sequencing - An Emerging Field of Cancer Personalized Medicine. **Gan to kagaku ryoho. Cancer & chemotherapy**, v. 43, n. 4, p. 391–7, abr. 2016.

KAUSHIK, A. K.; DEBERARDINIS, R. J. Applications of metabolomics to study cancer metabolism. **Biochimica et Biophysica Acta - Reviews on Cancer**, v. 1870, n. 1, p. 2–14, 2018.

KAWANISHI, M. et al. Expression of UCP2 is associated with sensitivity to platinum-based chemotherapy for ovarian serous carcinoma. **Oncology Letters**, v. 15, n. 6, p. 9923–9928, 1 jun. 2018.

KIDA, Y.; GOLIGORSKY, M. S. Sirtuins, Cell Senescence, and Vascular Aging. **Canadian Journal of Cardiology**, v. 32, n. 5, p. 634–641, 2016.

KIM, C. et al. Chemoresistance Evolution in Triple-Negative Breast Cancer Delineated by Single-Cell Sequencing. **Cell**, v. 173, n. 4, p. 879- 893.e13, 3 maio 2018.

KIM, J. et al. Functional influence of human CYP2D6 allelic variations: P34S, E418K, S486T, and R296C. **Archives of pharmacal research**, v. 36, n. 12, p. 1500–6, 2013.

KONG, H.; CHANDEL, N. S. **Reactive oxygen species and cancer**. [s.l.] Elsevier Inc., 2020a.

KONG, H.; CHANDEL, N. S. Reactive oxygen species and cancer. In: SIES, H. (Ed.). . **Oxidative Stress**. [s.l.] Academic Press, 2020b. v. 8p. 619–637.

KULKARNI, S. R. et al. Fasting induces nuclear factor E2-related factor 2 and ATP-binding cassette transporters via protein kinase a and sirtuin-1 in mouse and human. **Antioxidants and Redox Signaling**, v. 20, n. 1, p. 15–30, jan. 2014.

KULKOYLUOGLU-COTUL, E.; ARCA, A.; MADAK-ERDOGAN, Z. **Crosstalk between Estrogen Signaling and Breast Cancer MetabolismTrends in Endocrinology and Metabolism**Elsevier Inc., , 1 jan. 2019.

KUMAR, A. et al. Computational SNP analysis: current approaches and future prospects. **Cell biochemistry and biophysics**, v. 68, n. 2, p. 233–9, 2014.

KWON, D. N. et al. Oxidative stress and ROS metabolism via down-regulation of sirtuin 3 expression in Cmah-null mice affect hearing loss. **Aging**, v. 7, n. 8, p. 579–594, 2015.

LEE, I. H. Molecular Prognostic and Predictive Assays in Breast Cancer. **American Journal of Surgical Pathology: Review and Reports**, v. 21, n. 1, p. 4–10, 2016.

LIANG, B.; LI, C.; ZHAO, J. Identification of key pathways and genes in colorectal cancer using bioinformatics analysis. **Medical Oncology**, v. 33, n. 10, 1 out. 2016.

LITTON, J. K. et al. Talazoparib in Patients with Advanced Breast Cancer and a Germline *BRCA* Mutation. **New England Journal of Medicine**, v. 379, n. 8, p. 753–763, 23 ago. 2018.

LIU, B. et al. High expression of rac1 is correlated with partial reversed cell polarity and poor prognosis in invasive ductal carcinoma of the breast. **Tumor Biology**, v. 39, n. 7, p. 1–8, 3 jul. 2017.

LIU, P. H. et al. Prognosis of hepatocellular carcinoma: Assessment of eleven staging systems. **Journal of Hepatology**, v. 64, n. 3, p. 601–608, 1 mar. 2016.

LLOVET, J. M. et al. Molecular therapies and precision medicine for hepatocellular carcinoma. **Nature Reviews Clinical Oncology**, v. 15, n. 10, p. 599–616, 2018.

LOUBIÈRE, S. et al. Cost-effectiveness of KRAS, EGFR and ALK testing for decision making in advanced nonsmall cell lung carcinoma: the French IFCT-PREDICT.amm study. **The European respiratory journal**, v. 51, n. 3, 2018.

LU, D. et al. Cancer Bioinformatics in Cancer Therapy. **Advances in Proteomics and Bioinformatics**, n. February 2019, 2018.

LUO, M. et al. Targeting Breast Cancer Stem Cell State Equilibrium through Modulation of Redox Signaling. **Cell Metabolism**, v. 28, n. 1, p. 69- 86.e6, 3 jul. 2018.

LURIE, R. H. et al. **NCCN Guidelines Version 3Breast Cancer**. [s.l: s.n.].

MAHMOUD, A. M. et al. Possible involvement of Nrf2 and PPARγ up-regulation in the protective effect of umbelliferone against cyclophosphamide-induced hepatotoxicity. **Biomedicine and Pharmacotherapy**, v. 86, p. 297–306, 1 fev. 2017.

MENSCHAERT, G.; FENYÖ, D. **Proteogenomics from a bioinformatics angle: A growing fieldMass Spectrometry Reviews**John Wiley and Sons Inc., , 1 set. 2017.

MIRNEZAMI, R.; NICHOLSON, J.; DARZI, A. Preparing for Precision Medicine. **New England Journal of Medicine**, v. 366, n. 6, p. 489–491, 9 fev. 2012.

MOORE, R. L.; FALLER, D. V. SIRT1 represses estrogen-signaling, ligand-independent ERα-mediated transcription, and cell proliferation in estrogen-responsive

breast cells. **Journal of Endocrinology**, v. 216, n. 3, p. 273–285, 2013.

MURAKAMI, A. et al. Cullin-3/KCTD10 E3 complex is essential for Rac1 activation through RhoB degradation in human epidermal growth factor receptor 2-positive breast cancer cells. **Cancer Science**, v. 110, n. 2, p. 650–661, 1 fev. 2019.

MÜRDTER, T. E. et al. Activity levels of tamoxifen metabolites at the estrogen receptor and the impact of genetic polymorphisms of phase I and II enzymes on their concentration levels in plasma. **Clinical pharmacology and therapeutics**, v. 89, n. 5, p. 708–17, maio 2011.

MYANT, K. B. et al. ROS Production and NF-κB Activation Triggered by RAC1 Facilitate WNT-Driven Intestinal Stem Cell Proliferation and Colorectal Cancer Initiation. **Cell Stem Cell**, v. 12, n. 6, p. 761–773, 6 jun. 2013.

O'REILLY, E. A. et al. The fate of chemoresistance in triple negative breast cancer (TNBC). **BBA Clinical**, v. 3, p. 257–275, 2015.

OLAGNIER, D. et al. Nrf2, a pparγ alternative pathway to promote cd36 expression on inflammatory macrophages: Implication for malaria. **PLoS Pathogens**, v. 7, n. 9, p. e1002254, 15 set. 2011.

OLSON, M. V. The human genome project. **Proceedings of the National Academy of Sciences of the United States of America**, v. 90, n. May, p. 4338–4344, 1993.

ONG, A. L. C.; RAMASAMY, T. S. Role of Sirtuin1-p53 regulatory axis in aging, cancer and cellular reprogramming. **Ageing Research Reviews**, v. 43, n. January, p. 64–80, 2018.

PEROU, C. M. et al. Molecular portraits of human breast tumours. **Nature**, v. 406, n. 6797, p. 747–752, 2000.

PESTELL, R. et al. **Abstract P2-06-02: Pparg deacetylation by SIRT1 determines breast tumor lipid synthesis and growth**. American Association for Cancer Research (AACR), 15 dez. 2013

PINHEIRO, J. B. F.; TORRES, A. DE F.; PAZ, A. R. DA. Immunohistochemical profile of breast cancer subtypes in patients seen at Napoleão Laureano Hospital, Paraíba, Brazil. **Mastology**, v. 29, n. 2, p. 58–63, 2019.

POLVANI, S.; TAROCCHI, M.; GALLI, A. PPAR and oxidative stress: Con(β) catenating NRF2 and FOXO. **PPAR Research**, v. 2012, n. ID 641087, p. 1–15, 2012.

PONS, D. G. et al. UCP2 inhibition sensitizes breast cancer cells to therapeutic agents by increasing oxidative stress. **Free Radical Biology and Medicine**, v. 86, p. 67–77, 6 jul. 2015.

POSTOVIT, L. et al. Harnessing Oxidative Stress as an Innovative Target for Cancer Therapy. **Oxidative Medicine and Cellular Longevity**, v. 2018, p. 10–12, 2018.

RAMOS, N. et al. Hepatocellular Carcinoma In The Brazilian Public Health System: A Burden Of Illness Model. **Value in Health**, v. 21, p. S41, 2018.

RINALDI, G.; ROSSI, M.; FENDT, S. M. Metabolic interactions in cancer: cellular metabolism at the interface between the microenvironment, the cancer cell phenotype and the epigenetic landscape. **Wiley Interdisciplinary Reviews: Systems Biology and Medicine**, v. 10, n. 1, p. 1–18, 2018.

ROBSON, M. et al. Olaparib for Metastatic Breast Cancer in Patients with a Germline *BRCA* Mutation. **New England Journal of Medicine**, v. 377, n. 6, p. 523–533, 10 ago. 2017.

SALGADO, R. et al. Addressing the dichotomy between individual and societal approaches to personalised medicine in oncology. **European Journal of Cancer**, 3 maio 2019.

SCHMIDT, H. **What is The Warburg Effect and how can understanding it change the way we treat cancer? - Conversation Cancer**. Disponível em: <https://conversationcancer.com/what-is-the-warburg-effect-and-how-can-it-change-the-way-we-treat-cancer/>. Acesso em: 11 maio. 2019.

SCHNELZER, A. et al. Rac1 in human breast cancer: Overexpression, mutation analysis, and characterization of a new isoform, Rac1b. **Oncogene**, v. 19, n. 26, p. 3013–3020, 15 jun. 2000.

SEMENZA, G. L. Hypoxia-inducible factors: coupling glucose metabolism and redox regulation with induction of the breast cancer stem cell phenotype. **The EMBO Journal**, v. 36, n. 3, p. 252–259, 22 fev. 2017.

SENKUS, E. et al. Primary breast cancer: ESMO Clinical Practice Guidelines for diagnosis, treatment and follow-up † incidence and epidemiology. 2015.

SHI, Y. et al. Integrative comparison of mRNA expression patterns in breast cancers from Caucasian and Asian Americans with implications for precision medicine. **Cancer Research**, v. 77, n. 2, p. 423–433, 15 jan. 2017.

SHIEH, Y. et al. Breast Cancer Screening in the Precision Medicine Era: Risk-Based Screening in a Population-Based Trial. **Journal of the National Cancer Institute**, v. 109, n. 5, p. 1–8, 2017.

SHIN, S. et al. ERK2 regulates epithelial-to-mesenchymal plasticity through DOCK10-dependent Rac1/FoxO1 activation. **Proceedings of the National Academy of**

Sciences of the United States of America, v. 116, n. 8, p. 2967–2976, 19 fev. 2019.

SIA, D. et al. Liver Cancer Cell of Origin, Molecular Class, and Effects on Patient Prognosis. **Gastroenterology**, 2016.

SIMMONS, G. E.; PRUITT, W. M.; PRUITT, K. **Diverse roles of SIRT1 in cancer biology and lipid metabolismInternational Journal of Molecular Sciences**, 5 jan. 2015.

SIMON, S. D. et al. Characteristics and prognosis of stage I-III breast cancer subtypes in Brazil: The AMAZONA retrospective cohort study. **Breast**, v. 44, p. 113–119, 1 abr. 2019.

SONNENBLICK, A. et al. **An update on PARP inhibitors - Moving to the adjuvant settingNature Reviews Clinical Oncology**Nature Publishing Group, , 11 jan. 2015.

STORZ, P. Oxidative Stress in Cancer. In: **Oxidative Stress and Redox Regulation**. Dordrecht: Springer Netherlands, 2013. p. 427–447.

SU, H. et al. Profiling and bioinformatics analyses reveal differential circular RNA expression in radioresistant esophageal cancer cells. **Journal of Translational Medicine**, v. 14, n. 1, 28 jul. 2016.

SU, J. et al. Cytoprotective effect of the UCP2-SIRT3 signaling pathway by decreasing mitochondrial oxidative stress on cerebral ischemia–reperfusion injury. **International Journal of Molecular Sciences**, v. 18, n. 7, 2017.

SUNDARESAN, M. et al. Regulation of reactive-oxygen-species generation in fibroblasts by Rac1. **The Biochemical journal**, v. 318 (Pt 2), n. 2, p. 379–82, 1 set. 1996.

SZOSTAKOWSKA, M. et al. **Resistance to endocrine therapy in breast cancer: molecular mechanisms and future goalsBreast Cancer Research and Treatment**Springer New York LLC, , 15 fev. 2019.

TAFANI, M. et al. **The Interplay of Reactive Oxygen Species, Hypoxia, Inflammation, and Sirtuins in Cancer Initiation and ProgressionOxidative Medicine and Cellular Longevity**Hindawi Limited, , 2016.

TIAN, L. et al. Acetylation-defective mutants of Pparγ are associated with decreased lipid synthesis in breast cancer cells. **Oncotarget**, v. 5, n. 17, p. 7303–7315, 2014.

TSAI, C.-H. et al. Docosahexaenoic acid increases the expression of oxidative stress-induced growth inhibitor 1 through the PI3K/Akt/Nrf2 signaling pathway in breast cancer cells. **Food and Chemical Toxicology**, v. 108, p. 276–288, 1 out. 2017.

TUTT, A. et al. Carboplatin in BRCA1/2-mutated and triple-negative breast cancer

BRCAness subgroups: the TNT Trial. **Nature Medicine**, v. 24, n. 5, p. 628–637, 30 maio 2018.

TYANOVA, S.; COX, J. Perseus: A bioinformatics platform for integrative analysis of proteomics data in cancer research. In: **Methods in Molecular Biology**. [s.l.] Humana Press Inc., 2018. v. 1711p. 133–148.

VANDERLAAN, P. A. et al. Tumor biomarker testing in non-small-cell lung cancer: A decade of change. **Lung Cancer**, v. 116, n. July 2017, p. 90–95, 2018.

VARGAS, A. J.; HARRIS, C. C. Biomarker development in the precision medicine era: Lung cancer as a case study. **Nature Reviews Cancer**, v. 16, n. 8, p. 525–537, 2016.

VERLI, H. **Bioinformática da Biologia à Flexibilidade Molecular**. 1. ed. Porto Alegre: [s.n.].

VIDEIRA, M.; REIS, R. L.; BRITO, M. A. Deconstructing breast cancer cell biology and the mechanisms of multidrug resistance. **Biochimica et Biophysica Acta (BBA) - Reviews on Cancer**, v. 1846, n. 2, p. 312–325, 2014.

WANG, E. et al. Disease Biomarkers for Precision Medicine: Challenges and Future Opportunities. **Genomics, Proteomics and Bioinformatics**, v. 15, n. 2, p. 57–58, 2017a.

WANG, J. et al. Sirt1 inhibits gouty arthritis via activating PPARγ. **Clinical Rheumatology**, 31 jul. 2019.

WANG, M. et al. Uncoupling protein 2 downregulation by hypoxia through repression of peroxisome proliferator-activated receptor γ promotes chemoresistance of non-small cell lung cancer. **Oncotarget**, v. 8, n. 5, p. 8083–8094, 2017b.

WETTERSTRAND, K. **DNA Sequencing Costs: Data from the NHGRI Genome Sequencing Program (GSP)**. Disponível em: <https://www.genome.gov/about-genomics/fact-sheets/DNA-Sequencing-Costs-Data>. Acesso em: 11 maio. 2019.

WU, S.; LU, H.; BAI, Y. Nrf2 in cancers: A double-edged sword. **Cancer Medicine**, v. 8, n. 5, p. 2252–2267, 30 maio 2019.

YANG, D. et al. Regulation of Sirt1/Nrf2/TNF-α signaling pathway by luteolin is critical to attenuate acute mercuric chloride exposure induced hepatotoxicity. **Scientific Reports**, v. 6, 17 nov. 2016.

YU, T. M. et al. Budget Impact of Next-Generation Sequencing for Molecular Assessment of Advanced Non–Small Cell Lung Cancer. **Value in Health**, v. 21, n. 11, p. 1278–1285, 1 nov. 2018.

ZHAN, L. et al. Regulatory role of KEAP1 and NRF2 in PPARγ expression and

chemoresistance in human non-small-cell lung carcinoma cells. **Free Radical Biology and Medicine**, v. 53, n. 4, p. 758–768, 15 ago. 2012.

ZOU, W. et al. PI3K/Akt pathway mediates Nrf2/ARE activation in human L02 hepatocytes exposed to low-concentration HBCDs. **Environmental Science and Technology**, v. 47, n. 21, p. 12434–12440, 2013.

APÊNDICE A - CAPÍTULO DE LIVRO PUBLICADO

CAPITULO IV: OXIDATIVE STRESS AND DISEASE

Chapter 10

Oxidative Stress and Disease

Rosângela F.F de Araújo,
Danyelly Bruneska G. Martins and
Maria Amélia C.S.M. Borba

Additional information is available at the end of the chapter

http://dx.doi.org/10.5772/65366

Abstract

Typically in aerobic metabolism, organic compounds such as nucleic acids, proteins and lipids can undergo structural damage by oxidative reactions. This damage caused by reactive oxygen/nitrogen species has been recognized as "oxidative stress". Despite the biological systems present efficient enzymatic and nonenzymatic antioxidant systems, oxidative stress indicates a pro-oxidant/antioxidant imbalance in favor of excessive generation of free radicals or decrease in the removal rate. Various diseases such as cancer, diabetes, cardiovascular diseases and neurodegenerative clearly exemplify the chronic oxidative stress. Therefore, it is important to consider that at low and moderate ROS levels, it can, for example, act as signaling molecules that support cell proliferation and differentiation and activate survival pathways in response to stress. Correlations between oxidative stress and disease should be carefully investigated in order to understand whether oxidative stress actually increases susceptibility to a particular disease or opposite.

Keywords: oxidative stress, free radicals, oxidative damage, antioxidants, diseases

1. Introduction

The generation of free radicals is a continuous physiological process, fulfilling relevant biological functions. The mechanisms of generation of free radicals occur mostly in the mitochondria, cell membranes and cytoplasm. Reactive oxygen species (ROS) and reactive nitrogen species (RNS) are formed as unavoidable by-products of metabolism. During the metabolic processes, these radicals act as mediators for the transfer of electrons in various

biochemical reactions. Its production, in appropriate proportions, is possible to generate adenosine triphosphate (ATP) through the electron transport chain; fertilization of the ovum; activation of genes and participation of defense mechanisms during the infection process [1]. The continuous production of free radicals during the metabolic processes culminated in the development of antioxidant defense mechanisms (enzymes and substances such as glutathione, metallothionein, vitamin A, vitamin C and vitamin E). These are intended to limit the intracellular levels of these reactive species and control the occurrence of damage caused by them. However, excessive production can lead to oxidative damage. The structural modifications in the molecules of nucleic acids, proteins and lipids caused by increased concentration of reactive oxygen species (ROS) and/or reactive nitrogen species (RNS) lead to various metabolic changes that may contribute to the development of neurological diseases, cardiovascular diseases, cancer, among others [2].

2. Oxidative stress and molecular damage

The installation process of oxidative stress arises from an imbalance between oxidants and antioxidants in favor of excessive generation of free radicals or removal speed thereof. This process leads to the oxidation of biomolecules with consequent loss of its biological functions and/or homeostatic imbalances, whose manifestation is the potential oxidative damage to cells and tissues. Accumulation of ROS/RNS can result in a number of deleterious effects such as lipid peroxidation, protein oxidation and DNA damage [3].

2.1. Nucleic acids damage

DNA and RNA are chemically unstable and vulnerable to hydrolysis, nonenzymatic methylation and oxidation, due to its susceptibility to endogenous and exogenous damage. The endogenous genotoxic agents are mainly produced by cellular metabolism and composed of ROS and RNS, estrogen metabolites and aldehydes produced by lipid peroxidation [4, 5].

There are two major endogenous oxidants causing nucleic acids damage: hydroxyl radicals ($HO^{\bullet}$) and peroxynitrite (ONO_2^-). One major source of ROS is the mitochondrial respiration because up to 5% of oxygen undergoes single electron transfer and generates superoxide anion radical ($O_2^{\bullet-}$). The superoxide dismutase (SOD) converts $O_2^{\bullet-}$ to hydrogen peroxide that should be reduced by catalase (CAT) or glutathione peroxidase (GPx), however when transition metals are present, it is reduced to hydroxyl radicals ($HO^{\bullet}$). These radicals have a high reactivity, so it must be generated close to DNA or RNA in order to oxidize them. The generation of peroxynitrite (ONO_2^-) occurs by the reaction of nitric oxide (NO) and superoxide, both produced simultaneously in macrophages. Although these specimens can directly oxidize the nucleic acids, there is a secondary synergic mechanism of RNS to break the oxidative balance: the RNS are able to inhibit the enzyme FAPY glycosylase, a DNA repair mechanism to oxidation [6].

Oxidative stress can lead to different lesions in DNA, including direct modification of nucleotide bases, training sites apurinic/apyrimidinic, single strand break and much less frequently,

breaking double strands. Considering all the bases of the nucleotides, guanine is most susceptible to oxidative changes because it has lower reduction potential and hydroxyl radicals interact with the imidazole ring of this nitrogenous base at positions C4, C5 and C8 [7].

The most studied marker for DNA oxidation is 8-hydroxydeoxyguanosine, a product of guanosine oxidation by $HO^{\bullet}$ [6, 8]. This product is able to pair with adenine, generating a GC/TA mutation upon replication [6]. It is also known that oxidative stress regulates DNA methylation, playing a role in epigenetics regulation. Epigenetics constitutes several mechanisms of controlling gene expression without changing DNA sequence, but responding fast and precisely to environmental changes. One of the most characterized methods of epigenetic regulation is DNA methylation. The methylation of DNA CpG islands is mediated by DNA methyltransferases (DNMTs), but when the ROS or RNS interacts with cytosine, it is chemically modified from 5-methylcytosine to 5-hydroxymethylcytosine, which prevents DNMT binding and alters methylation patterns [9].

For RNA oxidation, the most relevant marker is the homologue 8-hydroxyguanosine. It has been made clear that RNA is more often oxidized than DNA, due to its cellular location closer to ROS and RNS occurrence. The major consequences of RNA oxidization are the breakage of the strand and ribosomal dysfunction, preventing correct protein production [8].

2.2. Protein damage

The effects of oxidation in proteins can be observed in impaired protein folding, side-chain oxidation and backbone fragmentation, resulting in loss of function and stop a variety of biochemical processes. Among the amino acids, the cysteines and methionines are more easily oxidizable, but this reaction is reversible through disulfite reductases activity. However, the cysteine can also suffer irreversible oxidation reactions leading to the formation of S-carboxymethylcysteine and S-(2-Succinyl)cysteine, which implies the formation of fumarate and dicarbonyl groups covalently bound to cysteine residues. When the amino acids lysine, proline, arginine and threonine are oxidized, occurs the production of carbonyl derivatives, which are used as markers for oxidative stress. In the oxidation of aromatic aminu acids, such as tyrosine, different products are formed due to interaction with ROS – dityrosine or RNS – 3-nitrotyrosine [8].

These oxidized-modified proteins are usually recognized and degraded in the cells, but some of them can accumulate over time and lead to cellular dysfunction. A physiological example is the lipofuscin, a brown-yellow pigment that is a product of iron-catalyzed oxidation (polymerization) of proteins and lipids, as it is extremely resistant to proteolysis, it accumulates and it is used as an aging marker [10].

2.3. Lipid damage

In biological systems, lipid peroxidation occurs in two forms, one enzymatically, involving the participation of cyclooxygenase and lipoxygenase in the oxidation of fatty acids and other nonenzyme medium, involving transition metal, the reactive species oxygen, nitrogen and others [11]. Excess peroxidation results are very damaging to the cell, despite contribute to the

inflammatory response, due to its importance in the cascade reaction from arachidonic acid to prostaglandin formation. The action of free radicals on lipids leads to the formation of lipid hydroperoxides and aldehydes, such as malondialdehyde, 4-hydroxynonenal and isoprostanes that contribute further to increased cellular toxicity and can be detected in biological samples to measure oxidative stress. Lipid peroxidation disrupts the normal structure and function of lipid bilayers surrounding both the cell itself and in the membranes of organelles. In particular, the lipid peroxidation can alter membrane permeability, transportation and fluidity [12]. The chronicity of the process in question has important implications for the etiologic process of many chronic diseases, including atherosclerosis, diabetes, obesity, neurodegenerative disorders and cancer [1].

3. Antioxidant defense system

The antioxidant defense system has the primary objective to maintain the oxidative process within physiological limits and subject to regulation by preventing oxidative damage from spreading, culminating in systemic irreparable damage. The enzymatic defense system includes enzymes such as superoxide dismutase (SOD), catalase (CAT) and glutathione peroxidase (GPx). These enzymes act through mechanisms of preventing and/or controlling the formation of free radicals and species nonradical, involved with the initiation of chain reactions that culminate in propagation and process amplification and, consequently, the occurrence of oxidative damage. CAT and GPx enzymes act with the same purpose, to prevent the hydrogen peroxide accumulation. Such integrated action is of great importance, since this reactive species through the reactions of Fenton and Haber-Weiss, with the participation of iron and copper metals, culminates in the generation of $OH^{\bullet}$ radical against which there is no enzyme system defense [13, 14].

The human organism is constantly exposed to a vast number of molecules that can lead to oxidative stress, such as drugs and alcohol. However, there is a conserved cellular component to oxidative stress response, which is constituted by over 100 genes responsible for detoxification and antioxidant protein production. The first line of the antioxidant defense to exogenous toxins includes the enzymes involved in phase I and II metabolism. The phase I metabolism is responsible for increased compound polarity through oxidation, reduction or hydrolysis reactions. The phase II metabolism, in the other hand, is responsible for facilitating the cellular export of those compounds; its reactions are mainly glucuronidation, acetylation and sulfation [15].

The enzymes that compose the cytochrome P450 are the most responsible for oxidation of drugs, chemicals and various endogenous substrates, such as eicosanoids, cholesterol, vitamin D3 and arachidonic acid [16]. The P450 is a superfamily of heme-thiolated enzymes with over 2000 members [17]. In humans, 57 functional genes and 58 pseudogenes are grouped according to the sequence similarity in 18 families and 44 subfamilies. The CYP-enzymes that belong to the families 1, 2 and 3 are responsible for metabolizing up to 90% of the drugs, this phase I drug oxidation system is frequently redundant, but many drugs are metabolized to a clinical concentration by one or few CYPs only [18].

In steroidogenic tissues (converts cholesterol into pregnenolone via the P450 side chain cleavage enzyme) there is a prevalence of CYP450 enzymes located in mitochondria and the electron transport system is very susceptible to oxidative stress. During the electron transport, a leakage of electron to the ultimate acceptor leads to their binding to oxygen, being considered a primary source of ROS, this may result in acceleration of ROS production in mitochondria. In this context, it is considered the effectiveness of electron transfer from NADPH to CYP enzymes for monooxygenation of substrates as a source of ROS because during the uncoupling reaction, without the presence of any substrates, the electron-transfer chain oxidizes NADPH and yields ROS. During CYP2E1 metabolism is frequently observed this kind of uncoupling reactions, thus this enzyme is strongly associated to ROS production and oxidative stress [16]. The enzyme CYP2E1 is associated with the metabolism of small molecules, and can be induced by ethanol, obesity, diabetes and polyunsaturated fatty acids; this induction is related to toxicity and oxidative stress. Another mechanism of CYP2E1 activation is the reduction of glutathione levels, upon acetaminophen administration, for example. Besides, this drug increases lipid peroxidation and protein carbonylation, enhancing the ROS production due to higher activity of CYP2E1 and being associated to hepatotoxicity mediated by MAP-kinase pathway [16, 19].

Glutathione S-transferase (GST) is a family of intracellular enzymes that prevent the action of endogenous and exogenous toxins on the cells. GSTs are multifunctional enzymes that participate in the phase II of the xenobiotic metabolism and catalyze the nucleophilic attack of the reduced form of glutathione (GSH) to potentially hazardous compounds. How are involved in the metabolism of many carcinogens, environmental pollutants and cancer-fighting drugs, it is therefore reasonable to assume that the lack of specific isoenzymes has a significant effect on the tolerance of an organism to carcinogens [20]. Human GSTs are categorized into cytosolic/nuclear, mitochondrial and microsomal. Based on their amino acid sequences and/or nucleotide substrate specificity and immunological properties, seven classes of cytosolic GSTs are described: Alpha, Mu, Pi, Sigma, Theta, Omega and Zeta. Microsomal GSTs are designated MAPEG (membrane-associated proteins in eicosanoid and glutathione metabolism) and the only mitochondrial GST confirmed in humans is GST-kappa, which is also present in peroxisomes. GSTs are normally found in biological medium as homo or heterodimers and these dimers have two active sites whose activities are independent. After combining with reduced glutathione (GSH), these enzymes have higher specificity for a second substrate (the electrophilic). GST enzymes participate in the metabolism of endogenous and exogenous compounds, for example, polycyclic aromatic hydrocarbons, phenylalanine and tyrosine amino acids, testosterone and progesterone. These enzymes target endogenous compounds, maybe derived from peroxidation of polyunsaturated fatty acids present in cell membranes and the activity of reactive oxygen species [21–23].

4. Oxidative stress and neurological disorders

Conclusive evidence suggests that oxidative stress is a major contributor to the pathophysiology of a variety of neurodegenerative diseases, including Alzheimer's, Parkinson's, Hunting-

ton's, tardive dyskinesia (TD), epilepsy and acute diseases of the central nervous system, such as spinal cord injuries and/or brain traumatic. The human brain is vulnerable to oxidative stress due to many facts such as (i) metabolism of catecholamines; (ii) decrease in antioxidants; (iii) presence of transition metals; (iv) occurrence of brain trauma/injury; and also (v) the brain is a organ that proportionally requires more oxygen and (vi) expresses low levels of antioxidant enzymes, which contribute to formation of ROS. As a consequence of redox unbalance in brain, one of the most affected structures is the lipid membrane [24].

Parkinson's disease (PD) is characterized by loss of dopaminergic neurons in the substantia nigra pars compacta of the brain, leading to rigidity or slowing movements and postural instability. Most of the cases of PD are idiopathic and some cases are genetic-related, but in general context, aging is a determinant factor. In both idiopathic and genetic cases of PD, the oxidative stress plays a critical role in pathogenesis, being a common underlying mechanism. There is an elevated level of oxidized lipids, proteins and DNA associated with decreased glutathione level in the brain of PD patients. This increased susceptibility to oxidative damage in the dopaminergic neurons is due to (i) the presence of ROS generating enzymes, such as tyrosine hydroxylase and monoamine oxidase and (ii) these neurons contain iron, a catalyser of Fenton reaction ($Fe(II) + H_2O_2 \rightarrow Fe(III) + OH^{\bullet} + OH^-$) that leads to superoxide radicals and hydrogen peroxide production [25].

A fact of Alzheimer's disease is the dysregulation of iron and copper homeostasis and various evidence of oxidative stress, mainly RNA oxidation. Neurons usually do not store big amounts of iron, but with aging there is an accumulation of iron in the brain, especially in microglia, astrocytes and neurons from cortex and hippocampus. If iron levels increase much more than ferritin, an iron-storage protein, it becomes free to catalyze Fenton's reaction [26].

The tardive dyskinesia (TD) is an adverse effect of antipsychotic use, it affects up to 25% of schizophrenic patients. However, as the majority of patients do not develop TD, it is considered that genetics factors may define its occurrence but TD pathophysiology remains unclear. One of the strongest hypotheses suggests that it is caused by oxidative stress originated from neurotoxic free-radical production upon antipsychotic medication. This affirmation is supported by genetic polymorphisms evaluated in genes that encode a mitochondrial enzyme that prevents oxidative damage due to energetic metabolism (manganese superoxide dismutase) and a cytosolic flavoenzyme that prevents quinone reduction (NADPH quinone oxidoreductase), playing a role in antioxidant defense [27].

5. Oxidative stress and metabolic syndrome

Metabolic syndrome is a term that designates a cluster of health problems often associated to modern life style, including obesity, insulin resistance, dyslipidemia, impaired glucose tolerance and high blood pressure. The metabolic syndrome is diagnosed when at least three of the following alterations are present: visceral obesity (waist circumference >102 cm in men or >88 cm in women); raised arterial blood pressure (>130/85 mm Hg); dysglycemia (fasting

plasma glucose >100 mg dL); raised triglyceride concentrations (>150 mg dL) and low high-density lipoprotein (HDL) cholesterol (<40 mg dL in men or < 50 mg dL in women) [28].

The oxidative stress is related to metabolic syndrome in several ways: (i) H_2O_2 promotes insulin signaling, being associated with increased insulin resistance; (ii) superoxide anion is generated by angiotensin stimulation of NADPH and angiotensin II/angiotensin II type I receptor (AT1R), which plays a critical role in blood pressure control; (iii) hyperglycaemia leads to overproduction of superoxide by mitochondrial electron transfer chain, activating oxidative stress; (iv) elevated low-density lipoprotein (LDL) and low high-density lipoprotein (HDL) are correlated with oxidative stress and the dyslipidemia treatment with rosuvastatin is known to reduce oxidative stress through raise of antioxidant enzymes [28].

Due to oxidative DNA damage there is a direct correlation between diabetes and cancer. Diabetic patients present high levels of ROS because of elevated glucose, fatty acids and insulin blood levels; combined to lower antioxidative capacity derived from reduced glutathione synthesis. To support those findings, it has been proved that polymorphisms in peroxisome proliferator-activated receptor-γ coactivator-1α (PPARGC1A) – a protein that regulates mitochondrial electron transport, leads to decontrolled redox activity [29].

6. Oxidative stress and atherosclerosis

Atherosclerosis is defined as an arterial disease characterized by fibrous and cholesterol rich plaques. Atherosclerosis progression causes blood flow obstruction, hemorrhage due to rupture and thrombosis leading to strokes or myocardial infarctions. Many risk factors are associated with atherosclerosis development, the most widely known are serum low-density lipoprotein (LDL) cholesterol, low serum high-density lipoprotein (HDL) cholesterol, diabetes, hypertension, smoking, aging and oxidative stress [30].

During LDL oxidation, a progressive process and very important for the beginning of the formation of atheromatous plaque, the cholesterol is target of oxidants, which generate a variety of oxysterols. On the other hand, lipid peroxidation products (MDA and 4-HNE) can react with histidine, cysteine or lysine residues of proteins, leading to formation of stable Michael adducts with a hemiacetal structure or to Schiff bases that undergo a rearrangement generating the Amadori products. These aldehydes can derivatize Lys residues of apoB, which decreases the number of positive charges and interferes on LDL binding to LDLR and scavenger receptors [31].

In endothelial cells, besides stimulating the antioxidant defense (mainly by glutathione), Nrf2 (nuclear factor (erythroid-derived 2)-like 2) suppresses inflammation-associated expression of adhesion molecules and cytokines, which are associated with the early stage of atherogenesis [29]. NAD(P)H oxidases (NOXs) are major sources of ROS in the vasculature, producing superoxide from molecular oxygen using NAD(P)H as the electron donor and endothelial NO synthase (eNOS) produce NO which represents a key element in the vasoprotective function of the endothelium. However, pathological conditions associated with oxidative stress may become eNOS inefficient and promote the rapid inactivation of NO by excess superoxide [32].

There is growing evidence that reversal of oxidative stress with antioxidants can reduce the degree of myocardial ischemic injury and heart dysfunction [33].

7. Oxidative stress and infection

The pathological effects of NO and O_2^- in virus infection are in clear contrast to their beneficial antimicrobial effects in bacterial and fungal infections. In virus infections, NO and $ONOO^-$, which are primitive host-defense molecules, cause nonspecific oxidative damage in virus-infected tissue, leading to various pathological events. Virus-induced oxidative stress has been reported during HIV, influenza virus, HBV, hepatitis C virus, encephalomyocarditis virus (EMCV), respiratory syncytial virus (RSV), dengue virus (DENV) and others [34].

Studies including rotavirus-infected patients showed that viral infection stimulates NO production, decreases superoxide dismutase and glutathione peroxidase activities and increases inducible nitric oxide synthase (iNOS) mRNA and iNOS expression in murine ileum [35].

Influenza virus is probably the best characterized pathogen modulating redox homeostasis. Influenza-induced ROS production has been associated with host immune and inflammatory responses, as well as modulation of viral replication. Oxygen radicals and their derivatives are recognized as principal mediators of influenza virus-induced lung injury [36].

Within the Flaviviridae family, hepatitis C virus infection promotes oxidative stress and manipulates antioxidant systems, leading to liver damage and chronic disease. Elevated levels of reactive oxygen species (ROS) are considered as a major factor contributing to HCV-associated pathogenesis. HCV core protein is considered as a major regulator affecting the release of ROS from mitochondria. In this context, mitochondria play a crucial role for the production of ROS in HCV-infected cells. Several pathways are affected upon HCV infection to result in an induction of autophagy that interferes with various steps of the viral life cycle to promote a permanent viral infection. The assembly and release of viral particles are closely linked to the VLDL synthesis and occur via the secretory pathway. Elevated glucose production, enhanced fatty acid uptake or upregulation of genes involved in lipid and cholesterol synthesis may contribute to oxidative stress-induced insulin resistance linked to HCV infection [36].

Induction of iNOS and production of NO, accumulation of ROS and RNS, as well as perturbation of the reduced glutathione (GSH) content are all signatures of Dengue virus (DENV) infection in different human cells and animal models. DENV infection resulted in an intracellular accumulation of NAD(P)H oxidase (NOX2)-derived ROS in monocyte-derived dendritic cells (Mo-DCs). Alteration in the redox status of DENV-infected patients has been associated with increased inflammatory responses, cell death and correlated with different parameters associated with dengue disease [37].

The HPV infection, although necessary, is not sufficient to cause cancer and several studies have been devoted to the search for concurrent carcinogenic factors. Among these cofactors,

many evidence support the role of ROS. It is clear that viral infection induces ROS that in turn causes damage to all types of biological macromolecules. Two different types of cooperative mechanisms are presumed to occur between ROS and HPV: (i) the ROS genotoxic activity and the HPV-induced genomic instability concur independently to the generation of the molecular damage necessary for the emergence of neoplastic clones. This first mode is merely a particular form of cocarcinogenesis and (ii) ROS specifically interacts with one or more molecular stages of neoplastic initiation and/or progression induced by the HPV infection [38, 39].

Therefore, it seems reasonable to hypothesize that, while in most cases the cells react to HPV infection and can overcome the virus-induced ROS by activating apoptosis leading to termination of viral replication and lesion regression, in some of the infected cells a steady state balance between ROS generation and detoxification is established, partly due to viral-induced antioxidant response. Thus, infected cells can aberrantly proliferate, paving the way to neoplastic progression HPV, exploit host cell survival mechanisms, through modulation of redox homeostasis, increasing the activity of catalase, SOD among other, as an adaptive response to the high ROS conditions of preneoplastic lesions. Elevated GST and GSH provide the HPV hosting cell with improved oxidative damage detoxifying systems, but suppression of p53 and iNOS together with induction of vascular endothelial growth factor (VEGF) and resistance to ROS leads to the suppression of apoptosis and generates an oxidant fitting cell phenotype. Therefore, the tumor cell adapts their metabolism in order to support their growth and survival, creating a paradox of high ROS production in the presence of high antioxidant levels [38, 39].

8. Oxidative stress and cancer

Many signaling pathways that regulate the metabolism of ROS are also linked to tumorigenesis [40, 41]. However, ROS can also promote tumor formation by inducing DNA mutations and pro-oncogenic signaling pathways. The production of low level of ROS is required for homeostatic signaling events. It can be driven by NAD(P)H and NAD(P)H oxidase (NOX), leading to the increase of cell proliferation and survival through the posttranslational modification of kinases and phosphatases. At moderate levels, ROS induce the expression of stress-responsive genes such as *HIF1A*, which in turn trigger the expression of proteins providing prosurvival signals, such as the glucose transporter GLUT1 (also known as SLC2A1) and vascular endothelial growth factor (VEGF). At low and moderate levels ROS can act as signaling molecules that sustain cellular proliferation and differentiation and activate stress-responsive survival pathways, stimulating the phosphorylation of protein kinase C (PKC), p38 mitogen-activated protein kinase (p38 MAPK), extracellular signal-regulated kinase (ERK)1/2, phosphoinositide 3-kinase/serine-threonine kinase (PI3K/Akt), protein kinase B (PKB) and JUN N-terminal kinase (JNK) [40, 42].

The regulation of oxidative stress is an important factor not only for tumor development but also for the responses to anticancer therapies. As high ROS levels are harmful to cells, oxidative stress can have a tumor-suppressive effect. This imparts pressure on cancer cells to adapt by developing strong antioxidant mechanisms. But despite having an enhanced antioxidant system, cancer cells maintain higher ROS levels than normal cells. At high levels, ROS can

cause damage to macromolecules, including DNA; induce the activation of protein kinase Cδ (PKCδ), triggering senescence; and/or cause permeabilization of the mitochondria, leading to the release of cytochrome *c* and apoptosis. ROS are also involved in the increased expression of antioxidant genes related to the activation of transcription factors such as the Nrf2, activator protein 1 (AP-1), nuclear factor kB (NF-kB) and p53 [40–42].

The role of ROS in carcinogenic process can be either pro or anti oncogenic, and it can be summarized as follows: (i) regulating tumor development and signaling pathways for cell progression through ERK1/2 activation and ligand-independent RTK activation; (ii) regulating chronic inflammation for example through NF-kB activation; (iii) controlling tumor suppressor expression and cell cycle inhibitors; (iv) mediating angiogenesis by the release of vascular endothelial growth factor (VEGF) and angiopoietin; (v) favoring metastasis and tissue invasion due to metalloproteinase secretion; (vi) avoiding cellular death by activating SRC and PI3K/AKT pathway. Additionally, generating ROS is the mechanism of attack used by most of chemotherapies and radiotherapy [43, 44].

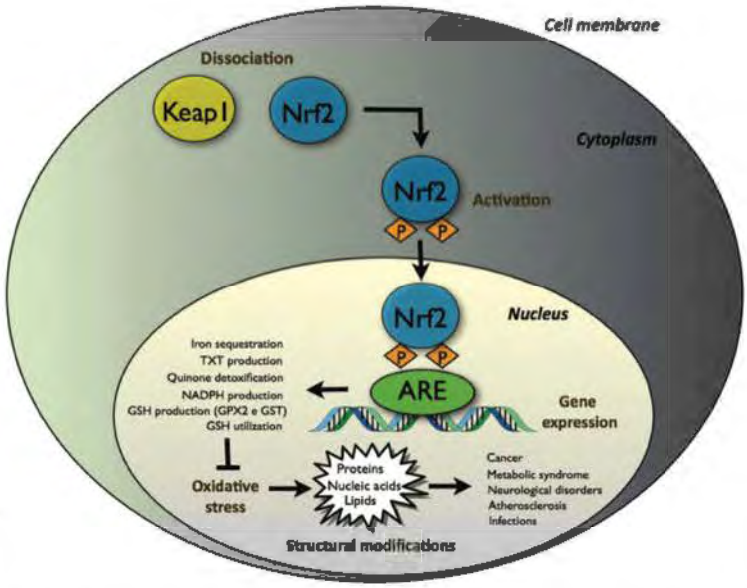

Figure 1. Keap1 (Kelch-like ECH-associated protein 1) sequesters Nrf2 (nuclear factor erythroid-derived 2) in the cytoplasm by binding to its aminoterminal regulatory domain. Keap1 is a sulfhydryl (S)-rich protein, and several cysteine residues mediate the Keap1–inducer interaction. When the interaction between Keap1 and Nrf2 disrupts, it allows Nrf2 to translocate to the nucleus. In the nucleus, Nrf2 controls several different antioxidant pathways by activating the expression of GSTs and other genes. This control is important to avoid cellular wear caused by oxidative stress, thus hindering the onset of various diseases.

The interindividual variation of the activity of antioxidant enzymes, for example, GST, considered by both environmental factors (e.g., diet and exposure to toxins such as cigarette) and genetic, is directly related to the etiology of cancer. Cytosolic GST present polymorphisms in humans and, this is probably the cause for differences in interindividual response to

xenobiotics. The first studies in this area have addressed the correlation between GSTM1 null and/or GSTT1 null genotypes and a higher incidence of lung cancer, bladder, breast, colorectal head/neck. The discovery of allelic variants of GSTP1, encoding enzymes with reduced catalytic activity, led many researchers to examine the hypothesis that the combinations of polymorphisms of the Mu class, Pi and Theta of GST contribute to disorders with environmental factors [45, 46]. Studies with mice that exhibited a homozygous deletion of Nrf2 showed that Nrf2 is critical for inducing hepatic glutathione S-transferase (GST), NAD(P)H: quinone oxidoreductase (NQO1) and regulating levels of glutathione (**Figure** 1) [47].

Besides genetic variants of GST, changes in phase I enzyme activity as encoded by the cytochrome P450 family can also have implications for the metabolism of specific nitrosamines from the tobacco, alcohol and other carcinogenic substances [48].

The GST enzymes are part of an integrated protection system, so it is important to note that the efficiency of this system depends on the combined action of other enzymes, such as γ-glutamylcysteine synthase γGluCysS) and glutathione synthase, in order to provide glutathione as well as carriers to facilitate the elimination of glutathione conjugates [21].

9. Conclusion

The modulation of intracellular ROS levels is crucial for cellular homeostasis, and different ROS levels can induce different biological responses. It can occur due to the accumulation of intrinsic and/or environmental factors, such as hypoxia, enhanced cellular metabolic activity, mitochondrial dysfunction, increased activity of oxidases, lipoxygenases and cyclooxygenases. The accumulation of free radicals can lead to important changes in the structure of nucleic acids, proteins and lipids, altering their functions with consequent impact on cellular metabolism. These changes create conditions favorable to the onset of different diseases. The determination of oxidative stress markers and plasma antioxidants can suggest a targeted therapy against deficiencies in cell protection systems and it could be useful in an attempt to minimize complications caused by increased oxidative stress, leading to a better prognosis of various diseases.

Author details

Rosângela F.F de Araújo[1,2*], Danyelly Bruneska G. Martins[1,2] and
Maria Amélia C.S.M. Borba[2]

*Address all correspondence to: rfrade@prospecmol.org

1 Department of Biochemistry – Federal University of Pernambuco, Recife, Brazil

2 Immunopathology Keizo Asami Laboratory – Federal University of Pernambuco, Recife, Brazil

References

[1] Lobo V, Patil A, Phatak A, Chandra N. Free radicals, antioxidants and functional foods: impact on human health. Pharmacognosy Reviews. 2010;4(8):118–126. DOI: 10.4103/0973-7847.70902.

[2] Rahman K. Studies on free radicals, antioxidants, and co-factors. Clinical Interventions in Aging. 2007;2(2):219–236. PMCID: PMC2684512.

[3] Lushchak VI. Free radicals, reactive oxygen species, oxidative stress and its classification. Chemico-Biological Interactions 2014;224:164–175. DOI: 10.1016/j.cbi.2014.10.016

[4] Ranchoux B, Meloche J, Paulin R, Boucherat O, Provencher S, Bonnet S. DNA damage and pulmonary hypertension. International Journal of Molecular Sciences. 2016;17(6): 990. DOI: 10.3390/ijms17060990

[5] Marengo B, Nitti M, Furfaro AL, Colla R, De Ciucis C, Marinari UM, et al. Redox homeostasis and cellular antioxidant systems: crucial players in cancer growth and therapy. Oxidative Medicine and Cellular Longevity 2016;2016:1–16. DOI: 10.1155/2016/6235641

[6] De Bont R, van Larebeke N. Endogenous DNA damage in humans: a review of quantitative data. Mutagenesis. 2004;19(3):169–185. DOI: 10.1093/mutage/geh025

[7] Smith JA, Park S, Krause JS, Banik NL. Oxidative stress, DNA damage, and the telomeric complex as therapeutic targets in acute neurodegeneration. Neurochemistry International. 2013; 62: 764–775. DOI:10.1016/j.neuint.2013.02.013.

[8] Pisoschi AM, Pop A. The role of antioxidants in the chemistry of oxidative stress: a review. European Journal of Medicinal Chemistry 2015;97:55–74. DOI: 10.1016/j.ejmech.2015.04.040

[9] Zhao H, Han Z, Ji X, Luo Y. Epigenetic regulation of oxidative stress in ischemic stroke. Aging and Disease. 2016;7(3):295–306. DOI: 10.14336/AD.2015.1009

[10] Amir Aslani B, Ghobadi S. Studies on oxidants and antioxidants with a brief glance at their relevance to the immune system. Life Sciences 2016;146:163–173. DOI: 10.1016/j.lfs.2016.01.014

[11] Ayala A, Muñoz MF, Argüelles S. Lipid peroxidation: production, metabolism, and signaling mechanisms of malondialdehyde and 4-hydroxy-2-nonenal. Oxidative Medicine and Cellular Longevity. 2014; 2014:1–31. DOI: 10.1155/2014/360438

[12] Morita M, Naito Y, Yoshikawa T, Niki E. Plasma lipid oxidation induced by peroxynitrite, hypochlorite, lipoxygenase and peroxyl radicals and its inhibition by antioxidants as assessed by diphenyl-1-pyrenylphosphine. Redox Biology 2016;8:127–135. DOI: 10.1016/j.redox.2016.01.005

[13] Schneider CD, Oliveira AR. Free radicals of oxygen and exercise: mechanisms of formation and adaptation to physical training. Revista Brasileira de Medicina do Esporte. 2004;10(4). DOI: 10.1590/S1517-86922004000400008

[14] Uhl L, Gerstel A, Chabalier M, Dukan S. Hydrogen peroxide induced cell death: one or two modes of action? Heliyon. 2015;1(4). DOI: 10.1016/j.heliyon.2015.e00049

[15] Jacob C, Winyard P. Redox Signaling and Regulation in Biology and Medicine. Wiley-VCH. 2009. Weinheim, Germany. DOI: 10.1002/9783527627585

[16] Bhattacharyya S, Sinha K, Sil PC. Cytochrome P450s: mechanisms and biological implications in drug metabolism and its interaction with oxidative stress. Current Drug Metabolism 2014;15:719–742. DOI: 10.2174/1389200215666141125121659

[17] Lewis DF Human cytochromes P450 associated with the phase 1 metabolism of drugs and other xenobiotics: a compilation of substrates and inhibitors of the CYP1, CYP2 and CYP3 families. Current Medicinal Chemistry. 2003;10(19):1955–1972. DOI: 10.2174/0929867033456855

[18] Zanger UM, Schwab M. Cytochrome P450 enzymes in drug metabolism: regulation of gene expression, enzyme activities, and impact of genetic variation. Pharmacology & Therapeutics. 2013;138(1):103–141. DOI: 10.1016/j.pharmthera.2012.12.007

[19] Tanaviyutpakdee P, Yoovathaworn K, Sirivarasai J, Chanprasertyothin S. Role of CYP2E1 and NQO1 polymorphisms in oxidative stress derived cancer in Thais with and without dyslipidemia. Asian Biomedicine. 2015;9(5):601–611. DOI: 10.5372/1905-7415.0904.430

[20] Zheng W, Wen W-Q, Gustafson DR, Gross M, Cerhan JR, Folsom AR. GSTM1 and GSTT1 polymorphisms and postmenopausal breast cancer risk. Breast Cancer Research and Treatment. 2002 Jul;74(1):9–16. DOI: 10.1023/A:1016005100958

[21] Huber PC, Almeida WP, Fátima Â de. Gluthathione and related enzymes: the biological role and importance in pathological process. Quimica Nova. 2008;31(5):1170–1179. DOI: 10.1590/S0100-40422008000500046

[22] Lo H-W, Ali-Osman F. Genetic polymorphism and function of glutathione S-transferases in tumor drug resistance. Current Opinion in Pharmacology. 2007;7(4):367–374. DOI: 10.1016/j.coph.2007.06.009

[23] Sheehan D, Meade G, Foley VM, Dowd CA. Structure, function and evolution of glutathione transferases: implications for classification of non-mammalian members of an ancient enzyme superfamily. The Biochemical Journal. 2001 Nov 15;360(Pt 1):1–16. DOI: 10.1042/0264-6021:3600001

[24] Rao AV, Balachandran B. Role of oxidative stress and antioxidants in neurodegenerative diseases. Nutritional Neuroscience. 2002;5: 291–309. DOI: 10.1080/1028415021000033767

[25] Hwang O. Role of oxidative stress in Parkinson's Disease. Experimental Neurobiology. 2013;22(1):11–17. DOI: 10.3233/JPD-130230

[26] Hofer T, Perry G. Nucleic acid oxidative damage in Alzheimer's disease-explained by the hepcidin-ferroportin neuronal iron overload hypothesis? Journal of Trace Elements in Medicine and Biology: Organ of the Society for Minerals and Trace Elements (GMS). 2016; in press. DOI:10.1016/j.jtemb.2016.06.005

[27] Cho C-H, Lee H-J. Oxidative stress and tardive dyskinesia: Pharmacogenetic evidence. Progress in Neuro Psychopharmacology and Biological Psychiatry. 2013 Oct 1; 46:207–13. DOI: http://dx.doi.org/10.1016/j.pnpbp.2012.10.018

[28] Bonomini F, Rodella LF, Rezzani R. Metabolic syndrome, aging and involvement of oxidative stress. Aging and Disease. 2015;6(2):109. DOI: 10.14336/AD.2014.0305

[29] Lee SC, Chan JC. Evidence for DNA damage as a biological link between diabetes and cancer. Chinese Medical Journal. 2015;128(11):1543–1548. DOI: 10.4103/0366

[30] Mimura J, Itoh K. Role of Nrf2 in the pathogenesis of atherosclerosis. Free Radical Biology and Medicine 2015;88:221–232. DOI: 10.1016/j.freeradbiomed.2015.06.019

[31] Salvayre R, Negre-Salvayre A, Camaré C. Oxidative theory of atherosclerosis and antioxidants. Biochimie 2016;125:281–296. DOI: 10.1016/j.biochi.2015.12.014

[32] Li H, Horke S, Förstermann U, Zhang DX, Gutterman DD, Stocker R, et al. Vascular oxidative stress, nitric oxide and atherosclerosis. Atherosclerosis. 2014 Nov;237(1):208–219. DOI: 10.1016/j.atherosclerosis.2014.09.001

[33] Wang D, Wang J, Liu Y, Zhao Z, Liu Q. Roles of Chinese herbal medicines in ischemic heart diseases (IHD) by regulating oxidative stress. International Journal of Cardiology 2016 Oct;220:314–319. DOI: 10.1016/j.ijcard.2016.06.161

[34] Akaike T, Maeda H. Nitric oxide and virus infection. Immunology. 2000 Nov;101(3): 300–308. DOI: 10.1046/j.1365-2567.2000.00142.x

[35] Guerrero CA, Acosta O. Inflammatory and oxidative stress in rotavirus infection. World Journal of Virology. 2016 May 12;5(2):38–62. DOI: 10.5501/wjv.v5.i2.38

[36] Medvedev R, Ploen D, Hildt E, Medvedev R, Ploen D, Hildt E. HCV and oxidative stress: implications for HCV life cycle and HCV-associated pathogenesis. Oxidative Medicine and Cellular Longevity 2016;2016:1–13. DOI: 10.1155/2016/9012580

[37] Olagnier D, Amatore D, Castiello L, Ferrari M, Palermo E, Diamond MS, et al. Dengue Virus Immunopathogenesis: Lessons Applicable to the Emergence of Zika Virus. Journal of Molecular Biology. 2016;428(17):3429–3448. DOI: 10.1016/j.jmb.2016.04.024

[38] Foppoli C, De Marco F, Cini C, Perluigi M. Redox control of viral carcinogenesis: the human papillomavirus paradigm. Biochimica et Biophysica Acta (BBA) – General Subjects. 2015;1850(8):1622–1632. DOI: 10.1016/j.bbagen.2014.12.016.

[39] De Marco F. Oxidative stress and HPV carcinogenesis. Viruses. 2013;5(2):708–731. DOI: 10.3390/v5020708.

[40] Gorrini C, Harris IS, Mak TW. Modulation of oxidative stress as an anticancer strategy. Nature Reviews. Drug Discovery. 2013;12(12):931–947. DOI: 10.1038/nrd4002.

[41] Cairns RA, Harris IS, Mak TW. Regulation of cancer cell metabolism. Nature Reviews. Cancer. 2011;11(2):85–95. DOI: 10.1038/nrc2981.

[42] Gupta SC, Pandey MK, Tyagi AK, Deb L, Prasad S, Deb L. Oxidative stress and cancer: advances and challenges. Oxidative Medicine and Cellular Lungevity. 2016.; 2016:1 page. DOI: 10.1155/2016/5010423.

[43] Sosa V, Moline T, Somoza R, Paciucci R, Kondoh H, LLeonart ME. Oxidative stress and cancer: an overview. Ageing Research Reviews. 2013;12(1):376–390. DOI: 10.1016/j.arr.2012.10.004.

[44] Dixon D, Edwards R. Glutathione transferases. In: The Arabidopsis Book. The American Society of Plant Biologists; 2010. p. e0131. DOI: 10.1199/tab.0131.

[45] Goto S, Kawakatsu M, Izumi S, Urata Y, Kageyama K, Ihara Y, et al. Glutathione S-transferase π localizes in mitochondria and protects against oxidative stress. Free Radical Biology and Medicine. 2009;46(10):1392–1403. DOI: 10.1016/j.freeradbiomed.2009.02.025.

[46] Chen C, Wang DW. Cytochrome P450-CYP2 family-epoxygenase role in inflammation and cancer. Advances in Pharmacology. 2015;74: 193–221. DOI: 10.1016/bs.apha.2015.04.005.

[47] Thimmulappa RK, Lee H, Rangasamy T, Reddy SP, Yamamoto M, Kensler TW, et al. Nrf2 is a critical regulator of the innate immune response and survival during experimental sepsis. The Journal of Clinical Investigation. 2006;116(4):984–995. DOI: 10.1172/JCI25790.984.

[48] Kolls JK. Oxidative stress in sepsis: a redox redux. The Journal of Clinical Investigation. 2006;116(4):860–863. DOI: 10.1172/JCI28111.

APÊNDICE B - CAPÍTULO DE LIVRO

CAPÍTULO V: AVALIAÇÃO DO ESTRESSE OXIDATIVO NO CÂNCER DE MAMA PELA EXPRESSÃO DOS GENES SIRT1, NFE2L2, UCP2, PPARG E RAC1 E SUA CORRELAÇÃO COM PARÂMETROS CLÍNICOS E HISTOPATOLÓGICOS.

TÍTULO: AVALIAÇÃO DO ESTRESSE OXIDATIVO NO CÂNCER DE MAMA PELA EXPRESSÃO DOS GENES SIRT1, NFE2L2, UCP2, PPARG E RAC1 E SUA CORRELAÇÃO COM PARÂMETROS CLÍNICOS E HISTOPATOLÓGICOS

1. INTRODUÇÃO

O câncer de mama é uma doença complexa e multifatorial que afeta mulheres em todo o mundo, sendo a causa mais comum de morte por câncer na população feminina em todo o mundo, segunda a Organização Mundial da Saúde (BRAY et al., 2018). Na busca por reduzir a mortalidade pelo câncer se mama se faz necessário compreender os mecanismos moleculares pelos quais estes tumores se desenvolvem e adquirem capacidades adaptativas de progressão tumoral (FENG et al., 2018). A regulação metabólica e o equilíbrio redox nas células tumorais são elementos chaves para esta adaptabilidade dos tumores de mama (KULKOYLUOGLU-COTUL; ARCA; MADAK-ERDOGAN, 2019; LUO et al., 2018; SEMENZA, 2017).

O NFE2L2 é gene que codifica o NRF2, um fator de transcrição crucial para a resposta antioxidante. Usualmente localizado no citoplasma ligado ao KEAP1, o que impede a translocação do NRF2 para o núcleo, onde exerce suas funções. O desligamento de KEAP1 leva A ativação e translocação do NRF2 para o núcleo e pode ocorrer por vários mecanismos: aumento da concentração de ROS, ligação de outras moléculas como p16, BRCA1, PALB2 ou PKC (GORRINI et al., 2014; KONG; CHANDEL, 2020b; TSAI et al., 2017; ZOU et al., 2013). Em estudos independentes e não-relacionados ao câncer de mama, a SIRT1 aumenta a expressão do NFE2L2 (KULKARNI et al., 2014; YANG et al., 2016) e inibe a expressão do UCP2 (BORDONE et al., 2005).

A Sirtuína 1 (SIRT1), por sua vez, é uma deacetilase cuja atividade de regulação da expressão gênica está associada a manutenção da homeostase celular, equilíbrio energético e metabólico e ao balanço redox (DAI et al., 2018; ONG; RAMASAMY, 2018). No câncer o papel da SIRT1 tem sido estudado em diversos tipos tumorais e sua integração em diversas vias metabólicas tem sido demonstrada (SIMMONS; PRUITT; PRUITT, 2015).

Um estudo em câncer de pulmão demonstrou que a expressão do NFE2L2 estava aumentada na situação de hipóxia nas células tumorais, devido ao aumento dos níveis de ROS e redução do UCP2 nestas células (WANG et al., 2017b). O gene UCP2 (Uncoupling Protein-2) codifica uma proteína que atua como transportadora de ânions na mitocôndria, este gene é amplamente expresso em células tumorais e regula a produção de espécies reativas de oxigênio (ROS) (BAFFY, 2019). A expressão de UCP2 foi associada a sensibilidade ao tratamento com quimioterapia baseada em platina no câncer de ovário seroso (KAWANISHI et al., 2018) e também a possível predição de resposta ao tratamento neoadjuvante do câncer de colo de útero localmente avançado (IMAI et al., 2017). No câncer de mama a expressão do UCP2 parece sensibilizar as células tumorais a alguns tratamentos, especialmente a terapia endócrina com tamoxifeno (PONS et al., 2015).

O PPAR*γ* (Peroxisome proliferator-activated receptor gamma, codificado pelo gene PPARG) é um fator de diferenciação que tem papel importante na regulação da adipogênese, crescimento celular, progressão e proliferação tumoral (JANANI; RANJITHA KUMARI, 2015). No câncer de bexiga o PPARG está ativado, seja por aumento da expressão ou pela presença de mutações, sendo um potencial alvo terapêutico em investigação preliminar para o tratamento desses tipos de tumores (GOLDSTEIN et al., 2017). Aparentemente o PPARG também é um alvo em potencial

para o câncer de próstata, pois parece ter papel chave no desenvolvimento do fenótipo metastático neste tumor (AHMAD et al., 2016). Por outro lado, no câncer de mama a expressão do PPARG foi associada a maior sobrevida, tendo sido apontada como preditor independente para o desfecho; de modo que maior expressão do PPARG foi associado a maior sobrevida em pacientes luminais (receptor de estrógeno positivo) que não receberam terapia endócrina para o câncer de mama (ABDULJABBAR et al., 2015).

O RAC1 (*Ras-related C3 botulinum toxin substrate 1*), por outro lado, é uma GTPase da família Ras que desempenha papéis importantes em diversos processos celulares, tais como organização do citoesqueleto, regulação da expressão gênica e migração celular (ISHII; WARABI, 2019). Além disso a RAC1 é um mediador no estresse oxidativo pois é ativado pelos ROS e através de retroalimentação positiva, ativa NOX1 e 2, aumentando a produção dos ROS (MYANT et al., 2013; SUNDARESAN et al., 1996).

A hipótese desse trabalho é que os genes NFE2L2, SIRT1, UCP2, PPARG e RAC1 tem expressões correlacionadas entre si, configurando uma via metabólica do estresse oxidativo em câncer de mama e que os perfis de expressão destes genes estão associados a parâmetros clínicos do câncer de mama.

2. METODOLOGIA

2.1 Amostras e Pacientes

Amostras tumorais de 62 pacientes com câncer de mama foram coletadas no momento da mastectomia no Hospital Barão de Lucena. As amostras foram armazenadas em RNAlater (Qiagen), e mantidas a -80ºC até o momento do uso. O trabalho tem aprovação do Comitê de Ética do Centro de Ciências da Saúde da UFPE

(47869315 0 00005208). Todas as pacientes forneceram o termo de consentimento livre e esclarecido (TCLE) antes de terem as amostras coletadas.

2.2 Análise de expressão gênica

O RNA foi purificado utilizando RNAeasy Kit (Qiagen), e em seguida quantificado pelo NanoDrop 2000 (Thermo). O cDNA foi sintetizado utilizando o kit QuantiNova Reverse Trancription (Qiagen), o cDNA foi quantificado e diluído para 100ng/µL. A análise de expressão dos genes NFE2L2, SIRT1, UCP2, PPARG e RAC1 foi realizada no equipamento StepOne Plus (Applied Biosystems) utilizando o kit GoTaq qPCR Master Mix (Promega). A expressão de β-actina foi utilizada como controle endógeno e o ΔCT (gene β-actina) foi calculado para analisar a quantificação relativa dos genes em cada amostra.

2.3 Análise estatística

As análises estatísticas foram realizadas com GraphPad Prism e R. Comparações de parâmetros com distribuição normal foram realizadas com o teste t de student, para amostras independentes, e teste não paramétrico Mann-Whitney. As análises de correlação entre as expressões gênicas foram feitas através do teste Spearman r, bicaudado. O teste t de Welch foi realizado para amostras paramétricas não pareadas. Os testes de hipóteses foram feitos considerando-se $\alpha=5\%$ ($p<0,05$).

3. RESULTADOS E DISCUSSÃO

3.1 Características Gerais da População

A **tabela 1** traz as características gerais da população do estudo. Ao todo foram coletadas 62 amostras de pacientes com câncer de mama. A média de idade foi de 54,74 anos, a maioria se declarou parda. Quase metade das pacientes (48,3%) têm histórico familiar de câncer e 35,5% delas tem histórico familiar de câncer de mama. Estas características observadas na população aqui estudada estão de acordo com as reportadas pelo estudo brasileiro AMAZONA, que avaliou mais de 4.900 casos de câncer de mama em todo o país (CALEFFI et al., 2018; SIMON et al., 2019). Com relação aos subtipos do câncer de mama, a maioria dos casos tem perfil histológico luminal, como reportado na literatura, neste estudo tivemos mais pacientes luminais B, similar ao que foi previamente reportado em estudo brasileiro conduzido no estado da Paraíba (PINHEIRO; TORRES; PAZ, 2019).

Tabela 1: Características basais da população de câncer de mama

Características	
Idade (média)	54,74 anos
Etnia (%)	
Branca	22,5%
Negra	9,67%
Parda	62,9%
Índia	1,61%
Tabagismo (%)	22,5%
Obesidade (%)	41,9%
Etilismo (%)	11,2%
Histórico Familiar de Câncer (%)	48,3%

Histórico Familiar de Câncer de Mama (%)	35,5%
Tratamento	
Quimioterapia Neoadjuvante (%)	22,5%
Quimioterapia Adjuvante (%)	69,35%
Quimioterapia Adjuvante + Tamoxifeno (%)	1,61%
Quimioterapia Adjuvante + Radioterapia + Tamoxifeno	3,22%
Tamanho (T)	
T1	19,35%
T2	29,03%
T3	27,41%
T4	4,83%
Linfonodos (N)	
N0	41,93%
N1	24,19%
N2	12,9%
N3	1,6%
Metástases (M)	
M0	69,35%
M1	12,9%
Grau Histológico	
Grau 1	1,61%
Grau 2	51,61%
Grau 3	24,19%
Luminais A n (%)	18 (29,03%)
Luminais B n (%)	27 (43,54%)
HER2 n (%)	6 (9,67%)
Triplo Negativo n (%)	7 (11,29%)

A população de pacientes com câncer de mama neste estudo em sua maioria é não obesa e não reportou tabagismo ou etilismo, e as análises estatísticas não

demonstraram correlação destes fatores com a expressão de dos genes testados, com exceção apenas do gene UCP2 com etilismo. Em um estudo populacional com mais de 2.600 casos de câncer de mama avaliados com relação ao consumo de álcool e tabagismo foi demonstrado que o consumo de álcool parece estar associado a menor risco de desenvolver subtipo HER2+ relativo ao ER+; mas o tabagismo não influenciou no risco relativo de nenhum dos subtipos (BAGLIA et al., 2018).

3.2 Análises de Expressão Gênica

A análise de expressão dos genes NFE2L2, SIRT1, UCP2, PPARG e RAC1 foi realizada em 62 pacientes, cuja distribuição de expressão e número de pacientes testadas para cada um dos genes está na **figura 1.** As proporções de expressão gênica nas amostras testadas foram as seguintes: NFE2L2 98,11% (52 de 53 amostras), SIRT1 82% (41 de 50 amostras), UCP2 62,5% (25 de 40 amostras), PPARG 82,6% (38 de 46 amostras) e RAC1 96,5% (55 de 57 amostras).

Figura 1: Distribuição geral da expressão dos genes estudados em câncer de mama.

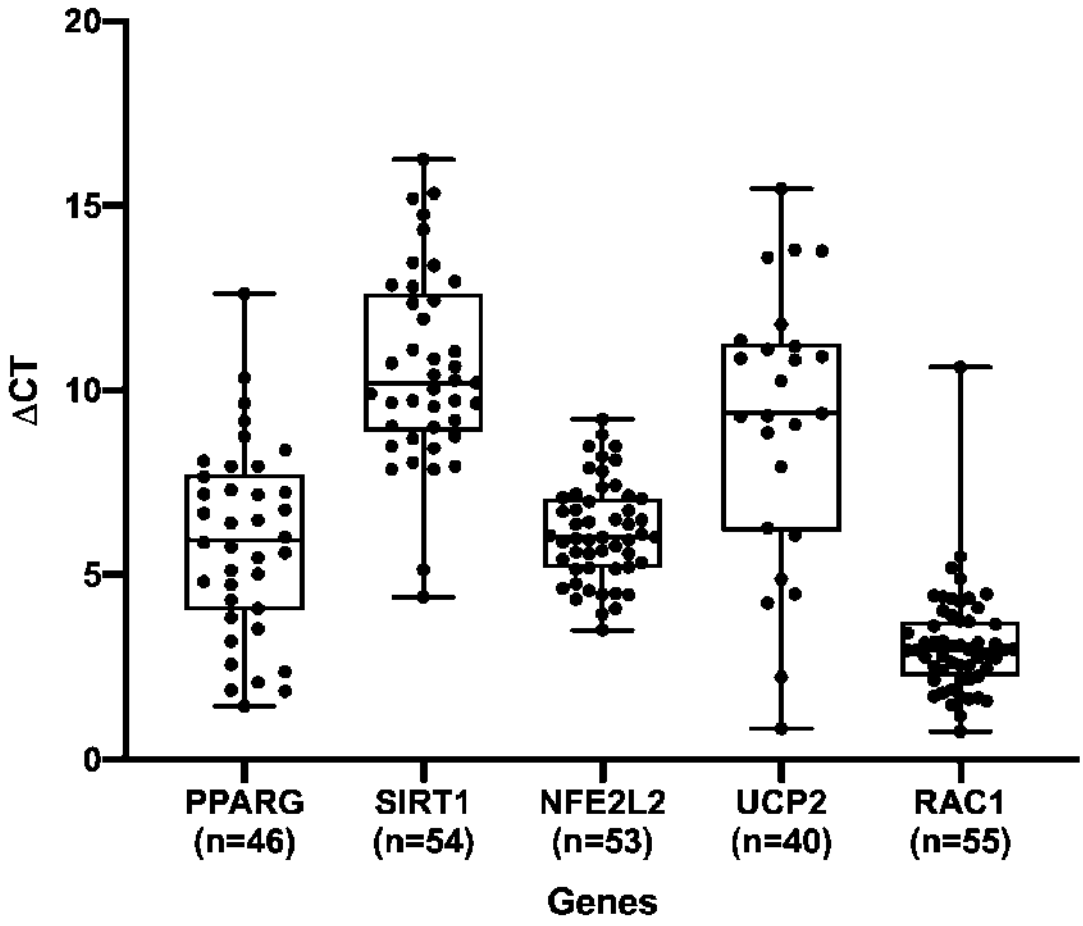

3.2.1 Análise de Correlação de Expressão Entre os Genes

Das 62 pacientes avaliadas neste trabalho, 9 foram testadas para todos os cinco genes em estudo. Nesta subpopulação foram realizados testes de correlação da expressão dos cinco genes entre si através do teste Spearman r de correlação e os resultados significativos estão apresentados na **figura 2.**

Figura 2: Correlação entre a expressão dos genes estudados pelo teste Spearman r, em (A) SIRT1-PPARG, em (B) NFE2L2-PPARG e em (C) NFE2L2-RAC1.

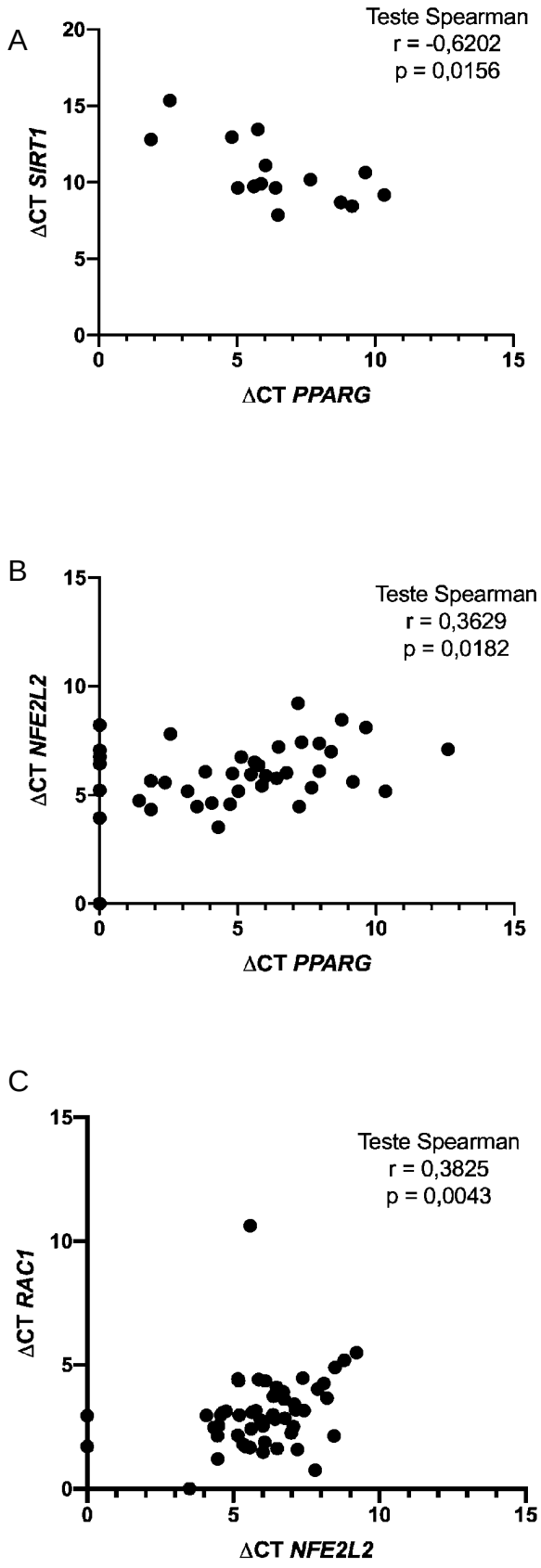

As expressões de SIRT1 e PPARG apresentaram correlação negativa (r=-0,6202, 95%CI -0,8637 a -0,1418, *p*=0,0156), indicando que quanto maior a expressão de SIRT1, menor a expressão do PPARG (e vice-versa) e retificando o que tem sido descrito na literatura do câncer e de outras patologias. Um estudo que avaliou as causas da disfunção cardíaca em modelo animal com diabetes tipo 2 mostrou que com aumento de PPARG houve redução da expressão de SIRT1, o que foi associado a disfunção cardíaca (KALLIORA et al., 2019). Um estudo conduzido em modelo animal avaliou a relação entre SIRT1 e PPARG na artrite gotosa e reportou que a SIRT1 parece ter papel na fase aguda da artrite gotosa através da inibição do infiltrado inflamatório e da secreção de citocinas pró-inflamatórias através do PPARG (WANG et al., 2019). No câncer, esta correlação tem sido descrita como um dos pilares para a manipulação das vias metabólicas, uma vez que o PPARG desempenha papel crucial na adipogênese (SIMMONS; PRUITT; PRUITT, 2015).

No câncer de mama, as evidências de correlação entre estes genes ainda são limitadas. Foi reportado em um estudo em cultura de células que a deficiência da acetilação pela SIRT1 do PPARG mutado está associada a menor síntese lipídica em câncer de mama, especialmente para o subtipo HER2 enriquecido (TIAN et al., 2014). Em cultura de células, demonstrou-se que a SIRT1 inibe a sinalização pela via do estrógeno, a transcrição mediada pelo receptor de estrógeno e a proliferação celular nas células de câncer de mama responsivas ao estrógeno (MOORE; FALLER, 2013). Ainda, de acordo com um trabalho apresentado em 2013 no *San Antonio Breast Cancer Symposium* (SABCS), a acetilação do PPARG induz uma assinatura genética que é aumentada no câncer de mama e está associada a redução da expressão da SIRT1 e um pior desfecho (PESTELL et al., 2013). Desta forma, a correlação da expressão gênica entre SIRT1 e PPARG que este estudo demonstrou parece ser a

primeira proveniente de análise de tecidos tumorais frescos em estudo observacional prospectivo.

A expressão do PPARG foi ainda positiva e significativamente correlacionada com a do NFE2L2 (r=0,3629 CI 95% 0,05706 a 0,6065 *p*=0,0182). Embora relativamente fraca, esta correlação corrobora com dados previamente reportados, que demonstram comunicação entre estas vias para regulação do estresse oxidativo em diferentes condições clínico-patológicas. Uma revisão de literatura que abordou a função do PPARG no estresse oxidativo aponta que ele desempenha função de conter o dano oxidativo e viabilizar a sobrevivência celular. O PPARG seria nesta situação, um ponto de interconexão entre as vias Wnt, FOXO e do NRF2 (proteína codificada pelo NFE2L2). Os dados demonstram que PPARG é um alvo transcricional do NRF2, e que existe entre eles uma retroalimentação positiva: NRF2 aumenta a expressão de PPARG que por sua vez contribui para a ativação do NRF2 (POLVANI; TAROCCHI; GALLI, 2012).

A correlação entre NFE2L2 e PPARG também foi descrita como crucial para a integração do estresse oxidativo com o metabolismo intermediário, no qual o NFE2L2 tem papel de proteção hepática contra esteatose através da estimulação da oxidação dos ácidos graxos e inibição da adipogênese, favorecendo que esta ocorra em tecidos periféricos pela ativação de C/EBPb (*CCAAT/enhancer-binding protein (C/EBP), b*) e PPARG (HAYES; DINKOVA-KOSTOVA, 2014). Um estudo em modelo animal conseguiu demonstrar que a ativação do PPARG pelo NRF2 na injúria pulmonar aguda foi essencial para proteger o tecido do dano oxidativo (CHO et al., 2010). Por outro lado, um estudo que avaliou como a correlação de PPARG e NFE2L2 influencia na reposta imunológica à malária demonstrou que através da estimulação do NFE2L2 houve aumento da expressão do CD36 nos macrófagos, possibilitando a fagocitose

dos eritrócitos infectados pelo *Plasmodium falciparum*, agente causador da malária (OLAGNIER et al., 2011).

No câncer, a expressão e função do PPARG e do NFE2L2 já foram descritas separadamente (WU; LU; BAI, 2019), mas a correlação entre eles tem sido particularmente associada a aspectos farmacogenômicos do tratamento. Um estudo em modelo animal demonstrou que a co-ativação de NFE2L2 e PPARG foi necessária para hepatoproteção por um derivado cumarínico (o umbeliforme) na presença de toxicidade hepática induzida pela ciclofosfamida (MAHMOUD et al., 2017). Já um estudo com células de câncer de pulmão conseguiu demonstrar experimentalmente e por modelo matemático que através da inibição do KEAP1 (responsável por inibir NRF2 no citoplasma) houve ativação de NFE2L2 e PPARG que resultou em sensibilização das células a agentes quimioterápicos (ZHAN et al., 2012). Estes resultados demonstram que o papel desta via de regulação metabólica e antioxidante o câncer vai além da etiopatologia tumoral e poderá ser uma estratégia para o desenvolvimento de novas terapias. No câncer de mama especificamente, não foi possível encontrar dados previamente reportados de correlação entre estes dois genes em estudo observacional prospectivo, de forma que a evidência apresentada neste trabalho abre novas possibilidades no estudo do câncer de mama.

A terceira correlação observada foi entre a expressão dos genes NFE2L2 e RAC1 (r=0,3825; CI95% 0,1199 a 0,5951; *p*=0,0043). Até o momento, esta é a primeira vez em que se observa em estudo prospectivo em amostras teciduais frescas de câncer de mama, algo interessante por quê o racional molecular entre os dois genes e o estresse oxidativo tem sido alvo de investigação *in vitro*. A correlação de NRF2 e SIRT1 foi previamente investigada em modelo experimental para análise de assinatura transcriptômica de perfis celulares inflamatórios. Foi observado que a

ativação de NFE2L2 por RAC1 parece ser independente do KEAP1, utilizando alternativamente o eixo do NF-κB para induzir o NRF2 (CUADRADO et al., 2014). Estudo *in vitro* avaliou quais eram os mecanismos que levam a expressão do HIF-1 (*Hypoxia-inducible factor 1*) em células de câncer de mama, onde foi demonstrado que a hipóxia pode além de induzir a expressão do HIF-1, ativa RAC1 através das vias de PI3K e ERK (DU et al., 2011). Uma análise *in vitro* avaliou os mecanismos de ativação no NRF2 a partir da sinalização do Receptor de estrógeno de membrana (ER- α36) acoplado a GPER (proteína G acoplada ao receptor de estrógeno). Pelo que foi observado neste estudo, a ativação do NRF2 em resposta a sinalização de ER- α36/GPER se dá de duas maneiras, a primeira pela CK2 (caseína quinase 2) fosforilando diretamente NRF2; e a segunda pelo eixo EGFR-Ras-PI3K-Akt que inibe GSK3β (*glycogen synthase kinase 3β*) e favorece a translocação de NRF2 (ISHII; WARABI, 2019). Juntas, estas evidências apontam que a expressão e atividade de RAC1 e NFE2L2 em câncer de mama fazem parte de um contexto metabólico que envolve outras vias clássicas das células tumorais mamárias, como PI3K e ER. Sendo assim, a correlação aqui descrita fornece nova evidência da importância desta via no câncer de mama, podendo ser ponto de partida para estudos de novas estratégias terapêuticas.

3.2.2 Associação de Expressão Gênica com Parâmetros Clínicos

A análise dos cinco genes estudados foi conduzida para avaliar se houve associação entre a expressão de cada um dos genes e os principais parâmetros clínicos do câncer de mama. Nesta etapa o teste de Mann-Whitney (para variáveis paramétricas) ou T de Welch (para variáveis não paramétricas) foram aplicados e os resultados combinados de acordo com cada um dos parâmetros clínicos avaliados.

A classificação do câncer de mama em subtipos biológicos é uma das primeiras etapas ao diagnóstico, pois direciona a diferentes condutas clínicas, visto que estes subtipos estão associados a diferentes sobrevida livre de recorrência e sobrevida global (GRADISHAR et al., 2019). Para fins de análises estatísticas, neste trabalho foram considerados três subgrupos: Luminais (incluindo luminal A e B), HER2 e Triplo Negativo. Os resultados das análises dos genes PPARG, SIRT1, RAC1, NFE2L2 e UCP2 para os três subtipos está apresentado na **figura 3**.

Não houve diferença estatística entre a expressão gênica de PPARG, SIRT1, NFE2L2 e UCP2 entre os subtipos do câncer de mama. No entanto, o gene RAC1 se apresentou significativamente mais expresso no subtipo HER2 enriquecido se comparado ao Luminal (p=0,0036), e menos expresso se comparado ao Triplo negativo (p=0,0152). Avaliação da expressão de RAC1 por imunohistoquímica e Western Blot em 37 pacientes (10 carcinomas ductais *in situ*, 20 com tumores comprometendo linfonodos, 5 controles saudáveis e 2 fibroadenomas) demonstrou aumento de expressão do RAC1 nas amostras com câncer de mama, mas não foi reportada análise dos subtipos biológicos e se há diferença entre eles (SCHNELZER et al., 2000). No câncer de mama HER2+ a via de sinalização do HER2 está muitas vezes mais ativa e expressa do que nos demais subtipos, conferindo a este subtipo um fenótipo mais agressivo. Um estudo *in vitro* foi capaz de demonstrar que o eixo CUL3/KCTD10/RhoB é responsável por regular positivamente o RAC1 nas células HER2+ (MURAKAMI et al., 2019). Sendo assim, o resultado aqui apresentado corrobora com este reportado por Murakami em 2019 pois demonstrou na população estudada que há associação entre HER2 e RAC1.

Figura 3: Análise da expressão dos genes (A) PPARG, (B) SIRT1, (C) NFE2L2, (D) UCP2 e (E) RAC1 nos subtipos luminal, HER2 e triplo negativo de câncer de mama.

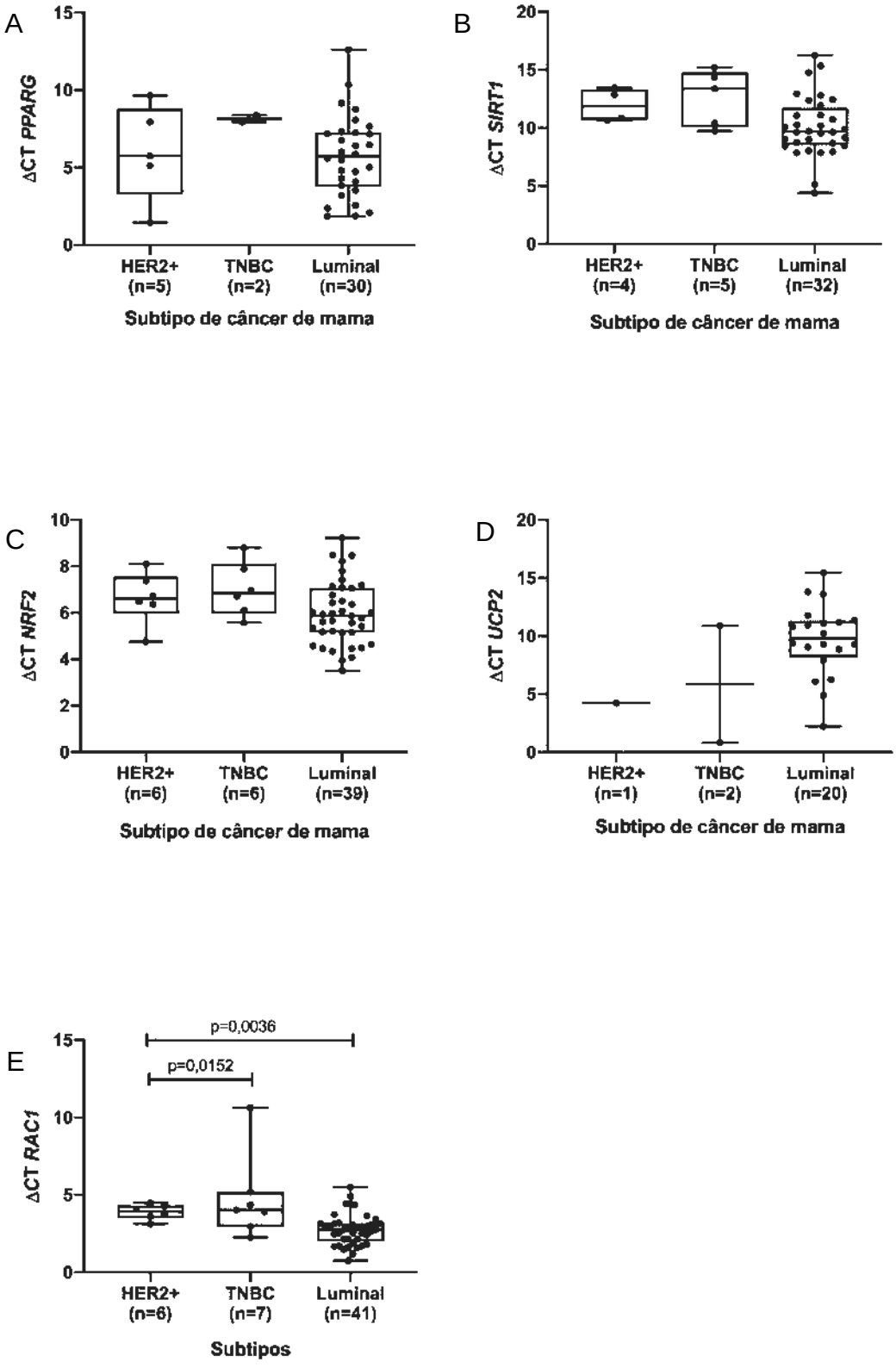

Adicionalmente, ainda nos tumores HER2+ o papel de RAC1 parece estar relacionado também a resistência ao tratamento com trastuzumabe, um anticorpo monoclonal anti-HER2, que é a base da terapia para este subtipo de câncer de mama

(DOKMANOVIC et al., 2009). Com isto, o resultado apresentado neste estudo reforça os achados prévios e também fornece embasamento para investigação do RAC1 como alvo para impedir ou reverter a resistência ao trastuzumabe.

Para avaliar a expressão dos genes estudados ao longo dos diferentes estágios do câncer de mama, foi considerada a classificação dos estádios pela recomendação do *National Cancer Comprehensive Network* (NCCN) (GRADISHAR et al., 2019) de forma simplificada. Sendo assim utilizamos estágio I (até 2 cm, comprometimento linfonodal de não mais que 2 mm e metástase ausente); estádio II (de 2 a 5 cm, linfonodos N0 ou N1 e metástase ausente); e estádio III (neste trabalho consideramos como estádio III também os casos de estádio IV, devido o número restrito de casos com metástase nesta casuística – logo, todos os tumores acima de 5 cm, que atingiram a parede toráxica, com linfodos N0 a N3 e/ou presença de metástase). Para determinação e análise do grau histológico a classificação tradicional foi adotada, mas foram agrupados os tumores de grau I e II para análise.

Os resultados das análises dos genes PPARG, SIRT1, RAC1, NFE2L2 e UCP2 para os três estádios está apresentado na **figura 4**. A expressão do PPARG foi avaliada de acordo com o estadiamento do câncer de mama através do teste t de variações desiguais de Welch (para amostras não pareadas), demonstrando diferença significativa entre a expressão do PPARG entre o estadiamento I e o III (p=0,0335) (**figura 4A**).

Figura 4: Análise da expressão dos genes (A) PPARG, (B) SIRT1, (C) NFE2L2, (D) UCP2 e (E) RAC1 nos estádios I, II e III do câncer de mama.

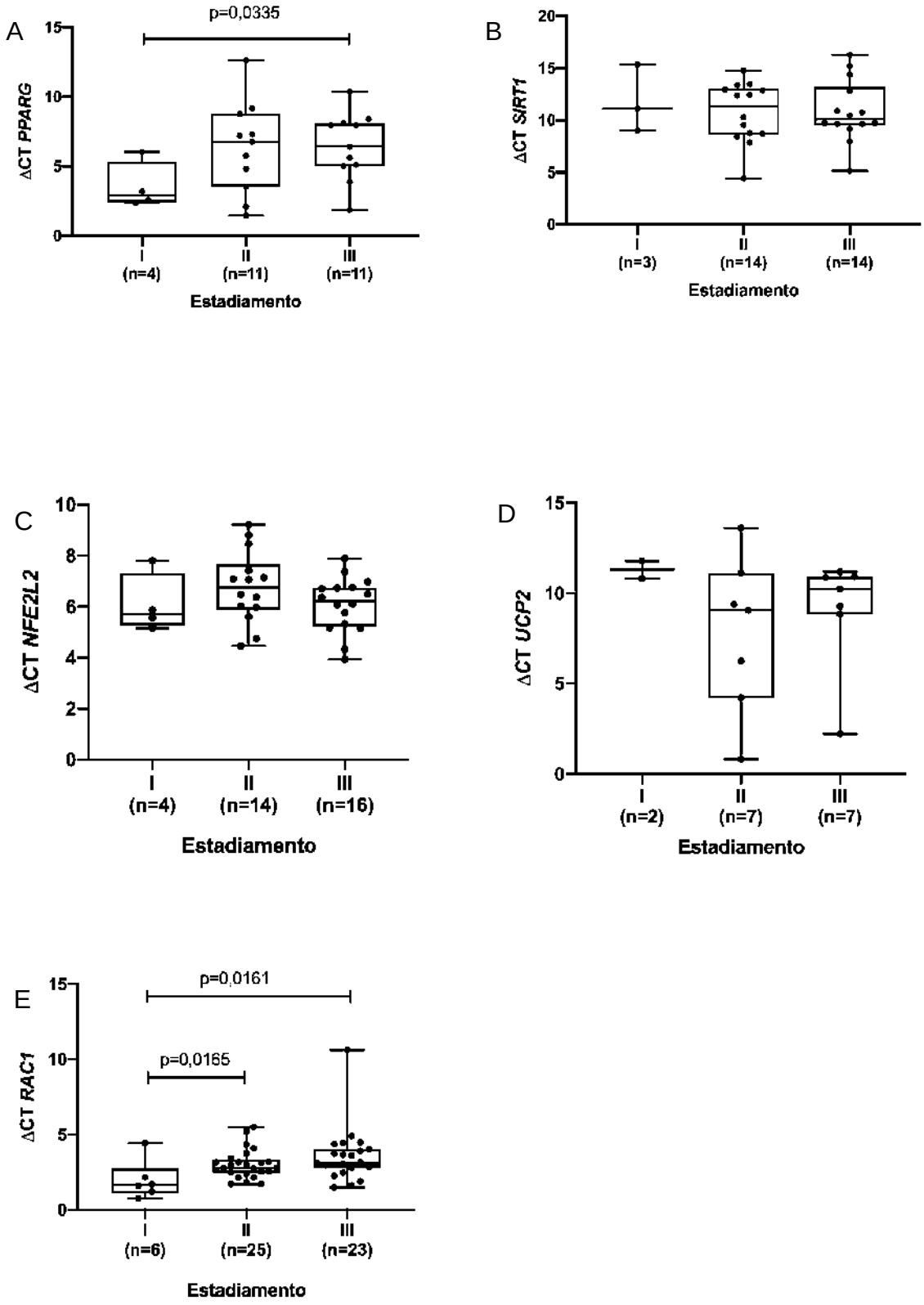

Não foram encontrados estudos reportando expressão de PPARG em amostras de câncer de mama e a associação aqui reportada parece ser a primeira a demonstrar diferença nos níveis de PPARG entre estádios I e III do câncer de mama. No entanto este trabalho corrobora com um estudo *in silico* que realizou análise integrada de bases de dados do *Gene Expression Omnibus of the National Center for Biotechnology Information* e reportou expressão aumentada de PPARG em câncer de mama (GONG et al., 2018).

Uma segunda análise integrativa de expressão de mRNA demonstrou que as vias do PPARG, juntamente com a do metabolismo do ácido araquidônico, parecem estar relacionadas a menor incidência de mortalidade de câncer de mama em americanos-asiáticos do que em americanos-caucasianos, sendo estas vias as responsáveis por integrar fatores ambientais e genéticos (SHI et al., 2017).

O gene RAC1 teve sua expressão significativamente diferente entre os estágios do câncer de mama, de forma que quanto maior o estágio, menor a expressão de RAC1 (**figura 4E**). Este dado se confirmou pela análise da expressão de acordo com o tamanho do tumor que demonstrou que RAC1 está significativamente mais expresso em T1 (até 2cm) do que em T3 (maior que 5cm) (p=0,0347). A expressão e atividade do RAC1 em câncer de mama têm sido estudadas e ele está associado ao fenótipo invasivo e metastático do (BAUGHER et al., 2005), sendo requerido para a transição epitélio-mesenquimal (SHIN et al., 2019) e para a reversão da polaridade celular (LIU et al., 2017). O perfil de expressão do RAC1 observado na população deste estudo vai de encontro ao que se esperaria, pois conforme demonstrado pelos estudos *in vitro* comentados, a expressão do RAC1 em estágios mais avançados deveria ser maior do que em estágios iniciais. Uma limitação importante nesta análise é que não temos a avaliação da expressão em tecido de mama sadio. Esta comparação foi feita

em outro estudo (SCHNELZER et al., 2000) e mostrou que a expressão no câncer é quase três vezes maior. Pode ser que mesmo sendo menor do que em estágios iniciais, a expressão do RAC1 que detectamos em estágios II e III seja suficiente para determinar as características de invasividade e metastatização tumoral observadas *in silico*.

A expressão dos genes PPARG, SIRT1, RAC1, NFE2L2 e UCP2 não foi diferente na comparação dos s graus histológicos, como mostra a **figura 5**. No presente estudo a única associação significativa observada para o gene UCP2 foi aumento da expressão em pacientes de câncer de mama não etilistas (p=0,0083 CI 95% 0,89 a 5,02). A observação da expressão de UCP2 em câncer de mama e hábito de consumo de álcool ainda não foi reportada. No entanto, existem evidencias que apontam que o aumento de UCP2 tem papel na redução do tempo de recuperação após intoxicação aguda por álcool (HORVATH et al., 2002). A expressão do UCP2 no câncer de mama foi reportada como aumentada e associada a propriedades tumorigênicas, inclusive a mediação do Efeito Warbug (AYYASAMY et al., 2011). Adicionalmente, a expressão do UCP2 também foi associada a promoção de quimiorresistência em células tumorais, indicando que este poderá ser um potencial alvo terapêutico para reverter resistência a tratamentos quimioterápicos (DERDAK et al., 2008). Embora neste estudo não tenha sido avaliada a incidência de quimiorresistência, foi observada expressão de UCP2 em 62% das amostras de câncer de mama, abrindo a possibilidade de se realizar análises posteriores para avaliação deste parâmetro de tratamento.

Figura 5: Análise da expressão dos genes (A) PPARG, (B) SIRT1, (C) NFE2L2, (D) UCP2 e (E) RAC1 no câncer de mama de acordo com o grau histológico.

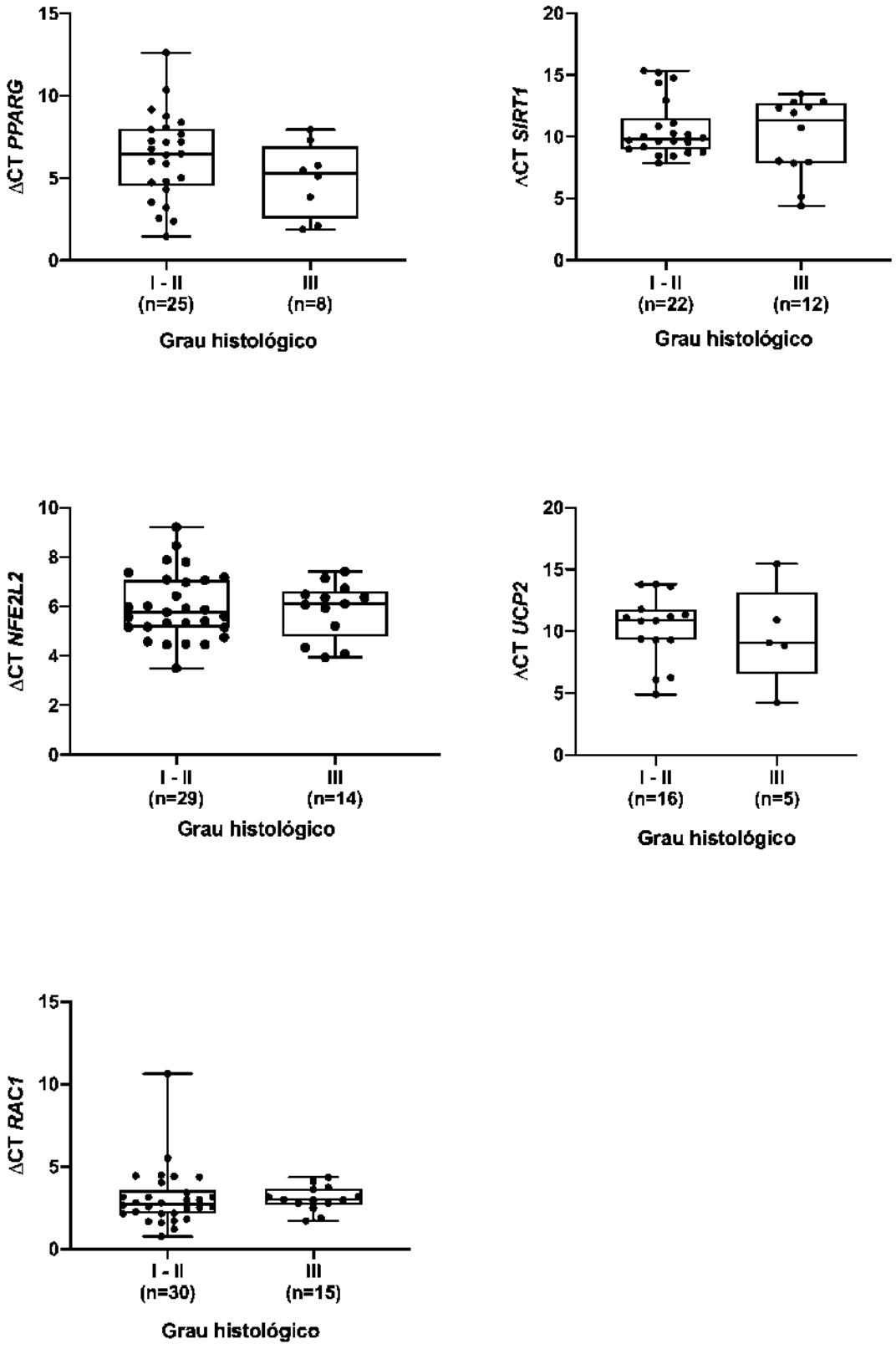

4. CONCLUSÕES

A modulação do estresse oxidativo e das vias moleculares pró e antioxidantes são um alvo do estudo do câncer dado que estão associados a várias das características que constituem os hallmarks do câncer. Diversas moléculas do estresse oxidativo tem, portanto, sido estudadas como potenciais alvos terapêuticos para o câncer (KONG; CHANDEL, 2020a).

Neste trabalho foi estudada a hipótese de que o NFE2L2, SIRT1, RAC1, PPARG e UCP2 têm suas expressões gênicas correlacionada no câncer de mama e estão associados a apresentação clínica destas pacientes. Os resultados aqui apresentados de correlação entre os genes PPARG-SIRT, PPARG-NFE2L2 e NFE2L2-RAC1 são, até onde vai o nosso conhecimento, inéditos em estudo prospectivo com amostras tumorais frescas; e indicam um potencial eixo metabólico no câncer de mama que é descrito aqui pela primeira vez. Adicionalmente, foram avaliados os principais parâmetros clínicos do câncer de mama: subtipo, estadiamento e grau histológico; o que demonstrou o perfil de expressão de cada gene nos diferentes subtipos e ao longo do desenvolvimento tumoral. Destacando-se que através dessas análises foram identificados potenciais marcadores de agressividade e sensibilidade ou resistência a tratamento. Em conclusão, os resultados deste trabalho trazem novas evidências para a busca de marcadores moleculares no câncer de mama, traçando o caminho para a oncologia de precisão.

5. REFERÊNCIAS

ABDULJABBAR, R. et al. Prognostic and biological significance of peroxisome proliferator-activated receptor-gamma in luminal breast cancer. Breast Cancer Research and Treatment, v. 150, n. 3, p. 511–522, 1 abr. 2015.

AHMAD, I. et al. Sleeping beauty screen reveals Pparg activation in metastatic prostate cancer. Proceedings of the National Academy of Sciences of the United States of America, v. 113, n. 29, p. 8290–8295, 19 jul. 2016.

AYYASAMY, V. et al. Cellular model of Warburg Effect identifies tumor promoting function of UCP2 in breast cancer and its suppression by genipin. PLoS ONE, v. 6, n. 9, p. e24792, 15 set. 2011.

BAFFY, G. Hanging in the balance: mitochondrial uncoupling protein-2 and the tumor microenvironment. Precision Cancer Medicine, v. 2, p. 12–12, 2019.

BAGLIA, M. L. et al. Alcohol, smoking, and risk of Her2-overexpressing and triple-negative breast cancer relative to estrogen receptor-positive breast cancer. International Journal of Cancer, v. 143, n. 8, p. 1849–1857, 2018.

BAUGHER, P. J. et al. Rac1 and Rac3 isoform activation is involved in the invasive and metastatic phenotype of human breast cancer cells. Breast cancer research : BCR, v. 7, n. 6, p. R965-74, 30 dez. 2005.

BORDONE, L. et al. Sirt1 Regulates Insulin Secretion by Repressing UCP2 in Pancreatic β Cells. PLoS Biology, v. 4, n. 2, p. e31, 27 dez. 2005.

BRAY, F. et al. Global cancer statistics 2018: GLOBOCAN estimates of incidence and mortality worldwide for 36 cancers in 185 countries. CA: A Cancer Journal for Clinicians, 12 set. 2018.

CALEFFI, M. et al. The AMAZONA Project: Retrospective Cohort Study Describing Breast Cancer Patients' Characteristics and Survival in Brazil. Journal of Global Oncology, n. 4_suppl_2, p. 219s-219s, out. 2018.

CHO, H. Y. et al. Nrf2-regulated PPARγ expression is critical to protection against acute lung injury in mice. American Journal of Respiratory and Critical Care Medicine, v. 182, n. 2, p. 170–182, 2010.

CUADRADO, A. et al. Transcription factors NRF2 and NF-κB are coordinated effectors of the rho family, GTP-binding protein RAC1 during Inflammation. Journal of Biological Chemistry, v. 289, n. 22, p. 15244–15258, 30 maio 2014.

DAI, H. et al. Sirtuin activators and inhibitors: Promises, achievements, and challenges. Pharmacology and Therapeutics, v. 188, p. 140–154, 2018.

DERDAK, Z. et al. The mitochondrial uncoupling protein-2 promotes chemoresistance in cancer cells. Cancer Research, v. 68, n. 8, p. 2813–2819, 15 abr. 2008.

DOKMANOVIC, M. et al. Rac1 contributes to trastuzumab resistance of breast cancer cells: Rac1 as a potential therapeutic target for the treatment of trastuzumab-resistant breast cancer. Molecular Cancer Therapeutics, v. 8, n. 6, p. 1557–1569, 2009.

DU, J. et al. PI3K and ERK-Induced Rac1 Activation Mediates Hypoxia-Induced HIF-1α Expression in MCF-7 Breast Cancer Cells. PLoS ONE, v. 6, n. 9, p. e25213, 27 set. 2011.

FENG, Y. et al. Breast cancer development and progression: Risk factors, cancer stem cells, signaling pathways, genomics, and molecular pathogenesisGenes and DiseasesChongqing yi ke da xue, di 2 lin chuang xue yuan Bing du xing gan yan yan jiu suo, , 1 jun. 2018.

GOLDSTEIN, J. T. et al. Genomic activation of PPARG reveals a candidate therapeutic axis in bladder cancer. Cancer Research, v. 77, n. 24, p. 6987–6998, 2017.

GONG, M. T. et al. Comprehensive integrated analysis of gene expression datasets identifies key anti-cancer targets in different stages of breast cancer. Experimental and Therapeutic Medicine, v. 16, n. 2, p. 802–810, 1 ago. 2018.

GORRINI, C. et al. Estrogen controls the survival of BRCA1-deficient cells via a PI3K-NRF2-regulated pathway. Proceedings of the National Academy of Sciences of the United States of America, v. 111, n. 12, p. 4472–7, 25 mar. 2014.

GRADISHAR, W. J. et al. NCCN Guidelines Version 3.2019 Breast Cancer. [s.l: s.n.].

HAYES, J. D.; DINKOVA-KOSTOVA, A. T. The Nrf2 regulatory network provides an interface between redox and intermediary metabolism. Trends in Biochemical Sciences, v. 39, n. 4, p. 199–218, 2014.

HORVATH, B. et al. Uncoupling protein 2 (UCP2) lowers alcohol sensitivity and pain threshold. Biochemical Pharmacology, v. 64, n. 3, p. 369–374, 1 ago. 2002.

IMAI, K. et al. UCP2 expression may represent a predictive marker of neoadjuvant chemotherapy effectiveness for locally advanced uterine cervical cancer. Oncology Letters, v. 14, n. 1, p. 951–957, 2017.

ISHII, T.; WARABI, E. Mechanism of rapid nuclear factor-e2-related factor 2 (Nrf2) activation via membrane-associated estrogen receptors: Roles of NADPH oxidase 1, neutral sphingomyelinase 2 and epidermal growth factor receptor (EGFR). Antioxidants, v. 8, n. 3, p. 1–17, 2019.

JANANI, C.; RANJITHA KUMARI, B. D. PPAR gamma gene - A reviewDiabetes and Metabolic Syndrome: Clinical Research and ReviewsElsevier Ltd, , 1 jan. 2015.

KALLIORA, C. et al. Dual PPARα/γ activation inhibitsSIRT1-PGC1α axis and causes cardiac dysfunction. JCI Insight, v. 4, n. 17, 5 set. 2019.

KAWANISHI, M. et al. Expression of UCP2 is associated with sensitivity to platinum-based chemotherapy for ovarian serous carcinoma. Oncology Letters, v. 15, n. 6, p. 9923–9928, 1 jun. 2018.

KONG, H.; CHANDEL, N. S. Reactive oxygen species and cancer. [s.l.] Elsevier Inc., 2020a.

KONG, H.; CHANDEL, N. S. Reactive oxygen species and cancer. In: SIES, H. (Ed.). . Oxidative Stress. [s.l.] Academic Press, 2020b. v. 8p. 619–637.

KULKARNI, S. R. et al. Fasting induces nuclear factor E2-related factor 2 and ATP-binding cassette transporters via protein kinase a and sirtuin-1 in mouse and human. Antioxidants and Redox Signaling, v. 20, n. 1, p. 15–30, jan. 2014.

KULKOYLUOGLU-COTUL, E.; ARCA, A.; MADAK-ERDOGAN, Z. Crosstalk between Estrogen Signaling and Breast Cancer MetabolismTrends in Endocrinology and MetabolismElsevier Inc., , 1 jan. 2019.

LIU, B. et al. High expression of rac1 is correlated with partial reversed cell polarity and poor prognosis in invasive ductal carcinoma of the breast. Tumor Biology, v. 39, n. 7, p. 1–8, 3 jul. 2017.

LUO, M. et al. Targeting Breast Cancer Stem Cell State Equilibrium through Modulation of Redox Signaling. Cell Metabolism, v. 28, n. 1, p. 69- 86.e6, 3 jul. 2018.

MAHMOUD, A. M. et al. Possible involvement of Nrf2 and PPARγ up-regulation in the protective effect of umbelliferone against cyclophosphamide-induced hepatotoxicity. Biomedicine and Pharmacotherapy, v. 86, p. 297–306, 1 fev. 2017.

MOORE, R. L.; FALLER, D. V. SIRT1 represses estrogen-signaling, ligand-independent ERα-mediated transcription, and cell proliferation in estrogen-responsive breast cells. Journal of Endocrinology, v. 216, n. 3, p. 273–285, 2013.

MURAKAMI, A. et al. Cullin-3/KCTD10 E3 complex is essential for Rac1 activation through RhoB degradation in human epidermal growth factor receptor 2-positive breast cancer cells. Cancer Science, v. 110, n. 2, p. 650–661, 1 fev. 2019.

MYANT, K. B. et al. ROS Production and NF-κB Activation Triggered by RAC1 Facilitate WNT-Driven Intestinal Stem Cell Proliferation and Colorectal Cancer Initiation. Cell Stem Cell, v. 12, n. 6, p. 761–773, 6 jun. 2013.

OLAGNIER, D. et al. Nrf2, a pparγ alternative pathway to promote cd36 expression on inflammatory macrophages: Implication for malaria. PLoS Pathogens, v. 7, n. 9, p. e1002254, 15 set. 2011.

ONG, A. L. C.; RAMASAMY, T. S. Role of Sirtuin1-p53 regulatory axis in aging, cancer and cellular reprogramming. Ageing Research Reviews, v. 43, n. January, p. 64–80, 2018.

PESTELL, R. et al. Abstract P2-06-02: Pparg deacetylation by SIRT1 determines breast tumor lipid synthesis and growth. American Association for Cancer Research (AACR), 15 dez. 2013

PINHEIRO, J. B. F.; TORRES, A. DE F.; PAZ, A. R. DA. Immunohistochemical profile of breast cancer subtypes in patients seen at Napoleão Laureano Hospital, Paraíba, Brazil. Mastology, v. 29, n. 2, p. 58–63, 2019.

POLVANI, S.; TAROCCHI, M.; GALLI, A. PPAR and oxidative stress: Con(β) catenating NRF2 and FOXO. PPAR Research, v. 2012, n. ID 641087, p. 1–15, 2012.

PONS, D. G. et al. UCP2 inhibition sensitizes breast cancer cells to therapeutic agents by increasing oxidative stress. Free Radical Biology and Medicine, v. 86, p. 67–77, 6 jul. 2015.

SCHNELZER, A. et al. Rac1 in human breast cancer: Overexpression, mutation analysis, and characterization of a new isoform, Rac1b. Oncogene, v. 19, n. 26, p. 3013–3020, 15 jun. 2000.

SEMENZA, G. L. Hypoxia-inducible factors: coupling glucose metabolism and redox regulation with induction of the breast cancer stem cell phenotype. The EMBO Journal, v. 36, n. 3, p. 252–259, 22 fev. 2017.

SHI, Y. et al. Integrative comparison of mRNA expression patterns in breast cancers from Caucasian and Asian Americans with implications for precision medicine. Cancer Research, v. 77, n. 2, p. 423–433, 15 jan. 2017.

SHIN, S. et al. ERK2 regulates epithelial-to-mesenchymal plasticity through DOCK10-dependent Rac1/FoxO1 activation. Proceedings of the National Academy of Sciences of the United States of America, v. 116, n. 8, p. 2967–2976, 19 fev. 2019.

SIMMONS, G. E.; PRUITT, W. M.; PRUITT, K. Diverse roles of SIRT1 in cancer biology and lipid metabolismInternational Journal of Molecular Sciences, 5 jan. 2015.

SIMON, S. D. et al. Characteristics and prognosis of stage I-III breast cancer subtypes in Brazil: The AMAZONA retrospective cohort study. Breast, v. 44, p. 113–119, 1 abr. 2019.

SUNDARESAN, M. et al. Regulation of reactive-oxygen-species generation in fibroblasts by Rac1. The Biochemical journal, v. 318 (Pt 2), n. 2, p. 379–82, 1 set. 1996.

TIAN, L. et al. Acetylation-defective mutants of Pparγ are associated with decreased lipid synthesis in breast cancer cells. Oncotarget, v. 5, n. 17, p. 7303–7315, 2014.

TSAI, C.-H. et al. Docosahexaenoic acid increases the expression of oxidative stress-induced growth inhibitor 1 through the PI3K/Akt/Nrf2 signaling pathway in breast cancer cells. Food and Chemical Toxicology, v. 108, p. 276–288, 1 out. 2017.

WANG, J. et al. Sirt1 inhibits gouty arthritis via activating PPARγ. Clinical Rheumatology, 31 jul. 2019.

WANG, M. et al. Uncoupling protein 2 downregulation by hypoxia through repression of peroxisome proliferator-activated receptor γ promotes chemoresistance of non-small cell lung cancer. Oncotarget, v. 8, n. 5, p. 8083–8094, 2017.

WU, S.; LU, H.; BAI, Y. Nrf2 in cancers: A double-edged sword. Cancer Medicine, v. 8, n. 5, p. 2252–2267, 30 maio 2019.

YANG, D. et al. Regulation of Sirt1/Nrf2/TNF-α signaling pathway by luteolin is critical to attenuate acute mercuric chloride exposure induced hepatotoxicity. Scientific Reports, v. 6, 17 nov. 2016.

ZHAN, L. et al. Regulatory role of KEAP1 and NRF2 in PPARγ expression and chemoresistance in human non-small-cell lung carcinoma cells. Free Radical Biology and Medicine, v. 53, n. 4, p. 758–768, 15 ago. 2012.

ZOU, W. et al. PI3K/Akt pathway mediates Nrf2/ARE activation in human L02 hepatocytes exposed to low-concentration HBCDs. Environmental Science and Technology, v. 47, n. 21, p. 12434–12440, 2013.

APÊNDICE C - ARTIGO EM COLABORAÇÃO

A SENSITVE AND SELECTIVE LABEL-FREE ELECTROCHEMICAL DNA BIOSENSOR FOR THE DETECTION O SPECIFIC DENGUE VIRUS SEROTYPE 3 SEQUENCES

Sensors **2015**, *15*, 15562-15577; doi:10.3390/s150715562

OPEN ACCESS

sensors

ISSN 1424-8220

www.mdpi.com/journal/sensors

Article

A Sensitive and Selective Label-Free Electrochemical DNA Biosensor for the Detection of Specific Dengue Virus Serotype 3 Sequences

Natália Oliveira [1,*], Elaine Souza [2], Danielly Ferreira [1], Deborah Zanforlin [1], Wessulla Bezerra [1], Maria Amélia Borba [1], Mariana Arruda [1], Kennya Lopes [3], Gustavo Nascimento [1], Danyelly Martins [1,4], Marli Cordeiro [4] and José Lima-Filho [1,4]

[1] Laboratório de Imunopatologia Keizo Asami (LIKA), Universidade Federal de Pernambuco-UFPE, Av. Prof. Moraes Rego, s/n, Campus da UFPE, 50670-901 Recife, PE, Brazil; E-Mails: daniellylsantos@hotmail.com (D.F.); deborahzanforin@gmail.com (D.Z.); wessullas@yahoo.com.br (W.B.); mariameliaborba@gmail.com (M.A.B.); mariana.s.arruda@gmail.com (M.A.); galvesn23@gmail.com (G.N.); bruneska@prospecmol.org (D.M.); joseluiz60@mac.com (J.L.-F.)

[2] Universidade Federal de Alagoas (UFAL), Campus Arapiraca, Av. Manoel Severino Barbosa, s/n, Bom Sucesso, 57.309-005 Arapiraca, AL, Brazil; E-Mail: elainevms@yahoo.com.br

[3] Departamento de Virologia e Terapia Experimental (LAVITE), Centro de Pesquisas Aggeu Magalhães (CPqAM), Fundação Oswaldo Cruz (Fiocruz)—Pernambuco, Av. Professor Moraes Rego, s/n, Campus da UFPE, 50.670-420 Recife, PE, Brazil; E-Mail: kennya.genne@bol.com.br

[4] Departamento de Bioquímica, Universidade Federal de Pernambuco-UFPE, Av. Professor Moraes Rego, s/n, Campus da UFPE, CEP: 50670-901 Recife, PE, Brazil; E-Mail: Marli@cpqam.fiocruz.br

* Author to whom correspondence should be addressed; E-Mail: nataliacybelle.89@gmail.com Tel: +55-81-2101-2508; Fax: +55-81-2126-8000.

Academic Editor: Stephen Holler

Received: 1 March 2015 / Accepted: 23 June 2015 / Published: 1 July 2015

Abstract: Dengue fever is the most prevalent vector-borne disease in the world, with nearly 100 million people infected every year. Early diagnosis and identification of the pathogen are crucial steps for the treatment and for prevention of the disease, mainly in areas where the co-circulation of different serotypes is common, increasing the outcome of dengue hemorrhagic fever (DHF) and dengue shock syndrome (DSS). Due to the lack of fast and inexpensive methods available for the identification of dengue serotypes, herein we report

the development of an electrochemical DNA biosensor for the detection of sequences of dengue virus serotype 3 (DENV-3). DENV-3 probe was designed using bioinformatics software and differential pulse voltammetry (DPV) was used for electrochemical analysis. The results showed that a 22-m sequence was the best DNA probe for the identification of DENV-3. The optimum concentration of the DNA probe immobilized onto the electrode surface is 500 nM and a low detection limit of the system (3.09 nM). Moreover, this system allows selective detection of DENV-3 sequences in buffer and human serum solutions. Therefore, the application of DNA biosensors for diagnostics at the molecular level may contribute to future advances in the implementation of specific, effective and rapid detection methods for the diagnosis dengue viruses.

Keywords: dengue fever; DNA biosensors; differential pulse voltammetry; electrochemical detection; guanine oxidation

1. Introduction

Dengue fever is the most prevalent vector-borne disease in the world. The World Health Organization (WHO) estimates that some 100 million people are infected every year; however, some studies have predicted that this number could be greatly underestimated, and is actually closer to 390 million [1–3]. The distribution of the disease is mainly in tropical and subtropical regions and recently, it is has been increasingly seen in urban and semi-urban areas. All these factors have contributed to reveal dengue fever as a major interuational public health problem [1,2,4,5].

The infection is caused by a single stranded RNA-virus (DENV) of about 10.7 kb, which belongs to the *Flaviviridae* family, with approximately four antigenically distinct serotypes (DENV-1–DENV-4) [6,7]. The disease exhibits a wide range of symptoms, such as fever, headache and myalgia, which are the most common in classic dengue. Nevertheless, it can also shows more severe manifestations, like in dengue hemorrhagic fever (DHF) or dengue shock syndrome (DSS), which present life-threatening symptoms, such as bleeding, thrombocytopenia and vascular leakage [8–10].

Early diagnosis and identification of the pathogen are necessary for the prevention and treatment of patients, as well as for the avoidance of new outbreaks and emergence of severe cases of dengue, since it is known that the co-circulation of different serotypes in an area increases the possibility of DHF and DSS outcomes [11,12].

Methods to confirm dengue virus infection may involve detection of the virion, viral RNA, antigens or antibodies [13]. Virus detection by cell culture, viral nucleic acid or antigen detection (nonstructural protein 1 or NS1 antigen) can be used to confirm dengue infection in the acute phase of the illness (0–7 days following the onset of the symptoms) [14,15]. In the later phase of the disease, serologic tests are more applied and preferred for diagnosis, as the sensitivity of virus isolation and antigen reactivity decreases [16]. Viral antigen (NS1) detection assays are rapid, reliable and easy to perform, however, they cannot allow to distinguish between different viral serotypes [17,18].

Viral isolation, although considered the gold standard diagnostic method, is time-consuming and highly complex compared with other direct virus detection techniques [1,19]. On the other hand, the

RT-PCR assay is widely used, it allows the detection of low copies of viral genes in less than 48 h [20]. However, both techniques are costly and labor-intensive, but they are more specific than serologic methods used for antibody detection and allow one to differentiate between the various dengue virus serotypes [21].

Application of DNA biosensors has emerged as an alternative method to the current molecular biology techniques [22,23]. These devices consist of a single-stranded DNA molecule (ssDNA) attached to a transducing surface that is able to detect a specific nucleic acid sequence, based on DNA hybridization events. Currently, there is a growing interest in developing label-free methods for DNA detection, considering their rapidness, easiness, low cost and minimal sample preparation requirements, compared to labeling methods, where the properties of the modified macromolecules often change, which may result in total loss of bioactivity or stability [24,25]. Label-free approaches rely on the direct detection of intrinsic electrochemical properties of DNA (e.g., oxidation of purine bases, particularly guanine) or on changes in some of the interfacial properties after hybridization. In addition, interference with the biological recognition between DNA molecules is minimized. Nevertheless, in labeling methods, these undesirable effects are more likely to occur due to steric hindrance and blocking of the binding sites [26–28].

Consequently, since biosensors allow to detect and identify DNA sequences in a fast and simple way, herein we report the first step to develop a cost-effective, sensitive and label-free electrochemical DNA biosensor for the detection of DENV-3 sequences in biological samples, as a part of an ongoing research previously published [29].

2. Experimental Section

2.1. Design of a Specific DENV-3 DNA Probe

The complete genomes of dengue virus serotype 3, corresponding to GenBank accession numbers AY099336, AY099337, AY099338S1,AY099338S2, AY099339S1, AY099339S2, AY099340S1, AY099340S2, AY09934S1, AY099342S1 were obtained from the National Center for Biotechnology Information (NCBI) database. These sequences correspond to strains that were introduced in the American continent, and caused the disease outbreaks in 2002 [30,31]. CLC Main Workbench v.6.0 software was used to analyze common sequences among those dengue genomes, by using an alignment tool. Then, a specific DNA probe for DENV-3 was selected by comparison of the homologous sequences with other organisms, using Basic Local Alignment Search Tool (BLAST). DENV-3 complementary (target) and non-complementary sequences were also designed using the same method.

2.2. Reagents and Materials

All chemicals were of reagent grade quality and were used directly as received without further purification. Tris base was obtained from Promega (Fitchburg, WI, USA) and sodium acetate was obtained from Sigma-Aldrich (St. Louis, MO, USA) DENV-3 probes were purchased as lyophilized powder from IDT Technologies (Coraville, IA, USA). The stock and diluted solutions (25 nM) were prepared in 0.5 M acetate buffer (pH 5.0) and kept frozen. Ultrapure RNAse/DNAse-free water was used in all buffer solutions. After bioinformatics analysis, the following DNA sequences were used in this study:

DENV-3 probe: 5′-TAA CAT CAT CAT GAG ACA GAG C-3′
DENV-3 target: 5′-GCT CTG TCT CAT GAT GAT GTT A-3′
Non-complementary sequence: 5′-TCT CTT GTT TAA GAC AAC AGA G-3′

Human serum used in this study was obtained from blood samples provided by the pathogenic virus collection of Centro de Pesquisas Aggeu Magalhães (CPqAM). Serum solutions were prepared by centrifugation at 3500 rpm for 5 min at 20 °C (3500 rpm for 5 min), in which the obtained supernatant was collected from each sample, and stored at 23 °C until further used for experiments testing.

2.3. Apparatus

Experiments were carried out using a PGSTAT302 potentiostat (METROHM Autolab, Utrecht, The Netherlands) with the GPES 4.9.007 software as a graphic interface. The electrochemical device was composed by a two-electrode system: A pencil graphite electrode (PGE) as a working electrode and silver/chloride silver electrode as a reference electrode. Each measurement consisted of a cycle of activation/immobilization/hybridization/detection by using a fresh PGE surface. All the experiments were performed in triplicate, at room temperature (23 °C).

2.4. Procedure

2.4.1. Preparation of Electrodes and Pre-Treatment of PGE

PGEs were obtained from Mercur (Santa Cruz do Sul, Brazil), as a pencil graphite lead type 4 B. Briefly, PGEs were produced by cutting graphite lead in pieces of 3 cm and polishing them with an emery polishing disc (Dremel, Mount Prospect, IL,USA). The PGEs were then washed with ultrapure water to remove any contaminant present on the surface of the working electrode. The reference electrode was made by immersing a golden pin into an Ag/AgCl ink (Henkel Acheson, Hemel Hempstead, UK) and dried at 40 °C overnight. The polished surface of PGEs was pre-treated by applying a potential of +1.80 V for 5 min in 0.5 M acetate buffer solution (pH 5.0) [32–34].

2.4.2. DNA Probe Immobilization onto PGE Surface

Immobilization of DENV-3 probe onto the PGE surface was performed by immersing the activated PGE in acetate buffer solution, with different concentrations of DENV-3 probes (250–1000 nM), by applying a fixed potential of +0.5 V for 300 s onto the electrode surface.

2.4.3. DNA Hybridization with Complementary and Non-Complementary Sequences

The hybridization of the immobilized DNA probe on the electrode (PGE/DENV-3 probe) was performed by immersing the electrode in an Eppendorf tube containing 70 µL of DENV-3 target sequences diluted in acetate buffer. The hybridization reaction was then carried out in a thermomixer, stirring at 300 rpm, under a specific annealing temperature of 52 °C, for 10 min. This same procedure was adopted to evaluate the hybridization of the PGE/DENV-3 probe with non-complementary sequences, as well as buffer solutions containing a mix of both 75 nM of DENV-3 complementary and non-complementary sequences (mixed DNA solution).

2.4.4. Detection of Complementary and Non-Complementary Sequences in Human Serum

As a way to evaluate the efficiency of the system to detect DENV-3 sequences in biological samples on the electrode surface, the complementary and non-complementary DNA sequences were diluted in human serum (75 nM concentration) and the hybridization assay was conducted using the same conditions described previously. This procedure was also adopted for tests human serum solutions mixed with both target and non-complementary sequences.

2.5. Electrochemical Analysis

Differential pulse voltammetry (DPV) was used for electrochemical analysis in this study. Current peaks were recorded after applying a potential range of +0.5 up to +1.2 V at a scan rate of 0.05 V/s onto the electrode surface, which was immersed in 20 mM Tris-HCl buffer (pH 7.0). The raw data obtained with DPV technique was treated using the Savitzky and Golay filter (level 2) of the GPES software, followed by moving the average baseline correction using a peak width of 0.01 V [35].

2.6. Statistical Data Analysis

Experimental data were analyzed with Statistica 8.0 software (StatSoft, Tulsa, OK, USA) using parametric tests; Tukey's test was used to compare multi-independent group data, and a level of $p < 0.05$ was considered significant. The reproducibility of the system was expressed as the coefficient of variation inter-assay (CV), which was calculated over three independent assays on the probe-modified PGEs.

3. Results and Discussion

3.1. Bioinformatics Analysis of DENV-3 DNA Probes

The design of DNA probes is one of the crucial steps in the development of a biosensor, because it determines the specificity of the device [36]. For genosensors, this can be achieved using bioinformatics analysis based on whole genome sequencing, in a way to predict the most specific region that is able to produce a steady double-strand DNA with the pathogen [37,38]. In this work, DNA probes specific for DENV-3 were designed mainly by using CLC Main Workbench software, based on a sequence alignment tool to identify regions of similarity between the dengue strains. After that, DNA sequences from the strains that showed specificity only for DENV-3 were compared with other organism genomes using BLAST tool, in order to exclude any correlations. Finally, the Oligonucleotide Properties Calculator (Oligo Calc) software (Northwestern University, IL, USA) was used to provide physical properties information of the selected DENV-3 sequences, in a way to establish the best match of DNA probe for biosensors. Figure 1 shows a flowchart containing the criteria of selection of DENV-3 probes used in this study.

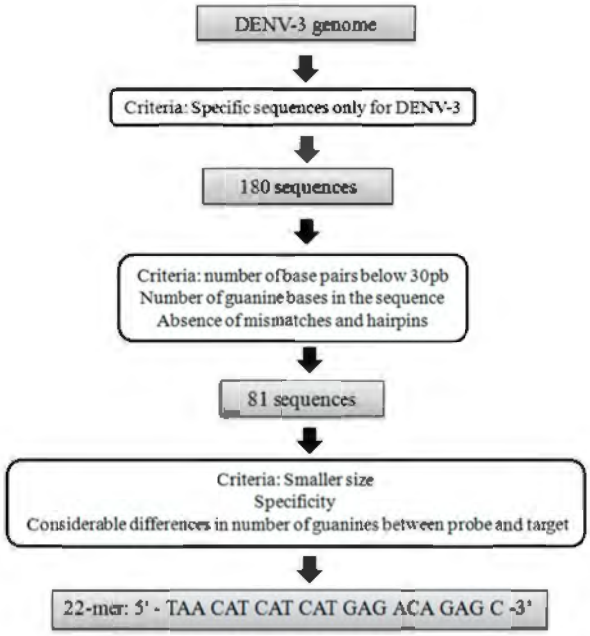

Figure 1. Flowchart of the selection criteria used to design the DENV-3 probe.

First, it was shown that 180 DNA sequences were specific only for dengue virus serotype 3. Among these, 81 were selected as DNA probes, based on the number of base pairs of the sequence, number of guanine bases and the absence of mismatches and hairpins. Finally, a 22-m oligonucleotide was selected to detect DENV-3, with the following sequence: 5′-TAA CAT CAT CAT GAG ACA GAG C-3′. This sequence was selected due to its suitable features that are desirable for electrochemical biosensors, such as shorter base pair length, high specificity and a considerable difference in the number of guanine base between the probe and target sequences, which is important to discriminate between ssDNA and dsDNA onto the PGE surface [33,39,40].

In addition, this probe was targeted to detect sequences from the envelope (E) gene, which is responsible for binding and fusion to host cell membranes [4,41]. This particular gene was chosen because of it is highly conserved sequence, which suffers less mutation process rather than other parts of dengue genome. Viral gene regions that interact with specific host cells are evolutionarily constrained, mainly in viruses that infect multiple organisms, like dengue virus. This is important to be considered in the development of DNA biosensors to detect dengue virus, once that it determines the selectivity and specificity of the method, avoiding cross-reactivity with non-related organisms [42–44].

3.2. Effect of DENV-3 Probes Concentration on Immobilization on the PGE

The immobilization of a biological element on the electrode is the first step to be considered in the development of a biosensor [45]. Determination of the optimal probe concentration is crucial to ensure a high performance of DNA biosensors, and reduce any interference in the electrochemical response of the system [46,47]. Thus, the effect of DENV-3 probes concentration was also investigated in this study.

Figure 2 shows current peaks of different DENV-3 probe concentrations on the PGE surface. As the electrochemical analysis in this study relies on label-free oxidation of guanine bases, the acquisition of higher current signals for DNA probes is well-suited for this system [29,48–50]. The results show that the current gradually rises with the increase of the probe concentration from 250 nM up to 500 nM, reaching the highest electrochemical signal of 777 ± 8.6 nA at 500 nM. The result obtained at 500 nM was also statistically different from that obtained at 750 nM ($p = 0.000178$). However, the decrease in the current peaks at higher concentrations of DNA probes after 500 nM could be due to the steric hindrance between the nitrogenous bases and the transducer. This prevents the electrons produced by the oxidation process to access the electrode surface [51–55]. Therefore, a concentration of 500 nM was selected as the optimal probe concentration for DNA immobilization on the PGE.

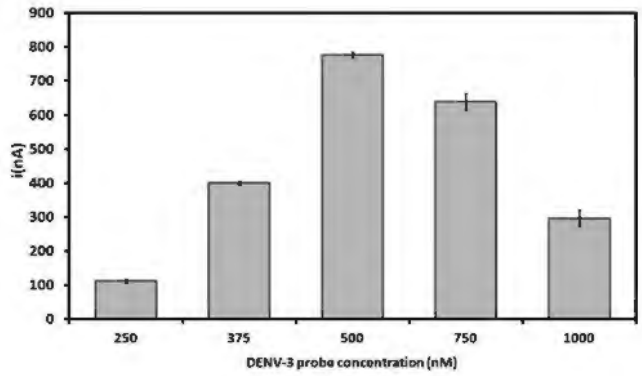

Figure 2. Electrochemical signals of different concentrations of DENV-3 probe onto pencil graphite electrodes (PGE). Differential pulse voltammetry (DPV) was used for electrochemical analysis based on guanine oxidation. Experimental conditions: Scanning potential range between +0.5 V and +1.2 V and scan rate of 0.05 V/s. The results represent the average of triplicates carried out at each DENV-3 probe concentration.

3.3. Electrochemical Analysis of Hybridization Assays

In this study, the biosensor performance was analyzed through the hybridization reaction between the DENV-3 probe and the complementary DENV-3 oligonucleotide. Hybridization was carried out with different amounts of the target sequence and this reaction was performed in an electrochemical cell containing 20 mM Tris-HCl buffer (pH 7.0). The electrochemical signals based on guanine oxidation are displayed in Figure 3. The results showed that the current peaks increase with the increasing concentration of the target sequence (10 nM to 500 nM); the highest concentration exhibited the highest current peak of the system (135 ± 2.15 nA). However, at concentrations higher than 500 nM, there is a decrease in the electrochemical signal that could be due to electrostatic hindrance of DNA molecules on the PGE surface [39,53,56].

The linear regression of the current peaks obtained from different concentrations of DENV-3 target is shown in the inset of Figure 3. The calibration curve (described by the equation $y = 0.8962x + 24.979$) is linear between 10 nM and 100 nM, with a correlation coefficient of 0.9883 ($p < 0.00536$, $n = 5$). A detection limit of 3.09 nM could be estimated with the following equation: $3\ s/m$, where s is the standard deviation of

most reproducible current peak result (corresponding to 75 nM concentration) and *m* is the slope of the linear regression [57]. The same experimental conditions were used to estimate the reproducibility of the method, which was 1.01%, indicating, thus, the significant reproducibility of the method.

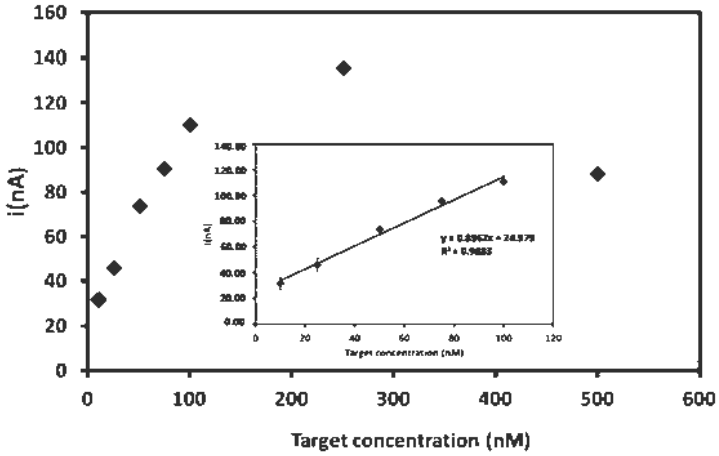

Figure 3. Current signals obtained for different DENV-3 target sequence concentrations after hybridization with probe-modified PGEs. Inset: Related calibration graph at a concentration range of 10–100 nM for the target sequence. Experimental conditions: Scanning potential range between +0.5 V and +1.2 V and scan rate of 0.05 V/s.

Figure 4 displays electrochemical signals of probe-modified PGE before and after hybridization with 250 nM of the target. A decrease of 83% in the current signal was observed after the reaction with the DENV-3 target; this is due to the fact that oxidizable regions of guanine bases in the ssDNA (777 nA) are bound through hydrogen bonds that held the double chain together, thus decreasing the electrochemical signal of the dsDNA (135 nA) on the electrode surface [24,58–60].

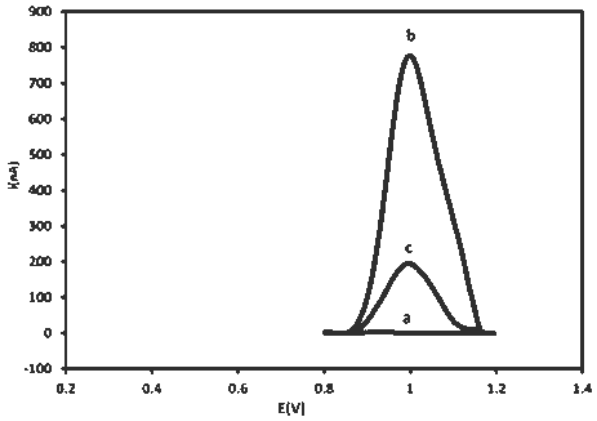

Figure 4. Differential pulse voltammograms corresponding to bare PGE (**a**), probe-modified PGE before (**b**) and after hybridization with 250 nM of target sequence (**c**) in 20mM Tris-HCl buffer solution (pH 7.0). Experimental conditions: Scanning potential range between +0.5 V and +1.2 V and scan rate of 0.05 V/s.

Furthermore, as is seen in Table 1, the present sensor has a lower detection limit (3.09nM) compared to other electrochemical DNA biosensors.

Table 1. Comparison of the analytical performance of different electrochemical DNA biosensors.

Nucleic Acid Biosensor	Electrode	Electrochemical Method	Linear Range of Hybridization	Detection Limit	Reference
Single-walled carbon nanotubes-polymer modified graphite electrodes for DNA hybridization	PGE [a]	DPV [d]	50–200μg/mL	5.14 μM	[61]
Hybridization biosensor for detection of hepatitis B virus	GCE [b]	DPV	0.36–1.32 μM	19.4 nM	[62]
Brilliant cresyl blue as electroactive indicator in electrochemical DNA oligonucleotide sensors	CPE [c]	DPV	10 nM–5μM	9 nM	[63]
Label-free DNA detection based on zero current potentiometry	PGE	LSV [e]	10 nM–1μM	6.9 nM	[64]
DNA biosensor detection of DENV-3 sequences onto PGE surfaces	PGE	DPV	10–100 nM	3.09 nM	This work

[a] Pencil graphite electrode; [b] Glassy carbon electrode; [c] Carbon paste electrode; [d] Differential pulse voltammetry; [e] Linear sweep voltammetry.

3.4. Selectivity Study

In a way to evaluate the selectivity of the DENV-3 biosensor, hybridization tests were performed with a non-complementary sequence. DPV voltammograms for bare PGE, probe-modified PGE before and after hybridization with DENV-3 target and non-complementary sequence are displayed in Figure 5. It was verified that no electrochemical signal was recorded with bare PGE, which is in agreement with the absence of DNA on the electrode surface. Probe-modified PGE presented the highest current peak of the system, whereas the probe-modified PGE after hybridization with target sequence showed a decrease in the current signal, as discussed previously.

As shown in Figure 5, a significant difference in the voltammetric signal was observed after hybridization of DENV-3 probe with the non-complementary sequence (600 nA) when compared with the complementary DNA (135 nA); however, the signal was slightly lower compared to the probe-modified electrode (777 nA). This may be attributed to some unspecific hybridization of non-complementary sequences with the probe. Nevertheless, the target sequence is clearly able to form a steady dsDNA on the electrode surface. Moreover, a decrease in the current peak was also noticed when the probe-modified PGE was added to the mixed DNA solution (~230 nA) when compared with the probe-modified electrode. Therefore, these results can confirm the ability of the PGE-modified biosensor to detect selectively dengue virus serotype 3 [34,61,62].

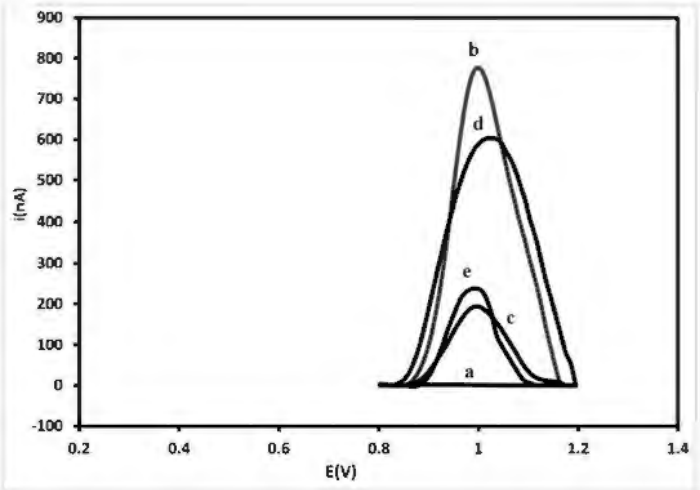

Figure 5. Differential pulse voltammograms for guanine oxidation of (**a**) bare PGE; (**b**) probe-modified PGE; (**c**) probe-modified PGE after hybridization with DENV-3 sequence; (**d**) non-complementary sequence and (**e**) a mixed solution of DENV-3 sequence and non-complementary sequence. Experimental conditions: Scanning potential range between +0.5 V and +1.2 V and scan rate of 0.05 V/s.

3.5. Electrochemical Measurement of Target Hybridization in Human Serum Solutions

In order to evaluate the efficiency of the probe surface for biosensing applications and in an attempt to test the performance if the biosensor for the detection DENV-3 in real samples, DPV was used to investigate DNA hybridization on PGE surface using human serum. This assay was tested with 75 nM of target sequence, non-complementary sequences and a solution mixed of both target and non-complementary sequences.

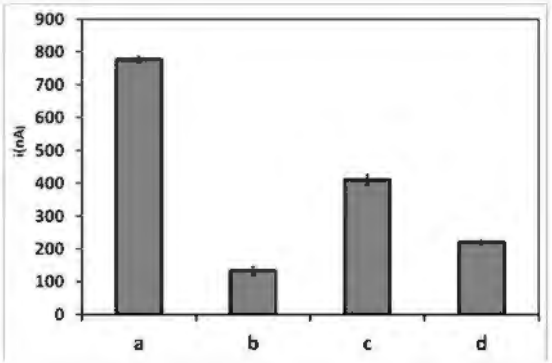

Figure 6. Current peaks related to guanine oxidation of the probe-modified-PGE after (**a**) and before hybridization with DENV-3 (**b**); in the presence of non-complementary sequences (**c**) and in a solution mixed with DENV-3 and non-complementary sequences (**d**), all diluted in human serum. Experimental conditions: Scanning potential range between +0.5 V and +1.2 V and scan rate of 0.05 V/s.

As shown in Figure 6, the biosensor displays the same electrochemical behavior observed previously in Tris-HCl buffer solutions. However, all the current signals of the probe-modified PGE after hybridization with the complementary, non-complementary sequences and mixed DNA solution diluted in human serum presented a slight decrease (134, 410.8 and 221 nA, respectively) when compared with those diluted in acetate buffer (135, 600 and 230 nA, respectively). This could be due to the hybridization kinetics and the efficiency of the PGE surface, which could be affected by non-specific adsorption of plasma proteins, and this may interfere with the detection of the electrochemical signal [63]. However, such interference with the detection of DNA molecules was observed previously with the optical DNA biosensor developed by Gong *et al.* [64,65]. Thus, these results confirm the high selectivity and sensitivity of the electrochemical DNA biosensor developed herein.

4. Conclusions

A sensitive DNA biosensor based on electrochemistry for the detection of dengue virus serotype 3 was proposed in the present study. A pencil graphite electrode, modified with a probe designed specifically for DENV-3, was able to identify selectively target sequences of the virus, with a low detection limit of 3.09 nM. Moreover, the probe-modified PGE allowed to detect specifically complementary sequences of the target DNA spiked with human serum.

The sensitivity of this assay can be further improved by testing other electrode materials, such as gold, platinum and grapheme electrodes. In addition, screen-printed electrodes could be also used for the implementation of a portable system. Therefore, the application of biosensors for the diagnosis of dengue virus at the molecular level may contribute to the future development and advancement of effective and rapid detection methods.

Acknowledgments

The authors would like to thank Centro de Pesquisas Aggeu Magalhães (CPqAM) that kindly provided biological samples for this project. In addition, they would like to thank Fundação de Amparo à Pesquisa do Estado de Pernambuco (FACEPE), Conselho Nacional de Desenvolvimento Científico e Tecnológico (CNPq) and Laboratório de Imunopatologia Keizo Asami (LIKA) for providing financial support and Graziella El Khoury for reviewing of the manuscript for English language.

Author Contributions

N.O. designed and performed the majority of the experiments. D.Z. performed bioinformatics analysis. W.B. and M.B. prepared PGEs, buffer solutions and performed part of electrochemical experiments. M.T. and K.T. were responsible for selecting and supplying biological samples for the experiments. D.M. processed human serum samples. G.N. and D.F. were responsible for statistical data analysis. N.O., E.S., M.A. and J.L.-F. drafted and revised critically the manuscript.

Conflicts of Interest

The authors declare no conflict of interest.

References

1. WHO. *Dengue—Guidelines for Diagnosis, Treatment, Prevention and Control*; WHO Press: Geneva, Switzerland, 2009; p. 147.
2. Sariol, C.A.; White, L.J. Utility, limitations, and future of non-human primates for dengue research and vaccine development. *Front. Immunol.* **2014**, *5*, 452, doi:10.3389/fimmu.2014.00452.
3. Bhatt, S.; Gething, P.W.; Brady, O.J.; Messina, J.P.; Farlow, A.W.; Moyes, C.L.; Drake, J.M.; Brownstein, J.S.; Hoen, A.G.; Sankoh, O.; Myers, M.F.; *et al.* The global distribution and burden of dengue. *Nature* **2013**, *496*, 504–507.
4. Vasilakis, N.; Cardosa, J.; Hanley, K.A.; Holmes, E.C.; Weaver, S.C. Fever from the forest: Prospects for the continued emergence of sylvatic dengue virus and its impact on public health. *Nat. Rev. Microbiol.* **2011**, *9*, 532–541.
5. Chien, L.C.; Yu, H.L. Impact of meteorological factors on the spatiotemporal patterns of dengue fever incidence. *Environ. Int.* **2014**, *73*, 46–56.
6. Cedillo-Barrón, L.; García-Cordero, J.; Bustos-Arriaga, J.; León-Juárez, M.; Gutiérrez-Castañeda, B. Antibody response to dengue virus. *Microbes Infect.* **2014**, *16*, 711–720.
7. Rovida, F.; Percivalle, E.; Campanini, G.; Piralla, A.; Novati, S.; Muscatello, A.; Baldanti, F. Viremic Dengue virus infections in travellers: Potential for local outbreak in Northern Italy Dengue-1 Dengue-4. *J. Clin. Virol.* **2011**, *50*, 76–79.
8. Ashley, E.A. Trends in Anaesthesia and Critical Care Dengue fever. *Trends Anaesth. Crit. Care* **2011**, *1*, 39–41.
9. Qing, X.; Sun, N.; Yeh, J.; Yue, C.; Cai, J. Dengue fever and bone marrow myelofibrosis. *Exp. Mol. Pathol.* **2014**, *97*, 208–210.
10. Halstead, S.B. Dengue. *Lancet* **2007**, *370*, 1644–1652.
11. Arora, P.; Sindhu, A.; Dilbaghi, N.; Chaudhury, A. Biosensors as innovative tools for the detection of food borne pathogens. *Biosens. Bioelectron.* **2011**, *28*, 1–12.
12. Chakravarti, A.; Arora, R.; Luxemburger, C. Fifty years of dengue in India. *Trans. R. Soc. Trop. Med. Hyg.* **2012**, *106*, 273–282.
13. Verma, R.; Sahu, R.; Holla, V. Neurological manifestations of dengue infection: A review. *J. Neurol. Sci.* **2014**, *346*, 26–34.
14. Pechansky, F.; Duarte, P.D.C.A.V.; de Boni, R.; Leukefeld, C.G.; von Diemen, L.; Bumaguin, D.B.; Kreische, F.; Hilgert, J.B.; Bozzetti, M.C.; Fuchs, D.F.P. Predictors of positive Blood Alcohol Concentration (BAC) in a sample of Brazilian drivers. *Rev. Bras. Psiquiatr.* **2012**, *34*, 277–285.
15. Ferraz, F.O.; Bomfim, M.R.Q.; Totola, A.H.; Ávila, T.V.; Cisalpino, D.; Pessanha, J.E.M.; da Glória de Souza, D.; Teixeira Júnior, A.L.; Nogueira, M.L.; Bruna-Romero, O.; *et al.* Evaluation of laboratory tests for dengue diagnosis in clinical specimens from consecutive patients with suspected dengue in Belo Horizonte, Brazil. *J. Clin. Virol.* **2013**, *58*, 41–46.
16. Peeling, R.W.; Artsob, H.; Pelegrino, J.L.; Buchy, P.; Cardosa, M.J.; Devi, S.; Enria, D.A.; Farrar, J.; Gubler, D.J.; Guzman, M.G.; *et al.* Evaluation of diagnostic tests: Dengue. *Nat. Rev. Microbiol.* **2010**, *8*, S30–S37.
17. Wattal, C.; Goel, N. Infectious Disease Emergencies in Returning Travelers—Special Reference to Malaria, Dengue Fever and Chikungunya. *Med. Clin. North Am.* **2012**, *96*, 1225–1255.

18. Korhonen, E.M.; Huhtamo, E.; Virtala, A.M.K.; Kantele, A.; Vapalahti, O. Approach to non-invasive sampling in dengue diagnostics: Exploring virus and NS1 antigen detection in saliva and urine of travelers with dengue. *J. Clin. Virol.* **2014**, *61*, 353–358.
19. Shenoy, B.; Menon, A.; Biradar, S. Science Direct Diagnostic utility of dengue NS1 antigen. *Pediatr. Infect. Dis.* **2014**, *6*, 110–113.
20. Hapugoda, M.D.; de Silva, N.R.; Khan, B.; Damsiri Dayanath, M.Y.; Gunesena, S.; Prithimala, L.D.; Abeyewickreme, W. A comparative retrospective study of RT-PCR-based liquid hybridization assay for early, definitive diagnosis of dengue. *Trans. R. Soc. Trop. Med. Hyg.* **2010**, *104*, 279–282.
21. Back, A.T.; Lundkvist, A. Dengue viruses—An overview. *Infect. Ecol. Epidemiol.* **2013**, *1*, 1–21.
22. Siddiquee, S.; Rovina, K.; Yusof, N.A.; Rodrigues, K.F. Nanoparticle-enhanced electrochemical biosensor with DNA immobilization and hybridization of Trichoderma harzianum gene. *Sens. Bio-Sens. Res.* **2014**, *2*, 16–22.
23. Teles, F.S.R.R. Biosensors and rapid diagnostic tests on the frontier between analytical and clinical chemistry for biomolecular diagnosis of dengue disease: A review. *Anal. Chim. Acta* **2011**, *687*, 28–42.
24. Lucarelli, F.; Tombelli, S.; Minunni, M.; Marrazza, G.; Mascini, M. Electrochemical and piezoelectric DNA biosensors for hybridisation detection. *Anal. Chim. Acta* **2008**, *609*, 139–159.
25. Souada, M.; Piro, B.; Reisberg, S.; Anquetin, G.; Noël, V.; Pham, M.C. Label-free electrochemical detection of prostate-specific antigen based on nucleic acid aptamer. *Biosens. Bioelectron.* **2014**, *68C*, 49–54.
26. Tosar, J.P.; Keel, K.; Laíz, J. Two independent label-free detection methods in one electrochemical DNA sensor. *Biosens. Bioelectron.* **2009**, *24*, 3036–3042.
27. Sadik, O.A; Aluoch, A.O.; Zhou, A. Status of biomolecular recognition using electrochemical techniques. *Biosens. Bioelectron.* **2009**, *24*, 2749–2765.
28. Conde, J.; Edelman, E.R.; Artzi, N. Target-responsive DNA/RNA nanomaterials for microRNA sensing and inhibition: The jack-of-all-trades in cancer nanotheranostics? *Adv. Drug Deliv. Rev.* **2015**, *81C*, 169–183.
29. Souza, E.; Nascimento, G.; Santana, N.; Ferreira, D.; Lima, M.; Natividade, E.; Martins, D.; Lima-Filho, J. Label-free electrochemical detection of the specific oligonucleotide sequence of dengue virus type 1 on pencil graphite electrodes. *Sensors* **2011**, *11*, 5616–5629.
30. Lourenço-de-Oliveira, R.; Honório, N.A.; Castro, M.G.; Schatzmayr, H.G.; Miagostovich, M.P.; Alves, J.C.R.; Silva, W.C.; Leite, P.J.; Nogueira, R. Dengue Virus Type 3 Isolation from Aedes aegypti in the Municipality of Nova Iguaçu, State of Rio de Janeiro. *Mem. Inst. Oswaldo Cruz* **2002**, *97*, 799–800.
31. Peyrefitte, C.N.; Couissinier-Paris, P.; Mercier-Perennec, V.; Bessaud, M.; Martial, J.; Kenane, N.; Durand, J.P.A.; Tolou, H.J. Genetic Characterization of Newly Reintroduced Dengue Virus Type 3 in Martinique (French West Indies). *J. Clin. Microbiol.* **2003**, *41*, 5195–5198.
32. Ensafi, A.A.; Heydari-bafrooei, E.; Amini, M. DNA-functionalized biosensor for riboflavin based electrochemical interaction on pretreated pencil graphite electrode. *Biosens. Bioelectron.* **2012**, *31*, 376–381.
33. Hejazi, M.S.; Alipour, E.; Pournaghi-Azar, M.H. Immobilization and voltammetric detection of human interleukine-2 gene on the pencil graphite electrode. *Talanta* **2007**, *71*, 1734–1740.

34. Pournaghi-Azar, M.H.; Alipour, E.; Zununi, S. Direct and rapid electrochemical biosensing of the human interleukin-2 DNA in unpurified polymerase chain reaction (PCR)-amplified real samples. *Biosens. Bioelectron.* **2008**, *24*, 524–530.
35. Özcan, A.; Yücel, S. A novel approach for the determination of paracetamol based on the reduction of *N*-acetyl-*p*-benzoquinoneimine formed on the electrochemically treated pencil graphite electrode. *Anal. Chim. Acta* **2011**, *685*, 9–14.
36. Ermini, M.L.; Scarano, S.; Bini, R.; Banchelli, M.; Berti, D.; Mascini, M.; Minunni, M. A rational approach in probe design for nucleic acid-based biosensing. *Biosens. Bioelectron.* **2011**, *26*, 4785–4790.
37. Huang, J.; Yang, X.; He, X.; Wang, K.; Liu, J.; Shi, H.; Wang, Q.; Guo, Q.; He, D. Design and bioanalytical applications of DNA hairpin-based fluorescent probes. *TrAC Trends Anal. Chem.* **2014**, *53*, 11 20.
38. O'Brien, B.; Zeng, H.; Polyzos, A.A.; Lemke, K.H.; Weier, J.F.; Wang, M.; Zitzelsberger, H.F.; Weier, H.U.G. Bioinformatics tools allow targeted selection of chromosome enumeration probes and aneuploidy detection. *J. Histochem. Cytochem.* **2013**, *61*, 134–147.
39. Campos-Ferreira, D.S.; Souza, E.; Nascimento, G.; Zanforlin, D.; Arruda, M.; Beltrão, M.; Melo, A.; Bruneska, D.; Lima-Filho, J.L. Electrochemical DNA biosensor for the detection of human papillomavirus E6 gene inserted in recombinant plasmid. *Arab. J. Chem.* **2014**, doi:10.1016/ j.arabjc.2014.05.023.
40. Corrigan, D.K.; Schulze, H.; McDermott, R.A.; Schmüser, I.; Henihan, G.; Henry, J.B.; Bachmann, T.T.; Mount, A.R. Improving electrochemical biosensor performance by understanding the influence of target DNA length on assay sensitivity. *J. Electroanal. Chem.* **2014**, *732*, 25–29.
41. Soares, R.O.S.; Caliri, A. Stereochemical features of the envelope protein Domain III of dengue virus reveals putative antigenic site in the five-fold symmetry axis. *Biochim. Biophys. Acta* **2013**, *1834*, 221–230.
42. Weaver, S.C.; Brault, A.C.; Kang, W.; John, J. Genetic and Fitness Changes Accompanying Adaptation of an Arbovirus to Vertebrate and Invertebrate Cells Genetic and Fitness Changes Accompanying Adaptation of an Arbovirus to Vertebrate and Invertebrate Cells. *J. Virol.* **1999**, *73*, 4316–4326.
43. Bennett, S.N.; Holmes, E.C.; Chirivella, M.; Rodriguez, D.M.; Beltran, M.; Vorndam, V.; Gubler, D.J.; McMillan, W.O. Molecular evolution of dengue 2 virus in Puerto Rico: Positive selection in the viral envelope accompanies clade reintroduction. *J. Gen. Virol.* **2006**, *87*, 885–893.
44. Weaver, S.C.; Vasilakis, N. Molecular evolution of dengue viruses: Contributions of phylogenetics to understanding the history and epidemiology of the preeminent arboviral disease. *Infect. Genet. Evol.* **2009**, *9*, 523–540.
45. Wang, Q.; Ding, Y.; Gao, F.; Jiang, S.; Zhang, B.; Ni, J.; Gao, F. A sensitive DNA biosensor based on a facile sulfamide coupling reaction for capture probe immobilization. *Anal. Chim. Acta* **2013**, *788*, 158–164.
46. Zhang, L.; Wang, Y.; Chen, M.; Luo, Y.; Deng, K.; Chen, D.; Fu, W. A new system for the amplification of biological signals: RecA and complimentary single strand DNA probes on a leaky surface acoustic wave biosensor. *Biosens. Bioelectron.* **2014**, *60*, 259 264.

47. Mohamadi, M.; Mostafavi, A.; Torkzadeh-Mahani, M. Electrochemical determination of biophenol oleuropein using a simple label-free DNA biosensor. *Bioelectrochemistry* **2015**, *101C*, 52–57.
48. Erdem, A.; Muti, M.; Karadeniz, H.; Congur, G.; Canavar, E. Colloids and Surfaces B: Biointerfaces Electrochemical monitoring of indicator-free DNA hybridization by carbon nanotubes—Chitosan modified disposable graphite sensors. *Colloids Surf. B Biointerfaces* **2012**, *95*, 222–228.
49. Paleček, E.; Fojta, M.; Tomschik, M.; Wang, J. Electrochemical biosensors for DNA hybridization and DNA damage. **1998**, *13*, 621–628.
50. Wang, J. Electrochemical biosensors: Towards point-of-care cancer diagnostics. *Biosens. Bioelectron.* **2006**, *21*, 1887–92.
51. Campos-Ferreira, D.S.; Nascimento, G.A.; Souza, E.V.M.; Souto-maior, M.A.; Arruda, M.S.; Zanforlin, D.M.L.; Ekert, M.H.F.; Bruneska, D.; Lima-filho, J.L. Electrochemical DNA biosensor for human papillomavirus 16 detection in real samples. *Anal. Chim. Acta* **2013**, *804*, 258–263.
52. Gao, Z.; Yang, W.; Wang, J.; Yan, H.; Yao, Y.; Ma, J.; Wang, B.; Zhang, M.; Liu, L. Electrochemical synthesis of layer-by-layer reduced graphene oxide sheets/polyaniline nanofibers composite and its electrochemical performance. *Electrochim. Acta* **2013**, *91*, 185–194.
53. Lucarelli, F.; Marrazza, G.; Palchetti, I.; Cesaretti, S.; Mascini, M. Coupling of an indicator-free electrochemical DNA biosensor with polymerase chain reaction for the detection of DNA sequences related to the apolipoprotein E. *Anal. Chim. Acta* **2002**, *469*, 93–99.
54. Teles, F.R.R.; Fonseca, L.P.Trends in DNA biosensors. *Talanta*, **2008**, *77*, 606–623.
55. Tichoniuk, M.; Ligaj, M.; Filipiak, M. Application of DNA Hybridization Biosensor as a Screening Method for the Detection of Genetically Modified Food Components. *Sensors* **2008**, *8*, 2118–2135.
56. Liu, X.; Fan, Q.; Huang, W. DNA biosensors based on water-soluble conjugated polymers. *Biosens. Bioelectron.* **2011**, *26*, 2154–2164.
57. Gumustas, M.; Ozkan, S.A. The Role of and tbe Place of Method Validation in Drug Analysis Using Electroanalytical Techniques. *Open Anal. Chem. J.* **2011**, *5*, 1–21.
58. Nascimento, G.A.; Souza, E.V.M.; Campos-ferreira, D.S.; Arruda, M.S.; Castelletti, C.H.M.; Wanderley, M.S.O.; Ekert, M.H.F.; Bruneska, D. Electrochemical DNA biosensor for bovine papillomavirus detection using polymeric film on screen-printed electrode. *Biosens. Bioelectron.* **2012**, *38*, 61–66.
59. Aydoğdu, G.; Günendi, G.; Zeybek, D.K.; Zeybek, B.; Pekyardımcı, Ş. A novel electrochemical DNA biosensor based on poly-(5-amino-2-mercapto-1,3,4-thiadiazole) modified glassy carbon electrode for the determination of nitrofurantoin. *Sens. Actuators B Chem.* **2014**, *197*, 211–219.
60. Wang, J.; Kawde, A. Pencil-based renewable biosensor for label-free electrochemical detection of DNA hybridization. *Anal. Chim. Acta* **2001**, *431*, 219–224.
61. Sehatnia, B.; Golabi, F.; Sabzi, R.E.; Hejazi, M.S. Modeling of DNA Hybridization Detection Using Methylene Blue as an Electroactive Label. *J. Iran. Chem. Soc.* **2011**, *8*, 115–122.
62. Souza, E.; Nascimento, G.; Santana, N.; Campos-ferreira, D.; Bibiano, J.; Arruda, M.S. Electrochemical DNA Biosensor for Sequences Related to the Human Papillomavirus Type 16 using Methylene Blue. *Biosens. J.* **2014**, *3*, 3–7.

63. Ren, Y.; Deng, H.; Shen, W.; Gao, Z. A Highly Sensitive and Selective Electrochemical Biosensor for Direct Detection of MicroRNAs in Serum. *Anal. Chem.* **2013**, *9*, 4784–4789.
64. Auer, S.; Nirschl, M.; Schreiter, M.; Vikholm-Lundin, I. Detection of DNA hybridisation in a diluted serum matrix by surface plasmon resonance and film bulk acoustic resonators. *Anal. Bioanal. Chem.* **2011**, *400*, 1387–1396.
65. Gong, P.; Lee, C.; Gamble, L.J.; Castner, D.G.; Grainger, D.W.; Chem, L.J. A. Hybridization Behavior of Mixed DNA/Alkylthiol Monolayers on Gold: Characterization by Surface Plasmon Resonance and 32 P Radiometric Assay rescence intensity measurements reported in a related. **2006**, *78*, 3326–3334.

APÊNDICE D - ARTIGO EM COLABORAÇÃO

DEVELOPMENT AND EVALUATION OF A RAPID MOLECULAR DIAGNOSTIC TEST FOR ZIKA VIRUS INFECTION BY REVERSE TRANSCRIPTION LOOP-MEDIATED ISOTHERMAL AMPLIFICATION

www.nature.com/scientificreports

SCIENTIFIC REPORTS

OPEN

Development and evaluation of a rapid molecular diagnostic test for Zika virus infection by reverse transcription loop-mediated isothermal amplification

Received: 9 May 2017
Accepted: 2 October 2017
Published online: 18 October 2017

Yohei Kurosaki[1], Danyelly Bruneska Gondim Martins[2], Mayuko Kimura[1], Andriu dos Santos Catena[2], Maria Amélia Carlos Souto Maior Borba[2], Sandra da Silva Mattos[2], Haruka Abe[1], Rokusuke Yoshikawa[1], José Luiz de Lima Filho[2] & Jiro Yasuda[1,3]

The recent outbreak of Zika virus (ZIKV) disease caused an enormous number of infections in Central and South America, and the unusual increase in the number of infants born with microcephaly associated with ZIKV infection aroused global concern. Here, we developed a reverse transcription loop-mediated isothermal amplification (RT-LAMP) assay using a portable device for the detection of ZIKV. The assay specifically detected ZIKV strains of both Asian and African genotypes without cross-reactivity with other arboviruses, including Dengue and Chikungunya viruses. The assay detected viral RNA at 14.5 $TCID_{50}$/mL in virus-spiked serum or urine samples within 15 min, although it was slightly less sensitive than reference real time RT-PCR assay. We then evaluated the utility of this assay as a molecular diagnostic test using 90 plasma or serum samples and 99 urine samples collected from 120 suspected cases of arbovirus infection in the states of Paraíba and Pernambuco, Brazil in 2016. The results of this assay were consistent with those of the reference RT-PCR test. This portable RT-LAMP assay was highly specific for ZIKV, and enable rapid diagnosis of the virus infection. Our results provide new insights into ZIKV molecular diagnostics and may improve preparedness for future outbreaks.

Zika virus (ZIKV) was first identified in Uganda in 1947. Since then, human infections were found across Africa and Southeast Asia[1,2]. In May 2015, the first case of infection with ZIKV on the South American continent was reported in Brazil[2,3]. By early 2016, the number of ZIKV infections in Brazil increased dramatically, and an unusual number of cases of foetal and newborn microcephaly associated with ZIKV infection in pregnant women were reported[4,5]. To control ZIKV disease outbreaks and the spread of ZIKV infections, the World Health Organization declared a Public Health Emergency of International Concern in February 2016. ZIKV infections have also been reported in other American countries and continue to expand.

A particular concern with respect to ZIKV infection is the increased risk of congenital central nerve system malformations, including microcephaly as well as arthrogryposis and spontaneous abortion caused by maternal infection during the first or second trimester of pregnancy[6,7]. In addition, sexual transmission and the probable transmission through blood transfusions have been reported[8–10]. ZIKV infection usually causes a mild and self-limiting illness, e.g., fever, rash, arthralgia, and conjunctivitis. Since these clinical symptoms are commonly observed in infections with other arboviruses, such as Dengue (DENV) and Chikungunya (CHIKV) viruses, it is difficult to diagnose ZIKV infection by clinical symptoms alone[1,2]. Therefore, accurate laboratory diagnosis to identify ZIKV infections is urgently required, especially for pregnant women who are at risk of bearing children with microcephaly.

[1]Institute of Tropical Medicine (NEKKEN), Nagasaki University, Nagasaki, 852-8523, Japan. [2]Laboratory of Immunopathology Keizo Asami (LIKA), Federal University of Pernambuco (UFPE), Recife, 50670-901, Brazil. [3]Graduate School of Biomedical Sciences and Program for Nurturing Global Leaders in Tropical and Emerging Communicable Diseases, Nagasaki University, Nagasaki, 852-8523, Japan. Correspondence and requests for materials should be addressed to J.Y. (email: j-yasuda@nagasaki-u.ac.jp)

Name	Type	Position*	Sequence (5′–3′)†	Specificity
ZIK-As4-F3	F3	1053–1071	AACATGGAGGTTGTGTCAC	Asian genotype
ZIK-As4-B3	B3	1315–1332	AACTTAGCGCATGTCACC	
ZIK-As4-FIP	FIP (F1c + F2)	1174–1192, 1114–1133	GCTGTCCGAAGCCATGTCT-TACAACAACAGTCAGCAACA	
ZIK-As4-BIP	BIP (B1c + B2)	1199–1220, 1262–1279	CCAACACAAGGTGAAGCCTACC-CCAGCCTCTGTCCACTAA	
ZIK-As4-LF	LF	1149–1170	ATTGATGCCTCATAGCAGTAGG	
ZIK-As4-LB	LB	1222–1242	TGACAAGCAATCAGACACTCA	Asian & African genotype
ZIK-Af41-F3	F3	1053–1071	AACATGGAGGTTGCGTCAC	African genotype
ZIK-Af41-B3	B3	1315–1332	AACTTGGCACATGTCACC	
ZIK-Af41-FIP	FIP (F1c + F2)	1174–1192, 1114–1133	ACTGTCCGAAGCCATGTCC-CACGACAACGGTTAGTAACA	
ZIK-Af41-BIP	BIP (B1c + B2)	1199–1220, 1262–1279	CCAACACAAGGTGAAGCCTACC-CCAACCTCTGTCCACCAA	
ZIK-Af41-LF	LF	1149–1170	ATTGATGCCTCGTAGCAATAGG	

Table 1. Sequences of LAMP primers. *Primer position in ZIKV strain MR766 (accession number: NC_012532). †Underlining indicates the positions of nucleic acids adapted to the African genotype.

ZIKV is a positive-stranded RNA virus belonging to the genus *Flavivirus* in the family *Flaviviridae*. ZIKV shares its vector, the *Aedes* mosquito, with other flaviviruses, including DENV, Yellow fever virus (YFV), and CHIKV[1]. ZIKV has been isolated from humans in East and West Africa and in Southeast Asia and Polynesian countries where the host mosquitoes, *A. aegypti* and *A. albopictus*, are found[1,11]. Based on phylogenetic analyses, these isolates can be categorised into two genotypes, African and Asian. Epidemiological studies have revealed that the recent outbreak of ZIKV in Brazil occurred via the introduction of a virus from French Polynesia, where an outbreak of the disease occurred in 2013[12]. All of the viruses isolated in Brazil and other countries on the American continent belong to the Asian genotype[13].

In patients with ZIKV infection, the virus can be detected in several sample types, including blood, urine, saliva, and other body fluids[14–18]. The viral load in blood reaches a peak at 2 to 5 days after the onset of illness, but decreases rapidly thereafter. Therefore, it is difficult to detect ZIKV in blood samples from patients after the acute phase of infection, even with sensitive molecular diagnostic methods, such as reverse transcription-polymerase chain reaction (RT-PCR)[14,18,19]. The virus can be detected in urine samples for longer durations (>7–14 days after the onset of symptoms) than in those for blood samples[14]. Currently, blood and urine samples are typically used for the molecular diagnosis of ZIKV.

ZIKV infection is diagnosed in the laboratory by nucleic acid amplification tests (NAATs) to detect viral RNA[20–24] or by ELISA to detect IgM or IgG antibodies[21,25]. The NAATs such as RT-PCR and other technologies (e.g. recombinase polymerase amplification) are highly accurate, and RT-PCR is considered the gold standard to confirm ZIKV infection[21,24]. RT-PCR, however, requires a step for viral RNA extraction prior to the assay and the use of expensive equipment, such as thermal cycler, to conduct the test. Moreover, there is a risk of reduced sample quality due to RNA degradation during transportation to the laboratory. For ELISA, serological cross-reaction between ZIKV and other circulating flaviviruses like DENV makes accurate diagnosis with serology difficult[21,26]. Therefore, novel diagnostic technologies that can be conducted at the point-of-care or in regional laboratories are greatly needed to control ZIKV infections.

Reverse transcription loop-mediated isothermal amplification (RT-LAMP) is a rapid, sensitive RNA detection method performed under isothermal conditions using four or six unique oligonucleotide primers[27,28]. Since LAMP reactions can be performed with simple inexpensive equipment, RT-LAMP assays can be conducted in the field and by under-funded laboratories[29]. We previously developed a RT-LAMP assay using a portable isothermal amplification and detection device for Ebola virus in response to the recent outbreak of Ebola virus disease in West Africa, and the assay has been deployed for field surveillance in Guinea[30,31]. Here, we developed a RT-LAMP assay for the detection of ZIKV with a portable battery-powered device. Then, we evaluated the utility of this assay for molecular diagnosis using clinical specimens collected from the recent ZIKV outbreak in Brazil.

Results

Sensitivity. We designed ZIKV genotype-specific LAMP primers that targeted conserved sequences in the E protein-coding region (Table 1). Each genotype-specific primer recognised the same genomic position. To detect all known ZIKV strains, we used a mixture of primers specific for each genotype in a single reaction. First, we examined the sensitivity of the assay using serial 10-fold dilutions of *in vitro* synthesised standard RNAs from strain 976Uganda, which was isolated from a rhesus macaque in Uganda, and strain PRVABC59, which was isolated at the Centres for Disease Control and Prevention (CDC) from a patient who travelled to Puerto Rico in 2015[32]. Ten copies of the RNA standards were detected from both strains in quadruplicate reactions (Fig. 1a). The times to obtain positive results (Tp) for RNA standards ranging from 10^6 to 10^1 copies were mostly less than 15 min, and within this range, Tp was correlated with the number of RNA copies (Fig. 1b and c). Single copies of the standard RNAs from the 976Uganda and PRVABC59 strains were detected with 75% and 50% positivity, respectively, and Tp values were dispersed. These results suggested that the RT-LAMP assay could be used as a

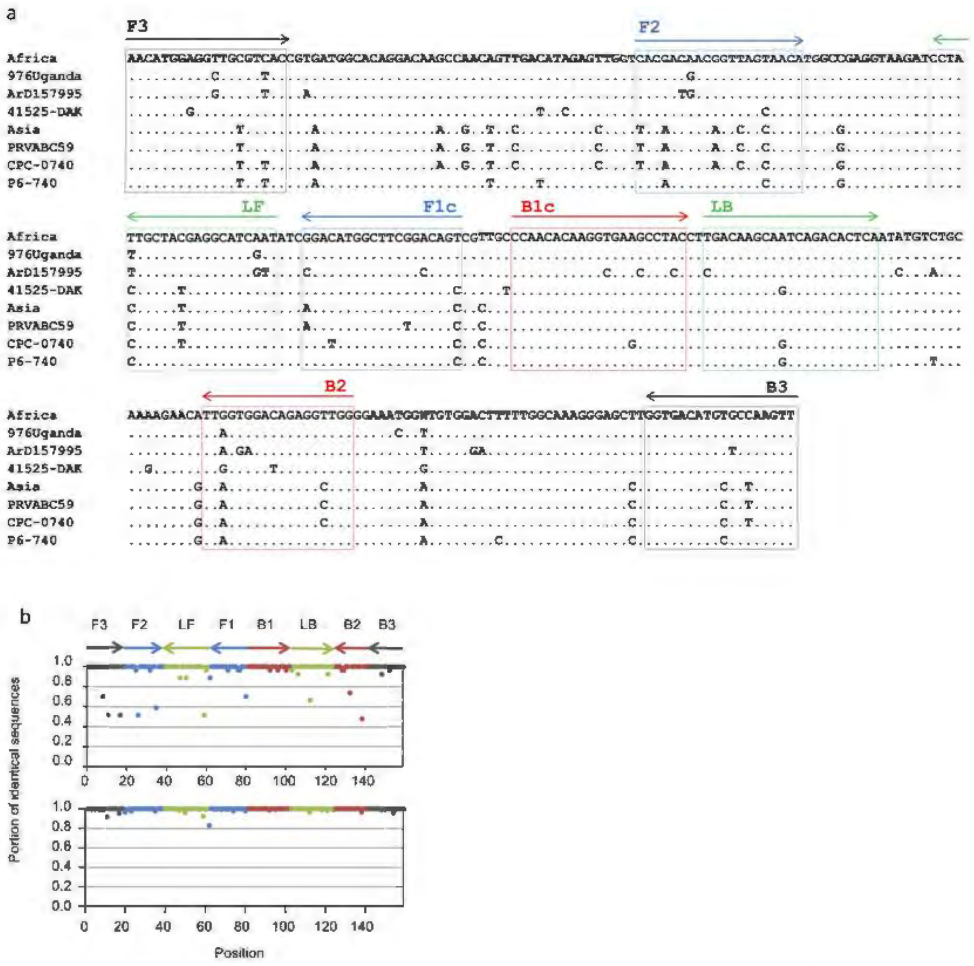

Figure 2. Specificity of the LAMP primers for ZIKV sequences. Alignment of ZIKV sequences and positions of LAMP primers (**a**). Boxes are the sites recognised by each oligonucleotide primer and arrows show the direction of each primer. Africa and Asia in the alignments indicate the consensus sequences of African and Asian genotypes, respectively. The accession numbers for the strains are LC002520.1, KF383118, KF955591, KU501215, HQ234499, and KU681082 (from top to bottom). Proportion of African (upper) and Asian (lower) genotype sequences that had identical nucleic acids with primers at respective positions in the LAMP primers (**b**).

strains. These RNA sequences were also detected using the RT-LAMP assay, in addition to the sequences in the 976Uganda and PRVABC59 strains (Table 2). Furthermore, no cross-reactions with other tested arboviruses, including DENV, YFV, West Nile virus (WNV), CHIKV, and Rift Valley fever virus (RVFV), and *Plasmodium falciparum* were observed. These results suggested that the RT-LAMP assay developed here was highly specific for detecting ZIKV strains of both African and Asian genotypes.

Detection of ZIKV in virus-spiked samples. In the routine molecular diagnosis of ZIKV infection, blood and/or urine is used, since viral RNA can be detected in these clinical specimens during the acute phase of infection. The feasibility of using the RT-LAMP assay for clinical specimens was evaluated using ZIKV-spiked human serum and urine samples. We prepared human serum and urine spiked with four-fold serially diluted ZIKV strain 976Uganda, and obtained samples with titres of 232.7–0.9 $TCID_{50}$/mL. The sensitivity of the RT-LAMP assay was compared to that of the real time RT-PCR (rRT-PCR) assay developed by the CDC[21]. Using the RT-LAMP assay, we detected viral RNA in both serum and urine samples at a titre of 14.5 $TCID_{50}$/mL in quadruplicate reactions. The Ct values in the rRT-PCR were 34.6 ± 0.8 and 35.4 ± 0.4 for serum and urine samples, respectively, which corresponded to 44.3 and 23.5 genome equivalents (geq) per reaction, respectively (Table 3). Using the rRT-PCR assay, we detected viruses in both serum and urine samples at a titre of 3.6 $TCID_{50}$/mL, which corresponded to 8.8 and 8.9 geq per reaction, respectively; however, the RT-LAMP assay failed for these samples, suggesting that the RT-LAMP assay was less sensitive than the CDC rRT-PCR assay for ZIKV detection. Together with the results

Family	Genus	Species	Strain	Amount of RNA/DNA	Results of RT-LAMP
Flaviviridae	*Flavivirus*	*Zika virus*	976Uganda	2.0×10^2 copies	+
		Zika virus	PRABC59	2.0×10^2 copies	+
		Zika virus	ArD157995*	2.0×10^2 copies	+
		Zika virus	41525-DAK*	2.0×10^2 copies	+
		Zika virus	CPC-0740*	2.0×10^2 copies	+
		Zika virus	P6-740*	2.0×10^2 copies	+
		Dengue virus serotype 1	Hawaii	2.4×10^4 copies	–
		Dengue virus serotype 2	ThNH7/93	9.5×10^4 copies	–
		Dengue virus serotype 3	PhMH-J1-97	2.2×10^5 copies	–
		Dengue virus serotype 4	SLMC 318	2.1×10^3 copies	–
		Yellow fever virus	17D	2.7×10^4 copies	–
		West Nile virus	NY99	3.5×10^4 copies	–
Togaviridae	*Alphavirus*	*Chikungunya virus*	10Mdy30	1.7×10^5 copies	–
Bunyaviridae	*Phlebovirus*	*Rift Valley fever virus*	SPU22/07	5.8×10^5 copies	–
Plasmodiidae	*Plasmodium*	*Plasmodium falciparum*	3D5	0.5 ng	–

Table 2. Species specificity of ZIKV RT-LAMP. *Synthesised partial genomic RNA sequences were used for these strains.

Sample	$TCID_{50}$/mL	RT-LAMP		rRT-PCR		geq/test
		Positive	Tp (min)	Positive	Ct	
Serum	232.7	4/4	12.5 ± 0.5	4/4	31.4 ± 0.2	329.5
	58.2	4/4	13.4 ± 0.9	4/4	33.1 ± 0.4	109.7
	14.5	4/4	14.3 ± 1.5	4/4	34.6 ± 0.8	44.3
	3.6	0/4	—	4/4	37.0 ± 0.7	8.8
	0.9	0/4	—	0/4	—	—
	mock	0/4	—	0/4	—	—
Urine	232.7	4/4	12.3 ± 0.4	4/4	31.0 ± 0.2	423.0
	58.2	4/4	14.4 ± 0.4	4/4	33.1 ± 0.2	105.8
	14.5	4/4	14.6 ± 2.1	4/4	35.4 ± 0.4	23.5
	3.6	1/4	23.8	4/4	37.1 ± 0.8	8.9
	0.9	0/4	—	1/4	37.5	5.8
	mock	0/4	—	0/4	—	—

Table 3. Detection of ZIKV in virus-spiked urine and serum samples.

obtained using standard RNA shown in Fig. 1, the limit of detection of the RT-LAMP assay was estimated to be 10 copies per reaction. The assay may be sufficiently sensitive for detecting ZIKV in clinical specimens.

Clinical evaluation of the RT-LAMP assay. We conducted a clinical evaluation of this assay using samples from patients with suspected arbovirus infection in the states of Paraíba and Pernambuco, Brazil in February–July 2016. The samples included 90 plasma/serum and 99 urine samples from 120 suspected arbovirus infection cases, including paired samples from 69 cases. To evaluate the diagnostic accuracy of this assay, we simultaneously conducted the CDC rRT-PCR assay as a reference test. In the RT-LAMP assay, eight out of sixteen serum samples collected in Pernambuco state in February 2016 were positive. However, all 74 plasma samples as well as urine samples collected in Paraíba state in March and July 2016 were negative. These results were concordant with those of the reference rRT-PCR assay (Table 4). The RT-LAMP assay did not show any false-positive results, even for six confirmed DENV samples (data not shown). The Ct values of these eight ZIKV-positive samples were 19.5–22.9, and the viral loads were estimated to be 1.6×10^6–1.4×10^7 geq/mL using the viral RNA standards (Table 5). These viral titres were higher than those reported in previous studies. To examine whether the assay can detect viral RNA in samples with lower titres, we randomly selected two ZIKV-positive samples confirmed in this study, MRL51 and MRL53, and conducted a dilution test (Table 6). While the RT-LAMP failed to detect samples with the Ct value > 37, however, it detected viral RNA at the Ct < 37, consistent with our earlier results obtained using the virus-spiked serum and urine samples (Table 3). These results show that the rRT-LAMP assay had sufficient specificity for the detection of ZIKV as a molecular diagnostic test. The assay can be used to detect an amount of viral RNA equivalent to that yielding Ct values of 36–37 in the reference rRT-PCR test.

Period	State	Type	No. samples	RT-LAMP		rRT-PCR	
				Positive	Negative	Positive	Negative
February, 2016	Pernambuco	Serum	16	8	8	8	8
March, 2016	Paraíba	Plasma	65	0	65	0	65
		Urine	69	0	69	0	69
July, 2016	Paraíba	Plasma	9	0	9	0	9
		Urine	30	0	30	0	30
Total		Serum/Plasma	90	8	82	8	82
		Urine	99	0	99	0	99

Table 4. Detection of ZIKV in samples from patients with suspected arbovirus infection collected in Paraíba and Pernambuco, Brazil in 2016.

Sample ID	RT-LAMP (Tt, min)	rRT-PCR (Ct)	Virus load (geq/ml)
LAV01	8.5	20.4	7.9×10^5
LAV04	8.8	20.8	6.2×10^5
LAV08	7.8	19.5	1.4×10^7
MRL51	8.3	21.6	3.7×10^6
MRL53	9.0	22.9	1.6×10^6
MRL55	8.5	21.4	4.2×10^6
MRL56	8.8	21.3	4.5×10^6
MRL57	8.8	21.2	4.8×10^6

Table 5. Viral load in ZIKV-positive samples tested in this study.

ID	Dilution ($\times 10^2$)	Estimated RNA copies	RT-LAMP		rRT-PCR	
			Positive	Tp (min)	Positive	Ct
MRL51	1	116.0	3/3	12.4 ± 1.0	3/3	32.9 ± 0.1
	3	38.7	3/3	12.8 ± 1.3	3/3	34.4 ± 0.1
	9	12.9	2/3	13.2 ± 1.1	3/3	36.3 ± 0.6
	27	4.3	0/3		2/3	36.7 ± 0.1
	81	1.4	0/3		1/3	37.2
	243	0.5	0/3		0/3	
MRL53	1	51.2	3/3	11.9 ± 0.4	3/3	34.5 ± 0.1
	3	17.1	3/3	15.8 ± 2.8	3/3	36.2 ± 0.2
	9	5.7	0/3		2/3	37.8 ± 0.1
	27	1.9	0/3		0/3	
	81	0.6	0/3		0/3	
	243	0.2	0/3		0/3	
No template control			0/3		0/3	

Table 6. Detection of ZIKV by RT-LAMP and rRT-PCR using diluted ZIKV-confirmed samples.

Discussion

We developed a rapid molecular detection assay for ZIKV in response to the recent outbreak in South America. LAMP assays and modified diagnostic methods for ZIKV have been reported; however, these molecular techniques have never been evaluated for clinical use[33–36]. This is the first evaluation of the clinical usage of a LAMP assay for molecular diagnostic testing in the recent outbreak of ZIKV infections. Since ZIKV shares a vector with DENV and CHIKV, these viral diseases can occur simultaneously, and Northeast Brazil is an endemic area for Dengue and Chikungunya[37]. Numerous severe mosquito-borne diseases, including arbovirus infections as well as Malaria, share clinical symptoms during the acute phase. However, ZIKV infection is generally associated with mild symptoms. A major concern with respect to molecular diagnostic testing for ZIKV is the potential for cross-reactivity with other flaviviruses, especially DNEV, which have close antigenic relation with ZIKV[21,23,25,38]. In contrast, our assay showed no cross-reactions with other arboviruses or *P. falciparum*, and did not show false-positive results when applied to ZIKV-negative samples. These results indicated that the RT-LAMP assay is specific for the detection of ZIKV and is a reliable molecular diagnostic test.

Another potential limitation of molecular diagnostic testing is that ZIKV-infected samples often have low titres after the acute or early phase of infection due to rapid clearance by the host immune system. This makes it difficult to identify ZIKV cases, even using RT-PCR-based tests. The limit of detection for this assay was 10 copies

for both genotypes. The assay was slightly less sensitive than the CDC rRT-PCR test, which was commonly used to confirm ZIKV infection during the recent outbreak. ZIKV-infected clinical samples often show high Ct values (>35)[19,23]. However, the ZIKV-positive samples detected in this evaluation showed Ct values of less than 22.9 (more than 1.6×10^6 geq/mL), which was a higher titre than that reported in other studies. To confirm its clinical utility, this assay should be tested using samples with lower titres or borderline ZIKV infections.

It has been reported that viral RNA can be detected for longer periods in urine than in blood[19,23]. Therefore, we considered urine to be one of the best sample types for detecting ZIKV infections. Recently, Paz-Bailey *et al.* reported contradictory results for the persistence of viral RNA in blood samples of ZIKV patients; RNA can be detected 1 or 2 weeks after the onset of illness[17]. In some cases, viral RNA can also be detected at higher titres in saliva than in blood, but persists for shorter periods[15,17]. It is necessary to determine the sample types suitable for the RT-LAMP assay and to establish a standardised RNA extraction protocol adjusted to each clinical specimen type in order to improve the sensitivity of this assay.

Owing to the sequence diversity among ZIKV isolates, we designed LAMP primers specific for each genotype and used a mixture of these primers to detect all known isolates of both African and Asian genotypes. As shown in Fig. 2, we conducted an *in silico* evaluation of each primer using available ZIKV sequences. African genotype strains supposedly have a longer history of circulation in African mosquitos and humans than that of Asian genotype strains[11], and African genotype sequences showed a lower identity at some positions in the LAMP primers. The LAMP primers designed here showed high identities at most positions against the sequences of strains involved in the recent outbreak on the American continent, as well as its ancestral Southeast Asian and Polynesian isolates. During the outbreak of ZIKV in Americas, confirmed or probable ZIKV-infected cases has been continuously reported in Southeast Asia[39]. Our assay will be useful for virus detection and may contribute to preparedness for future outbreaks in these ZIKV endemic countries as well as in Asia and Africa. However, the evolution of ZIKV sequences must be constantly monitored to guarantee primer specificity.

Using samples obtained from subjects with suspected arbovirus infection, we did not find any ZIKV-positive samples in Paraíba in March or July 2016 by rRT-PCR or our RT-LAMP test. These samples were collected from patients within 1 or 2 weeks after the onset of arbovirus infection-like symptoms as part of an education and follow-up campaign for cardiovascular diseases. Many samples might have been collected after the acute or early stage of infection. In addition, when this campaign was conducted, the prevalence of ZIKV infection may have been low, since most cases were reported from November 2015 to March 2016[40], which is closely linked to the ecology of the vector *Aedes* mosquito.

The main advantages of this assay are its speed (positive results can be obtained within 15 min) and the use of a battery-operated portable device. Since the device has a user-friendly interface, training is not necessary to conduct the assay and interpret the results. Recently, freeze-dried reagents for LAMP assays have been made available, making cold-chain-free LAMP assays a possibility. Our assay is suitable for use in field surveillance or remote areas where it is difficult to implement laboratory diagnostic tests. The assay should be evaluated in a prospective study to confirm its utility for molecular diagnostic testing, especially under limited resources and by field laboratories in ZIKV endemic countries.

In this paper, we successfully developed a RT-LAMP assay for the detection of ZIKV by designing Asian and African genotype-specific primers. The assay showed results consistent with those of the reference rRT-PCR assay in diagnostic tests with suspected cases of ZIKV infection. Our results provide a potential new molecular diagnostic test for ZIKV and may serve as a basis for the development of alternative rapid diagnostic techniques to prepare for potential outbreaks.

Methods

Cells and viruses. Vero 76 cells were obtained from the Health Science Research Resources Bank (JCRB9007) and were maintained in Dulbecco's modified Eagle's medium (DMEM) supplemented with 1% penicillin/streptomycin and 10% foetal bovine serum (FBS). ZIKV strain 976Uganda was kindly provided by Dr. Shigeru Tajima (National Institute of Infectious Diseases; NIID). The virus was propagated in Vero 76 cells grown in DMEM supplemented with 2% FBS. Two days after infection, culture supernatants were harvested, clarified by low-speed centrifugation, and then stored as virus stock at −80 °C until use. The infectious titre of the virus stock was determined by the 50% tissue culture infective dose ($TCID_{50}$) using Vero 76 cells; titres are expressed as $TCID_{50}$/mL. Viral RNA was extracted from 140 μL of infected culture supernatant using the QIAamp Viral RNA Mini Kit according to the manufacturer's protocol. The RNA was eluted in 60 μL of elution buffer and stored at −80 °C until use. Viral RNA from ZIKV strain PRABC59 was kindly provided by Dr. Shigeru Tajima (NIID). Viral RNAs from other arboviruses, including DENV serotype 1–4, YFV, WNV, CHIKV, and RVFV, as well as genomic DNA from *P.falciparum* strain 3D7 were kindly provided by Dr. Kouichi Morita and Dr. Osamu Kaneko (Institute of Tropical Medicine, Nagasaki University).

Preparation of RNA standards. RNA standards, consisting of partial genome sequences of ZIKV strains 976Uganda and PRVABC59, were amplified by RT-PCR using forward (5′-GGAGTCAGGATGGTACTTGTACC-3′) and reverse (5′-AAAATTGGATATTCAGGAACC-3′) primers with the PrimeScriptII High Fidelity One Step RT-PCR Kit (Takara Bio, Shiga, Japan). The reactions were performed using the TaKaRa PCR Thermal Cycler Dice with the following program: 45 °C for 10 min, 94 °C for 2 min, followed by 40 cycles of 98 °C for 10 s, 55 °C for 15 s, and 68 °C for 20 s. Amplified PCR fragments were cloned into the pCR2.1 vector using the TOPO-TA-Cloning Kit (Invitrogen, Carlsbad, CA, USA). The plasmids were digested with *Bam*HI, purified from the agarose gel slice using a column purification kit (Qiagen, Hilden, Germany), and used as templates for RNA synthesis. The partial genomic RNAs of each ZIKV strain were synthesised *in vitro* using T7 RNA polymerase (Promega, Madison, WI, USA) and purified using the RNeasy Mini Kit (Qiagen). The RNA concentration was determined by measuring the optical density at 260 nm (OD_{260}) with

a NanoDrop 2000 (Thermo Fisher Scientific, Waltham, MA, USA), and the RNAs were diluted in DEPC-treated water to achieve the desired concentrations.

Primer design. LAMP primers for ZIKV detection were designed based on the coding sequences for the E protein. The ZIKV sequences available in GenBank were aligned using CLUSTALX to identify conserved regions. A consensus sequence for a region in the *E* gene was used to design LAMP primers using LAMP Designer (Optigene; http://www.optigene.co.uk/lamp-designer/). Primers specific for Asian genotype viruses were designed first, and then African genotype-specific primers were designed by adapting each position to the African genotype consensus sequence. The RT-LAMP assay required a set of six primers, two outer primers (F3 and B3), a forward inner primer (FIP), a reverse inner primer (BIP), a forward loop primer (LF), and a reverse loop primer (LB). The FIP consisted of the F1c sequence, which was complementary to the F1 and F2 sequences. The BIP consisted of the B1c sequence, which was complementary to the B1 and B2 sequences[27]. The LB primer was designed to detect both Asian and African genotype sequences. The sequences and locations of the oligonucleotide primers are shown in Table 1.

RT-LAMP. RT-LAMP was performed with Isothermal Master Mix reagent (Optigene, West Sussex, UK) using the Genelyzer FIII real-time fluorescence detection platform (TOSHIBA Medical Systems, Otawara, Japan). The reaction mixture (total volume, 25 μL) contained 15 μL of Isothermal Master Mix; 1 μL of WarmStart RTx reverse transcriptase (1 U; New England BioLabs, Ipswich, MA, USA); 4 μL of the LAMP primer mix consisting of 5 pmol F3 and B3, 20 pmol FIP and BIP, 10 pmol LF and LB; and 5 μL of RNA sample (template). The assay was carried out using a mixture of primers specific for the Asian and African genotypes. All primers were cartridge-purified oligonucleotides purchased from Hokkaido System Science (Sapporo, Japan). The reaction was performed at 65 °C for 30 min, followed by a dissociation analysis at 95 °C–80 °C. DEPC-treated distilled water and RNA synthesised from 976Uganda or PRVABC59 were used for the negative and positive controls, respectively. Nonspecific amplification was excluded by comparing the melting temperature to that of the positive control[31].

Real time RT-PCR. Real time RT-PCR for ZIKV was performed using the QuantiTect Probe RT-PCR Kit (Qiagen) as reported previously[21]. The reaction mixture (total volume, 25 μL) contained 12.5 μL of 2× QuantiTect Probe RT-PCR Master Mix, 0.5 μL of QuantiTect RT Mix, 10 pmol each of primers 1086 and 1162c, and 5 pmol FAM-labelled 1086 probe for ZIKV. Then, aliquots of the RNA samples (2 μL) were added to the 25-μL reaction mixtures. Each reaction was performed using the 7500 Real-Time PCR System (Applied Biosystems, Tokyo, Japan) with a thermal cycle profile consisting of 48 °C for 30 min, 95 °C for 15 min, followed by 40 cycles of 95 °C for 15 s and 60 °C for 1 min. Cut-off values were set at Ct 38.5. To quantify viral RNA, a standard curve, generated with 10-fold serial dilutions of synthesised standard RNA from 976Uganda or PRVABC59, was used.

Droplet digital PCR. Each arbovirus RNA listed in Table 2 except ZIKV was quantified by droplet digital PCR (ddPCR). The complementary DNA (cDNA) of each arbovirus RNA was synthesised from an extracted RNA stock using the SuperScript III First-Strand Synthesis System (Invitrogen) with forward primer for RVFV and reverse primers for DENV, WNV, YFV, and CHIKV, respectively (Supplementary Table 1). The primers used for ddPCR were designed using Primer3 (Supplementary Table 1). All 20-μL ddPCR mixtures contained 2× EvaGreen ddPCR Supermix (Bio-Rad, Hercules, CA, USA), 0.1 μM forward and reverse primers, and 2 μL of cDNA. Each oil compartment of the droplet generator DG8 cartridge (Bio-Rad) was filled with 70 μL of droplet generation oil for EvaGreen (Bio-Rad), and approximately 20,000 droplets were generated in each well by the QX200 Droplet Generator (Bio-Rad). The reactions were performed in a 40-μL droplet emulsion using a GeneAmp PCR System 9700 (Applied Biosystems) under the following thermal cycling conditions: 95 °C for 10 min, followed by 45 cycles of 94 °C for 30 s and 60 °C for 2 min, with a final step at 98 °C for 10 min. Controls without the template were used to monitor for signals from contamination or primer-dimer formation. The cycled droplets were read individually using the QX200 droplet reader (Bio-Rad) and analysed with QuantaSoft Droplet Reader software (Bio-Rad).

Clinical specimens. Peripheral blood and urine samples were obtained from patients between 2 and 65 year old with suspected arbovirus infection, who presented with fever, rash, and/or arthralgia symptoms. Venous whole blood samples were collected in one VACUETTE® Z Serum Separator Clot Activator and two Vacuette® EDTA Tubes (Greiner Bio-One, Kremsmünster, Austria). To one EDTA tube, RNA*later* (Thermo Fisher Scientific) was added at half the volume of the collected blood samples to prevent RNA degradation during transport. In total, 90 plasma/serum and 99 urine samples from 120 patients with suspected arbovirus infection, including paired samples from 69 cases, were used in this study. The separated plasma or serum samples and urine samples were stored at −80 °C until use. RNAs were extracted from sera and urine using the QIAamp Viral RNA Mini Kit (Qiagen) according to the manufacturer's instructions. RNA samples were eluted with 60 μL of elution buffer and stored at −80 °C until use.

Ethical declaration. This study was approved by the CCS-UFPE Ethical Committee (CAAE: 61603316.7.0000.5208) and all patients gave informed consent. Whole blood and urine samples were collected as part of an education and follow-up campaign for arboviruses and cardiovascular diseases conducted by LIKA in the states of Paraíba and Pernambuco, Brazil in February–July 2016. All experiments were performed in accordance with relevant guidelines and regulations.

References

1. Petersen, L. R., Jamieson, D. J., Powers, A. M. & Honein, M. A. Zika Virus. *N Engl J Med* **374**, 1552–1563 (2016).
2. Wikan, N. & Smith, D. R. Zika virus: history of a newly emerging arbovirus. *Lancet Infect Dis* **16**, e119–126 (2016).
3. Campos, G. S., Bandeira, A. C. & Sardi, S. I. Zika Virus Outbreak, Bahia, Brazil. *Emerg Infect Dis* **21**, 1885–1886 (2015).
4. Mlakar, J. *et al.* Zika Virus Associated with Microcephaly. *N Engl J Med* **374**, 951–958 (2016).
5. Schuler-Faccini, L. *et al.* Possible Association Between Zika Virus Infection and Microcephaly - Brazil, 2015. *MMWR Morb Mortal Wkly Rep* **65**, 59–62 (2016).
6. de Araujo, T. V. *et al.* Association between Zika virus infection and microcephaly in Brazil, January to May, 2016: preliminary report of a case-control study. *Lancet Infect Dis* **16**, 1356–1363 (2016).
7. Franca, G. V. *et al.* Congenital Zika virus syndrome in Brazil: a case series of the first 1501 livebirths with complete investigation. *Lancet* **388**, 891–897 (2016).
8. Barjas-Castro, M. L. *et al.* Probable transfusion-transmitted Zika virus in Brazil. *Transfusion* **56**, 1684–1688 (2016).
9. Hills, S. L. *et al.* Transmission of Zika Virus Through Sexual Contact with Travelers to Areas of Ongoing Transmission - Continental United States, 2016. *MMWR Morb Mortal Wkly Rep* **65**, 215–216 (2016).
10. Moreira, J., Peixoto, T. M., Machado de Siqueira, A. & Lamas, C. C. Sexually acquired Zika virus: a systematic review. *Clin Microbiol Infect* (2017).
11. Faye, O. *et al.* Molecular evolution of Zika virus during its emergence in the 20(th) century. *PLoS Negl Trop Dis* **8**, e2636 (2014).
12. Musso, D. Zika Virus Transmission from French Polynesia to Brazil. *Emerg Infect Dis* **21**, 1887 (2015).
13. Faria, N. R. *et al.* Zika virus in the Americas: Early epidemiological and genetic findings. *Science* **352**, 345–349 (2016).
14. Gourinat, A. C., O'Connor, O., Calvez, E., Goarant, C. & Dupont-Rouzeyrol, M. Detection of Zika virus in urine. *Emerg Infect Dis* **21**, 84–86 (2015).
15. Musso, D. *et al.* Detection of Zika virus in saliva. *J Clin Virol* **68**, 53–55 (2015).
16. Bingham, A. M. *et al.* Comparison of Test Results for Zika Virus RNA in Urine, Serum, and Saliva Specimens from Persons with Travel-Associated Zika Virus Disease - Florida, 2016. *MMWR Morb Mortal Wkly Rep* **65**, 475–478 (2016).
17. Paz-Bailey, G. *et al.* Persistence of Zika Virus in Body Fluids - Preliminary Report. *N Engl J Med* (2017).
18. St George, K. *et al.* Zika Virus Testing Considerations: Lessons Learned from the First 80 Real-Time Reverse Transcription-PCR-Positive Cases Diagnosed in New York State. *J Clin Microbiol* **55**, 535–544 (2017).
19. Fourcade, C. *et al.* Viral load kinetics of Zika virus in plasma, urine and saliva in a couple returning from Martinique, French West Indies. *J Clin Virol* **82**, 1–4 (2016).
20. Faye, O. *et al.* Quantitative real-time PCR detection of Zika virus and evaluation with field-caught mosquitoes. *Virol J* **10**, 311 (2013).
21. Lanciotti, R. S. *et al.* Genetic and serologic properties of Zika virus associated with an epidemic, Yap State, Micronesia, 2007. *Emerg Infect Dis* **14**, 1232–1239 (2008).
22. Waggoner, J. J. & Pinsky, B. A. Zika Virus: Diagnostics for an Emerging Pandemic Threat. *J Clin Microbiol* **54**, 860–867 (2016).
23. Campos Rde, M. *et al.* Prolonged detection of Zika virus RNA in urine samples during the ongoing Zika virus epidemic in Brazil. *J Clin Virol* **77**, 69–70 (2016).
24. Abd El Wahed, A. *et al.* Rapid Molecular Detection of Zika Virus in Acute-Phase Urine Samples Using the Recombinase Polymerase Amplification Assay. *PLoS Curr* **9** (2017).
25. Tappe, D. *et al.* First case of laboratory-confirmed Zika virus infection imported into Europe, November 2013. *Euro Surveill* **19** (2014).
26. Felix, A. C. *et al.* Cross reactivity of commercial anti-dengue immunoassays in patients with acute Zika virus infection. *J Med Virol* **89**, 1477–1479 (2017).
27. Notomi, T. *et al.* Loop-mediated isothermal amplification of DNA. *Nucleic Acids Res* **28**, E63 (2000).
28. Hong, T. C. *et al.* Development and evaluation of a novel loop-mediated isothermal amplification method for rapid detection of severe acute respiratory syndrome coronavirus. *J Clin Microbiol* **42**, 1956–1961 (2004).
29. Notomi, T., Mori, Y., Tomita, N. & Kanda, H. Loop-mediated isothermal amplification (LAMP): principle, features, and future prospects. *J Microbiol* **53**, 1–5 (2015).
30. Kurosaki, Y. *et al.* Deployment of a Reverse Transcription Loop-Mediated Isothermal Amplification Test for Ebola Virus Surveillance in Remote Areas in Guinea. *J Infect Dis* **214**, S229–S233 (2016).
31. Kurosaki, Y. *et al.* Development and Evaluation of Reverse Transcription-Loop-Mediated Isothermal Amplification (RT-LAMP) Assay Coupled with a Portable Device for Rapid Diagnosis of Ebola Virus Disease in Guinea. *PLoS Negl Trop Dis* **10**, e0004472 (2016).
32. Yun, S. I. *et al.* Complete Genome Sequences of Three Historically Important, Spatiotemporally Distinct, and Genetically Divergent Strains of Zika Virus: MR-766, P6-740, and PRVABC-59. *Genome Announc* **4** (2016).
33. Wang, X. *et al.* Rapid and sensitive detection of Zika virus by reverse transcription loop-mediated isothermal amplification. *J Virol Methods* **238**, 86–93 (2016).
34. Tian, B. *et al.* Attomolar Zika virus oligonucleotide detection based on loop-mediated isothermal amplification and AC susceptometry. *Biosens Bioelectron* **86**, 420–425 (2016).
35. Song, J. *et al.* Instrument-Free Point-of-Care Molecular Detection of Zika Virus. *Anal Chem* **88**, 7289–7294 (2016).
36. Lee, D. *et al.* Simple and Highly Sensitive Molecular Diagnosis of Zika Virus by Lateral Flow Assays. *Anal Chem* **88**, 12272–12278 (2016).
37. Pessoa, R. *et al.* Investigation Into an Outbreak of Dengue-like Illness in Pernambuco, Brazil, Revealed a Cocirculation of Zika, Chikungunya, and Dengue Virus Type 1. *Medicine (Baltimore)* **95**, e3201 (2016).
38. Zammarchi, L. *et al.* Zika virus infections imported to Italy: clinical, immunological and virological findings, and public health implications. *J Clin Virol* **63**, 32–35 (2015).
39. Duong, V., Dussart, P. & Buchy, P. Zika virus in Asia. *Int J Infect Dis* **54**, 121–128 (2017).
40. Pan American Health Organization and World Health Organization. *Zika – Epidemiological Update* 10 March. http://www2.paho.org/hq/index.php?option=com_content&view=article&id=11599&Itemid=41691&lang=en (2016).

Acknowledgements

The authors would like to thank Sayaka Okada, Shota Koyano and Olamide K. Oloniniyi for technical assistance with the experiments at Nagasaki University, Renato P. Melo Neto and Carlos Henrique M. Castelletti for bioinformatics support at LIKA, and all members of the staff for their hospitality during the visit when the main results of this paper were obtained. This work was supported by the Japan Agency for Medical Research and Development, Japan Society for the Promotion of Science Research Fellowship PD (15J06242), National Council for Scientific and Technological Development of Brazil (CNPq - 459406/2014-0), and Foundation for Science and Technology of Pernambuco (FACEPE - APQ-0142-2.08/2016).

Author Contributions

Y.K., D.B.G.M., J.L.L.F., and J.Y. designed the experiments and analysed the data. Y.K., D.B.G.M., M.K., A.d.S.C., M.A.C.S.M.B., S.d.S.M., H.A., R.Y., and J.Y. performed the experiments. Y.K. and H.A. performed sequence analysis and designed the primers. Y.K., D.B.G.M., and J.Y. wrote the paper and prepared all of the figures and tables.

Additional Information

Supplementary information accompanies this paper at https://doi.org/10.1038/s41598-017-13836-9.

Competing Interests: The authors declare that they have no competing interests.

Publisher's note: Springer Nature remains neutral with regard to jurisdictional claims in published maps and institutional affiliations.

APÊNDICE E - ARTIGO EM COLABORAÇÃO

ELECTROCHEMICAL APTASENSOR FOR THE DETECTION OF HER2 IN HUMAN SERUM TO ASSIST IN THE DIAGNOSIS OF EARLY STAGE BREAST CANCER

Analytical and Bioanalytical Chemistry
https://doi.org/10.1007/s00216-019-02040-5

RESEARCH PAPER

Electrochemical aptasensor for the detection of HER2 in human serum to assist in the diagnosis of early stage breast cancer

Giselda Bezerra[1] · Carolina Córdula[1] · Danielly Campos[1] · Gustavo Nascimento[1] · Natália Oliveira[1] · Maria Aparecida Seabra[1] · Valeria Visani[1] · Sampaio Lucas[1] · Iasmim Lopes[1] · Joana Santos[1] · Francisco Xavier Jr[1] · Maria Amélia Borba[1] · Danyelly Martins[1] · José Lima-Filho[1]

Received: 4 May 2019 / Revised: 7 July 2019 / Accepted: 17 July 2019

Abstract
Human epidermal growth factor receptor-2 (HER2) is an important biomarker in the diagnosis and prognosis of breast cancer. This work aimed to develop an aptasensor to detect HER2 in human serum. HER2 aptamer was immobilized by electrostatic adsorption on the surface of a homemade screen-printed electrode modified with poly-L-lysine. Measurements were made by differential pulse voltammetry using methylene blue as a redox indicator. A calibration curve was constructed ($R^2 = 0.997$) using different concentrations of HER2 protein (10–60 ng/mL) in PBS buffer (pH 7.4), with a detection limit of 3.0 ng/mL. The aptasensor showed good reproducibility with relative standard deviations (RSDs) of 3% and remained stable for 3 days with an RSD around 2%. When the tests were performed with serum from a healthy woman, a peak of 6.72 μA was found without the addition of the protein. When we tested the serum of a woman with HER2+ breast cancer, we obtained a signal of 2.65 μA; the same pattern was found when adding to protein in serum control, i.e., the higher the concentration of protein, the lower the signal. The aptasensor was characterized by scanning electron microscopy and isothermal titration calorimetry (ITC), showing excellent interaction between aptamer and target protein. The results revealed a promising and sensitive tool capable of detecting HER2 protein in human serum with albumin depletion, aiding in the molecular diagnosis of breast cancer.

Keywords Aptasensor · Aptamer · Diagnosis · Breast cancer · HER2 · Screen-printed electrode

Introduction

Nearly 2.1 million new cases of breast cancer and about 630,000 deaths were estimated in 2018 worldwide. In Brazil, 60,000 new cases of breast cancer were expected [1]. The ideal interval between diagnosis and treatment should be up to 60 days for a better prognosis [2]; however, in Brazil, Mexico, and India, this period reaches up to 240 days [2]. This highlights the need for new strategies, such as public policies and new techniques, to decrease the time required for diagnostic testing.

Breast cancer is a disease with high mortality rate among women around the world and has a heterogeneous clinical nature [3]. There are four main subtypes of breast cancer: luminal A, luminal B, HER2 positive, and triple negative/basal-like; the SKBR3 breast tumor line is equivalent to the subtype molecular model HER2 positive, and the MDA-MB-231 cell line is equivalent to the triple-negative molecular subtype [4].

The human epidermal growth receptor-2 (*HER2*) gene expresses a HER2 transmembrane protein and has three domains: an extracellular domain (ECD), a transmembrane region, and an intracellular tyrosine kinase domain; the ECD can be released into the bloodstream when the cell is lysed and can be detected. Overexpression of the *HER2* oncogene characterizes the HER2 positive subtype of breast cancer, an aggressive tumor with a poor clinical outcome [5, 6]. In serum, HER2 concentration ranges from 0 to 15 ng mL^{-1} in healthy women, and values above this point are considered overexpressed [4].

Nowadays, breast cancer is diagnosed through screening methods, such as ultrasound, mammography, and, in a few cases, nuclear magnetic resonance. These methods have some

✉ Giselda Bezerra
giseldamilamari@hotmail.com

[1] Laboratório de Imunopatologia Keizo Asami – LIKA, Universidade Federal de Pernambuco – UFPE, Av. Prof. Moraes Rego 1235, Recife, PE 50670-901, Brazil

Published online: 05 August 2019

limitations: for example detection by mammography is impaired in areas with dense breast tissue [7].

Immunohistochemistry (IH) is recommended to determine HER2 expression in tissues, followed by fluorescence in situ hybridization (FISH) to evaluate *HER2* gene amplification, and these two methods to detect HER2 are invasive because they are performed with a fragment of the breast tissue by biopsy [8]. Siemens has an immunoenzymatic assay (ELISA), approved by the US Food and Drug Administration (FDA) in 2000, for the determination of HER2 protein in serum, for monitoring the treatment and prognosis of HER2-type breast cancer [9]. Despite these already established methods for detecting HER2, the possibility of developing a simple, rapid, inexpensive, safe, and point-care device, such as biosensors [10], will be of great help in the diagnosis of subtype of breast cancer type HER2 [11]. The quantification of this molecule in serological samples is considered a promising, less invasive method for the early diagnosis of the disease.

Aptasensors are biosensors that use an aptamer as the biological recognition element. They exhibit high sensitivity and selectivity, good stability in complex environments, and resistance to denaturation and degradation [12]. Electrochemical aptasensors are faster, cheaper, and more sensitive platforms with potential for application in point-of-care diagnosis, monitoring, and treatment guidance [13]. Aptamers are single-stranded DNA or RNA molecules with tridimensional folding that serve as ligands to a specific target [13]. As a biological recognition element, aptamers have some advantages over antibodies, which make them preferable in the development of biosensors, such as simpler structure, which makes them highly reproducible, and thus, they are cheaper, easier to store, and more stable owing to their greater resistance to denaturation [14].

The literature contains publications on several electrochemical immunosensors [10, 15–19] and aptasensors [12, 14] which detect HER2 in serum. These biosensors used a gold transducer [10, 12, 14, 15, 17] with a reaction time and signal that varied between 20 and 60 min [10, 12, 14].

In this work, we used an aptamer capable of recognizing HER2 ECD in human serum after depletion of serum albumin. The use of a carbon transducer produced in our laboratory made the experiment cheaper. It also showed a shorter detection time than previously published sensors. Since our system is affected by albumin, it required the depletion of the serum albumin; in turn, the used kit also removes the immunoglobulin IgG. Insulin was used as a non-complementary protein for the system selectivity test because it is increased in cases of breast cancer and the results showed that the sensor did not detect insulin. It can have a positive impact in the early diagnosis and continuous monitoring of this cancer of high incidence and aggressiveness.

Materials and methods

Materials

All reagents used were of high purity and solutions were prepared in ultrapure water. L-Lysine, insulin, and methylene blue (MB) were purchased from Sigma-Aldrich (USA); phosphate buffered saline (PBS) and RNA aptamer (5' GGG AGA UAC CAG CUU AUU CAA UUU GGA UGG GGA GAU CCG UUG AGU AAG CGG GCG UGU CUC UCU GCC GCC UUG CUA UGG GGA GAU AGU AAG UGC AAU CU 3') extracellular domain (ECD) were acquired from Aptagen (USA) and HER2 protein extracellular domain (ECD) (fragment ab168896) was from Abcam (USA). All inks (carbon and silver/silver chloride) were purchased from Gwent Group. Albumin & IgG Depletion SpinTrap was from GE Healthcare (USA).

Stock solutions

HER2 RNA aptamer was prepared according to the manufacturer's instructions for 50 μM and HER2 protein (specific target) was dissolved to 1.02 μM in ultrapure water. Insulin (non-specific target) was diluted to 17.2 μM in ultrapure water. All stock solutions were stored at − 20 °C and showed stability during the experiments that occurred throughout 1 year.

Clinical samples

The research was approved by the Ethics Committee Involving Human Beings, Federal University of Pernambuco, Health Sciences Center (Universidade Federal de Pernambuco, CCS Centro de Ciências da Saúde), with numbers 1.215.006 and 1.514.122-B. Patient blood samples with HER2 positive breast cancer subtype and negative control were obtained from files from the Keizo Asami Immunopathology Laboratory (LIKA), Federal University of Pernambuco. All samples were validated using gold standards for diagnosis (IH and FISH).

Screen-printing and modified electrodes

All electrodes were homemade (Fig. 1a). A three-electrode system was used employing carbon as working electrode (surface area 7 mm^2) (Fig. 1, a1) and counter electrode. Silver/silver chloride (Ag/AgCl) was used as reference electrode.

The working electrode surface was modified with a poly-L-lysine film (PLLF) (which occurs by electrostatic adsorption) (Fig. 1b) to provide a support for aptamer immobilization. L-

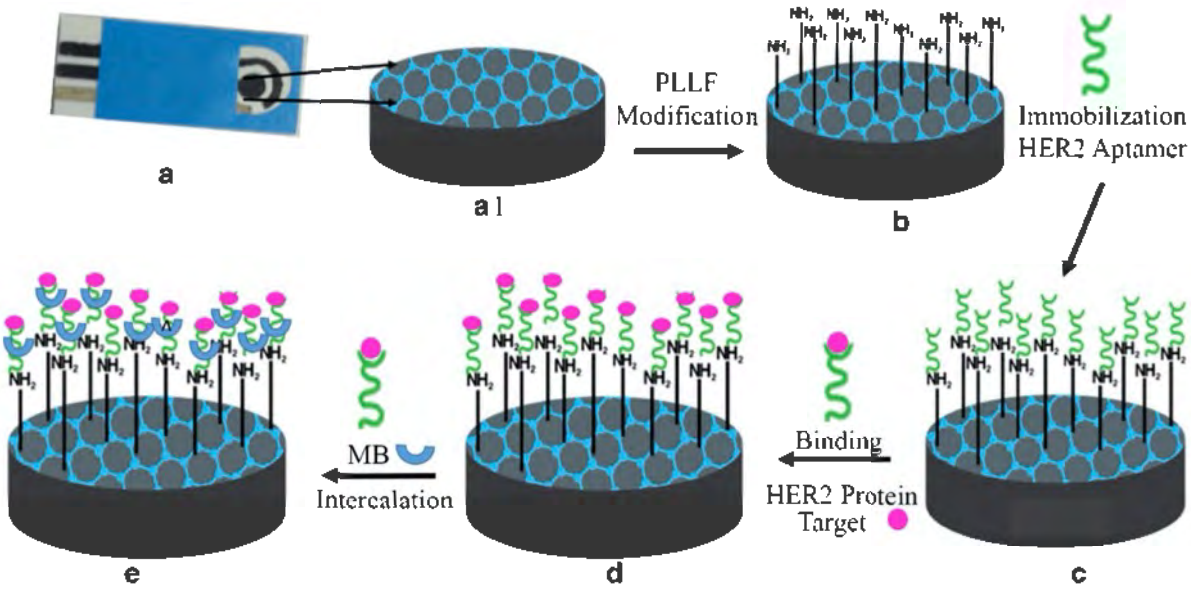

Fig. 1 Schematic of aptasensor production. (a) Screen-printed electrode; (a1) working electrode; (b) modified working electrode with PLLF; (c) HER2 aptamer immobilized on modified electrode; (d) HER2 protein bound to the aptamer; (e) MB/aptamer interaction

Lysine solution (1 mM) was prepared in PBS buffer pH 7.4. Then, L-lysine was electropolymerized for PLLF formation by cyclic voltammetry (CV) scanning from 1.8 to 2.0 V for 10 cycles with a scan rate of 100 mV s^{-1}.

Schematic aptasensor production

Figure 1 shows a schematic of the preparation of the aptasensor.

RNA aptamer immobilization and target binding assay

The aptamer in stock solution at a temperature of 20 °C showed stability during the experiments that occurred throughout 1 year.

Different aptamer concentrations (0.10 2.0 µM) were immobilized on the modified working electrode (Fig. 1c) at 25 °C for 30 min. The unbound aptamer was removed by washing with Tris-HCl (pH 7.4).

HER2 protein was diluted at concentrations ranging from 10 to 60 ng/mL in PBS at pH 7.4 and in whole human serum, human serum after albumin depletion of positive and negative patients for breast cancer subtype HER2. All diluted samples were added to the aptamer immobilized on the working electrode surface (Fig. 1d). Non-specific binding was performed using insulin with the same conditions as described above. The binding reaction occurred at 25 °C for 30 min. MB (500 µM) was added to the modified electrode (Fig. 1e) and incubated for 5 min at 25 °C followed by washing with 20 mM Tris-HCl (pH 7.4) to remove the unbound molecules. This protocol is already used in our research group [20].

Electrochemical analysis

Electrochemical signal analysis was performed by differential pulse voltammetry (DPV) in the phases of immobilization of aptamer HER2-RNA and after the recognition process between the interaction of the aptamer and the HER2 protein to detect the best signal of these phases. A 500 mM MB solution in Tris-HCl buffer (20 mM, pH 7.0) was used as the chemical mediator, 5 µL of which was pipetted onto the surface of the working electrode for 5 min, then washed with Tris-HCl buffer. The DPV measurement was performed on Tris-HCl for electrochemical reduction of MB under the following conditions: with a potential scanning between 0.6 and 0 V, amplitude modulation of 50 mV, and scan rate of 20 mV s^{-1}, during 4 min. Electrochemical analysis was conducted using the potentiostat (Autolab) set up with NOVA 2.0 software.

Characterization of aptasensor

Characterization of bare, modified electrode and immobilized aptamer

All electrodes were metallized with pure gold and palladium (80% and 20%, respectively). All images were taken in a Zeiss microscope model EVO-LS.

Thermodynamic characterization of binding process and affinity between RNA aptamer and HER2 protein were studied by ITC (ITC-200 MicroCal/GE, Northampton, Massachusetts)

Isothermal titration calorimetry (ITC) is an established analytical technique routinely used to determine thermodynamic interaction for a variety of chemical and biological systems. For the ITC experiments, all solutions were prepared in 0.1 M modified PBS, pH 7.4. Before each experiment, all solutions were filtered through a 0.22-μm membrane (Millex®, Millipore, France) and degassed. The titrant solutions of RNA (0.75 μM) were prepared in PBS pH 7.4 and placed in the stirring syringe. The sample cell was filled with 200 μL of HER2 (0.15 μM). The first injection of 0.4 μL was discarded to eliminate diffusion effects of material from the syringe to the sample cell. Experiments consisted of 19 consecutive injections (2 μL), each one lasting 4.0 s at spaced time intervals of 120 s and a stirring speed of 400 rpm at 25, 35, and 45 °C. The data consisted of a series of heat flows as a function of time. The interaction process between RNA aptamer and HER2 protein was analyzed by one-site binding model (Origin 7 software). Stoichiometry of the interaction (n), binding constant (K), and changes in enthalpy (ΔH), entropy (ΔS), and the Gibbs free energy (ΔG) were obtained.

Results and discussion

Screen-printed electrode structural analysis

The working electrode was modified to allow the aptamer immolization. Thus, L-lysine was electropolymerized on the carbon surface electrode by cyclic voltammetry. L-Lysine monomer is oxidized to an amino free radical at a higher positive potential, and then subsequently forms a carbon nitrogen linkage at the working electrode surface [21, 22]. PLLF formation on the working electrode can be monitored by cyclic voltammetry. In general, redox signal increases with cycle number until stabilizing, leading to a full covering on the working electrode area. The modified working electrode with PLLF has free amine groups on its surface which interact with the negatively charged RNA phosphate groups [23, 24, 35]. Therefore, this is a fundamental step in the aptamer immobilization as observed in the literature.

Electron micrographs in Fig. 2a–c show the change in the surface of the working electrode covered by PLLF, and after immobilization of the aptamer observed in the literature [22].

Once modification and immobilization steps on the working electrode were confirmed, an aptamer concentration curve was constructed to determine the optimal aptamer concentration.

Study of aptamer concentration

Methylene blue is a widely used electrochemical mediator owing to its capacity to intercalate with nucleic acids through interaction with guanines [22, 23]. This reaction can be monitored by DPV and is applied to aptasensor analyses [22, 23].

Figure 3 shows that the current peak increased significantly as the concentration of the aptamer increased, reaching its highest point (8.03 μA) at a concentration of 1.5 μM, followed by a decrease to 6.37 μA at a concentration of 2.0 μM. This may be explained by the excessive accumulation of probe on the carbon electrode, with the resulting saturation leading to lower availability of guanine bases, which overlap. Increasing interaction occurs between MB and the guanines of the RNA aptamer until saturation on the working electrode surface, resulting in an increase in the signal [24, 25]. Therefore, 1.5 μM was the best concentration in this experiment.

Effect of interaction between aptamer and HER2 protein

In this work, a screen-printed homemade electrode was prepared in order to detect HER2+. A study was performed using HER2-PBS (protein HER2 added to PBS), HER2-HS (protein HER2 added to human serum), HER2-HSAD (protein HER2 added to human serum after albumin depletion), and then a positive and negative controls.

Once the best concentration of the aptamer was determined, we began tests using the target (HER2 protein) added to PBS, human serum (HS), human serum after albumin depletion (HSAD) as well as HSAD positive (HER2+) and negative (HER−) biological samples. Figure 3 shows the study concentration of immobilized aptamer used (Fig. 3).

With the HER2 protein added to PBS, pH 7.4, the increase in the concentration resulted in a decrease in the signal (10 ng/mL = 6.60 μA and 15 ng/mL = 6.07 μA). These values were used to simulate an organic system of a healthy woman, whereas 25 ng/mL = 5.47 μA, 40 ng/mL = 4.07 μA, 50 ng/mL = 3.06 μA, and 60 ng/mL = 2.22 μA were used to simulate a patient with HER2+ cancer. In this range (10–60 ng/mL) (Fig. 4a), the system was linear and these values were used to calculate the calibration curve of the aptasensor [26].

The reduction in the signal with the increase in concentration was caused by the presence of the target, which opened the aptamer hairpin and either hindered or impeded the access of methylene blue to the guanines [25].

Application of HER2-aptasensor-RNA/LOD

The linear regression was calculated from the difference between the methylene blue samples on the surface of the

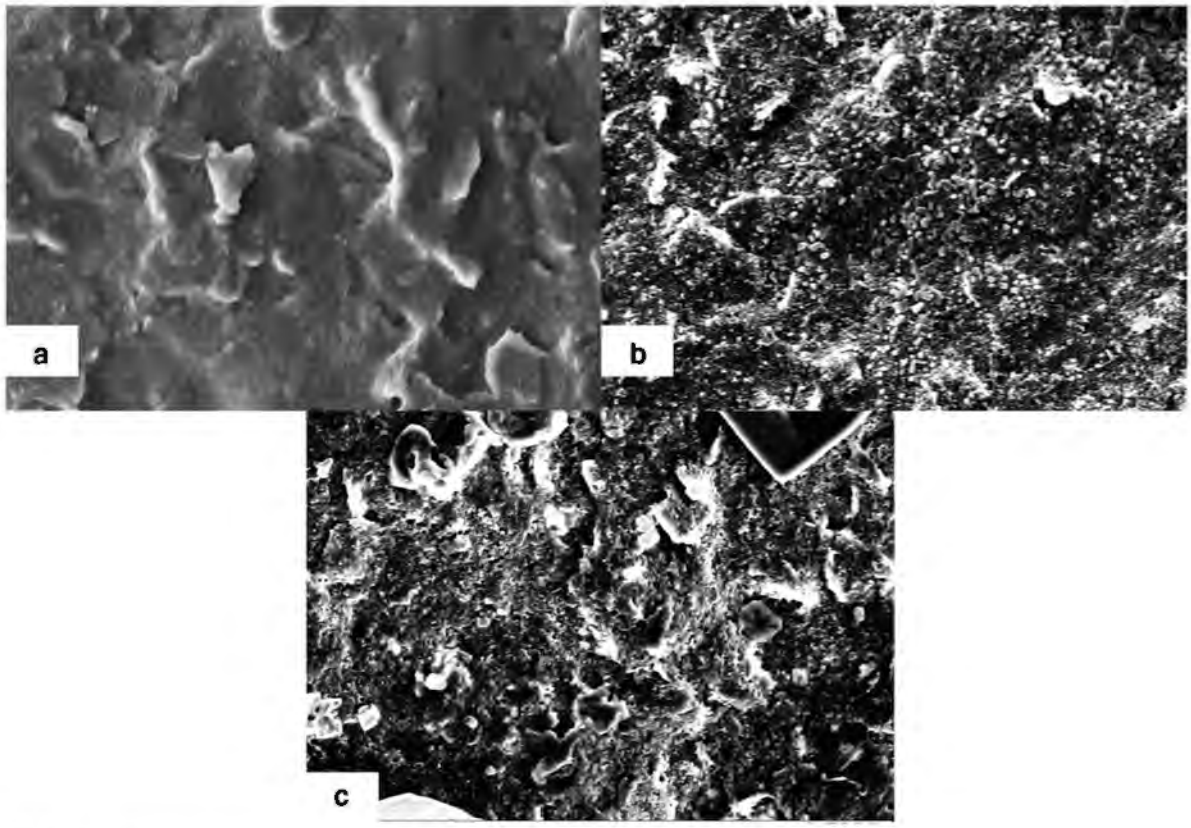

Fig. 2 a Electrode bare and b modified carbon electrode with PLLF (c) aptamer immobilization at ×5000 magnification

immobilized electrode in the presence and absence of the target diluted in PBS (Δi). Samples in PBS have also been used as the standard for the calculation of the detection limit in previous studies [26]. The calibration curve ($y = 0.0879x + 0.5378$) (Fig. 4b) was linear between 10 and 60 ng/mL Fig. 4b. A detection limit of 3.0 ng/mL was estimated by the equation $3\sigma/\alpha$, in which α is the decline of the slope and σ is the intercept, with $R^2 = 0.997$.

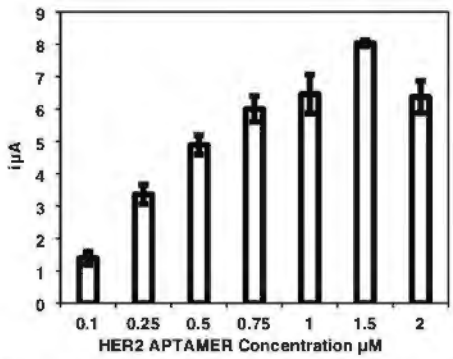

Fig. 3 Differential pulse voltammetry of HER2 aptamer immobilized on the working electrode surface at different concentrations

Interference study

The next test was performed with a sample of human serum from a healthy woman (control serum) with the addition of the HER2 protein (HER2-HS) (15 ng/mL = 3.8 μA; 30 ng/mL = 4.27 μA; 50 ng/mL = 5.7 μA; 60 ng/mL = 6.80 μA) (Fig. 4c), simulating HER2 overexpression. Since the serum already contained HER2, adding 15 ng/mL leads to a concentration higher than 15 ng/mL. In contrast, the interaction between the HER2 aptamer and HER2-HS exhibited a linear response in the opposite direction.

This was attributed to the interference of albumin, which is an abundant protein in serum [27]. One of the important constraints observed in the aptamer system for detection of HER2 protein in serum is the possibility of protein albumin being in the milligram per milliliter range overlapping binding sites, competing and masking the detection of proteins appearing in a range of nanograms per milliliter as is the

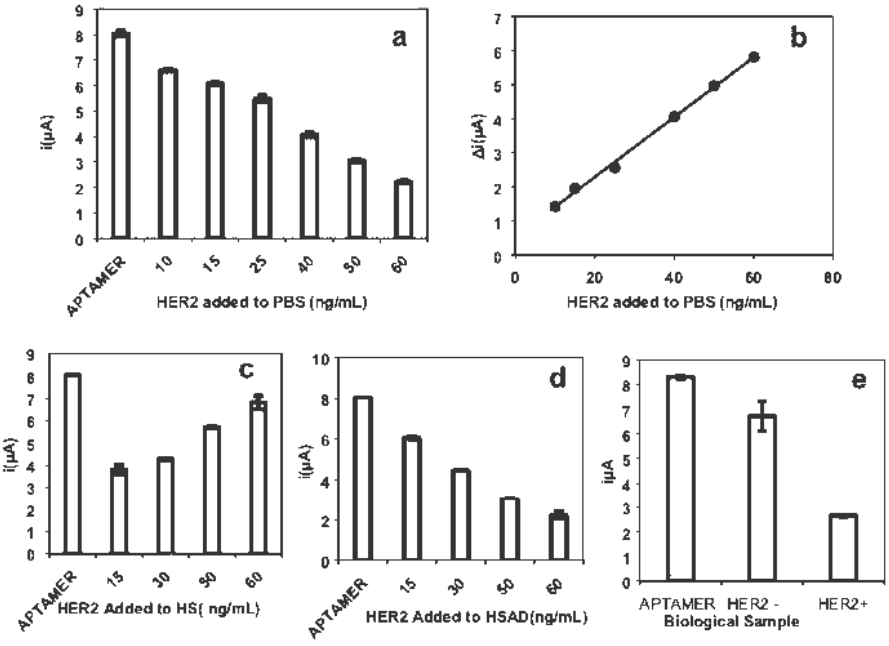

Fig. 4 Histogram of the effect on the electrochemical reduction of methylene blue following the interaction between the HER2 aptamer probe and spiking protein HER2 target; **a** HER2-PBS; **b** linear response of HER2 protein diluted in PBS at concentrations of 10 to 60 ng/mL and aptasensor detection limit **c** HER2-HS; **d** HER2-HSAD; **e** biological samples [HER2-HSAD negative (−) and HER2-HSAD positive (+)]

case of the HER2 protein, with a false positive, because of non-specific adsorption of the protein albumin [28].

Considering the direct interaction between the aptamer, the protein albumin, and the target protein that caused a pronounced change in the reduction current recorded by the measurements, as demonstrated in Fig. 4c, there is need to remove albumin [29] with the use of an albumin depletion kit [30]. After depletion of the albumin from the biological sample of the control serum (following the manufacturer's instructions) and addition of the HER2 protein (15 ng/mL = 5.91 μA; 30 ng/mL = 4.5 μA; 50 ng/mL = 3.35 μA; 60 ng/mL = 2.1 μA) (HER2-HSAD) (Fig. 4d), the result was similar to that found in the PBS experiment [9] (Fig. 4a).

The need to deplete albumin in the detection of proteins in a lower concentration of serum has also been described

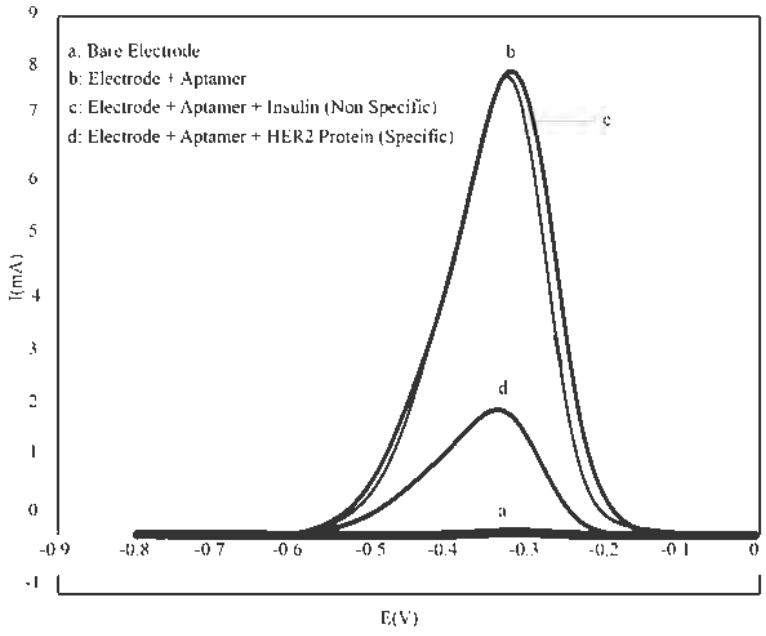

Fig. 5 Electrochemical reduction of MB. (a) Bare electrode; (b) electrode with an immobilized aptamer; (c) aptamer with non-specific insulin protein (1 ng/mL = 26 IU); (d) aptamer with HER2-PBS protein specific (60 ng/mL)

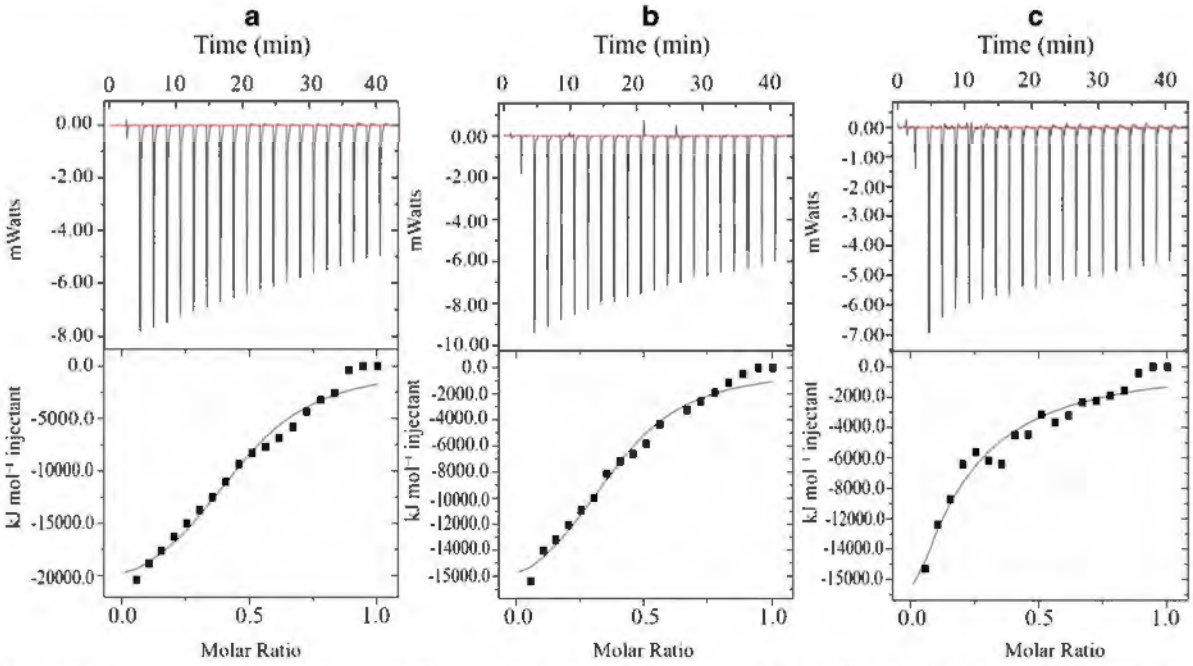

Fig. 6 ITC titration curves of interaction between RNA aptamer (0.75 μM) and HER2 protein (0.15 μM) obtained at 25 °C (**a**), 35 °C (**b**), and 45 °C (**c**)

elsewhere [30] since highly abundant proteins (such as albumin) tend to mask those that are less abundant (such as the protein of interest). The strategy of depleting albumin and globulins was crucial to enable the detection of HER2 protein on the aptamer surface. The electrochemical analysis of small amounts of proteins, such as HER2 protein, can be prevented by an undesirable adsorption of proteins present in serum, predominantly serum albumin (2/3 of total proteins) and globulins (1/3) [27, 28]. Therefore, one should consider alternative ways of combating this non-specific protein adsorption. For this reason, the depletion of albumin and globulins allowed use to exclude the interference of non-specific protein adsorption in the trial results.

The tests were performed with serum from a healthy woman, in which a peak of 6.72 μA was found without the addition of the protein. When we tested the serum of a woman with HER2+ breast cancer, we obtained a signal of 2.65 μA, demonstrating the decreasing patterns shown in Fig. 4e and d, respectively. Figure 4 shows the effect of the interaction between the aptamer and HER2 protein and the application of the HER2-aptasensor-RNA and LOD.

Selectivity studies and affinity for HER2

The absence of the ligand enables MB to bind with the free guanines of the RNA with high efficiency, producing an electrochemical signal. In contrast, the presence of the ligand (analyte of interest, i.e., HER2 protein in the present case) either forces the exit of the redox indicator or hinders its interaction, consequently producing a lower

Table 1 Stoichiometry (n), binding constant (K), enthalpy (ΔH), entropy ($-T\Delta S$), and Gibbs free energy (ΔG) of binding between RNA aptamer and HER2 protein according to a single binding site model

Temperature (°C)	N^a	K (μM)^b	ΔH (kJ mol^{-1})^c	$-T\Delta S$ (kJ mol^{-1})^d	ΔG (kJ mol^{-1})
25	0.459	89	−229.3	169.3	−60.0
35	0.387	82.1	−189.7	158.4	−31.3
45	0.101	16.4	−73.4	58.9	−14.5

[a] Standard deviations are less than 4%

[b] Errors in K values ranged from 1% to 6%

[c] Errors in ΔH ranged from 1% to 4%

[d] Errors in $-T\Delta S$ are 1–5%

Table 2 Main features between existing HER2 biosensors and biosensor developed in this work

Detection method[a]	Analyzed sample	Time (min)[b]	Selective	LOD	LR	Ref.
Electrochemical aptasensor |1/6|	Human serum Albumin/depletion	4	Insulin	3 ng/mL	10–60 ng/mL	This work
Electrochemical aptasensor |2/7|	Protein HER2 Diluted ultrapure water	60	Glucose, IgG, DNA RNA	5 ng/mL	10^{-5}–10^{2} ng/mL	[12]
Electrochemical aptasensor |2/7|	1% Fetal bovine calf serum	30	BSA	10^{-12} M	10^{-12}–10^{-8} M	[14]
Electrochemical immunosensor |3/8|	Human serum diluted in PBS	60	Not shown	4.4 ng/mL	15–100 ng/mL	[10]
Electrochemical immunosensor |2/8|	Serum diluted in PBS 20×	Not shown	Not shown	0.995 pg/mL	0.01–10 ng/mL 10–100 ng/mL	[15]
Magneto-immunosensor |5/8|	Serum Sigma + human serum	Not shown	HSA, HIgG, TNFa, BSA	26 pg/mL	0.1–32.0 ng/mL	[16]
Electrochemical immunosensor |3/8|	Human serum in PBS	Not shown	BSA, CEA, PSA	7.4 ng/mL	10–110 ng/mL	[17]
Electrochemical immunosensor |4/8|	Human serum diluted in PBS 20×	Not shown	BSA	2.0×10^{-5} ng mL	5.0×10^{-4} 50 ng/mL	[18]
Electrochemical immunosensor |3/8|	Male human serum	20	CA 15-3 BSA Cystatin C	0.16 ng/mL 8.5 ng/mL	7.5–50 ng/mL	[19]

[a] Transducer/probe is presented in brackets: [1] Carbon (homemade); [2] Gold; [3] Carbon and gold nanoparticles; [4] Glassy carbon; [5] Carbon (industrialized); [6] HER2 RNA; [7] HER2 DNA; [8] Antibody

[b] Time of analysis includes only the biorecognition reaction and measurements of the signal

signal, because the hairpin is closed in the absence of the specific target [25, 29].

No signal was found with the bare electrode (Fig. 5a). The peak of the immobilized probe on the carbon electrode was 8.03 μA (Fig. 5b), demonstrating a considerable increase in the signal. The interaction between the probe and non-specific protein (insulin) (Fig. 5c) was similar to that found for the probe alone, demonstrating that the aptasensor has no affinity for the non-specific target. Insulin was chosen as the non-specific target owing to its solubility in water, like HER2, and because there is a significant increase in insulin levels in women with cancer [31, 32]. The positive signal was seen for the HER2-HSAD (Fig. 5c), demonstrating that the aptasensor is specific to HER2. The ability of aptamers to bind to specific targets, such as HER2, enables the creation of biosensors for monitoring HER2 in serum [30]. Figure 5 shows the results of selectivity studies.

Reproducibility and stability

In order to study the reproducibility, measurements in DPV for detection of the HER2 target, at concentrations of 10–60 ng/mL, diluted in PBS, were performed in triplicate for each concentration, using 18 different electrodes, prepared with the same methodology, resulting in relative standard deviations (RSDs) of 10 ng/mL (3%), 15 ng/mL (2%), 25 ng/mL (3%), 40 ng/mL (3.0%), 50 ng/mL (2%), and 60 ng/mL (2%), showing good reproducibility of the aptasensor. The aptasensor was stored at 4 °C for 5 days. HER2 was measured at a concentration of 60 ng/mL in triplicate by DPV using different electrodes and the same methodology; the aptasensor remained stable for 3 days, with a relative standard deviation around 2%. However, after this period, it showed a relative standard deviation of 27%, denoting that stability had declined considerably.

Thermodynamic characterization of recognition event between aptamer and target

ITC titration curves of interaction between RNA aptamer and protein

Isothermal titration calorimetry (ITC) is an established analytical technique routinely used to determine thermodynamic interaction for a variety of chemical and biological systems [31]. Figure 6 shows typical calorimetric titration profiles between RNA aptamer (0.75 μM) and HER2 protein (0.15 μM) obtained at 25, 35, and 45 °C. Each peak in the binding isotherm represents a single injection of the titrant solutions into the cell containing HER2. All titration profiles provide exothermic heats of binding, which decrease in magnitude with subsequent injections.

The stoichiometry and binding affinity between RNA aptamer and HER2 protein decreases when the temperature increases (Table 1). This effect could be associated with the degradation of the compounds or steric blockage of the binding sites due to a conformational change of the molecule. All interactions showed favorable enthalpy changes, indicating an

exothermic process (Table 1). The experiment performed at 25 °C presented higher enthalpy associated with good hydrogen bonding. In contrast, high temperatures show lower enthalpy due reduction in binding sites between the molecules which promote hydrophobic interaction such as van der Waals bonding [29, 33]. The entropy effects ($-T\Delta S$) of all interactions were positive corresponding to unfavorable conformational change responsible for exposing active sites of the molecules. Gibbs free energy (ΔG) measures the ability of a thermodynamic system to do maximum or reversible isothermic and isobaric works. ΔG is one of the most important thermodynamic quantities to characterize the driving forces of binding [33]

All ΔG negative values indicate that the binding affinity of a ligand to a given acceptor is a spontaneous process, with more negative values of ΔG (60.0 kJ mol ^{1}). Gathering all results shows that the favorable binding mechanism between the aptamer and protein is temperature dependent and predominantly governed by enthalpy associated with hydrogen bond formation and unfavorable conformational changes, which expose interaction sites of the molecules [29].

Table 2 shows the comparison between the analytical characteristics of some aptasensors and electrochemical HER2 immunosensors and those of the proposed aptasensor. These clearly show that they were able to detect HER2, in serum diluted in PBS, using transducer platforms with gold electrodes and carbon and gold nanoparticles in a time ranging from 20 to 60 min, with selectivity testing using BSA, HSA, HIgG, TNFα, CEA, PSA, CA 15-3, and cystatin C [16–19] with an interval ranging from (LR) 0.01 to 100 ng/mL with LOD between 0.995 pg/mL and 8.5 ng/mL [15, 19].

The aptasensor presented in this study can also detect HER2 in serum after albumin depletion, in 4 min with the use of carbon electrode (homemade screen-printed electrode), further reducing the experimental time. This indicates that the optimized strategy in this work is promising, as shown in the comparison in Table 2.

Conclusion

In this article, we use an electrochemical carbon transducer modified by the electropolymerization of L-lysine, forming a poly-L-lysine (PLL) film deposited on the surface, exposing amines. Studies with PLL as a modifier generally use gold electrodes [20]. The chemical mediator was methylene blue as an intercalator of guanines, because the aptamer of RNA HER2 (purchased from Aptagen) has guanines in the hairpin region [34]. This type of reaction with methylene blue is common in the construction of electrochemical biosensors that interact with the target probe through hybridization [34]. The advantages of electrochemical biosensors over calorimetric, optical, and piezoelectric biosensors are portability, low cost, practicality, and fast results. Therefore, such biosensors can assist in the diagnosis of different diseases, such as breast cancer [5], in a less invasive manner (blood samples) than current methods, which only detect the disease once it has been established and require the removal of breast tissue through a biopsy [5].

The aptasensor used in the present study exhibited a good linear response (10 60 ng/mL) diluted in PBS and had a detection limit of 3.0/mL. The aptasensor showed good reproducibility with relative standard deviations (RSDs) of 3% and it remains stable for 3 days with an RSD around 2%. The HER2 aptamer is not complementary to the insulin protein. In the tests performed with a healthy woman's serum, it showed a peak of 6.72 μA and in the serum of a woman with HER2+ breast cancer, we obtained a signal of 2.65 μA, showing the decreasing patterns found in the calibration curve. The sensor is sensitive to HER2 protein and has considerable potential as an effective alternative method for the early detection of HER2 in human serum.

Acknowledgments We would like to thank Laboratório de Imunopatologia Keizo Asami (LIKA), Federal University of Pernambuco UFPE-Brazil. We would like to express our sincere gratitude to all those who helped us develop this research.

Funding This research did not receive any specific grant from funding bodies in the public, commercial, or not-for-profit sectors.

Compliance with ethical standards

Conflict of interest There are no conflicts to declare.

References

1. Bray F, Ferlay J, Soerjomataram I, Siegel RL, Torre LA, Jemal A. Global cancer statistics 2018: GLOBOCAN estimates of incidence and mortality worldwide for 36 cancers in 185 countries. CA Cancer J Clin. 2018. https://doi.org/10.3322/caac.21492.
2. Medeiros GC. Determinants of the time between breast cancer diagnosis and initiation of treatment in Brazilian women. Cad Saude Publica. 2015. https://doi.org/10.1590/0102-311X00048514.
3. Unger-saldaña K. Challenges to the early diagnosis and treatment of breast cancer in developing countries. World J Clin Oncol. 2014. https://doi.org/10.5306/wjco.v5.i3.465.
4. Vondeling GT, Menezes GL, Dvortsin EP, Jansman FGA, Konings IR, Postma MJ, et al. Burden of early, advanced and metastatic breast cancer in the Netherlands. BMC Cancer. 2018. https://doi.org/10.1186/s12885-018-4158-3.
5. Zhang X-H, Xiao C. Diagnostic value of nineteen different imaging methods for patients with breast cancer: a network meta-analysis. Cell Physiol Biochem. 2018. https://doi.org/10.1159/000489443.
6. Khanjani F, Sajedi RH, Hasanvia S. Rapid screening of drug candidates against EGFR/HER2 signaling pathway using fluorescence assay. Anal Bioanal Chem. 2018;410(30):7827–35.
7. Tagliafico AS, Valdora F, Mariscotti G, Durando M, Nori J, La Forgia D, et al. An exploratory radiomics analysis on digital breast tomosynthesis in women with mammographically negative dense breasts. Breast. 2018. https://doi.org/10.1016/j.breast.2018.04.016.

8. Efared B, Sidibé IS, Gamrani S, El Otmani I, Erregad F, Hammas N, et al. The assessment of HER2 gene status by fluorescence in situ hybridization in invasive breast carcinomas with equivocal HER2 immunostaining: experience from a single institution. Int J Surg Pathol. 2018. https://doi.org/10.1177/1066896918767546.
9. Carney WP. Circulating oncoproteins HER2/neu, EGFR and CAIX (MN) as novel cancer biomarkers. Expert Rev Mol Diagn. 2007;7(3):309–19.
10. Marques RCB, Viswanathan S, Nouws HPA, Delerue-Matos C, González-García MB. Electrochemical immunosensor for the analysis of the breast cancer biomarker HER2 ECD. Talanta. 2014;129:594–9. https://doi.org/10.1016/j.talanta.2014.06.035.
11. Gohring JT, Dale PS, Fan X. Detection of HER2 breast cancer biomarker using the opto-fluidic ring resonator biosensor. Sensors Actuators B Chem. 2010;146(1):226–30.
12. Chun L, Kim SE, Cho M, Choe WS, Nam J, Lee DW, et al. Electrochemical detection of HER2 using single stranded DNA aptamer modified gold nanoparticles electrode. Sensors Actuators B Chem. 2013;186:446–50. https://doi.org/10.1016/j.snb.2013.06.046.
13. Pfeiffer F, Mayer G. Selection and biosensor application of aptamers for small molecules. Front Chem. 2016. https://doi.org/10.3389/fchem.2016.00025.
14. Salimian R, Kékedy-Nagy L, Ferapontova EE. Specific picomolar detection of a breast cancer biomarker HER-2/neu protein in serum: electrocatalytically amplified electroanalysis by the aptamer/PEG-modified electrode. ChemElectroChem. 2017. https://doi.org/10.1002/celc.201700025.
15. Emami M, Shamsipur M, Saber R, Irajirad R. An electrochemical immunosensor for detection of a breast cancer biomarker based on antiHER2–iron oxide nanoparticle bioconjugates. Analyst. 2014. https://doi.org/10.1039/c4an00183d.
16. Eletxigerra U, Martinez-Perdiguero J, Merino S, Barderas R, Torrente-Rodríguez RM, Villalonga R, et al. Amperometric magnetoimmunosensor for ErbB2 breast cancer biomarker determination in human serum, cell lysates and intact breast cancer cells. Biosens Bioelectron. 2015. https://doi.org/10.1016/j.bios.2015.03.017.
17. Arkan E, Saber R, Karimi Z, Shamsipur M. A novel antibody-antigen based impedimetric immunosensor for low level detection of HER2 in serum samples of breast cancer patients via modification of a gold nanoparticles decorated multiwall carbon nanotube-ionic liquid electrode. Anal Chim Acta. 2015. https://doi.org/10.1016/j.aca.2015.03.022.
18. Shamsipur M, Emami M, Farzin L, Saber R. A sandwich-type electrochemical immunosensor based on in situ silver deposition for determination of serum level of HER2 in breast cancer patients. Biosens Bioelectron. 2018. https://doi.org/10.1016/j.bios.2017.12.022.
19. Freitas M, Nouws HPA, Delerue-Matos C. Electrochemical sensing platforms for HER2-ECD breast cancer biomarker detection. Electroanalysis. 2018. https://doi.org/10.1002/elan.201800537.
20. Nascimento GA, Souza EVM, Campos-Ferreira DS, Arruda MS, Castelletti CHM, Wandedey MSO, et al. Electrochemical DNA biosensor for bovine papillomavirus detection using polymeric film on screen-printed electrode. Biosens Bioelectron. 2012;38(1):61–6.
21. Ouyang Y, Cai X, Shi QS, Liu L, Wan D, Tan S, et al. Poly-L-lysine-modified reduced graphene oxide stabilizes the copper nanoparticles with higher water-solubility and long-term additively antibacterial activity. Colloids Surf B: Biointerfaces. 2013. https://doi.org/10.1016/j.colsurfb.2013.01.073.
22. Sun W, Zhang Y, Ju X, Li G, Gao H, Sun Z. Electrochemical deoxyribonucleic acid biosensor based on cadboxyl functionalized graphene oxide and poly-L-lysine modified electrode for the detection of tlh gene sequence related to vibrio parahaemolyticus. Anal Chim Acta. 2012. https://doi.org/10.1016/j.aca.2012.09.009.
23. Bang GS, Cho S, Kim BG. A novel electrochemical detection method for aptamer biosensors. Biosens Bioelectron. 2005;21(6):863–70.
24. Rohs R, Sklenar H, Lavery R, Ro B. Methylene blue binding to DNA with alternating GC base sequence: a modeling study. J Am Chem Soc. 2000;11:2860–6.
25. Abnous K, Danesh NM, Alibolandi M, Ramezani M, Taghdisi SM. Amperometric aptasensor for ochratoxin A based on the use of a gold electrode modified with aptamer, complementary DNA, SWCNTs and the redox marker methylene blue. Microchim Acta. 2017;184:1151–9.
26. Chou J, Yan S, Liao Y, Lai C, Wu Y. Fabrication of flexible arrayed lactate biosensor based on immobilizing LDH-NAD+ on NiO film modified by GO and MBs. Sensors (Basel). 2017. https://doi.org/10.3390/s17071618.
27. Cortez CM, Silva D, Silva CMC, Missailidis S. Interactions of aptamers with sera albumins. Spectrochim Acta A Mol Biomol Spectrosc. 2012;95:270–5.
28. Jarczewska M, Kékedy-Nagy L, Nielsen JS, Campos R, Kjems J, Malinowska E, et al. Electroanalysis of pM-levels of urokinase plasminogen activator in serum by phosphorothioated RNA aptamer. Analyst. 2015;140(11):3794–802.
29. Cai S, Yan J, Xiong H, Liu Y, Peng D, Liu Z. Investigations on the interface of nucleic acid aptamers and binding targets. Analyst. 2018. https://doi.org/10.1039/C8AN01467A.
30. Björhall K, Miliotis T, Davidsson P. Comparison of different depletion strategies for improved resolution in proteomic analysis of human serum samples. Proteomics. 2005;5(1):307–17.
31. Bronsveld HK, De Bruin ML, Wesseling J, Sanders J, Hofland I, Jensen V, et al. The association of diabetes mellitus and insulin treatment with expression of insulin-related proteins in breast tumors. BMC Cancer. 2018. https://doi.org/10.1186/s12885-018-4072-8.
32. Khalid S, Hwang D, Babichev Y, Kolli R, Altamentova S, Koren S, et al. Evidence for a tumor promoting effect of high-fat diet independent of insulin resistance in HER2/Neu mammary carcinogenesis. Breast Cancer Res Treat. 2010;122(3):647–59.
33. Pang Y, Xu Z, Sato Y, Nishizawa S, Teramae N. Base pairing at the abasic site in DNA duplexes and its application in adenosine aptasensors. ChemBioChem. 2012;13(3):436–42.
34. Campos-Ferreira DS, Souza EVM, Nascimento GA, Zanforlin DML, Arruda MS, Beltrão MFS, et al. Electrochemical DNA biosensor for the detection of human papillomavirus E6 gene inserted in recombinant plasmid. Arab J Chem. 2016;9(3):443–50.
35. Yang W, Ozsoz M, Hibbert DB, Gooding JJ. Evidence for the direct interaction between methylene blue and guanine bases using DNA-modified carbon paste electrodes. Electroanalysis. 2002;14(18):1299–302.